JPRS Report

Science & Technology

USSR: Engineering & Equipment

AUTOMATIC STABILIZATION OF OPTICAL IMAGE

19980121 179

DTIC QUALITY INSPECTED 3

SCIENCE & TECHNOLOGY

USSR: ENGINEERING & EQUIPMENT

AUTOMATIC STABILIZATION OF OPTICAL IMAGE

CONTENTS

[Text] Annotation

The methods and means of stabilization of an image during optical observations from mobile bases by acting on individual elements of the optical apparatus are analyzed systematically in the book. Special attention is devoted to promising automatic systems, in which stabilization is carried out according to information of image displacements. Systems of indirect image stabilization, based on information about the three-dimensional displacements of movable bases, are also considered.

The book is intended for engineering and technical personnel in instrument building.

Preface

The modern requirements imposed on optical instruments reduce mainly to a combination of two contradictory characteristics: high angular resolution and minimal mass and size of the instrument. These requirements are also retained for apparatus, operating on a moving or insufficiently stable base. Various types of supplementary mechanical devices, which reduce the influence of the motion of the base on image quality, are most frequently used to retain the potential capabilites of optical instruments in the area of resolution. The most widespread procedure is mounting the optical instrument on a gyro-stabilized platform. One must frequently do away with using a gyro-stabilized platform in real cases with all the theoretical evidence of the correctness of selecting this variant of solving the stabilization problem. The latter is explained by the fact that the relations between the mass of the instrument to be stabilized and the stabilizing setting are equal to 1:3-1:4 at low compensation level. Moreover, there is a

specific dependence of the mass of the mount on the accuracy of its operation. The mass of the mount increases with an increase of accuracy and the ratio presented above deteriorates. Therefore, the basic direction in development of optical instruments of this class will undoubtedly be related to stabilization of the image with respect to the image detector or of the detector with respect to a randomly fluctuating image (due to stabilization of displacement of individual components or assemblies of the instrument, the mass of which is at least an order of magnitude less than that of the entire instrument). It is obvious that a somewhat different approach both toward selection of the optical layout of the instrument and toward selection of its entire schematic diagram is required for this.

More than 300 publications on different circuit solutions and on specific devices, related to photographic and movie equipment, to telescopes mounted both on the earth and in space, to aerospace observation equipment, to helioequipment and also to visual devices-- binoculars, telescopes, sights, surveyor's instruments--and to hologram- receiving units are now known.

Selection of one or another layout of an optical device with image stabilization is largely determined by the principle of designing the control system, which should respond with high sensitivity to external perturbations of a wide frequency range, which cause displacement of the image. Two directions are possible in development of a stabilization system. The first direction is related to the use of highly sensitive mechanical or laser gyroscopes, which record nonprogrammed displacements of the movable base in space and emit the corresponding signals to the follow-up systems, which control the actuating devices in the optical circuit of the instrument and which compensate for dynamic shifts of the image. This direction is related to indirect image stabilization, since the image itself is not monitored and information about it is not fed to the control system. The use of highly sensitive and compact laser gyroscopes, which have not yet been considered in problems of design of image stabilization systems, is promising.

The second direction is related to the use of information image displacement monitoring systems in the coordinate axes of the focal plane and to development of closed control systems directly for the image. One-coordinate systems are made in the simplest case, but it frequently becomes necessary to make two- and three-coordinate systems that shape the given quality of the image. Those principles of designing information systems, the drives of actuating devices and of control systems as a whole, which would have the highest speed and greatest dynamic accuracy, would be simple in organization and flexibility in functional adjustment upon variation of the operating mode of the optical equipment, must be used with regard to the high sensitivity of systems to external effects of a broad spectrum, which cause dynamic shifts of the image. The second direction is more promising, although it is related to solution of a combination of new problems, development of which many organizations in the Soviet Union

and abroad are involved.   These problems determine the need to develop:
1) active actuating devices for the equipment which would function most
efficiently in automatic control systems, 2) highly sensitive
information image checking systems according to the coordinates of the
image plane, 3) precision devices that would guarantee the necessary
linear and angular displacements of the actuating devices, and 4) one-,
two-, and three-coordinate image stabilization systems that provide a
given quality to it.

It should be emphasized that design of multicoordinate control systems
for apparatus with high image resolution is a very complicated
scientific engineering problem.   This problem can be solved with
accurate knowledge of the influence of each component of the system on
the measurement error and by processing the extent of displacement for
each coordinate axis of spatial displacements of the optical equipment.
The answers to individual problems that occur upon solution of the above
problems are contained in numerous articles and patents.   The first
well-known prominent publications in the field of image stabilization
should be considered [5, 62].

General data are presented in [5] on the use of gyroscopes in optical
instrument building, specifically, on the use of gyro-stabilized
platforms.   Systems containing these devices are developed in [4], in
which random vibrations of the ship, the essence of modern methods of
gyroscopic stabilization of the carrier and of the equipment mounted on
it, the mathematical fundamentals of solution of problems of coordinate
conversion, different methods of stabilization and hardware for
achieving them are considered.   The book gives a rather complete idea of
the methods of solving the theoretical and practical problems which the
developers of traditional gyroscopic stabilizers encounter.

The design principles and methods of design of image stabilization
systems, in which the active devices of optical instruments, controlled
by information signals on displacement of the bases and on misalignments
of the image directly are used, were not reflected in the above papers.
This circumstance determines the absence of papers on information image
misalignment checking systems, and on precision drives of the actuating
devices of image motion control systems.

Gyro sensors and gyro units, designed on precision gyroscopes, have
reached the limit in an increase of sensitivity and a reduction of mass
and size in their specifications.   Image stabilization systems will be
improved further toward use of new systems for measuring the spatial
displacements of the object, including laser instruments.

Stabilization systems are described in the book, in which displacements
of individual components or assemblies of optical instruments are used,
are described in the book.   The use of gyro-stabilized platforms, which
are described in detail in the above monographs, is essentially not
considered in the book.

3

The book has six chapters. General data on shaping the image in the focal plane of optical instruments are presented in Chapter 1. A mathematical description of the processes of image misalignment, caused by the functional modes of the equipment and by random motions of the base, is given. Methods of active effects on the image to stabilize it are considered. Methods and means of image stabilization during optical observations with a moving base are considered in Chapter 2 with regard to the characteristics of different optical systems. The methods and means of parametric stabilization of the image in control systems with feedback according to coordinates of displacements of the moving base and misalignment of the image is presented. The design principles of functional image stabilization devices are considered and specific solutions of realizing these devices for optical equipment are given in Chapter 3. A detailed outline of the principles of organizing information systems for monitoring spatial displacement of moving bases and misalignment of the image is given in Chapter 4, according to the problems of image stabilization, formulated in Chapter 1. Main attention is devoted to information systems for checking misalignment of the image in two coordinates. The errors of the information systems are analyzed and the main methods of error compensation are considered.

Precision instruments of actuating devices in image motion control systems are described in Chapter 5. The design principles of drives for formation of the angular and linear displacements of the assemblies of the equipment, which meet the requirements of high dynamic accuracy and functional characteristics of the apparatus, are outlined.

Chapter 6 is devoted to automatic image stabilization systems. Automatic indirect image stabilization systems according to information about spatial displacements of moving bases and automatic stabilization systems for information about shifting of the image are considered. Methods of optimization of local and correlated stabilization systems according to the criteria of image quality are outlined.

Chapter 1. General Data on Misalignment of Image and Methods of Image Stabilization During Optical Observations With Moving Base

1.1. Main Characteristics of Image

Images are considered in iconics in the unity of physical and information properties and the developers of equipment can select different mathematical descriptions of images with regard to specific problems [50].

Adequate mathematical models correspond to the physical level of description of images within this book and two transformations of information are taken into account: shaping of images and recording of images.

These transformations are typical, for example, for aerial photographic equipment (AFA), mounted on a moving base.

The optical image is shaped in the plane of the photographic film by the optical system of the AFA. The mathematical model of the shaped image can be the function f(x, y, t) of two rectangular coordinates x, y and of time t, where the value of f is the intensity of the optical image at a given point of plane x, y, at given moment of time t.

Shaping can be presented as a sequence of two steps (Figure 1.1). The hypothetical ideal optical system initially shapes an ideal image f(x, y, t), being an accurate projection of the object to be photographed onto plane x, y, and image f*(x, y, t) is then distorted by a linear spatial filter, which takes into account the aberrations, inaccuracy of focusing of the optical system, diffraction and scattering of light and other physical phenomena.
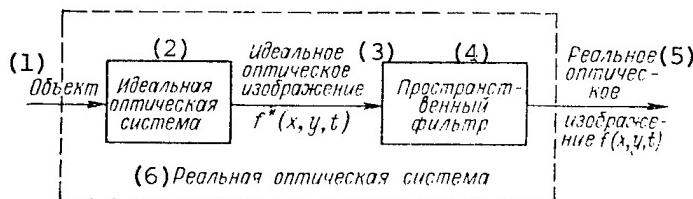
Figure 1.1. Diagram of Shaping of Optical Image

KEY:
1. Object
2. Ideal optical system
3. Ideal optical image
4. Spatial filter
5. Real optical image
6. Real optical system

The optical system in most applications is considered isoplanar (spatially invariant) and distortions are described by a convolution integral

$$f(x, y, t) = \int\int_{-\infty}^{+\infty} f^*(x - \varkappa, y - \eta, t) h_0(\varkappa, \eta) \, d\varkappa \, d\eta, \qquad (1.1)$$

where $h_0(x, y)$ is a scattering function of a point of the optical system (pulsed characteristic of the filter).

We note that the optical system is practically inertialless. This is formally expressed in the fact that the kernel of the integral transform h_0 is independent of time t. In practice, the inertialless nature of the optical system means that any time changes of the object (for example, displacement of the object with respect to the AFA or displacement of the AFA with respect to a fixed object) are transmitted without distortions to plane x, y. This property is used in design of image displacement sensors, considered in detail in Chapter 4.

The image is recorded by photographic film. The final result of recording (after photochemical processing of the film) is a fixed (time-invariable) g (x, y), where g is the intensity of the photographic image at point x, y. If the photographic film is an ideal recorder, transformation of the image f(x, y, t) to an ideal image g*(x, y) was described as time integration

$$g^*(x, y) = \int_0^T f(x, y, t) \, dt, \qquad (1.2)$$

where [0, T] is an interval of exposure time.

The recording of a real image g(x, y) is accompanied by the appearance of spatial distortions and noise, caused by the stochastic discrete structure of the photographic emulsion, by the quantum nature of light, by scattering of light within the photographic emulsion and by other factors [73].
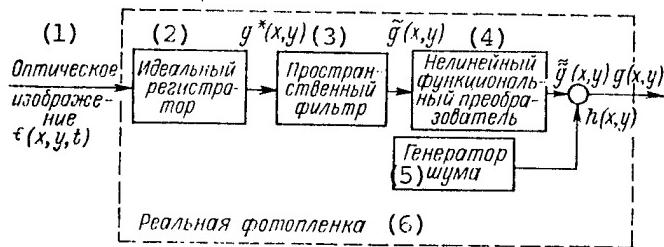
Figure 1.2. Diagram of Shaping Spatial Images and Noise

KEY:

1. Optical image
2. Ideal recorder
3. Spatial filter

4. Nonlinear functional converter
5. Noise generator
6. Real photographic film
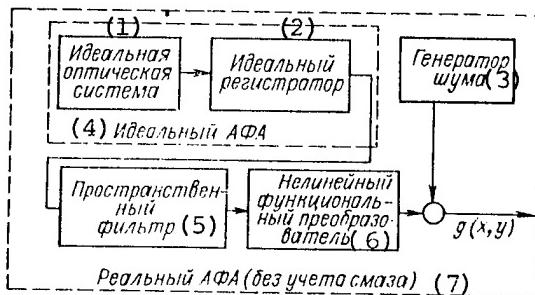
Figure 1.3. Diagram of Shaping of Image in AFA

KEY:

1. Ideal optical system
2. Ideal recorder
3. Noise generator
4. Ideal AFA
5. Spatial filter

6. Nonlinear functional converter
7. Real AFA (without regard to blurring)

The enumerated distortions are reduced in most applications to linear spatially invariant filtration, to nonlinear functional transformation and to addition of noise realization, generated by some hypothetical noise generator (Figure 1.2), i.e.,

$$g(x, y) = \widetilde{\widetilde{g}}(x, y) + n(x, y). \qquad (1.3)$$

Here n(x, y) is the realization of noise, $\widetilde{\widetilde{g}}(x, y) = \varphi[\widetilde{g}(x, y)]$, where $\widetilde{\widetilde{g}}(x, y) = \varphi$ is the characteristic of nonlinearity (the characteristic

7

curve of the photographic emulsion), $\tilde{g}(x, y) = \int\int\limits_{-\infty}^{+\infty} g^*(x - \varkappa, y - \eta) h_\phi$

$(\varkappa, \eta) d\varkappa d\eta$, and $h_\phi(x, y)$ is a scattering function of the point of the photographic emulsion.

Spatial filtration in the optical system and on the photographic film can be taken into account by a single linear spatially invariant filter of the AFA (Figure 1.3). The pulsed characteristic of this filter $h_{AFA}(x, y)$ is expressed by convolution of functions $h_0(x, y)$ and $h_\phi(x, y)$, i.e.,

$$h_{AФA}(x, y) = \int\int\limits_{-\infty}^{+\infty} h_0(x - \varkappa, y - \eta) h_\phi(\varkappa, \eta) d\varkappa d\eta. \qquad (1.4)$$

We note that functions f, g, h_0, h_ϕ, and h_{AFA} can be replaced by different mathematical equivalants. The most widespread equivalent of the function of two coordinates and time $a(x, y, t)$ in practical applications is the complex spectrum $T_a(N_x, N_y, f_t)$ of spatial frequencies N_x, N_y along axes x, y and time frequencies f_t. Both functions are linked by operators of direct and inverse Fourier transforms F, F^{-1}:

$$
\left.
\begin{aligned}
T_a(N_x, N_y, f_t) &= F\left[a(x, y, t)\right] = \\
= \int\int\int\limits_{-\infty}^{+\infty} a(x, y, t) &\exp\left[-j2\pi(N_x x + N_y y + f_t t)\right] dN_x dN_y dt; \\
a(x, y, t) &= F^{-1}\left[T(N_x, N_y, f_t)\right] = \\
= \int\int\int\limits_{-\infty}^{+\infty} & T_a(N_x, N_y, f_t) \times \\
\times \exp\left[-j2\pi(N_x x + N_y y + f_t t)\right] &dN_x dN_y dt.
\end{aligned}
\right\} \qquad (1.5)
$$

The concept of the Fourier transform is generalized by the concept of expansion of function $a(x, y, t)$ in orthogonal basis [79]. The wide distribution of the apparatus of Fourier transforms is related to the fact that the trigonometric functions are eigenfunctions of the linear filtration kernel. In other words, the multiplication operation in the area of space and time frequencies corresponds to the convolution operation in the space-time region, i.e., if

$$a(x, y, t) = \int\int\int\limits_{-\infty}^{+\infty} b(x - \varkappa, y - \eta, t - \tau) C(\varkappa, \eta, \tau) d\varkappa d\eta d\tau, \qquad (1.6)$$

8

then

$$T(N_x, N_y, f_t) = T_b(N_x, N_y, f_t) T_c(N_x, N_y, f_t).$$

Transition to the frequency range, without changing the physical and mathematical meaning of calculations of the AFA, simplifies the calculations in some practical cases and finds application in this book.

Typical distortion of moving images, which has been named blurring, is related to the recording process. The phenomenon of blurring determines to a significant degree the spatial resolution of the AFA, and this paper is essentially devoted to methods of measuring blurring, and also to methods of preventing blurring on the basis of compensating the displacements of images in the exposure interval. One other method of controlling blurring is also known—a posteriori processing of blurred photographic images [79]. This method is not considered in this book. The gradually complicated mathematical descriptions of blurring are presented below.

Let us begin with the simplest case: let us assume that there is a bright point, displaced along axis x at constant rate v_x, in an optical image on the surface of the photographic film $f(x, y, t)$. This point can be displaced by distance $X = v_x T$ in the exposure range $[0, T]$. Accordingly, blurring is manifested in the photographic image $g(x, y) =$

$= \int_0^T f(x, y, t)\, dt$ as transformation of the image of a point to an image of

a straight line with length X.

Let us turn attention to the fact that the extent of blurring X is proportional to the rate of displacement v_x and of the exposure time T. Two directions of controlling blurring hence follow: reducing the exposure time T by using highly sensitive photographic films and reducing the speed v_x by improving the design of the AFA.

Let us consider the more complicated case: let us assume that the entire image $f(x, y, t)$ is displaced along axis x during interval $[0, T]$, and that the result of recording is a blurred image $\hat{g}(x, y)$. This blurring can be formally described as a convolution of the image $g(x, y)$ by formula (1.3) with pulsed characteristic $h_{CM}(x)$ of the hypothetical blurring filter [70]

$$\hat{g}(x, y) = \int_{-\infty}^{+\infty} g(x - \varkappa, y) h_{CM}(\varkappa)\, d\varkappa =$$

$$= \int_0^x g(x - \varkappa, y) h_{CM}(\varkappa)\, d\varkappa.$$

(1.7)

9

where

$$h_{\text{c}_M}(x) = \begin{cases} v_x^{-1} & \text{at} \quad 0 \leqslant x < X; \\ 0 - & \text{in remaining cases.} \end{cases}$$

The blurring filter can be combined by formula (1.7) to the distorting filter of the AFA by equation (1.4)

$$h^{\text{экв}}_{\text{АФА}}(x, y) = \int_0^X h_{\text{АФА}}(x - \varkappa, y) h_{\text{c}_M}(\varkappa) d\varkappa, \tag{1.8}$$

where $h^{\text{экв}}_{\text{АФА}}(x, y)$ is the equivalent scattering function of the point of the AFA with regard to smearing.

Relation (1.8) is convenient for comparison of the spatial distortions of the image g(x, y). If the diameter D_{AFA} (Figure 1.4, a) of function $h_{\text{AFA}}(x, y)$ is considerably less than blurring X (Figure 1.4, b), the resolution in the direction of blurring is determined mainly by the blurring. Resolution is independent of blurring in the perpendicular direction (along axis y) and is determined by the value of D_{AFA} (Figure 1.4, c).
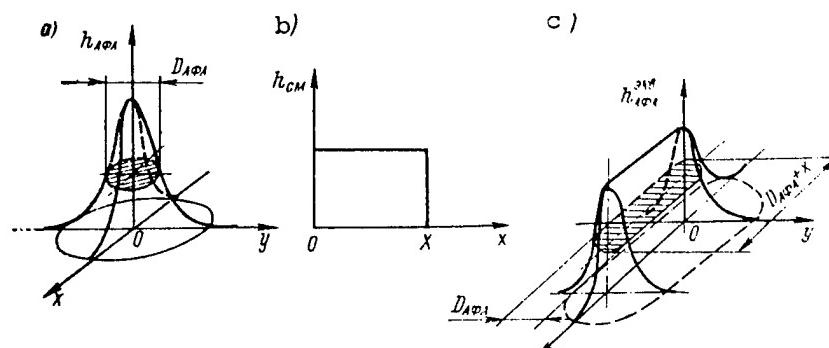
Figure 1.4. Characteristics of Image Blurring:
a--equivalent scattering function of point in AFA;
b--function of blurring point along one coordinate;
c--spatial function of blurring of point

10

Let us generalize the previous case: let us assume that the image is displaced at constant rate v with components v_x, v_y along axes x and y; moreover,

$$v = \sqrt{v_x^2 + v_y^2}. \tag{1.9}$$

Then $h^{\text{ЭКВ}}_{\text{АFА}}$ is determined by double convolution along axes x and y:

$$
\begin{aligned}
h^{\text{ЭКВ}}_{\text{АФА}}(x, y) &= \int_0^X \bar{h}(x - \varkappa, y) h_{\text{СМ}}(\varkappa) d\varkappa; \\
\bar{h}(x, y) &= \int_0^Y h_{\text{АФА}}(x, y - \eta) h^{\bullet}_{\text{СМ}}(\eta) d\eta,
\end{aligned}
\tag{1.10}
$$

where

$$
h^{\bullet}_{\text{СМ}}(y) = \begin{cases} v_y^{-1} & \text{at} \quad 0 \leqslant y \leqslant Y; \\ 0 & \text{—in remaining cases}, \end{cases}
$$
$$
y = v_y T.
$$

Expansion of the rate along the coordinate axes according to expression (1.9) at each given moment of time t is also possible in those cases when the rate is not constant, i.e., v = v(t). Specifically, when moving along axis x at constant acceleration a_x, the characteristic $h_{\text{СМ}}(x)$ has the following form [66]:

$$
h_{\text{СМ}}(x) = \begin{cases} 0{,}5 \sqrt{a_x x} & \text{at} \quad 0 \leqslant x \leqslant a_x T^2; \\ 0 & \text{—in remaining cases}. \end{cases}
\tag{1.11}
$$

During oscillatory motion when the period of motion coincides with the exposure time T, characteristic $h_{\text{СМ}}(x)$ is written in the form [92]

$$
h_{\text{СМ}}(x) = \begin{cases} (T/\pi) \sqrt{1 - x^2} & \text{at} \quad -1 \leqslant x \leqslant 1; \\ 0 & \text{—in remaining cases}. \end{cases}
\tag{1.12}
$$

Relations (1.7)-(1.12) express the relationship between displacement of the image to be recorded with respect to the photographic film and the

11

parameters of blurring. The operations of multiplication of the integrated spectrum of the image $T(N_x, N_y, f_t)$ by the complex frequency characteristic of blurring filter $T_{CM}(N_x, N_y)$ correspond to relations (1.7)-(1.12) in the frequency region by formula (1.6)

$$T_g(N_x, N_y, f_t) = T_f(N_x, N_y, f_t) T_{CM}(N_x, N_y).$$

Specifically, blurring caused by uniform displacement of the image along axis x by distance X by formula (1.7) is described by the following frequency characteristic:

$$T_{CM}(N_x) = Fh_{CM}(x) = \frac{1}{W_x^{-1}} \frac{\sin \pi x N_x}{\pi x N_x}.$$

The equivalent frequency characteristic of the AFA corresponds to the equivalent scattering of the point of the AFA with regard to blurring by formula (1.8)

$$T_{A\Phi A}^{\ni K B}(N_x, N_y) = T_{A\Phi A}(N_x, N_y) T_{CM}(N_x, N_y).$$

In addition to the complex frequency response curves, their normalized modules, called the modulation transfer function (FPM), will be used in the later sections of the book [81].

The equivalent modulation transfer function of the AFA is determined with regard to blurring by the following relation:

$$T_{A\Phi A}^{\ni K B}(N_x, N_y) = T_{A\Phi A}(N_x, N_g) T_{CM}(N_x, N_y),$$

where $T_{AFA}(N_x, N_y)$ is the modulation transfer function of the AFA without regard to blurring and $T_{CM}(N_x, N_y)$ is the normalized modulus of the frequency response curve of the blurring filter.

The second part of the problem--establishment of the correlation between the properties of displacements and structural parameters of the AFA--is considered in the next section. These displacements are generally different for different points of plane x, y.

12

1.2. Mathematical Description of Image Misalignment During Optical Observations From Moving Base

General mathematical description of image misalignment. Let us consider photography from a moving base. Let fixed coordinate system Oxyz be related to the space of the observation objects (Figure 1.5). Coordinate system $Ox_0y_0z_0$ is correlated with the moving base of the optical device. Let us use the following order of rotation of the moving coordinate system: yaw angle ψ in plane Oxy, pitch angle ϑ in plane Oy_0z, and bank angle γ in plane Ox_0y_0. If the angular rotational velocities are denoted by $\dot{\psi}$, $\dot{\vartheta}$, and $\dot{\gamma}$, respectively, the projections of the angular velocities of the base onto the axes of the moving coordinate system can be written in the form:

$$
\left.
\begin{aligned}
\omega_{x0} &= \dot{\vartheta}\cos\gamma - \dot{\psi}\cos\vartheta\sin\gamma; \\
\omega_{y0} &= \dot{\gamma} + \dot{\psi}\sin\vartheta; \\
\omega_{z0} &= \dot{\vartheta}\sin\gamma + \dot{\psi}\cos\vartheta\cos\gamma.
\end{aligned}
\right\}
\qquad (1.13)
$$

Angular velocities ω_{x0}, ω_{y0}, ω_{z0} can be measured by gyroscopes that are oriented along the axes of the moving coordinate system and that are attached to the base.
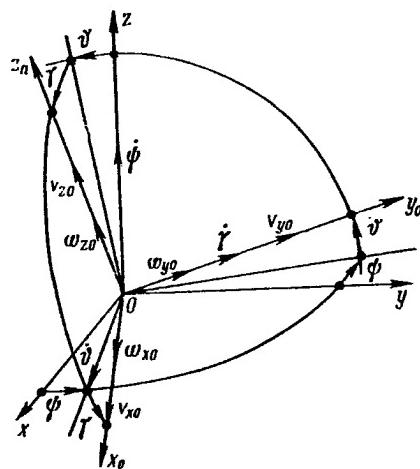
Figure 1.5. Coordinate System of Moving Base

13
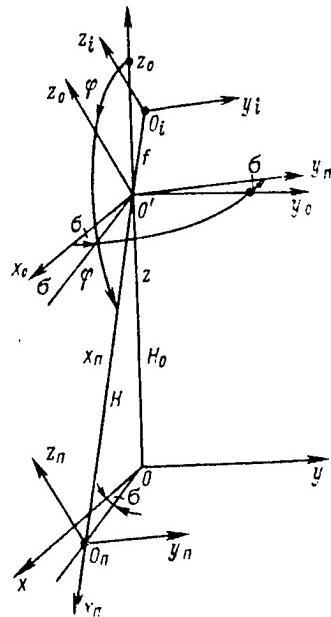
Figure 1.6. Coordinate System of Subject
Field and of Image Field of AFA

The orientation of the optical device on board is determined by the
method of photography and can be given by two angles of perspective:
laterally σ and downard φ (Figure 1.6).

Coordinate system $O'x_{II}y_{II}z_{II}$, bound to the optical device, is rotated
with respect to the base by these angles. Let us select this
coordinate system such that axis $O'x_{II}$ coincides with the principal
optical axis of the device and so that axes $O'y_{II}$ and $O'z_{II}$ be oriented
along and perpendicular to the frame. The vector of the linear velocity
of the center of gravity of the base can be represented in the form of
its projection onto the axes of the base v_{x0}, v_{y0}, v_{z0} (see Figure 1.5).

Let us consider the equations of motion of the system at initial moment
of time when the axes of the base coincide with the axes of the fixed
coordinate system, i.e., $\psi = \vartheta = \gamma = 0$. Let us place two additional
coordinate systems, parallel to those transferred from point O to image
field $O_i x_i y_i z_i$ (Figure 1.6) and to the object field $O_{II}x_{II}y_{II}z_{II}$. One can
then, with regard to the distance between the origins of the coordinate
systems, write the coupling equations of the coordinates in two systems:

14

$$x_{\text{II}} = H + z_{\text{II}}\,\text{ctg}\,\varphi;$$
$$y_{\text{II}} = -\frac{1}{f}\,x_{\text{II}}y_i;$$
$$z_{\text{II}} = -\frac{1}{f}\,x_{\text{II}}z_i,$$
(1.14)

where $H = O'O_{\text{II}}$; $f = O'O_i$.

Having differentiated in time the last two equations and having made the transformations with respect to variables $\dot{y}_i$ and $\dot{z}_i$, we find:

$$\dot{y}_i = -\frac{f}{x_{\text{II}}}\,\dot{y}_{\text{II}} + f\frac{y_{\text{II}}}{(x_{\text{II}})^2}\,\dot{x}_{\text{II}};$$
$$\dot{z}_i = -\frac{f}{x_{\text{II}}}\,\dot{z}_{\text{II}} + f\frac{z_{\text{II}}}{(x_{\text{II}})^2}\,\dot{x}_{\text{II}}.$$
(1.15)

Making the transformation in equations (1.15), one can find:

$$x_{\text{II}} = \frac{H}{1 + \dfrac{1}{f}\,z_i\,\text{ctg}\,\varphi};$$
$$y_{\text{II}} = -\frac{Hy_i}{f\left(1 + \dfrac{1}{f}\,z_i\,\text{ctg}\,\varphi\right)};$$
$$z_{\text{II}} = -\frac{Hz_i}{f\left(1 + \dfrac{1}{f}\,z_i\,\text{ctg}\,\varphi\right)}.$$
(1.16)

Having substituted relations (1.16) into equation (1.15), we find:

$$\dot{y}_i = -\left(1 + \frac{1}{f}\,z_i\,\text{ctg}\,\varphi\right)\left(\frac{f}{H}\,\dot{y}_{\text{II}} + \frac{1}{H}\,y_i\dot{x}_{\text{II}}\right);$$
$$\dot{z}_i = -\left(1 + \frac{1}{f}\,z_i\,\text{ctg}\,\varphi\right)\left(\frac{f}{H}\,\dot{z}_{\text{II}} + \frac{1}{H}\,z_i\dot{x}_{\text{II}}\right).$$
(1.17)

Projections of the angular and linear velocities of the base onto the axes of the device $O'x_{\text{II}}y_{\text{II}}z_{\text{II}}$ can be found from the equations:

$$[\omega_{x\text{II}}\omega_{y\text{II}}\omega_{z\text{II}}]^T = M\,[\omega_{xo}\omega_{yo}\omega_{zo}]^T;$$
$$[v_{x\text{II}}v_{y\text{II}}v_{z\text{II}}]^T = M\,[v_{xo}v_{yo}v_{zo}]^T,$$
(1.18)

where T is the sign of transposition of the matrix, M is the matrix of the direction cosines; it is determined in the form

$$M = \begin{bmatrix} \cos\varphi\cos\sigma & \cos\varphi\sin\sigma & -\sin\varphi \\ -\sin\sigma & \cos\sigma & 0 \\ \sin\varphi\cos\sigma & \sin\varphi\sin\sigma & \cos\varphi \end{bmatrix}.$$

The motion of the base with respect to the object field is equivalent to the oncoming displacement of the object field; therefore, one can write:

$$\left.\begin{aligned} \dot{x}_{II} &= -v_{xII} - z_{II}\omega_{yII} + y_{II}\omega_{zII}; \\ \dot{y}_{II} &= -v_{yII} - x_{II}\omega_{zII} + z_{II}\omega_{xII}; \\ \dot{z}_{II} &= -v_{zII} - y_{II}\omega_{xII} + x_{II}\omega_{yII}. \end{aligned}\right\} \tag{1.19}$$

Having substituted relations (1.16) into equations (1.19), we find:

$$\left.\begin{aligned} \dot{x}_{II} &= -v_{xII} - \frac{H}{1 + \frac{z_i}{f}\operatorname{ctg}\varphi}\left(\frac{y_i}{f}\omega_{zII} - \frac{z_i}{f}\omega_{yII}\right); \\ \dot{y}_{II} &= -v_{yII} - \frac{H}{1 + \frac{z_i}{f}\operatorname{ctg}\varphi}\left(\frac{z_i}{f}\omega_{xII} - \omega_{zII}\right); \\ \dot{z}_{II} &= -v_{zII} - \frac{H}{1 + \frac{z_i}{f}\operatorname{ctg}\varphi}\cdot\left(\omega_{yII} - \frac{y_i}{f}\omega_{xII}\right). \end{aligned}\right\} \tag{1.20}$$

After substitution of relations (1.20) into equations (1.17), one can write

$$\left.\begin{aligned} \dot{y}_i &= A_4 y_i^2 + A_3 y_i + A_2 y_i z_i + A_1 z_i + A_0; \\ \dot{z}_i &= B_4 z_i^2 + B_3 z_i + B_2 y_i z_i + B_1 y_i + B_0, \end{aligned}\right\} \tag{1.21}$$

where

$$A_4 = \frac{\omega_{zII}}{f}; \quad A_3 = \frac{v_{xII}}{H};$$

$$A_2 = \frac{1}{f}\left(\frac{v_{xII}}{H}\operatorname{ctg}\varphi - \omega_{yII}\right);$$

$$A_1 = \omega_{xII} + \frac{v_{yII}}{H}\operatorname{ctg}\varphi;$$

$$A_0 = f\frac{v_{yII}}{H} - f\omega_{zII};$$

16

$$B_4 = \frac{v_{x\text{II}}}{fH} \operatorname{ctg} \varphi - \frac{\omega_{y\text{II}}}{f};$$

$$B_3 = \frac{v_{x\text{II}}}{H} + \frac{v_{z\text{II}}}{H} \operatorname{ctg} \varphi;$$

$$B_2 = \frac{\omega_{z\text{II}}}{f}; \quad B_1 = -\omega_{x\text{II}};$$

$$B_0 = f \left(\omega_{y\text{II}} + \frac{v_{z\text{II}}}{H} \right).$$

Having denoted the flight altitude by H_0, we find

$$H = H_0/\sin \varphi. \qquad (1.22)$$

Having substituted relation (1.22) into expressions (1.21), we find the following values of the coefficients of the equations:

$$
\left.
\begin{aligned}
A_0 &= f \left(\frac{v_{y\text{II}}}{H_0} \sin \varphi - \omega_{z\text{II}} \right); \\[4pt]
A_1 &= \omega_{x\text{II}} + \frac{v_{y\text{II}}}{H_0} \cos \varphi; \\[4pt]
A_2 &= \frac{1}{f} \left(\frac{v_{x\text{II}}}{H_0} \cos \varphi - \omega_{y\text{II}} \right); \\[4pt]
A_3 &= \frac{v_{x\text{II}}}{H_0} \sin \varphi; \quad A_4 = \frac{\omega_{z\text{II}}}{f}; \\[4pt]
B_0 &= f \left(\frac{v_{z\text{II}}}{H_0} \sin \varphi + \omega_{y\text{II}} \right); \\[4pt]
B_1 &= -\omega_{x\text{II}}; \quad B_2 = \frac{\omega_{z\text{II}}}{f}; \\[4pt]
B_3 &= \frac{1}{H_0} (v_{x\text{II}} \sin \varphi + v_{z\text{II}} \cos \varphi); \\[4pt]
B_4 &= \frac{1}{f} \left(\frac{v_{x\text{II}}}{H_0} \cos \varphi - \omega_{y\text{II}} \right).
\end{aligned}
\right\} \qquad (1.23)
$$

Thus, the rate of shift of the image is determined by equations (1.21) and is dependent on the position of the element of the image to be considered with respect to the center of the frame and also on the angular and linear rates of displacement of the base, on which the device is mounted.

Besides the indicated factors, the shift of the image is also determined by the mutual displacements of the optical components of the device (objective, mirrors and so on) and these displacements can be both those

to be checked and random in nature. A series of these displacements can be used to stabilize the image.

Analysis of equations of image misalignmentfor case of frame and slot aerial photography. The type of matrix of direction cosines M is determined in equations (1.18) by the orientation of the optical device with respect to the moving base. All the components of the optical system of the AFA are fixed with respect to each other during frame aerial photography, while the principal optical axis of the AFA is fixed with respect to the base and is rotated by perspective angles $0 \leq \sigma \leq 90°$ and $0 \leq \varphi \leq 90°$ with respect to the base.

The equations for the rates of misalignment of the image can generally be found by substitution of equations (1.18) into equations (1.21). Let us consider a number of widely used versions of orientation of the AFA. Let us assume that photography is from a base, moving horizontally to velocity v_{y0}, i.e., let us assume that $v_{x0} = v_{z0} = 0$.

Vertical frame photography (frame along axis Oy_i). In this case, the perspective angles correspond to equalities $\sigma = 0$, $\varphi = 90°$. For the matrix of direction cosines from equations (1.18), we find:

$$M = \begin{bmatrix} 0 & 0 & -1 \\ 0 & 1 & 0 \\ 1 & 0 & 0 \end{bmatrix}. \tag{1.24}$$

Let us find the projections of the angular and linear velocities of the base onto the axes of the optical device and let us substitute them into shift equations (1.21). We find the following functions:

$$\left. \begin{aligned} \dot{y}_i &= y_i^2 \frac{\omega_{x0}}{f} - z_i \omega_{z0} + \frac{f}{H_0} v_{y0} - f \omega_{x0}; \\ \dot{z}_i &= -z_i^2 \frac{\omega_{y0}}{f} + y_i z_i \frac{\omega_{x0}}{f} y_i \omega_{x0} + f \omega_{y0}. \end{aligned} \right\} \tag{1.25}$$

For vertical frame photography with the frame arranged along axis Oz_i ($\sigma = 90°$, $\varphi = 90°$), by analogy, one can write:

$$\left. \begin{aligned} \dot{y}_i &= y_i^2 \frac{\omega_{y0}}{f} + \frac{\omega_{x0}}{f} y_i z_i - \omega_{z0} z_i - f \omega_{y0}; \\ \dot{z}_i &= z_i^2 \frac{\omega_{x0}}{f} + \frac{\omega_{y0}}{f} y_i z_i + \omega_{z0} y_i - f \omega_{x0} + f \frac{v_{y0}}{H_0}. \end{aligned} \right\} \tag{1.26}$$

Perspective frame photography laterally ($\sigma = 0$, $0 \leq \varphi \leq 90°$). For the matrix of direction cosines, instead of equations (1.18), we find:

$$M = \begin{bmatrix} \cos\varphi & 0 & -\sin\varphi \\ 0 & 1 & 0 \\ \sin\varphi & 0 & \cos\varphi \end{bmatrix}. \qquad (1.27)$$

The equations of the image misalignment can be written in the form:

$$
\left.
\begin{aligned}
\dot{y}_i &= \frac{y_i^2}{f}\left(\omega_{xo}\sin\varphi + \omega_{zo}\cos\varphi\right) - y_i z_i \frac{\omega_{yo}}{f} + \\
&\quad + z_i\left(\omega_{xo}\cos\varphi - \omega_{zo}\sin\varphi\right) + z_i \frac{v_{yo}}{H_0}\cos\varphi + \\
&\quad + f\frac{v_{yo}}{H_0}\sin\varphi - f\left(\omega_{xo}\sin\varphi + \omega_{zo}\cos\varphi\right); \\
\dot{z}_i &= -\frac{\omega_{yo}}{f}z_i^2 + \frac{y_i z_i}{f}\left(\omega_{xo}\sin\varphi + \omega_{zo}\cos\varphi\right) - \\
&\quad - y_i\left(\omega_{xo}\cos\varphi - \omega_{zo}\sin\varphi\right) + f\omega_{yo}.
\end{aligned}
\right\} \qquad (1.28)
$$

Perspective frame photography forward ($\sigma = 90°$, $0 \le \varphi \le 90°$). We find for the matrix of direction cosines:

$$M = \begin{bmatrix} 0 & \cos\varphi & -\sin\varphi \\ -1 & 0 & 0 \\ 0 & \sin\varphi & \cos\varphi \end{bmatrix}. \qquad (1.29)$$

The misalignment equations are written in the form:

$$
\begin{aligned}
\dot{y}_i &= \frac{y_i^2}{f}\left(\omega_{yo}\sin\varphi + \omega_{zo}\cos\varphi\right) + \\
&\quad + \frac{y_i}{2}\frac{v_{yo}}{H_0}\sin 2\varphi + \frac{y_i z_i}{f}\left(\frac{v_{yo}}{H_0}\cos^2\varphi + \omega_{xo}\right) + \\
&\quad + z_i\left(\omega_{yo}\cos\varphi - \omega_{zo}\sin\varphi\right) - \left(f\omega_{yo}\sin\varphi + f\omega_{zo}\cos\varphi\right);
\end{aligned}
\qquad (1.30)
$$

$$
\begin{aligned}
\dot{z}_i &= \frac{z_i^2}{f}\left(\frac{v_{yo}}{H_0}\cos^2\varphi + \omega_{xo}\right) + z_i\frac{v_{yo}}{H_0}\sin 2\varphi + \\
&\quad + \frac{z_i y_i}{f}\left(\omega_{yo}\sin\varphi + \omega_{zo}\cos\varphi\right) + y_i\left(\omega_{zo}\sin\varphi - \omega_{yo}\cos\varphi\right) + \\
&\quad + f\left(\frac{v_{yo}}{H_0}\sin^2\varphi - \omega_{xo}\right).
\end{aligned}
\qquad (1.31)
$$

Characteristic features of image shift equations during slit photography. The above expressions for vertical photography are also valid for slit photography. The film is exposed through a narrow slit, located along axis Oz_i, near the focal plane of the objective. If the width of the slit is small compared to the width of the frame, one can assume that $y_i = 0$ in the expressions found for vertical photography.

We then find for vertical photography ($\sigma = 0$, $\varphi = 90°$):

$$\begin{aligned}
\dot{y}_i &= -z_i \omega_{z0} + \frac{f}{H_0} v_{y0} - f \omega_{x0}; \\
\dot{z}_i &= -z_i^2 \frac{\omega_{y0}}{f} + f \omega_{y0}.
\end{aligned} \right\} \qquad (1.32)$$

In the case of different orientation of the AFA ($\sigma = 90°$, $\varphi = 90°$), we have:

$$\begin{aligned}
\dot{y}_i &= -\omega_{z0} z_i - f \omega_{y0}; \\
\dot{z}_i &= z_i^2 \frac{\omega_{x0}}{f} + f \frac{v_{y0}}{H_0} - f \omega_{x0}.
\end{aligned} \right\} \qquad (1.33)$$

Other types of orientation during slit photography are rarely used in practice.

Analysis of equations of image shift for panoramic aerial photography. Let us consider the general case of vertical panoramic aerial photography. Let the panning be carried out by rotating the principal axis of the optical device about axis Oz_{III} (Figure 1.7), rotated by angle β with respect to the axes of the device about axis Oy_{II}. Let us denote the panning angle by α. Transition from the coordinate system of the base to a coordinate system, bound to the instrument, $Ox_{II}y_{II}z_{II}$ is achieved by sequential rotations by angles σ, $\varphi + \beta$, α, and $(-\beta)$.

Thus, we find for the matrix of direction cosines:

$$\mathbf{M} = \begin{bmatrix} \cos\beta & 0 & \sin\beta \\ 0 & 1 & 0 \\ -\sin\beta & 0 & \cos\beta \end{bmatrix} \begin{bmatrix} \cos\alpha & \sin\alpha & 0 \\ -\sin\alpha & \cos\alpha & 0 \\ 0 & 0 & 1 \end{bmatrix} \times \qquad (1.34)$$

$$\times \begin{bmatrix} \cos(\varphi+\beta) & 0 & -\sin(\varphi+\beta) \\ 0 & 1 & 0 \\ \sin(\varphi+\beta) & 0 & \cos(\varphi+\beta) \end{bmatrix} \begin{bmatrix} \cos\sigma & \sin\sigma & 0 \\ -\sin\sigma & \cos\sigma & 0 \\ 0 & 0 & 1 \end{bmatrix}$$

20

We generally find for matrix M:

$$M = \begin{bmatrix} m_{11} & m_{12} & m_{13} \\ m_{21} & m_{22} & m_{23} \\ m_{31} & m_{32} & m_{33} \end{bmatrix},$$

where

$m_{11} = \cos\alpha \cos\beta \cos\sigma \cos(\varphi + \beta) - \cos\beta \sin\alpha \sin\sigma + {} + \sin\beta \cos\sigma \sin(\varphi + \beta)$; $m_{12} = \cos\alpha \cos\beta \sin\sigma \cos(\varphi + \beta) + {} + \sin\alpha \cos\beta \cos\sigma + \sin\beta \sin\sigma \sin(\varphi + \beta)$; $m_{13} = \sin\beta \cos \times {} \times (\varphi + \beta) - \cos\alpha \cos\beta \sin(\varphi + \beta)$; $m_{21} = -\sin\alpha \cos\sigma \cos(\varphi + {} + \beta) - \sin\sigma \cos\alpha$; $m_{22} = -\sin\alpha \sin\sigma \cos(\varphi + \beta) + \cos\alpha \cos\sigma$; $m_{23} = \sin\alpha \sin(\varphi + \beta)$; $m_{31} = -\sin\beta \cos\alpha \cos\sigma \cos(\varphi + \beta) + {} + \sin\alpha \sin\beta \sin\sigma + \cos\beta \cos\sigma \sin(\varphi + \beta)$; $m_{32} = -\sin\beta \times {} \times \cos\alpha \sin\sigma \cos(\varphi + \beta) - \sin\alpha \sin\beta \cos\sigma + \cos\beta \sin\sigma \sin(\varphi + \beta)$; $m_{33} = \sin\beta \cos\alpha \sin(\varphi + \beta) + \cos\beta \cos(\varphi + \beta)$.

In the special case, when the panning axis coincides with axis $Oz_\text{П}$ ($\beta = 0$), we find

$$M = \begin{bmatrix} \cos\alpha \cos\sigma \cos\varphi - & \cos\alpha \sin\sigma \cos\varphi + & -\cos\alpha \sin\varphi \\ -\sin\alpha \sin\sigma & +\sin\alpha \cos\sigma & \\ -\sin\alpha \cos\sigma \cos\varphi - & -\sin\alpha \sin\sigma \cos\varphi + & \sin\alpha \sin\varphi \\ -\sin\sigma \cos\alpha & +\cos\alpha \cos\sigma & \\ \cos\sigma \sin\varphi & \sin\sigma \sin\varphi & \cos\varphi \end{bmatrix}. \qquad (1.36)$$

The film is exposed during panoramic photography through a slit, while the film itself can be displaced with respect to the axes of the device.

Moreover, the angular rate of panning $\dot{\alpha}$, the vector of which is directed along axis $Oz_\text{П}$, will be projected onto the axes of the device $Ox_\text{П}y_\text{П}z_\text{П}$; therefore, instead of equations (1.18), we find

$$\left. \begin{aligned} \overset{*}{\omega}_{x\text{П}} &= \omega_{x\text{П}} + \dot{\alpha}\sin\beta; \\ \overset{*}{\omega}_{y\text{П}} &= \omega_{y\text{П}}; \\ \overset{*}{\omega}_{z\text{П}} &= \omega_{z\text{П}} + \dot{\alpha}\cos\beta. \end{aligned} \right\} \qquad (1.37)$$

21
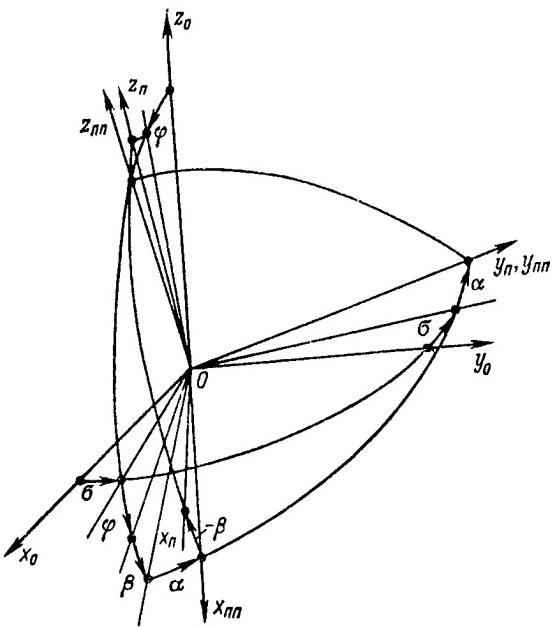
Figure 1.7. Coordinate System of Panoramic Aerial Camera

Moreover, for panoramic photography, instead of expression (1.22), it is easy to find the relation

$$H = H_0 \sqrt{1 + \text{tg}^2 \alpha \cos^2 \beta} / \sin \varphi,$$

or at $\beta = 0$

$$H = H_0/(\sin \varphi \cos \alpha). \tag{1.38}$$

Having substituted this expression into equations (1.21), we find the following values of the coefficients instead of (1.23):

$$
\left.
\begin{aligned}
A_0 &= f \frac{v_{y\Pi}}{H_0} \sin \varphi \cos \alpha - f\omega_{z\Pi}; \\
A_1 &= \omega_{x\Pi} + \frac{v_{y\Pi}}{H_0} \cos \varphi \cos \alpha; \\
A_2 &= f \frac{v_{x\Pi}}{H_0} \cos \varphi \cos \alpha - \frac{\omega_{y\Pi}}{f}; \\
A_3 &= \frac{v_{x\Pi}}{H_0} \sin \varphi \cos \alpha; \quad A_4 = \frac{\omega_{z\Pi}}{f};
\end{aligned}
\right\} \tag{1.39}
$$

$$B_0 = f\omega_{yII} + f\frac{v_{zII}}{H_0}\sin\varphi\cos\alpha;$$

$$B_1 = -\omega_{xII}; \quad B_2 = \frac{\omega_{zII}}{f};$$

$$B_3 = \frac{v_{xII}}{H_0}\sin\varphi\cos\alpha + \frac{v_{zII}}{H_0}\cos\varphi\cos\alpha;$$

$$B_4 = \frac{v_{xII}}{fH_0}\cos\varphi\cos\alpha - \frac{\omega_{yII}}{f}.$$

Let us consider the different versions of orientation of the device with respect to the base.

Vertical panoramic photography ($\sigma = 90°$, $\varphi = 90°$). For matrix M, we have

$$M = \begin{bmatrix} -\sin\alpha\cos\beta & \frac{1}{2}\sin 2\beta\,(1-\cos\alpha) & -(\sin^2\beta + \cos\alpha\cos^2\beta) \\ -\cos\alpha & \sin\alpha\sin\beta & \sin\alpha\cos\beta \\ \sin\alpha\sin\beta & \cos^2\beta + \cos\alpha\sin^2\beta & -\frac{1}{2}\sin 2\beta\,(1-\cos\alpha) \end{bmatrix}. \quad (1.40)$$

At $\beta = 0$, instead of matrix (1.40), we find

$$M = \begin{bmatrix} -\sin\alpha & 0 & -\cos\alpha \\ -\cos\alpha & 0 & \sin\alpha \\ 0 & 1 & 0 \end{bmatrix}. \quad (1.41)$$

Let us assume as before that $v_{x0} = v_{z0} = 0$.

Taking into account that one can assume that $y_i \approx 0$ during panoramic photography (the same as during slit photography, we find for the image misalignment equations:

$$\dot{y}_i = -z_i\,(\omega_{x0}\sin\alpha + \omega_{z0}\cos\alpha) - f\,(\omega_{y0} + \dot{\alpha});$$

$$\dot{z}_i = \frac{z_i^2}{f}\,(\omega_{x0}\cos\alpha - \omega_{z0}\sin\alpha) +$$

$$+ \frac{f}{H_0}\,v_{y0}\cos\alpha - f\omega_{x0}\cos\alpha + f\omega_{z0}\sin\alpha. \qquad (1.42)$$

23

Forward panoramic perspective photography ($\sigma = 90°$, $0 < \varphi < 90°$). In this case ($\beta = 0$), the matrix of direction cosines has the form

$$
M = \begin{bmatrix} -\sin\alpha & \cos\alpha\cos\varphi & -\cos\alpha\sin\varphi \\ -\cos\alpha & -\sin\alpha\cos\varphi & \sin\alpha\sin\varphi \\ 0 & \sin\varphi & \cos\varphi \end{bmatrix}. \tag{1.43}
$$

The misalignment equations are written in the form:

$$
\dot{y}_i = z_i\left(-\omega_{xo}\sin\alpha + \omega_{yo}\cos\alpha\cos\varphi - \omega_{zo}\cos\alpha\sin\varphi - \right.
$$
$$
- z_i\frac{1}{2}\frac{v_{yo}}{H_0}\cos^2\varphi\sin2\alpha - \frac{f}{4}\frac{v_{yo}}{H_0}\sin2\alpha\sin2\varphi - f\omega_{yo}\sin\varphi - \tag{1.44}
$$
$$
- f\omega_{zo}\cos\varphi - f\dot{\alpha};
$$

$$
\dot{z}_i = z_i^2\frac{1}{f}\frac{v_{yo}}{H_0}\cos^2\varphi\cos^2\alpha +
$$
$$
+ \frac{z_i^2}{f}(\omega_{xo}\cos\alpha + \omega_{yo}\sin\alpha\cos\varphi - \omega_{zo}\sin\alpha\sin\varphi) +
$$
$$
+ z_i\frac{v_{yo}}{H_0}\cos\varphi\cos\alpha(\sin\alpha + \sin\varphi\cos\alpha) + \tag{1.45}
$$
$$
+ \frac{f}{2H_0}v_{yo}\sin2\alpha\sin\varphi + f(-\omega_{xo}\cos\alpha -
$$
$$
- \omega_{yo}\sin\alpha\cos\varphi + \omega_{zo}\sin\alpha\sin\varphi).
$$

Panoramic perspective photography with leveled horizontal line ($\sigma = 90°$, $\varphi + \beta = 0$). The matrix of direction cosines is generally written in the form

$$
M = \begin{bmatrix} -\sin\alpha\cos\alpha & \cos\alpha\cos\beta & \sin\beta \\ -\cos\alpha & -\sin\alpha & 0 \\ \sin\alpha\sin\beta & -\sin\beta\cos\alpha & \cos\beta \end{bmatrix}. \tag{1.46}
$$

In the special case (at $\beta = 0$), the image misalignment equations will assume the following form:

$$\dot{y}_i = z_i \left(\omega_{yo} \cos \alpha - \omega_{xo} \sin \alpha \right) -$$

$$- f \left(\frac{v_{yo}}{H_0} \sin \alpha \cos \alpha + \omega_{zo} + \dot{\alpha} \right);$$

$$\dot{z}_i = \frac{z_i^2}{f} \left(\omega_{xo} \cos \alpha + \omega_{yo} \sin \alpha \right) +$$

$$+ z_i \frac{v_{yo}}{H_0} \cos^2 \alpha - f \left(\omega_{xo} \cos \alpha + \omega_{yo} \sin \alpha \right).$$

(1.47)

Panoramic perspective photography with leveled verticals ($\sigma = 90°$, $\varphi + \beta = 90°$). For matrix M, we find in this case

$$\mathbf{M} = \begin{bmatrix} -\sin \alpha \cos \beta & \sin \beta & -\cos \alpha \cos \beta \\ -\cos \alpha & 0 & \sin \alpha \\ \sin \alpha \sin \beta & \cos \beta & \cos \alpha \sin \beta \end{bmatrix}.$$

(1.48)

In the special case, $\beta = 0$

$$\mathbf{M} = \begin{bmatrix} -\sin \alpha & 0 & -\cos \alpha \\ -\cos \alpha & 0 & \sin \alpha \\ 0 & 1 & 0 \end{bmatrix}.$$

(1.49)

Vertical panoramic photography along flight line ($\sigma = 0$, $\varphi = 90°$). For matrix M, we find

$$\mathbf{M} = \begin{bmatrix} \frac{1}{2} \sin 2\beta \, (1 - \cos \alpha) & \sin \alpha \cos \beta & -(\sin^2 \beta + \cos \alpha \cos^2 \beta) \\ (\sin \alpha \sin \beta - \cos \alpha) & \cos \alpha & \sin \alpha \cos \beta \\ (\sin^2 \beta \cos \alpha + \cos^2 \alpha) & -\sin \alpha \sin \beta & -\frac{1}{2} \sin 2\beta \, (1 - \cos \alpha) \end{bmatrix}.$$

(1.50)

In the special case at $\beta = 0$

$$\mathbf{M} = \begin{bmatrix} 0 & \sin \alpha & -\cos \alpha \\ -\cos \alpha & \cos \alpha & \sin \alpha \\ \cos^2 \alpha & 0 & 0 \end{bmatrix}.$$

(1.51)

We find for the misalignment equations:

25

$$\dot{y}_i = z_i(\omega_{yo}\sin\alpha - \omega_{zo}\cos\alpha) + f\frac{v_{yo}}{H_0}\cos^2\alpha - f\omega_{xo}\cos^2\alpha - f\dot{\alpha};$$

$$\dot{z}_i = \frac{z_i^2}{f}(\omega_{xo}\cos\alpha - \omega_{yo}\cos\alpha - \omega_{zo}\sin\alpha) +$$

$$+ \frac{z_i}{2}\frac{v_{yo}}{H_0}\sin 2\alpha - f(\omega_{xo}\cos\alpha - \omega_{yo}\cos\alpha - \omega_{zo}\sin\alpha). \qquad (1.52)$$

Table 1.1

(1) Вид съемки	σ	ϕ	$\dot{y}_i$	$\dot{z}_i$
(2) Кадровая плановая	0	90°	$f v_{yo}/H_0$	0
	90°	90°	0	$f v_{yo}/H_0$
(3) Кадровая перспективная вбок	0	$0 < \phi < 90°$	$f\frac{v_{yo}}{H_0}\left(\sin\phi + \frac{z_i}{f}\cos\phi\right)$	0
(4) Кадровая перспективная вперед	90°	$0 < \phi < 90°$	$y_i \frac{v_{yo}}{H_0}\cos\phi \times \left(\sin\phi + \frac{z_i}{f}\cos\phi\right)$	$f\frac{v_{yo}}{H_0}\left(\frac{z_i}{f}\cos\phi + \sin\phi\right)^2$
Панорамная плановая (5)	90°	90°	0	$f\frac{v_{yo}}{H_0}\cos\alpha$
Панорамная перспективная вперед (6)	90°	$0 < \phi < 90°$	$-\frac{f}{2}\frac{v_{yo}}{H_0}\sin 2\phi \times \cos\phi\left(\sin\phi + \frac{z_i}{f}\cos\phi\right)$	$f\frac{v_{yo}}{H_0}\frac{z_i^2}{f^2}\cos^2\phi \times \cos^2\alpha + \frac{z_i}{f}\cos\phi \times \cos\alpha(\sin\alpha + \cos\alpha\sin\phi) + \frac{1}{2}\sin 2\alpha\sin\phi$
(7) Панорамная с выровненной линией горизонта	90°	0	$-\frac{f}{2}\frac{v_{yo}}{H_0}\sin 2\alpha$	$z_i\frac{v_{yo}}{H_0}\cos^2\alpha$
(8) Панорамная вдоль линии полета	0	90°	$f\frac{v_{yo}}{H_0}\cos^2\alpha$	$\frac{z_i}{2}\frac{v_{yo}}{H_0}\sin 2\alpha$

KEY:

1. Type of photography
2. Vertical frame
3. Lateral perspective frame
4. Forward perspective frame
5. Vertical panoramic
6. Forward perspective panoramic
7. Panoramic with leveled horizontal line
8. Panoramic along flight line

The formulas for determination of the image misalignment, caused by the flight speed of the base, are presented in Table 1.1 for different types of photography.

1.3. Methods of Active Response to Image Misalignment for Stabilization of It During Optical Observations

Let us arbitrarily present an optical system in the form of separate components, located at specific distance d_i with respect to each other along optical axis Ox. By considering the path of a paraxial beam in the system, one can state that the parameters of the beam A_i undergo variations only upon passage through the principal planes of the optical components (Figure 1.8). The nature of variation of the beam parameters upon passage of the beam through each optical element can be described by optical arrays [28]. The beam parameters A_i before passage through the i-th element and the beam parameters A_{i+1} after passage are linked by the equation:

$$\mathbf{A}_{i+1} = \mu_i \mathbf{A}_i. \tag{1.53}$$

Here μ_i is the transformation matrix of the beam by the i-th element;

$$\mathbf{A}_i = [z_i y_i \alpha_i \beta_i]^{\mathrm{T}}; \quad \mathbf{A}_{i+1} = [z_{i+1} y_{i+1} \alpha_{i+1} \beta_{i+1}]^{\mathrm{T}},$$

where z_i, y_i, α_i, and β_i are the beam parameters A_i.
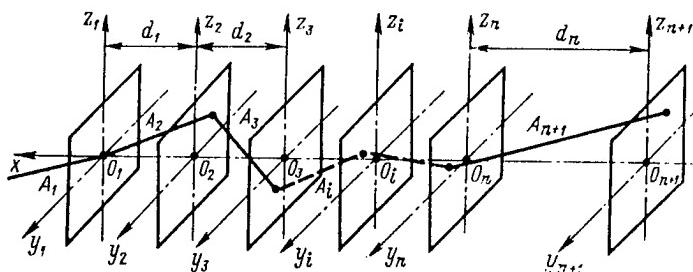
Figure 1.8. Layout of Optical System of Device

Let the image be checked in plane $O_{n+1} y_{n+1} z_{n+1}$.

The beam parameters in the image plane are then determined from the expression

$$\mathbf{A}_{n+1} = \left(\prod_{i=1}^{n} \mu_i \right) \mathbf{A}_1. \tag{1.54}$$

27

Not only the matrices of the optical elements, but also the transformation matrices in the space between the elements are taken into account in the product of the matrices.

When using radial matrices [28], the beam parameters in the i-th plane, perpendicular to the optical axis of the system, are characterized by coordinates y_i, z_i of the point of intersection of the plane by the beam and by angles β_i and α_i of the inclination of projection of the beam in the meridional and sagittal planes, respectively. Rotation of coordinate axes Oxyz of the base, on which the optical system is located, can be described with respect to the coordinate system, bound to the observation object $O\kappa\eta\zeta$, by the matrix of direction cosines.

If, for example, the order of rotation of the coordinate system of the base is assumed as follows: yaw angle θ, pitch angle ψ, and bank angle φ, one can write at small angles

$$
\begin{bmatrix} x \\ y \\ z \end{bmatrix} = \begin{bmatrix} 1 & -\theta & \psi \\ \theta & 1 & -\varphi \\ -\psi & \varphi & 1 \end{bmatrix} \begin{bmatrix} \kappa \\ \eta \\ \xi \end{bmatrix}. \tag{1.55}
$$

The linear displacements of the input beam can be reduced to the corresponding angular misalignments; therefore, one can assume that the input beam intersects plane $O_1 z_1 y_1$ at the origin, i.e., $A_1 = |0 \ 0 \ \beta_i \ \alpha_i|$.

Using equation (1.55), we find

$$
\begin{aligned}
\beta_2 &= \frac{\theta + \beta_1 - \varphi\alpha_1}{1 - \theta\beta_1 + \psi\alpha_1}; \\
\alpha_2 &= \frac{\alpha_1 - \psi + \varphi\beta_1}{1 - \theta\beta_1 + \psi\alpha_1}.
\end{aligned}
$$

At small angles α_1 and β_1, we have

$$
A_1 + dA_1 \approx [0 \ 0 \ (\beta_1 + \theta) \ (\alpha_1 - \psi)]^T,
$$

where $dA_1 = |0 \ 0 \ \theta \ -\psi|^T$.

Thus, variation of the position of the optical system in space can be represented as equivalent variation of the coordinates of the input beam.

The matrix of transformation of the beam coordinates by the space between the i-th and the (i + 1)-th optical elements can be written in the form

$$\mu_i = \begin{bmatrix} 1 & 0 & \lambda_{i\,(i+1)} & 0 \\ 0 & 1 & 0 & -d_{i\,(i+1)} \\ 0 & 0 & 1 & 0 \\ 0 & 0 & 0 & 1 \end{bmatrix}.$$

If matrix μ_i varies by the value $d\mu_i$, the variation of the beam coordinate in the plane of the next element can be written in the form

$$\mathbf{A}_{i+1} + d\mathbf{A}_{i+1} = [\mu_i + d\mu_i]\,\mathbf{A}_i.$$

Hence,

$$dA_{i+1} = [d\mu_i]\,\mathbf{A}_i. \tag{1.56}$$

If all n transformation matrices vary simultaneously, then we find for the beam coordinates at the output of the n-th element

$$\mathbf{A}_{n+1} + d\mathbf{A}_{n+1} = [\mu_n + d\mu_n][\mu_{n+1} + d\mu_{n-1}]\ldots[\mu_1 + d\mu_1](\mathbf{A}_1 + d\mathbf{A}_1).$$

Disregarding second-order terms, we have

$$dA_{n+1} = \sum_{j=1}^{n} \left\{ \left(\prod_{i=j+1}^{n} \mu_i \right) (d\mu_j) \left(\prod_{i=1}^{j=1} \mu_i \right) \right\} \mathbf{A}_1 +$$
$$+ \left(\prod_{i=1}^{n} \mu_i \right) d\mathbf{A}_1; \quad i = \overline{1,\,n}; \quad j = \overline{1,\,n}. \tag{1.57}$$

If the beam at the output of the n-th element contains information about the controlled image, its parameters should remain fixed and the problem of stabilization reduces to fulfillment of the condition

$$dA_{n+1} \to 0. \tag{1.58}$$

We find from equations (1.57) and (1.58)

$$\sum_{j=1}^{n} \left\{ \left(\prod_{i=j+1}^{n} \mu_i \right) (d\mu_j) \left(\prod_{i=1}^{j-1} \mu_i \right) \right\} = - \left(\prod_{i=1}^{n} \mu_i \right) d\mathbf{A}_1 \mathbf{A}_1^{-1}. \tag{1.59}$$

29

Let the image be stabilized only due to variation $d\mu_k$ of the k-th matrix. We then have from equation (1.59)

$$d\mu_k = -\left(\prod_{i=1}^{k}\mu_i\right) dA_1 A_1^{-1} \left(\prod_{i=1}^{k-1}\mu_i\right)^{-1}.$$

Hence,

$$d\mu_k = -\left(\prod_{i=1}^{k}\mu_k\right) dA_1 A_1^{-1} \left(\prod_{i=1}^{k-1}\mu_i\right). \tag{1.60}$$

If the parameters of matrix $d\mu_k$ can be varied and if the reaction matrix B that leads to these changes is known, we find at small deviations of the parameters from nominal values instead of equation (1.56):

$$dA_{i+1} = \frac{\partial}{\partial A_{ij}}[d\mu_i] A_i + \frac{\partial}{\partial B_{ij}}[d\mu_i] B_i. \tag{1.61}$$

For most optical elements, assuming that the angles and misalignments are small, one can assume

$$\frac{\partial}{\partial A_{ij}}[d\mu_i] = 0,$$

i.e., one can assume that the parameters of the transformation matrix of the element are independent of the parameters of the input beam. Expression (1.59) then assumes the form

$$\left(\prod_{i=1}^{n}\mu_i\right) dA_i = -\sum_{i=2}^{n}\left(\prod_{i=j}^{n}\mu_i G_i B_i\right), \tag{1.62}$$

where $G = \frac{\partial}{\partial B_{ij}}[d\mu_i]$ is a matrix of the coefficients of the sensitivity of the parameters of matrix μ_i to reactions B_{ij}.

In the special case for variation of the parameters of only the k-th element of the system, instead of equation (1.60), we find

$$B_h = -\left(\prod_{i=k}^{n} \mu_h\right)^{-1} (G_h)^{-1} \left(\prod_{i=1}^{n} \mu_i\right) dA_i. \qquad (1.63)$$

Expressions (1.60) and (1.63) permit one to estimate the sensitivity of the optical system to variation of the parameters of the elements comprising the system, even at the phase of selecting the optical layout of the device and, thus, to select the most efficient version from the viewpoint of the stability of the entire device. On the other hand, these expressions permit one to determine the parameters and order of arrangement in the optical circuit of the controlled elements for achieving the greatest control effect with least expenditures of energy and retention of the stability of resolution of the entire optical device.

It is obvious that a multicircuit and multiconnected stabilization system using two or more control elements in the optical circuit can be employed to stabilize the image under conditions of significant variation of the parameters of the input beam over a wide frequency range. The functions of processing slow misalignments, significant in value, and of processing insignificant misalignments, but rapid in value, are divided among these elements.

Thus, the problem of image stabilization upon variation of matrix A_1 reduces to formulation of matrix B_k according to equation (1.63) and by which the compensation displacements of the k-th element of the optical system are also determined. This problem is solved by using automatic stabilization systems.

1.4. Example of Analysis of Image Shift in Optical System

Let us consider the simplest optical system, consisting of a deflecting mirror (OZ) and photodetector (FP), mounted on a common base. Let us assume that the base has angular displacements with respect to the object of observation. Let us link to the optical device the coordinate system $Ox_0 y_0 z_0$ (Figure 1.9, a), and axis Ox_0 coincides with the incident beam. The angular displacements of the base with respect to this coordinate system can then be described in projections of angular velocities ω_{x0}, ω_{y0}, ω_{z0}.

Let us consider the motion of a central beam that links the center of the original and the center of the image on the photodetector.

31
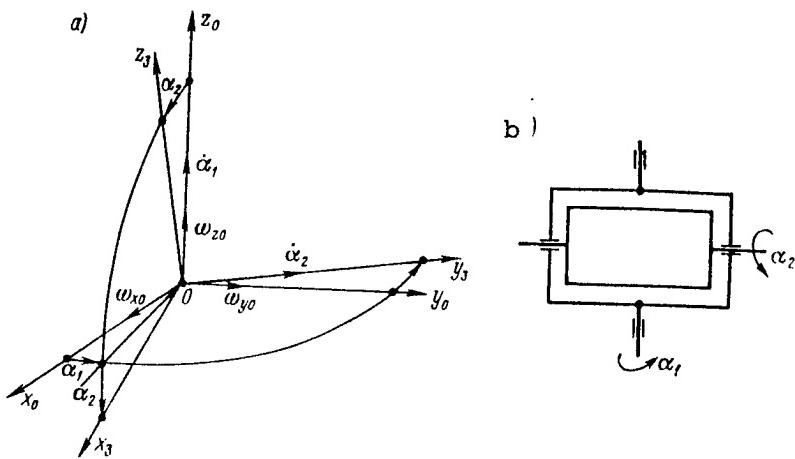
Figure 1.9. Variant of Attachment of Mirror to Outer
Gimbal, Oriented According to Reflected Beam:
a--coordinate system bound to deflecting mirror;
b--gimbal of deflecting mirror

The nature of motion of the central beam along the photodetector will be
determined by a number of factors: by displacement of the base, by
displacement of the photodetector and deflecting beam with respect to
the base, and by the design of the assembly for attachment of the
deflecting mirror to the base. Let us consider a version of attaching
the deflecting mirror in a gimbal suspension (Figure 1.9, b), which
permits one to rotate the deflecting mirror by angle α_1 about axis Oz_0
and by angle α_2 about an axis perpendicular to the deflecting mirror

(axis OY_0). If these rotations occur at angular rates $\dot{\alpha}_1$ and $\dot{\alpha}_2$,
respectively, one can then write for projections of the angular
velocities of the mirror onto axes $Ox_0 y_0 z_0$

$$
\left.
\begin{aligned}
\omega'_{xo} &= \omega_{xo} - \dot{\alpha}_2 \sin \alpha_1; \\
\omega'_{yo} &= \omega_{yo} + \dot{\alpha}_2 \cos \alpha_1; \\
\omega'_{zo} &= \omega_{zo} + \dot{\alpha}_1.
\end{aligned}
\right\}
\qquad (1.64)
$$

Transition from one coordinate system to another is achieved by using
the matrix of direction cosines, which is the product of the matrices of
sequential rotations about axes Ox_Π, Oy_Π, and Oz_Π:

32

$$M_x(\alpha) = \begin{bmatrix} 1 & 0 & 0 \\ 0 & \cos\alpha & -\sin\alpha \\ 0 & \sin\alpha & \cos\alpha \end{bmatrix}; \quad M_y(\alpha) = \begin{bmatrix} \cos\alpha & 0 & -\sin\alpha \\ 0 & 1 & 0 \\ \sin\alpha & 0 & \cos\alpha \end{bmatrix};$$

$$M_z(\alpha) = \begin{bmatrix} \cos\alpha & \sin\alpha & 0 \\ -\sin\alpha & \cos\alpha & 0 \\ 0 & 0 & 1 \end{bmatrix}.$$

To switch to coordinate systems, bound to the mirror $Ox_3y_3z_3$, we find the matrix equation

$$[\omega_{x3}\omega_{y3}\omega_{z3}]^T = M_\Pi(\alpha_i)(\omega'_{xo}\omega'_{yo}\omega'_{zo})^T, \tag{1.65}$$

where ω_{x3}, ω_{y3}, ω_{z3} are projections of the angular velocities onto axes $Ox_3y_3z_3$; and

$$M_\Pi(\alpha_i) = M_y(\alpha_2)M_z(\alpha_1) =$$

$$= \begin{bmatrix} \cos\alpha_2 & 0 & -\sin\alpha_2 \\ 0 & 1 & 0 \\ \sin\alpha_2 & 0 & \cos\alpha_2 \end{bmatrix} \begin{bmatrix} \cos\alpha_1 & \sin\alpha_1 & 0 \\ -\sin\alpha_1 & \cos\alpha_1 & 0 \\ 0 & 0 & 1 \end{bmatrix} =$$

$$= \begin{bmatrix} \cos\alpha_1\cos\alpha_2 & \sin\alpha_1\cos\alpha_2 & -\sin\alpha_2 \\ -\sin\alpha_1 & \cos\alpha_1 & 0 \\ \cos\alpha_1\sin\alpha_2 & \sin\alpha_1\sin\alpha_2 & \cos\alpha_2 \end{bmatrix}.$$

It should be noted that axis Ox_3 coincides with the perpendicular to the surface of the mirror; therefore, the component of the angular velocity of the mirror ω_{x3} does not result in motion of the beam reflected from the mirror. On the other hand, according to the law of reflection, the angular rates of displacement of the reflected beam along axes Oy_3 and Oz_3 will be twice as much as the corresponding angular velocities of the mirror. Thus, for projections of the angular velocities of the reflected (i.e., output) beam onto the axes of the mirror $Ox_3y_3z_3$, one can write

$$[\omega_{xB}\omega_{yB}\omega_{zB}]^T = [0 \ 2\omega_{y3} \ 2\omega_{z3}]^T. \tag{1.66}$$

33

To find the projections of the angular velocities of the output beam onto axes $Ox_0y_0z_0$, one should multiply expression (1.66) by the matrix of direction cosines, which fulfills the inverse transformation compared to matrix $M_\Pi(\alpha_i)$, i.e.,

$$[\omega_{x\text{в}}^o\omega_{y\text{в}}^o\omega_{z\text{в}}^o]^T = M'_\Pi(\alpha_i)[0\quad 2\omega_{y3}\quad 2\omega_{z3}]^T, \tag{1.67}$$

where $\omega_{x\text{в}}^o$, $\omega_{y\text{в}}^o$, $\omega_{z\text{в}}^o$ are projections of the angular velocities of the output beam onto axes $Ox_\Pi y_\Pi z_\Pi$;

$$M'_\Pi(\alpha_i) = M_z(-\alpha_1)M_y(-\alpha_2) =$$

$$= \begin{bmatrix} \cos\alpha_1 & -\sin\alpha_1 & 0 \\ \sin\alpha_1 & \cos\alpha_1 & 0 \\ 0 & 0 & 1 \end{bmatrix} \begin{bmatrix} \cos\alpha_2 & 0 & \sin\alpha_2 \\ 0 & 1 & 0 \\ -\sin\alpha_2 & 0 & \cos\alpha_2 \end{bmatrix} =$$

$$= \begin{bmatrix} \cos\alpha_1\cos\alpha_2 & -\sin\alpha_1 & \cos\alpha_1\sin\alpha_2 \\ \sin\alpha_1\cos\alpha_2 & \cos\alpha_1 & \sin\alpha_1\sin\alpha_2 \\ -\sin\alpha_2 & 0 & \cos\alpha_2 \end{bmatrix}.$$

Multiplying out expressions (1.65) and (1.67) and having substituted relation (1.64), we find

$$\left. \begin{aligned} \omega_{x3} &= \cos\alpha_1\cos\alpha_2(\omega_{xo} - \dot{\alpha}_2\sin\alpha_1) + \\ &+ \sin\alpha_1\cos\alpha_2(\omega_{yo} + \dot{\alpha}_2\cos\alpha_1) - \sin\alpha_2(\omega_{zo} + \dot{\alpha}_1); \\ \omega_{y3} &= -\sin\alpha_1(\omega_{xo} + \dot{\alpha}_2\sin\alpha_1) + \cos\alpha_1(\omega_{yo} + \dot{\alpha}_2\cos\alpha_1); \\ \omega_{z3} &= \cos\alpha_1\sin\alpha_2(\omega_{xo} - \dot{\alpha}_2\sin\alpha_1) + \\ &+ \sin\alpha_1\sin\alpha_2(\omega_{yo} + \dot{\alpha}_2\cos\dot{\alpha}_1) + \cos\alpha_2(\omega_{zo} + \dot{\alpha}_1); \end{aligned} \right\} \tag{1.68}$$

$$\left. \begin{aligned} \omega_{x\text{в}}^o &= -2\omega_{y3}\sin\alpha_1 + 2\omega_{z3}\cos\alpha_1\sin\alpha_2; \\ \omega_{y\text{в}}^o &= 2\omega_{y3}\cos\alpha_1 + 2\omega_{z3}\sin\alpha_1\sin\alpha_2; \\ \omega_{z\text{в}}^o &= 2\omega_{z3}\cos\alpha_2. \end{aligned} \right\} \tag{1.69}$$

Having substituted matrix (1.68) into relations (1.69) after certain transformations, we find

34

$$\omega_{xn}^{o} = \omega_{xo}\left(2\sin^2\alpha_1 + 2\cos^2\alpha_1\sin^2\alpha_2\right) +$$
$$+ \omega_{yo}\left(-2\sin\alpha_1\cos\alpha_1 + \sin 2\alpha_1\sin^2\alpha_2\right) +$$
$$+ \omega_{zo}\left(\cos\alpha_1\sin 2\alpha_2\right) + \dot{\alpha}_1\cos\alpha_1\sin 2\alpha_2 -$$
$$- \dot{\alpha}_2\, 2\sin\alpha_1;$$
$$\omega_{yn}^{o} = -\omega_{xo}\left(\sin 2\alpha_1\cos^2\alpha_2\right) +$$
$$+ \omega_{yo}\left(2\cos^2\alpha_1 + 2\sin^2\alpha_1\sin^2\alpha_2\right) +$$
$$+ \omega_{zo}\sin\alpha_1\sin 2\alpha_2 + \dot{\alpha}_1\sin\alpha_1\sin 2\alpha_2 +$$
$$+ \dot{\alpha}_2\, 2\cos\alpha_1;$$
$$\omega_{zn}^{o} = \omega_{xo}\sin 2\alpha_2\cos\alpha_1 + \omega_{yo}\sin\alpha_1\sin 2\alpha_2 +$$
$$+ \omega_{zo}2\cos^2\alpha_2 + \dot{\alpha}_1\, 2\cos^2\alpha_2. \qquad (1.70)$$

Blurring of the image on the photodetector will be determined by the difference of angular velocities of the beam, impinging on the photodetector, and by the photodetector itself. If the photodetector is attached to the base, it moves with the angular velocity of the base with respect to the object of observation. Thus, projections of the angular rates of blurring of the image onto axes $Ox_0y_0z_0$ can be found from the expressions:

$$\omega_{\delta x}^{o} = \omega_{xn}^{o} - \omega_{xo};$$
$$\omega_{\delta y}^{o} = \omega_{yn}^{o} - \omega_{yo}; \qquad (1.71)$$
$$\omega_{\delta z}^{o} = \omega_{zn}^{o} - \omega_{zo}.$$

It is obvious that the problem of stabilization of the image will be written in the form:

$$\omega_{\delta x}^{o} = 0;$$
$$\omega_{\delta y}^{o} = 0; \qquad (1.72)$$
$$\omega_{\delta z}^{o} = 0.$$

To guarantee equalities (1.72), one can select the corresponding angular velocities with respect to rotation of the mirror $\dot{\alpha}_1$ and $\dot{\alpha}_2$. A more effective method is introduction of the corresponding angular displacements of the photodetector or of the entire optical system with respect to the base. The projections of the angular velocities of the photodetector onto axes $Ox_0y_0z_0$, i.e., $\omega_{x\phi}^{o}$, $\omega_{y\phi}^{o}$, $\omega_{z\phi}^{o}$ should be substituted into expression (1.71).

35
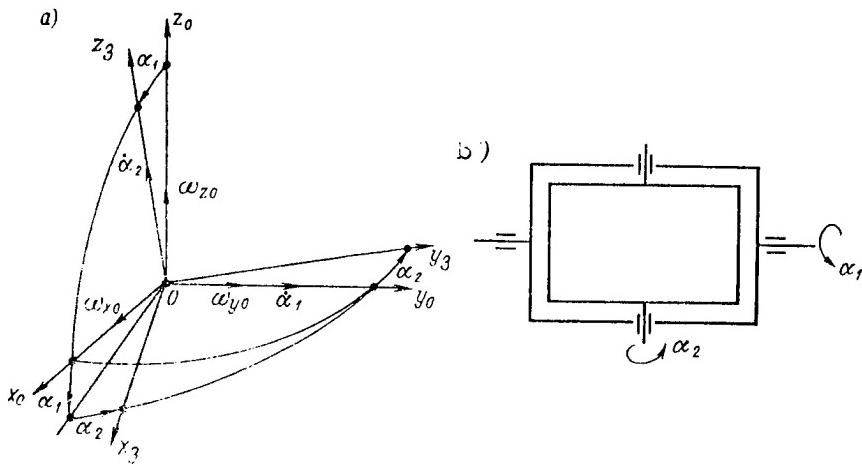
Figure 1.10. Variant of Attaching Mirror to Outer Gimbal,
Oriented According to Incident Beam:
a—coordinate system bound to deflecting mirror;
b—gimbal suspension of deflecting mirror

The basic element of most optical systems is the objective, mounted in front of the photodetector such that the photodetector is in its focal plane. The angular displacements of the photodetector are rational only about the principal axis of the objective, while the other angular displacements of the photodetector can be reduced to linear displacements in the corresponding directions at velocities v_ϕ. This motion is equivalent to angular displacement of the vector at velocity $\omega_{\phi.э} = v_\phi f'$, where f' is the focal distance of the objective. The corresponding projections of vector $\omega_{\phi.э}$ are substituted into expression (1.71).

Let us consider other versions of a design for attachment of the mirror. A coordinate system and the design for attachment of the deflecting mirror, corresponding to this system and corresponding to the order of rotation, are shown in Figure 1.10, a and b. As before, let us assume that the light beam from the object of observation coincides with axis Ox_Π.
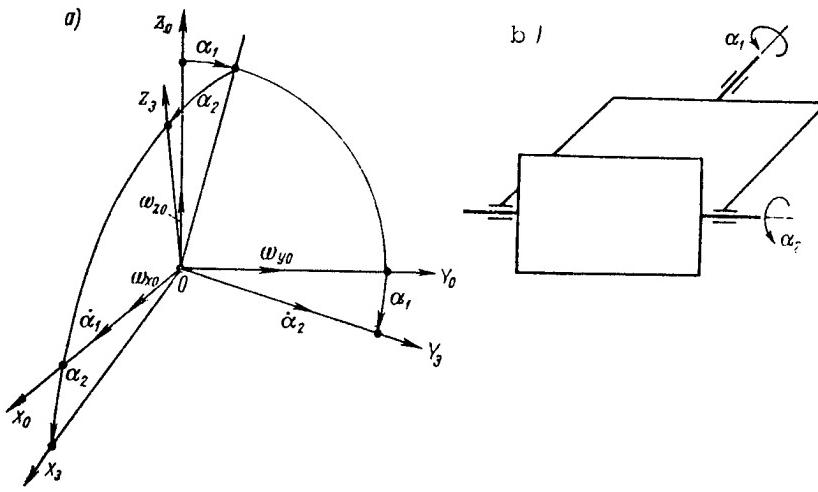
Figure 1.11. Variant for Attachment of Mirrors:
a--coordinate system bound to deflecting mirror;
b--gimbal suspension of deflecting mirror

For this case, instead of expressions (1.70), we find:

$$
\begin{aligned}
\omega^{\text{o}}_{x\text{B}} &= \omega_{x\Pi}2\left(\sin^2\alpha_1 - \cos^2\alpha_1\sin^2\alpha_2\right) - \omega_{y\Pi}2\cos\alpha_1\sin\alpha_2\cos^2\alpha^2 + \\
&\quad + \omega_{z\Pi}\sin 2\alpha_1\cos^2\alpha_2 - \dot\alpha_1 2\cos\alpha_1\sin\alpha_2\cos^2\alpha_2 + \dot\alpha_2 2\sin\alpha_1; \\
\omega^{\text{o}}_{y\text{B}} &= \omega_{x\Pi}\left(-2\cos\alpha_2\cos\alpha_1\sin\alpha_2\right) + \omega_{y\Pi}2\cos^3\alpha_2 + \\
&\quad + \omega_{z\Pi}2\sin\alpha_1\sin\alpha_2\cos\alpha_2 + \dot\alpha_1 2\cos^3\alpha_2; \\
\omega^{\text{o}}_{z\text{B}} &= \omega_{x\Pi}\left(\sin 2\alpha_1\cos 2\alpha_2\right) + \omega_{y\Pi}\left(2\sin\alpha_1\sin\alpha_2\cos^2\alpha^2\right) + \\
&\quad + \omega_{z\Pi}2\left(\sin^2\alpha_1\sin^2\alpha_2 + \cos^2\alpha_1\right) + \\
&\quad + \dot\alpha_1\left(2\sin\alpha_1\sin\alpha_2\cos^2\alpha_2\right) + \dot\alpha_2 2\cos\alpha_1.
\end{aligned}
\qquad (1.73)
$$

By analogy with equations (1.72) and (1.73) for the case shown in Figure 1.11, a and b, one can write

$$
\begin{aligned}
\omega^{\text{o}}_{x\text{B}} &= \omega_{x\Pi}2\sin^2\alpha_2 + \omega_{y\Pi}\left(-\sin\alpha_1\sin 2\alpha_2\right) + \\
&\quad + \omega_{z\Pi}\left(\cos\alpha_1\sin 2\alpha_2\right) + \dot\alpha_1 2\sin^2\alpha_2; \\
\omega^{\text{o}}_{y\text{B}} &= \omega_{x\Pi}\left(-\sin\alpha_1\sin 2\alpha_2\right) + \omega_{y\Pi}\left(2\cos^2\alpha_1 - 2\sin^2\alpha_1\cos^2\alpha_2\right) - \\
&\quad - \omega_{z\Pi}\left(\sin 2\alpha_1 + \sin 2\alpha_1\cos^2\alpha_2\right) + \\
&\quad + \dot\alpha_1\left(-\sin\alpha_1\sin 2\alpha_2\right) + \dot\alpha_2\left(2\cos\alpha_1\right); \\
\omega^{\text{o}}_{z\text{B}} &= \omega_{x\Pi}\left(\cos\alpha_1\sin 2\alpha_2\right) + \omega_{y\Pi}\sin 2\alpha_1\left(1 + \cos^2\alpha_2\right) + \\
&\quad + \omega_{z\Pi}2\left(\cos^2\alpha_1\cos^2\alpha_2 - \sin^2\alpha_1\right) + \dot\alpha_1\left(\cos\alpha_1\sin 2\alpha_2\right) + \dot\alpha_2 2\sin\alpha_1.
\end{aligned}
\qquad (1.74)
$$

Chapter 2. Principles of Image Stabilization

2.1. General Principles of Image Stabilization for Different Optical Systems

Various optical devices, mounted on a moving base and requiring the use of an image field stabilization system, are ordinarily recording devices. Photographic, television, image converter, and other image detectors are used as the image recorder in them. In this regard, these systems will be further designed on examples of recording-type apparatus, specifically, on examples of AFA.

Misalignment of the image by two of its coordinates, caused by displacement of the optical device in space, can be compensated by the following basic methods: 1) by displacement of the camera objective, 2) by displacement or rotation of the reflecting or refracting optical elements contained in the device, and 3) by displacement or rotation of the optical elements, additionally introduced to the layout of the device to compensate for misalignment of the image, and 4) by displacement of the image detector.

The problem of selecting one or another method of compensation is determined by analysis of alternative variants of making the image stabilization system. This problem can seemingly be solved without introduction of additional elements into the optical layout of the device. However, an increase of the energy expenditures and of the mass of the device, related to introduction of a stabilization system, at high intensities and broad range of displacements of the base, is mainly dependent on the coefficients of inertia of the moving elements of the optical system. Those solutions at which these values would be minimal must be used. It follows from the foregoing that additional elements with small coefficients of inertia, specially designed for stabilization, can be introduced into the optical circuit.

Let us consider the design principles of optical systems with stabilization of the image field on examples of various types of known cameras.

1. Misalignment of the image can be compensated in cameras with flat image field, without resorting to additional optical elements, by displacement of: the objective in two coordinates, the film holder part containing the film, or an leveling table with segment of the photographic film on it also in two coordinates. The mass of all three image misalignment compensation devices can be estimated in the first step of analysis of alterative solutions and the problem of selecting the best variant can be solved.

Introduction of additional compensating elements of the mirror, prism, wedge and other types can be substantiated for all types of cameras only if the mass of the introduced compensation assembly is related to the mass of the variant selected from the above three variants as 1:2 or less.

2. Misalignment can also be compensated by several methods in cameras which take photographs by a scanning system or without it on fixed film, arranged on a cylindrical surface, for example, in panoramic AFA, in AFA of PACA-70 type (the Netherlands), and in cameras with special wide-angle objectives: a) by displacement of the objective parallel to the generatrix of the cylindrical surface of the leveling table containing the film, b) by displacement of the film holder part in the same direction, c) by rotation of the film holder part about the cylindrical surface of the leveling table, and d) by additional rotation of the scanning element about the scanning axis.

3. The objective in cameras with spherical image field may not be used as the compensation element in the image stabilization system. The image can be compensated only by angular rotations of the leveling table containing the film about the central axes of symmetry of the spherical surface of the image.

The problem of selecting the element of the optical system, by which one should compensate the image misalignment upon misalignments of the base, is one of the problems of designing the stabilization system. Other problems are related to the principles of designing automatic stabilization systems and to database organization and management. Those systems in which the possibility of a direct check of misalignment of the device together with the moving base provide the best database organization and management.

The design principles of automatic image stabilization systems and the models of optical systems for different types of cameras are similar. The difference is only in the methods of displacement of the compensation elements, of the selected alternatives and in the properties of the given type of camera. This representation can also be made for other image detectors, such as television camera tubes, IR detectors, and solid-state structures. The shapes of their light-sensitive surfaces can be the same as the shape of the film on the leveling table of the camera. For this reason, image stabilization systems can be made similar to each other. However, one should note that misalignment of the image can be compensated using television receivers and image converter tubes not only by moving the entire detector (as was considered in the example of a camera), but also by acting on the speed of the reading electron beam (in the case of television camera tubes) or on the control readout signal (for solid-state image detectors). However, the functional diagrams of control of image stabilization devices remain the same.
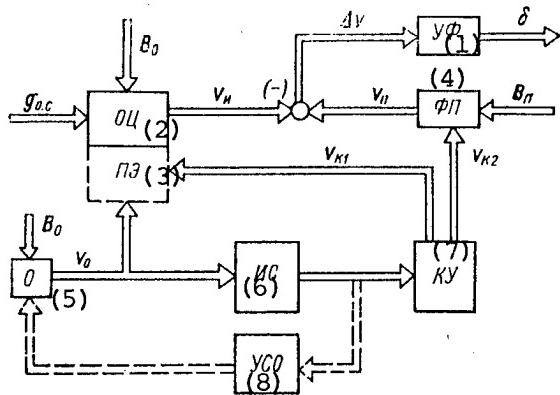
Figure 2.1. Generalized Functional Diagram of
Optical Device

KEY:

1. Recording device
2. Optical circuit
3. Moving elements
4. Photodetector
5. Base
6. Misalignment of base
7. Control system
8. Base stabilization device

Most existing image stabilization systems are based on the use of
information obtained by one or another method about the current value of
the parameters of motion of the base.

Data on misalignment of the image can obviously be found only
indirectly.

Let us consider a generalized functional diagram of an optical device
(Figure 2.1). An optical signal $g_{0.c}$ is fed to the input of the optical
circuit (OTs). The motion of the image in the focal plane of the
objective is characterized by vector $v_{\text{и}}$. Vector $v_{\text{п}}$ of the motion of the
photodetector (FP) together with vector $v_{\text{и}}$ yields the vector of the
difference motion Δv, which in turn is fed to the recording device (UF).
The film (together with the shutter), a solid-stage image sensor and so
on can be used as the image recording devices.

A shift of the image δ on the recording device is determined not only by
the parameters of vector Δv, but also by the characteristics of the
recording device.

One of the main causes of misalignment of the image is the motion of the
base O due to perturbations B_0. The vector of motion v_0 is determined
by using the parameters of motion of the base. The parameters of this
vector are calculated by the base misalignment meter (IS) and are
delivered as the control actions on the controller (KU) of the motion of

40

the moving elements (PE) of the optical circuit and photodetector. To do this, the controller generates compensating motions v_{K1} and v_{K2}. For partial compensation of the image shift, the information at the output of the base misalignment meter can be used as the base stabilizer (USO).

It follows from the diagram presented in Figure 2.1 that the image stabilization system is designed in the given case on the open principle and may not be used effectively to compensate for perturbing effects B_0 and B_{π} on the optical circuit and the photodetector, respectively. The errors of the base misalignment sensor result in uncompensated errors of the system as a whole.

The obvious deficiencies of stabilization systems, designed on the use of data on displacement of a moving base, resulted in the need to develop essentially new approaches.

One of the natural directions of improving the accuracy of image stabilization is design of a system using data directly about the misalignment itself.
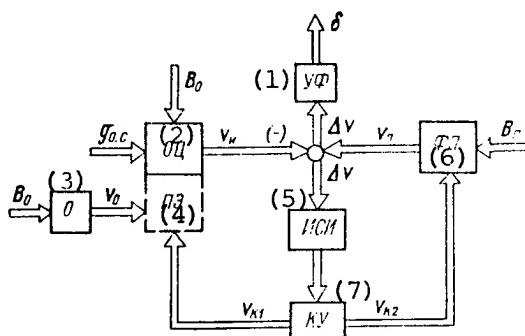
Figure 2.2. Generalized Functional Diagram of
Optical Device With Image Misalignment Sensor

KEY:

1.	Recorder	5.	Image shift sensor
2.	Optical circuit	6.	Photodetector
3.	Base	7.	Control system
4.	Moving elements		

A generalized functional diagram of this device is presented in Figure 2.2. The previous notations are retained in the figure. An image shift sensor (ISI) is used to measure the current value of the parameters of difference motion Δv. It follows from the given functional diagram that the image stabilization system becomes closed upon difference motion.

41

This circumstance permits effective suppression of all perturbations acting on the system, regardless of their physical nature.

High requirements on accuracy and speed are imposed on the image shift sensor as on the element of the closed image stabilization system. It is obvious that the range of measured frequencies of variations Δv should exceed severalfold the highest frequency of the perturbations acting on the system. The motion of the base v_0 is ordinarily the strongest perturbation, while an image stabilization system can rationally be structured on the combination control principle for partial suppression of this perturbation. Both of the above principles are combined in the control system.
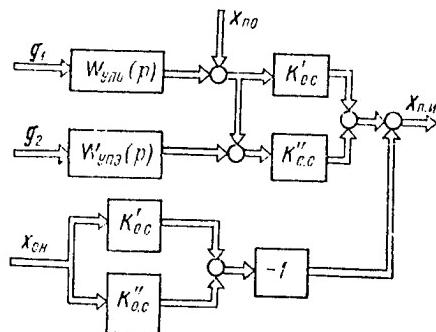
Figure 2.3. Block Diagram of Formulation of
Image Displacement

Obvious causes of the image displacement of the optical device are mutual displacements of the base of the device and of the object of observation in inertial space. This situation can be reflected in the block diagram as the effect of the vectors of displacements of the base $x_{\text{п.о}}$ and of displacement of the object of observation $x_{\text{о.н}}$ on the elements of the optical system (Figure 2.3). The matrix of the transfer coefficients of the elements, fixed with respect to the base of the device, is denoted by $K'_{\text{о.с}}$, while that of the moving elements is denoted by $K''_{\text{о.с}}$. It is obvious that the effect of vector $x_{\text{о.н}}$ is equal in value and opposite in sign to the effect of vector $x_{\text{п.о}}$ on all elements of the optical system simultaneously. Additional displacements of the image can be achieved by introducing base displacement devices (UPO) and moving element displacement devices (UPE) with matrices of transfer functions $W_{\text{UPO}}(p)$ and $W_{\text{UPE}}(p)$, respectively. Control signals g_1 and g_2 should be delivered to the control inputs of these devices.

The problem of stabilization reduces to fulfillment of condition $x_{\text{п.и}} =$ $= 0$, i.e., to suppression of image misalignments.

42

The control channels of different parameters in most cases of engineering realization of stabilization systems do not actually have cross-couplings and the matrices in description of these systems will be diagonal or can be reduced to diagonal. This circumstance permits one to linearize the mathematical description of the optical system, considering the transformation of the coordinates of displacements of the base of the observation object and of the elements of the optical system in coordinates of image displacements.

It should be noted that the optical image detector is also included among the elements of the optical system in this interpretation of the problem.

Parametric stabilization of image. It follows from the block diagram presented in Figure 2.3 that if the following condition is fulfilled

$$K'_{o.c} + K''_{o.c} = 0 \qquad\qquad (2.1)$$

perturbations $x_{\text{п.о}}$ and $x_{\text{о.н}}$ do not influence the displacements of the image. The details of engineering realization of these optical systems will be considered in the next chapter. We note only that introduction of high-speed image recorders in the system permits one to reduce the time of analysis of the image and, accordingly, the amount of smearing during this time. This circumstance can be represented as the result of inclusion of an element with matrix of transfer coefficients less than unity into the optical system of the device.

Image stabilization system with programmed processing of perturbing effects. A stabilization system, designed on the open control principle, is simplest to realize. The values of vectors $x_{\text{о.н}}$ and $x_{\text{п.о}}$ either remain constant or vary by known law in a number of cases. An example of this device is the AFA. The effect of displacement of the base (the aircraft) at specific velocity v_0 at a specific altitude H_0 can be compensated by corresponding displacement of the entire optical device or of the elements of its optical system during photography. A programmer with matrix of transfer coefficients $K_{\text{п.у}}$, which transforms the introduced and predicted estimates of vectors $\hat{x}_{\text{п.о}}$ and $\hat{x}_{\text{о.н}}$ to the vectors of control signals g_1 and g_2, is introduced into the structure of the system for this purpose. It is obvious that real displacements will differ to one or another degree from the predicted displacements: therefore, image stabilization on this principle does not yield satisfactory results in most cases.

Image stabilization system with control by perturbing influences. Condition (2.1) is difficult or impossible to fulfill in most cases; therefore, the design of the optical device should vary the position of

43

the entire device in space or of the number of elements of the optical system.

The corresponding control systems, which also include base displacement sensors (IPO), components of the optical system (IPE), and components of the object of observation (ION), besides base displacement devices and moving element displacement, should in turn be used to control the position in space. The cross-couplings through different control channels are ordinarily small or can be reduced to a minimum. Therefore, the spatial control problem breaks down into a number of one-dimensional control problems for each of the parameters of the vectors of input actions.
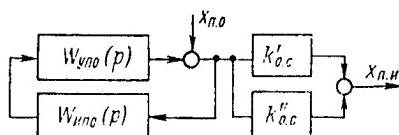
Figure 2.4. Block Diagram of Optical Device
With Base Position Stabilizer
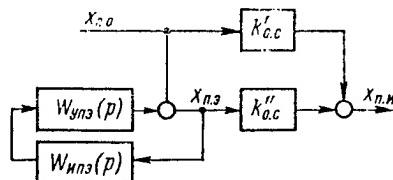
Figure 2.5. Block Diagram of Optical Device
With Control Circuit of Position of Elements
of Optical System

Moreover, it is sufficient in some practical problems to eliminate the effect of displacement of the base. The block diagram presented in Figure 2.4 for the scalar case corresponds to a stabilizer of the position of the base in inertial space. The transfer function for one coordinate for input $x_{\text{п.о}}$ can be written in the form

$$\Phi_{\text{п.о}}(p) = \frac{x_{\text{п.и}}}{x_{\text{п.о}}} = \frac{k'_{\text{о.с}} + k''_{\text{о.с}}}{1 + W_{\text{упо}}(p)W_{\text{ипо}}(p)} . \qquad (2.2)$$

It follows from expression (2.2) that the condition $\Phi_{\text{п.о}}(p) \to 0$ must be fulfilled to stabilize the image. In the frequency band reproduced by

44

the base stabilization circuits, we find with regard to expression (2.2)
the condition of image stabilization in the form

$$W_{\text{упо}}(p)\, W_{\text{нпо}}(p) \gg k'_{\text{о. с}} + k''_{\text{о. с}}. \tag{2.3}$$

Expression (2.3) imposes a restriction on the minimum possible speed of
the base position stabilization system. It is obvious that condition
(2.3) should be fulfilled over the entire range of frequencies of
variations of $x_{\text{п.о}}$.

The problem of image stabilization can also be solved by controlling the
position of the elements of the optical system in inertial space (Figure
2.5). Instead of expression (2.2), we find

$$\Phi_{\text{п. о}}(p) = k'_{\text{о. с}} + \frac{k''_{\text{о. с}}}{1 + W_{\text{упэ}}(p)\, W_{\text{ипэ}}(p)}. \tag{2.4}$$

The condition of image stabilization $\Phi_{\text{п.о}}(p) = 0$ is written in the form

$$W_{\text{упэ}}(p)\, W_{\text{ипэ}}(p) = -\left(1 - \frac{k''_{\text{о. с}}}{k'_{\text{о. с}}}\right). \tag{2.5}$$

It follows from expression (2.5), that, first, the system for
stabilization of the position of elements of the optical system should
be static with transfer factor according to the control circuits,

determined by this expression. Secondly, the condition $|k''_{\text{о. с}}| > |k'_{\text{о. с}}|$.

should be fulfilled to eliminate the appearance of positive feedback and
instability of the system. Moreover, the signs of $k''_{\text{о.с}}$ and $k'_{\text{о.с}}$
should be different.

A sensor of the parameters of displacements of the observation object
(ION) with transfer function $W_{\text{ION}}(p)$ should be introduced into the
structure of the system for complete image stabilization.

One can write for the block diagram shown in Figure 2.6

$$x^{*}_{\text{п. о}} = x_{\text{п. о}}\Phi_{\text{в}}(p) + x_{\text{о. н}}W_{\text{ион}}(p)\,\Phi(p),$$

45

where

$$\Phi(p) = \frac{W_{\text{ипо}}(p)\, W_{\text{упо}}(p)}{1 + W_{\text{ипо}}(p)\, W_{\text{упо}}(p)};$$

$$\Phi_{\text{в}}(p) = \frac{1}{1 + W_{\text{ипо}}(p)\, W_{\text{упо}}(p)}.$$

We find for displacement of the optical elements

$$x_{\text{п. э}} = x_{\text{п. о}}^{*} + x_{\text{п. о. э}} =$$

$$= [x_{\text{п. о}}\Phi_{\text{в}}(p) + x_{\text{о. н}}\Phi(p)\, W_{\text{нон}}(p)][1 - W_{\text{ипо}}(p)\, W_{\text{упэ}}(p)] +$$

$$+ x_{\text{о. н}}W_{\text{нон}}(p)\, W_{\text{упэ}}(p).$$

Based on the previous expression for displacement of the image, one can write

$$x_{\text{п. н}} = - x_{\text{о. н}}(k_{\text{о. c}}' + k_{\text{о. c}}'') + x_{\text{п. о}}^{*}k_{\text{о. c}}' + x_{\text{п. э}}k_{\text{о. c}}'' =$$

$$= x_{\text{п. о}}\{k_{\text{о. c}}'\Phi_{\text{в}}(p) + k_{\text{о. c}}''\Phi_{\text{в}}(p)[1 - W_{\text{ипо}}(p)\, W_{\text{упэ}}(p)]\} +$$

$$+ x_{\text{о. н}}\{k_{\text{о. c}}'\Phi(p)\, W_{\text{нон}}(p) - (k_{\text{о. c}}' + k_{\text{о. c}}'') + \Phi(p)\, W_{\text{нон}}(p)k_{\text{о. c}}'' \times$$

$$\times [1 - W_{\text{ипо}}(p)\, W_{\text{упэ}}(p) + k_{\text{о. c}}''W_{\text{нон}}(p)\, W_{\text{упэ}}(p)]\}.$$
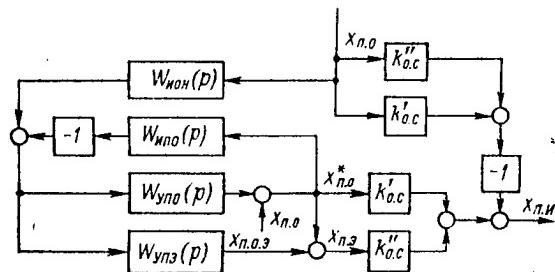

Figure 2.6.   Block Diagram of Optical Device With
Sensor of Parameters of Displacement of Observation
Object

The condition of invariance to perturbing effects is written in the form

$$k_{\text{о. c}}' + k_{\text{о. c}}''[1 - W_{\text{ипо}}(p)\, W_{\text{упэ}}(p)] = 0.$$

Hence,

$$W_{\text{уно}}(p) = \frac{1}{W_{\text{упэ}}(p)}\left(1 + \frac{k'_{\text{о. с}}}{k_{\text{о. с}}}\right).$$ (2.6)

Moreover,

$$\Phi(p)\, W_{\text{нон}}(p)\, [k'_{\text{о. с}} + k''_{\text{о. с}}(1 - W_{\text{шно}}(p)\, W_{\text{упэ}}(p)] -$$
$$- (k'_{\text{о. с}} + k''_{\text{о. с}}) + k''_{\text{о. с}} W_{\text{нон}}(p)\, W_{\text{упэ}}(p) = 0.$$ (2.7)

Having substituted expression (2.6) into equation (2.7), we find

$$W_{\text{нон}}(p) = \frac{1}{W_{\text{упэ}}(p)}\left(1 + \frac{k'_{\text{о. с}}}{k''_{\text{о. с}}}\right).$$

Thus, the transfer functions of sensors of both perturbing effects should be identical and their value is determined only by the ratio of coefficients $k'_{\text{о.с}}/k''_{\text{о.с}}$ and transfer function $W_{\text{упэ}}(p)$.
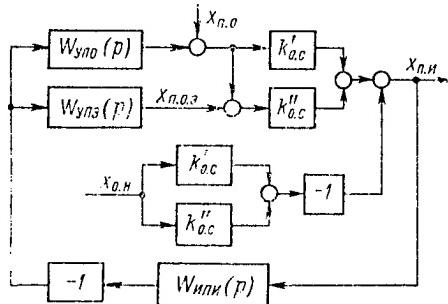
Figure 2.7. Block Diagram of Optical Device
With Image Displacement Sensor

It is obvious from the derived equations that the speed of the closed control circuit with transfer function $\Phi(p)$ has no influence on fulfillment of the condition of invariance.

Image stabilization system with control by image displacement. A radical means of improving the quality of the image stabilization system is to develop image feedback in its structure. To do this, current data must be found about displacement of the image $x_{\text{п.н}}$, which is taken from the output of the image displacement sensor (IPI) with transfer function

47

$W_{ИПИ}$(p) (Figure 2.7). The condition of image stabilization appears in the form of the matrix of transfer functions being equal to zero according to perturbations in a closed system.

One can find the following relation from this condition:

$$W_{ИПИ}(p)\, W_{УПО}(p) + \frac{k''_{o.c}}{k'_{o.c} + k''_{o.c}}\, W_{ИПИ}(p)\, W_{УПЭ}(p) \gg 1,$$

from which it follows that control of the position of the components of the optical circuit in the given structure can be introduced only at

$$k''_{o.c} > k'_{o.c}.$$

Retention of two control channels is rational in this case to expand the dynamic range of the compensated values of displacements $x_{o.н}$ and $x_{п.о}$. It is obvious that the channel of the base displacement device permits control at practically unlimited values of displacement $x_{o.н}$ and permits one to reduce considerably the possible displacement of the base $x_{п.о}$. On the other hand, the channel of the moving component displacement permits one to trigger comparatively small misalignments of the image at high speed, and accordingly, with smaller dynamic error.

2.2. Mounting Equipment on Moving Base and Methods of Initial Orientation of It With Respect to Object of Optical Observations

The resolving capabilities of optical devices located on a moving base are considerably determined by the method of attaching them. It is obvious that the equipment can be mounted on shock absorbers to suppress vibration misalignments of the base (specifically in the high-frequency range). The effectiveness of shock absorption is enhanced when the frequency of natural vibrations of the device, connected to the base through a flexible coupling, is reduced. On the other hand, the stiffness of this elastic coupling should provide the required accuracy of orientation of the optical axis of the device.

Let us consider an AFA in the side-looking mode as an example of the requirement on the accuracy of orientation of the main optical axis.

It follows from expressions (1.21) that the rate of misalignment of the image along axis Oy is determined by the approximation formula

$$\dot{y}_i = f' v_{п} \sin \varphi / H_0, \qquad (2.8)$$

48

where φ is the angle between the horizontal plane and the principal optical axis of the device.

Let us represent this angle in the form of the sum of the basic angle φ_0 and of the orientation error $\Delta\varphi$. Then, instead of expression (2.8), we find

$$\dot{y}_i \approx f' \frac{V_{11}}{H_0} \sin \varphi_0 (1 + \Delta\varphi \, \text{ctg} \, \varphi_0).$$

One can determine the component of the rate of misalignment of the image, determined by the orientation error, in the last expression. The permissible value of this error can then be found in the form

$$\Delta\varphi_{\text{доп}} = \frac{\Delta\dot{y}_{i\,\text{доп}}}{f' \dfrac{v_{11}}{H_0} \cos \varphi_0},$$

where $\Delta\dot{y}_{i\text{доп}}$ is the permissible value of the uncompensated rate of misalignment of the image.

It follows from this formula that the requirements on the accuracy of initial orientation increase as the angle φ_0 decreases and as the ratio $v_{\text{П}}/H_0$ increases.

All the foregoing is related to image stabilization systems, designed on the open principle. If there is an image displacement sensor, the errors of orientation of the main optical axis of the device have no effect on misalignment of the image, since they are suppressed jointly with other perturbations.

An initial orientation system should be introduced into the structure of the device to maintain specific orientation of the main optical axis, which assumes the presence of the corresponding information channels and devices that permit one to measure and record in space the position of the principal optical axis. The latter requirement can easily be fulfilled if the optical device includes an image stabilization system. Correction signals, which permit one to assign a specific position of the principle optical axis with respect to the object of photography at the beginning of each operating cycle, should be suppressed for the additional inputs of the local drive control modules of the moving components of the optical system of the device. The function of the information channels is clear from the foregoing. The navigation and orientation equipment that already exist on the base can be used.

49

Thus, the signals from the output of the onboard gyro unit can be used on the aircraft for initial orientation of the aerial camera. The required frequency of correction of the autonomous image stabilization equipment of the optical device can be established experimentally or can be determined from the ratio of the permissible orientation error and the drift rate of the gyroscopes of the stabilization system. The design principles of gyroscopic orientation systems and methods of calculating them are outlined in [53]. Besides gyroscopic systems, systems for orientation by astronomical objects are also considered in [3].

2.3. General Characteristic of Image Misalignment Compensation Devices

Various additional components, on which the effects of the compensating motion of the image up to a value which essentially does not deteriorate the quality of the image to be recorded have an active influence and are added, are introduced into the optical system to eliminate the effect of stabilization errors. Let us consider only the components themselves in this section and let us evaluate the possibilities of using them, without touching on the design features of the optical device itself.

Functions that determine the direction of the beam (reflected or refracted), which are ordinarily found by using the following expression, are used to design stabilization devices

$$A' = A - 2N(AN),\qquad(2.9)$$

where A is the unit vector of the direction of the impinging beam, N is the unit vector of the direction of the normal of the reflecting surface, and AN is the scalar product of the vectors [60].
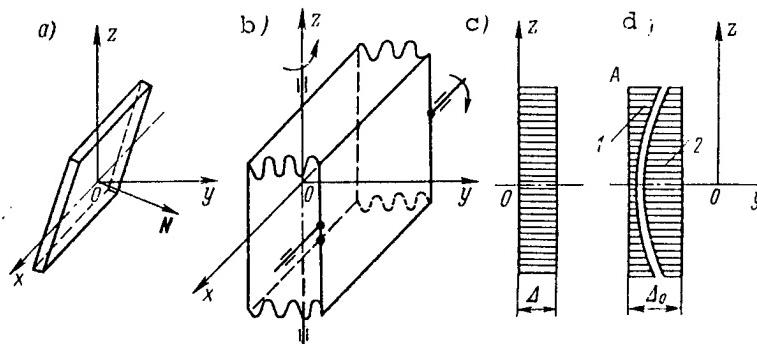

Figure 2.8. Layouts of Main Image Misalignment
Compensation Devices:
a—coordinate system of flat mirror; b—wedge
with variable refracting angle; c—planoparallel
fiber optic element (VOE); d—image misalignment
compensator using VOE; 1, 2—parts of compensator

50

One can write A' = M'A, where M' is the transformation matrix, in matrix form.

The transformation matrix for a flat mirror (Figure 2.8, a) is determined in the following form:

$$\mathbf{M}' = \begin{bmatrix} 1 - 2N_x^2 & -2N_xN_y & -2N_xN_z \\ -2N_xN_y & 1 - 2N_y^2 & -2N_yN_z \\ -2N_xN_z & -2N_yN_z & 1 - 2N_z^2 \end{bmatrix}, \qquad (2.10)$$

where N_x, N_y and N_z are projections of the unit vector N of the direction of the normal of the mirror onto axes x, y, and z of an arbitrary fixed coordinate system.

It is quite sufficient to use the indicated expressions to determine the effect of rotations of the mirror about one or another axis. Thus, even if the mirror, the plane of which is perpendicular to plane Oyz and if its principal cross-section comprises an angle of 45° with axes Oz and Oy, is located in coordinate system Oxyz, the normal N' is determined by the expression

$$\mathbf{N}' = \mathbf{j} \sin 45° - \mathbf{k} \cos 45°.$$

The incident beam is determined by the unit vector

$$\mathbf{A} = \mathbf{i} \cos i \sin \xi + \mathbf{j} \cos i \cos \xi + \mathbf{k} \sin i.$$

The mirror is rotated about axis Ox by angle ψ. Equation (2.10) must be solved to find the unit vector of the reflected beam, having first determined the normals of the inverted mirror, i.e., N' = MN. Multiplying out the matrix M, we find

$$\mathbf{N}' = \begin{bmatrix} 1 & 0 & 0 \\ 0 & \cos\psi & \sin\psi \\ 0 & \sin\psi & \cos\psi \end{bmatrix} \begin{bmatrix} 0 \\ \sin 45° \\ \cos 45° \end{bmatrix} = \mathbf{j} \sin(45° + \psi) - \mathbf{k} \cos(45° + \psi).$$

It follows from this equation that

$$N_x = 0; \quad N_y = \sin(45° + \psi); \quad N_z = -\cos(45° + \psi).$$

51

The unit vector of the output beam then assumes the form

$$\mathbf{A}' = \mathbf{M}_x'\mathbf{A} = - \mathbf{i}\cos\gamma\sin\xi + \mathbf{j}\,(\cos 2\psi\sin\gamma - \sin 2\psi\cos\xi\cos\gamma) +$$
$$+ \mathbf{k}\,(\cos 2\psi\cos\xi\cos\gamma + \sin 2\psi\sin\gamma).$$

The turns by the other axes can also be found in similar fashion. The following expression is valid for a refracting surface

$$\mathbf{A}' = \frac{n}{n'}\,\mathbf{A} - \mathbf{N}\left\{\frac{n}{n'}\,(\mathbf{A}\mathbf{N}) - \sqrt{1 + \left(\frac{n}{n'}\right)^2 \left[(\mathbf{A}\mathbf{N})^2 - 1\right]}\,\right\} = \qquad (2.11)$$
$$= \frac{n}{n'}\,\mathbf{A} + \mathbf{N}\left(\frac{n}{n'}\cos i - \cos i'\right),$$

where n and n' are the refractive indices of the first and second media, separated by the refracting surface, and i and i' is the angle of incidence and the angle of refraction of the beam on the surface.

It is shown in [60] that the operation matrix of a refracting wedge is determined by the following expression:

$$\mathbf{M}_{\text{кл}} = \begin{bmatrix} \cos\varkappa + 2p_x\sin^2\dfrac{\varkappa}{2} \\[2mm] p_z\sin\varkappa + 2p_xp_y\sin^2\dfrac{\varkappa}{2} \\[2mm] -p_y\sin\varkappa + 2p_xp_z\sin^2\dfrac{\varkappa}{2} \end{bmatrix}$$

$$\begin{array}{ccc} 2p_xp_y\sin^2\dfrac{\varkappa}{2} - p_z\sin\varkappa & \quad p_y\sin\varkappa + 2p_xp_z\sin^2\dfrac{\varkappa}{2} & \quad \\[2mm] 2p_y^2\sin^2\dfrac{\varkappa}{2} + \cos\varkappa & \quad -p_x\sin\varkappa + 2p_yp_z\sin^2\dfrac{\varkappa}{2} & \quad, \\[2mm] 2p_yp_z\sin^2\varkappa + p_x\sin\varkappa & \quad \cos\varkappa + 2p_z^2\sin\dfrac{\varkappa}{2} & \end{array}$$

where $\varkappa$ is the angle of rotation of the refracted beam (output beam) with respect to the incident (input) beam and p_x, p_y, and p_z are projections of the unit vector of the edge of the wedge onto the corresponding coordinate axes.

Angle $\varkappa$ for a wedge with small refracting angle θ is equal to

$$\varkappa \approx \Theta\left(1 - \sqrt{n^2 + (n^2 - 1)\,\text{tg}^2\gamma}\,\right) \approx$$
$$\approx \sigma(1 - n)\left(1 + \frac{n+1}{2n}\,\text{tg}^2\gamma\right).$$

The value of angle $\mathbf{æ}$ in the first approximation (at small angles and at angles of incidence γ not more than $45°$) is dependent only on the angle of incidence of the beam on the wedge and is independent of the orientation of the plane of incidence with respect to the principal cross-section of the wedge.

A wedge with variable refracting beam can also be used. This type of wedge can be formed by two methods: by using two glass plates, mounted with the capability of rotating about two mutually perpendicular axes, or by a combination of positive and negative lenses that form a planoparallel plate in combination. The operation matrix of this wedge will be determined in both cases in the form of the product of two matrices $M_{КЛI}$ and $M_{КЛII}$, which differ both by the value of angle $\mathbf{æ}$ and by unit vectors of the edge of the wedge. For the case corresponding to Figure 2.8, b, we have:

$$p_\mathrm{I} = i; \quad p_\mathrm{II} = k.$$

The matrix assumes the form:

$$
M_{КЛ} =
\begin{bmatrix}
\cos\varkappa_2\left(\cos\varkappa_1 + 2\sin^2\frac{\varkappa_1}{2}\right) & -\sin\varkappa_2\left(\cos\varkappa_1 + 2\sin^2\frac{\varkappa_1}{2}\right) & 0 \\
\cos\varkappa_1\sin\varkappa_2 & \cos\varkappa_1\cos\varkappa_2 & -\sin\varkappa_1\left(\cos\varkappa_2 + 2\sin^2\frac{\varkappa_1}{2}\right) \\
0 & \sin\varkappa_1\cos\varkappa_2 & \cos\varkappa_1\left(\cos\varkappa_2 + 2\sin^2\frac{\varkappa_1}{2}\right)
\end{bmatrix}.
$$

When using a telescopic system mounted in front of the objective of the optical apparatus as a stabilization element of the image field, the angle between the direction of the beams emerging from the eyepiece and the sighting line is determined in the form of $\beta = \epsilon + \epsilon'$ or $\beta* = \epsilon + \Gamma\epsilon = \epsilon(1 + \Gamma)$, where ϵ and ϵ' are the angles of the beams and Γ is the visible magnification.

The dependence between ϵ and ϵ' can be expressed by the angular magnification of the telescopic system in the form

$$\varepsilon' = \gamma\varepsilon.$$

On the other hand, for a telescopic system, we have $\gamma = \Gamma - f'_{o6}/f'_{oK}$, and $\varepsilon' = -\varepsilon f'_{o6}/f'_{oK}$.

The angle between the direction of the beams emerging from the eyepiece and the sighting line is determined as $\beta = \epsilon + \epsilon'$ or $\beta* = \varepsilon + I\varepsilon = \varepsilon(1 + \Gamma)$.

The angle between the direction of the beams emerging from the eyepiece and the sighting line at $\gamma = -1$ is equal to the angle between the incoming beam and the sighting axis.

Image speed compensators, based on the use of fiber optic elements (VOE), can operate only when they are mounted in the image plane.

Let us consider the effect of one fiber optic element in the form of a planoparallel plate, the fibers in which are laid parallel to each other (Figure 2.8, c). The relationship of the image coordinates, located on the input and output surfaces, is determined by the following expression:

$$
\begin{bmatrix} x' \\ y' \\ z' \end{bmatrix} = \begin{bmatrix} 1 & 0 & 0 \\ 0 & 1 & 0 \\ 0 & 0 & 1 \end{bmatrix} \begin{bmatrix} x_0 \\ y_0 \\ z_0 \end{bmatrix} + \begin{bmatrix} 0 \\ \Delta \\ 0 \end{bmatrix}
$$

where Δ is the thickness of the plate.

The second term of this equation shows the operation of the fiber optic element. It is clear that rotation does not change the initial correlation of the coordinates upon rotation of the plate about axis Oy, i.e., upon multiplication of the second term by the corresponding matrix. We arrive at a trivial conclusion that a planoparallel fiber optic element with parallel placement of the fibers, perpendicular to the input and output surfaces, causes no misalignment of the transmitted image upon movement of it.

Let us consider another case when the elementary fibers in this planoparallel plate remain parallel to each other and at the same time form some constant angle (for example, ξ) with the input and output surfaces. The previous equation then assumes the form

$$
\begin{bmatrix} x' \\ y' \\ z' \end{bmatrix} = \begin{bmatrix} 1 & 0 & 0 \\ 0 & 1 & 0 \\ 0 & 0 & 1 \end{bmatrix} \begin{bmatrix} x_0 \\ y_0 \\ z_0 \end{bmatrix} + \begin{bmatrix} 1 & 0 & 0 \\ 0 & 1 & 0 \\ 0 & 0 & 1 \end{bmatrix} \begin{bmatrix} 0 \\ \Delta \\ \Delta \, \text{tg}\, \xi \end{bmatrix}.
$$

The second term is the operation matrix of the fiber optic element. If the fiber optic element is rotated about axis Oy, the operation matrix of the fiber optic element assumes the form

$$M_{ВОЭ} = \begin{bmatrix} \Delta \, \text{tg} \, \xi \, \sin \varphi \\ \Delta \\ \Delta \, \text{tg} \, \xi \, \cos \varphi \end{bmatrix}.$$

It follows from the last expression that each point of the image upon rotation of the fiber optic element by some angle φ receives identical increments with respect to the corresponding coordinate axes.

A flat fiber compensator, consisting of two lens-like fiber optic elements (Figure 2.8, d), in which the elementary light guides are arranged perpendicular to the flat surfaces and one of the plates is rigidly attached, while part 1 can rotate about the axis passing through the center of curvature of the contiguous surfaces, can be used. The image passing through the plate undergoes the following changes: part 1 is transferred from the flat surface to a cylindrical or spherical surface, and part 2 on the contrary is transferred from the cylindrical or spherical surface to the plane. Because part 1 is the movable element, the origin of the coordinates of the system can be transferred to the center of curvature of the parts (to the center of oscillation). By analogy with the previous case, the transformations of the coordinates in matrix form assume the form

$$\begin{bmatrix} x'' \\ y'' \\ z'' \end{bmatrix} = \begin{bmatrix} 1 & 0 & 0 \\ 0 & 1 & 0 \\ 0 & 0 & 1 \end{bmatrix} \begin{bmatrix} x_0 \\ -y_0 \\ z_0 \end{bmatrix} + \begin{bmatrix} 1 & 0 & 0 \\ 0 & 1 & 0 \\ 0 & 0 & 1 \end{bmatrix} \times$$

$$\times \begin{bmatrix} 0 \\ \sqrt{r^2 - z_{0\,max}^2} + \sqrt{r^2 - z_0^2} \\ 0 \end{bmatrix} + \begin{bmatrix} 1 & 0 & 0 \\ 0 & 1 & 0 \\ 0 & 0 & 1 \end{bmatrix} \times$$

$$\times \begin{bmatrix} 0 \\ \sqrt{r^2 - z_0^2} - (r + \Delta_0) \\ 0 \end{bmatrix},$$

where r is the radius of a sphere, $z_{0\,max}$ is the dimension of the fiber optic element along axis OZ, and Δ_0 is the total thickness of the plates.

The second term in this expression is the operation matrix of the first fiber component, while the third term is the operation matrix of the second fiber component.

When one part rotates with respect to the other about the axis passing through the center of curvature of adjacent surfaces, the elementary light guides of the first part rotate; the image with curvilinear surface to be transmitted onto a plane does not occupy the previous

position. The image is shifted, which can be used to compensate for the motion of the image, caused by other factors.

The operation matrix of the inverted first component has the form

$$
M_I = \begin{bmatrix} 0 \\ \left(\sqrt{r^2 - z_0^2} - \sqrt{r^2 - z_{0\,max}^2}\right)\cos\varphi \\ \left(\sqrt{r^2 - z_0^2} - \sqrt{r^2 - z_{0\,max}^2}\right)\sin\varphi \end{bmatrix}.
$$

Since the image detector is combined with plane A, the image will be shifted along axis Oz at the following rate due to rotation of the fiber component about axis Ox, passing through the center of curvature of the part

$$
\dot{z}_i = \left(\sqrt{r^2 - z_0^2} - \sqrt{r^2 - z_{0\,max}^2}\right)\dot{\varphi}\sin\varphi,
$$

i.e., the value of $\dot{z}_i$, variable with respect to axis Oz, also approaches zero at $z_0 = z_{0\,max}$.

2.4. Methodical Errors of Image Misalignment Stabilization System

It was shown earlier that the rate of misalignment of the image is complexly dependent on the coordinates of the image field, on the orientation of the optical device with respect to the object plane, and on the values of the angular and linear rates of displacement of the base of the optical device with respect to the object field.

Let us transform equation (1.21) to the following form to analyze the possibility of compensating for image displacement:

$$
\begin{aligned}
\dot{y}_i &= \frac{\omega_{zn}}{f}y_i^2 + \frac{v_{xn}}{H_0}y_i\sin\varphi + \frac{y_iz_i}{f}\left(\frac{v_{xn}}{H_0}\cos\varphi - \omega_{yn}\right) + \\
&\quad + z_i\left(\omega_{xn} + \frac{v_{yn}}{H_0}\cos\varphi\right) + f\left(\frac{v_{yn}}{H_0}\sin\varphi - \omega_{zn}\right) = \\
&= \omega_{xn}z_i - \omega_{yn}\frac{y_iz_i}{f} + \omega_{zn}\left(\frac{y_i^2}{f} - f\right) + \\
&\quad + \frac{v_{xn}}{H_0}\left(y_i\sin\varphi + \frac{y_iz_i}{f}\cos\varphi\right) + \frac{v_{yn}}{H_0}(z_i\cos\varphi + f\sin\varphi);
\end{aligned} \qquad (2.12)
$$

56

$$\dot{z}_i = \frac{1}{f}\left(\frac{v_{x\text{п}}}{H_0}\cos\varphi - \omega_{y\text{п}}\right)z_i^2 + \frac{z_i}{H_0}\left(v_{x\text{п}}\sin\varphi + v_{z\text{п}}\cos\varphi\right) +$$

$$+ \omega_{z\text{п}}\frac{y_i z_i}{f} - \omega_{x\text{п}}y_i + f\left(\frac{v_{z\text{п}}}{H_0}\sin\varphi + \omega_{y\text{п}}\right) =$$

$$= -\omega_{x\text{п}}y_i + \omega_{y\text{п}}\left(f - \frac{z_i^2}{f}\right) + \omega_{z\text{п}}\frac{y_i z_i}{f} +$$

$$+ \frac{v_{x\text{п}}}{H_0}\left(z_i\sin\varphi + \frac{z_i^2}{f}\cos\varphi\right) + \frac{v_{z\text{п}}}{H_0}\left(z_i\cos\varphi + f\sin\varphi\right).$$

$$(2.13)$$

It follows from the above expressions that the stabilization system can be made in the following manner to fulfill the image stabilization conditions $(\dot{z}_i = \dot{y}_i = 0)$.

1. The entire device is placed on a base, stabilized with respect to angular coordinates in inertial space. In this case, $\omega_{x\text{п}} = \omega_{y\text{п}} = \omega_{z\text{п}} = 0$. The effect of the linear velocity of the base can be compensated by shifting the photodetector or object at rates $\dot{y}_{\varphi\text{п}} = \dot{y}_i;\ \dot{z}_{\varphi\text{п}} = \dot{z}_i$.

The same effect can be achieved by introducing image shift compensators that operate in a parallel bundle of beams, which cause misalignment of the image according to the following expressions: $\omega_{z\text{к}}f = \dot{y}_{i\text{к}};\ \omega_{y\text{к}}f = -\dot{z}_{i\text{к}}$, where $\omega_{z\text{к}}$ and $\omega_{y\text{к}}$ are the additional angular velocities of the bundle of beams obtained due to introduction of the compensator, into the optical system of the device.

The compensators are used in this case to reduce the misalignment caused by the linear rate of displacement of the base.

Three-axis stabilization of the optical device and the possibility of displacement of the moving element of the optical system in two coordinates are obviously required in the case under consideration. Even in this case, total compensation of misalignment for the entire image field is possible only at $v_{x\text{п}} = 0$ and $\varphi = 90°$, i.e., if the principal optical axis of the device is perpendicular to the plane of the objects.

2. There are moving elements in the optical system of the device that guarantee rotation of the coordinate system, bound to the bundle of beams, sequentially about all three axes, or corresponding displacement of the photodetector. It is obvious that even in this case only partial compensation of image misalignment is possible.

Let displacement of the compensating elements result in an additional angular momentum of the principal optical axis. The projections of this additional angular momentum onto the axes of the device can be denoted

by ω_{xK}, ω_{yK}, and ω_{zK}. Instead of expressions (2.12) and (2.13), we find:

$$\dot{y}_i = (\omega_{x\text{п}} + \omega_{x\text{к}}) z_i + (\omega_{y\text{п}} + \omega_{y\text{к}}) \left(-\frac{y_i z_i}{f}\right) + (\omega_{z\text{п}} + \omega_{z\text{к}}) \left(\frac{y_i^2}{f} - f\right) +$$

$$+ \frac{v_{x\text{п}}}{H_0} \left(y_i \sin \varphi + \frac{y_i z_i}{f} \cos \varphi\right) + \frac{v_{y\text{п}}}{H_0} (z_i \cos \varphi + f \sin \varphi);$$

$$\dot{z}_i = -y_i (\omega_{x\text{п}} + \omega_{x\text{к}}) + (\omega_{y\text{п}} + \omega_{y\text{к}}) \left(f - \frac{z_i^2}{f}\right) +$$

$$+ (\omega_{z\text{п}} + \omega_{z\text{к}}) \frac{y_i z_i}{f} + \frac{v_{x\text{п}}}{H_0} \left(z_i \sin \varphi + \frac{z_i^2}{f} \cos \varphi\right) +$$

$$+ \frac{v_{z\text{п}}}{H_0} (z_i \cos \varphi + f \sin \varphi).$$

The condition of image stabilization $\dot{y}_i = \dot{z}_i = 0$ can be fulfilled, for example, if $\omega_{x\text{п}} = -\omega_{x\text{к}}$, $\omega_{y\text{п}} = -\omega_{y\text{к}}$. We find for ω_{zK} from equations (2.12) and (2.13):

$$-(\omega_{z\text{п}} + \omega_{z\text{к}}) = f (v_{x\text{п}} y_i + v_{y\text{п}} f) \frac{\sin \varphi + \frac{z_i}{f} \cos \varphi}{H_0 \left(y_i^2 - f^2\right)};$$

$$-(\omega_{z\text{п}} + \omega_{z\text{к}}) = f (v_{x\text{п}} z_i + v_{z\text{п}} f) \frac{\sin \varphi + \frac{z_i}{f} \cos \varphi}{H_0 z_i y_i}.$$

Adding these equations, we find

$$\omega_{z\text{к}} = -\omega_{z\text{п}} - \frac{f}{2H_0} \left(\sin \varphi + \frac{z_i}{f} \cos \varphi\right) \times$$

$$\times \left[v_{x\text{п}} \left(\frac{y_i}{y_i^2 - f^2} + \frac{1}{y_i}\right) + v_{y\text{п}} \frac{f}{y_i^2 - f^2} + v_{z\text{п}} \frac{f}{z_i y_i}\right].$$

It follows from the last expression that the linear velocity of the base can not be completely compensated at all points of the frame.

In the center of the frame, $y_i = z_i = 0$ and instead of equations (2.12) and (2.13), we find:

$$\dot{y}_i = -(\omega_{z\text{п}} + \omega_{z\text{к}}) f + \frac{v_{y\text{п}}}{H_0} f \sin \varphi;$$

$$\dot{z}_i = (\omega_{y\text{п}} + \omega_{y\text{к}}) f + \frac{v_{z\text{п}}}{H_0} f \sin \varphi.$$

58

The image misalignment in the center of the frame should be compensated

$$\omega_{z\kappa} = -\omega_{z\pi} + \frac{v_{y\pi}}{H_0} \sin \varphi;$$

$$\omega_{y\kappa} = -\omega_{y\pi} - \frac{v_{z\pi}}{H_0} \sin \varphi.$$

The stabilization error is determined in the following manner:

$$\Delta \dot{y}_i = \omega_{x\pi} z_i + \frac{v_{z\pi}}{H_0} \frac{y_i z_i}{f} \sin \varphi + \frac{v_{y\pi}}{H_0} f \left[\frac{y_i^2}{f^2} \sin \varphi + \frac{z_i}{f} \cos \varphi \right] +$$

$$+ \frac{v_{x\pi}}{H_0} y_i \left(\sin \varphi + \frac{z_i}{f} \cos \varphi \right);$$

$$\Delta \dot{z}_i = -\omega_{x\pi} y_i + \frac{v_{x\pi}}{H_0} z_i \left(\sin \varphi + \frac{z_i}{f} \cos \varphi \right) +$$

$$+ \frac{v_{y\pi}}{H_0} \sin \varphi \frac{y_i z_i}{f} + \frac{v_{z\pi}}{H_0} z_i \left(\cos \varphi + \frac{z_i}{f} \sin \varphi \right).$$

Compensating actions by integral estimates of misalignment of the image must be introduced when the parts of the image over the entire field of the frame are important.

Integrating the input eauations (2.12) and (2.13), we find the mean values of the velocities:

$$\dot{y}_i^{\text{cp}} = \frac{1}{z_m y_m} \int_{-z_m}^{z_m} \int_{-y_m}^{y_m} \dot{y}_i \, dz_i \, dy_i = \omega_{z\pi} \left(\frac{2}{3} \frac{y_m^2}{f} - f \right) + v_{y\pi} \frac{f}{H_0} \sin \varphi; \qquad (2.14)$$

$$\dot{z}_i^{\text{cp}} = \frac{1}{z_m y_m} \int_{-z_m}^{z_m} \int_{-y_m}^{y_m} \dot{z}_i \, dz_i \, dy_i = \omega_{y\pi} \left(f - \frac{2}{3} \frac{z_m^2}{f} \right) + v_{z\pi} \frac{f}{H_0} \sin \varphi. \qquad (2.15)$$

The image stabilization system realizes the relation $\dot{y}_i^{\text{cp}} = \dot{z}_i^{\text{cp}} = 0$. Let compensation (as before) be determined by introduction of displacements $\omega_{z\text{K}}$ and $\omega_{y\text{K}}$.

We then find from expressions (2.14) and (2.15):

$$\omega_{z\text{к}} = v_{y\text{п}} \frac{f^2}{H_0} \sin \varphi \frac{1}{f^2 - \frac{2}{3} y_m^2} - \omega_{z\text{п}};$$

$$\omega_{y\text{к}} = v_{z\text{к}} \frac{f^2}{H_0} \sin \varphi \frac{1}{\frac{2}{3} z_m^2 - f^2} - \omega_{y\text{п}}.$$

Having substituted these values into input expressions (2.12) and (2.13), we find the remaining misalignment of the image

$$\Delta \dot{y}_i = \omega_{x\text{п}} z_i - \frac{y_i z_i}{f} v_{z\text{п}} \frac{f^2}{H_0} \frac{\sin \varphi}{\frac{2}{3} z_m^2 - f^2} +$$

$$+ v_{y\text{п}} \frac{f}{H_0} (y_i^2 - f^2) \frac{\sin \varphi}{f^2 - \frac{2}{3} y_m^2} + v_{y\text{п}} \frac{f}{H_0} \left(\sin \varphi + \frac{z_i}{f} \cos \varphi \right) +$$

$$+ v_{x\text{п}} \frac{y_i}{H_0} \left(\sin \varphi + \frac{z_i}{f} \cos \varphi \right) =$$

$$= \omega_{x\text{п}} z_i + v_{x\text{п}} \frac{y_i}{H_0} \left(\sin \varphi + \frac{z_i}{f} \cos \varphi \right) + v_{y\text{п}} \frac{f}{H_0} \sin \varphi \frac{\frac{2}{3} y_m^2 - y_i^2}{\frac{2}{3} y_m^2 - f^2};$$

$$\Delta \dot{z}_i = -\omega_{x\text{п}} y_i + v_{z\text{п}} \frac{f}{H_0} \sin \varphi \frac{\frac{2}{3} z_m^2 - z_i^2}{\frac{2}{3} z_m^2 - f^2} +$$

$$+ v_{x\text{п}} \frac{z_i}{H_0} \left(\sin \varphi + \frac{z_i}{f} \cos \varphi \right).$$

We have at the origin $z_i = y_i = 0$. Then at $f \gg z_m$, we have:

$$\Delta \dot{z}_i \approx -v_{z\text{п}} \frac{2}{3} \frac{z_m^2}{f H_0} \sin \varphi; \quad \Delta \dot{y}_i \approx -v_{y\text{п}} \frac{2}{3} \frac{y_m^2}{f H_0} \sin \varphi.$$

The derived expressions permit one to perform comparative analysis of the engineering capabilities of image misalignment stabilization systems, which are designed by using different information devices and image misalignment compensation devices.

60

Chapter 3. Functional Image Stabilization Devices

3.1. Stabilization Devices With Optical Wedges

One of the methods of solving the problem of stabilizing the position of
a beam in space upon rotations of an optical system about two mutually
perpendicular axes is to use an optical wedge with variable angle of
refraction with the corresponding rotation of the edge of the wedge.
Both glass wedge systems and liquid wedges are used.

Let us consider the possible design versions of these devices.

Stabilization devices with optical wedges, formed by lenses. The
operation matrix of an optical wedge with variable angle of refraction,
which permits one to calculate the path of the beam at any angle of
incidence of it on the optical wedge, was presented in the previous
chapter. Since the optical axis is perpendicular at the initial moment
to the input edge of the wedge, one can limit oneself to consideration
of the paraxial beams to evaluate one or another design of an optical
wedge compensator. Let us consider optical wedge compensation devices
with variable deflection angle, in which a pair of contiguous optical
lenses is used, and one of the lenses is attached such that it can be
shifted in two mutually perpendicular directions with respect to the
center of curvature of the surfaces of the adjacent parts (Figure 3.1).
All the surfaces of the adjacent lenses can generally have a radius of
curvature. The angular displacement of the beam is then determined by
the following function (Footnote) (Japanese patent 56-23125):

$$\varkappa = \frac{n_1 - n_0}{n_1 n_3} \left(1 + \frac{R_2 + d_1}{R_1} \right) \left\{ \frac{n_2 + n_3}{R_3} d_1 + \right. \tag{3.1}$$
$$\left. + \left[\left(\frac{d_2}{R_3} + 1 \right) (n_2 - n_3) + n_3 \right] \frac{n_1 R_2 - (n_2 - n_1)}{n_2 R_2} \right\} \Theta,$$

while the rate of deflection is determined by the following relation

$$\dot{\varkappa} = \frac{n_1 - n_0}{n_1 n_3} \left(1 + \frac{R_2 + d_1}{R_1} \right) \left\{ \frac{n_2 + n_3}{R_3} d_1 + \right. \tag{3.2}$$
$$\left. + \left[\left(\frac{d_2}{R_3} + 1 \right) (n_2 - n_3) + n_3 \right] \frac{n_1 R_2 - (n_2 - n_1)}{n_2 R_2} \right\} \dot{\Theta},$$

where $\varkappa$ is the angle of deflection of the beam, i.e., the angle between
the incident and output beams, R_1, R_2, and R_3 are the radii of curvature
of the corresponding surfaces of adjacent lenses, n_0, n_1, n_2, and n_3 are

61

the refractive indices of the media and marks of glass from which the lenses are made, θ is the angle of rotation of the movable lens, and d_1 and d_2 are the thickness of the lenses along their optical axis.
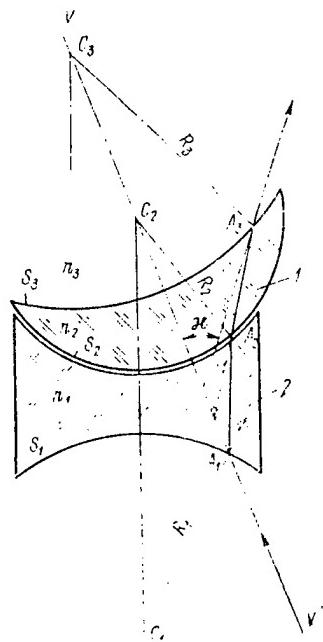

Figure 3.1. Optical Wedge Formed by Two Lenses:
1--moving; 2--fixed

It is assumed in derivation of formula (3.1) that $\sin \Theta = \Theta$, $\sin i = i$,

$\operatorname{tg} \Theta = \Theta$, $\operatorname{tg} i = i$, $\cos \Theta = 1$, $\cos i = 1$.

Formula (3.1) permits one to calculate the misalignment of the beam at any ratios of the radii of curvature and of the thickness of the lenses. Moreover, it permits one to determine the misalignment of the image when the system is operating from a finite distance, and also when estimating the effect of shifting the image during misalignment of the lenses.   In the specific case during operation of an optical device with infinite distance, i.e., in parallel beams and when using a combination of planoconvex and planoconcave lenses having identical refractive index in the stabilization system, i.e., at $n_0 = n_3 = 1$, $n_2 = n_1 = n$ and $R_1 = = R_3 = \infty$, formula (3.1) assumes the following form:

$$\varkappa = (n - 1)\,\Theta. \qquad (3.3)$$

Several identical pairs of lenses, which permit one to increase the angle of deflection of the sighting axis of the device, can generally be

mounted in front of the objective. The optical accessory should be afocal in order that the wedge compensators not change the parameters of the system itself. The following condition must be fulfilled

$$\sum_{i=1}^{N} \Phi_i = 0, \qquad (3.4)$$

where Φ is the optical intensity of the lenses and N is the number of lenses. (Footnote) (U.S. patent 3,959,088)

The design of such a complex wedge compensator is simplified considerably if the centers of curvature of all the lenses are joined at one point. The movable lenses can be combined and synchronous rotation of them from one motor can thus be guaranteed. The condition of the afocal nature of the system will thus assume the form

$$\sum_{i=1}^{N} R_i \Phi_i = 1, \qquad (3.5)$$

where R_i is the distance from the nodal point of the i-th lens to the center of rotation. Taking into account that $\Phi = 1/f'$, function (3.5) can be represented in the form

$$\sum_{i=1}^{N} \frac{R_i}{f_i'} = 1. \qquad (3.6)$$

It follows from formula (3.6) that the condition $R = f'$ should be fulfilled when using a single pair of lenses.

The total angle by which the beam is deflected after passing through the system, consisting of several pairs of lenses, is equal to $\sum_{i=1}^{N} (n_i - 1)\,\Theta$, where N is the number of pairs of lenses. It is understandable that the following relation must be fulfilled to retain the position of the sighting axis in space

$$\sum_{i=1}^{N} (n_i - 1)\,\Theta_i = \Theta, \qquad (3.7)$$

i.e., from the equality of the angles of rotation of the sighting axis of the device θ and the angles of rotation of the lenses θ_i follows:

63

$$\sum_{i=1}^{N} (n_i - 1) = 1, \qquad (3.8)$$

or

$$\sum_{i=1}^{N} n_i = 1 + N. \qquad (3.9)$$

For example, when using two pairs of lenses, the total of the refractive indices for parametric stabilization of the axis of the device should be equal to $n_1 + n_2 = 3$.
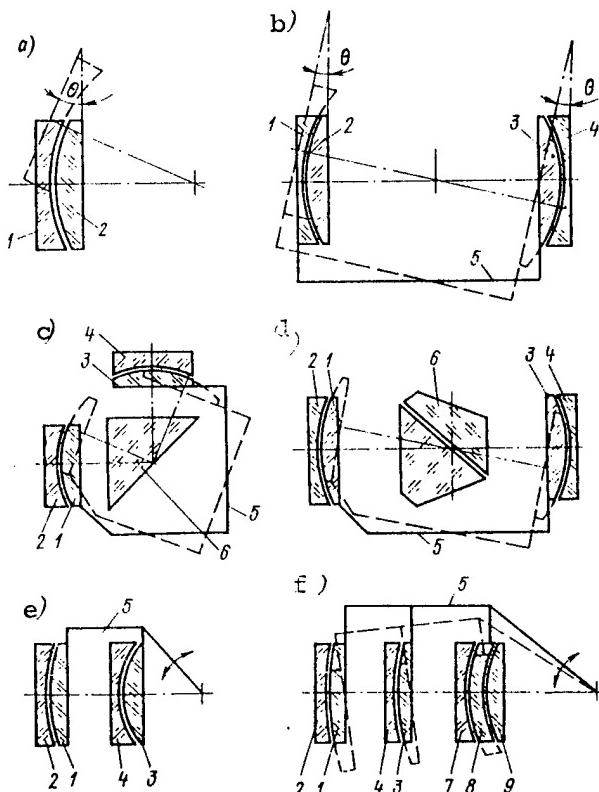

Figure 3.2. Layouts of Stabilization Devices
With Optical Wedges, Formed:
a--by one pair of lenses; b, c, d, e--by two pairs of
lenses; f--by three pair of lenses; 1, 3, 8--movable
lenses; 2, 4, 7, 9--fixed lenses; 5--mechanical coupling;
6--rotating element

One can assume from general concepts of design of optical systems that additional optical systems with magnification equal to Γ are mounted in front of one or several pairs of movable lenses. Function (3.6) then assumes the form

$$\sum_{i=1}^{N} (R_i/f'_i)\Gamma_i = 1. \qquad (3.10)$$

Magnification Γ equal to +1 should be used in expression (3.10) for all pairs of lenses that do not operate with additional optical systems having magnification Γ_i. If rotating systems (for example, mirrors or prisms) are mounted between pairs of lenses, magnification Γ in formula (3.10) should be assumed equal to -1. The functional solutions of these compensators are presented in Table 3.2. Specifically, the simplest layout of an image field stabilization device, consisting of two lenses—a planoconvex 2 and planoconcave 1, is presented in Figure 3.2, a. This stabilizer can automatically stabilize the sighting axis at specific reduction coefficient k_p, which links the angle of rotation of the device to that of the movable lens. It follows from expression (3.7) that it will be determined by the ratio $k_K = 1/(n - 1)$ for a single pair of lenses.

Specifically, the angle of rotation of the lens should be twofold greater than that of the device at n = 1.5. Automatic reducerless stabilization can also be achieved by using high-density glass, the refractive index of which is equal to 2. It also follows from expressions (3.7) and (3.9) that automatic reducerless stabilization of the optical axis is also possible when using widely distributed marks of glass; two pairs of wedge compensators can be used. A sufficient condition for total stabilization is fulfillment of equality (3.9) and the sum of the refractive indices of the first and second pair should be equal to 3. The parameters of the constituent lenses and the coordinates of the center of curvature of surfaces with respect to the constituent wedges are determined from expressions (3.7) and (3.6). Analysis of the possible design layouts of a reducerless stabilizer of the sighting axis, in which two pairs of lenses are used, indicates that motion to the negative lens must be provided in the first pair and motion to the positive lens must be provided in the second pair when there is a combination center of curvature between pairs of lenses (Figure 3.2, b). If rotating systems, mirrors, rectangular prism, Pechan prism with covers and similar optical elements having magnification of -1 (Figure 3.2, c and d) are introduced between the pairs of lenses, the lenses of the same type in both pairs becomes fixed. The design of the device, especially sealing of it, is simplified considerably. A version in which the lens is not rotated, but is displaced positively in a direction perpendicular to the optical axis of the instrument, is also possible.

The overall dimensions of the stabilization device are reduced if the design layout shown in Figure 3.2, e is used. This layout provides for the use of moving optical elemnts of the same type, which have combined centers of curvature. The radii of curvature of these elements have identical sign and are not equal to each other.

Chromatic aberrations, which occur as a result of variance in the optical wedges, introduced the greatest errors in wedge systems mounted in parallel beams. To reduce them, the system is achromatized, introducing yet another pair of lenses, which has chromatic aberration of opposite sign.
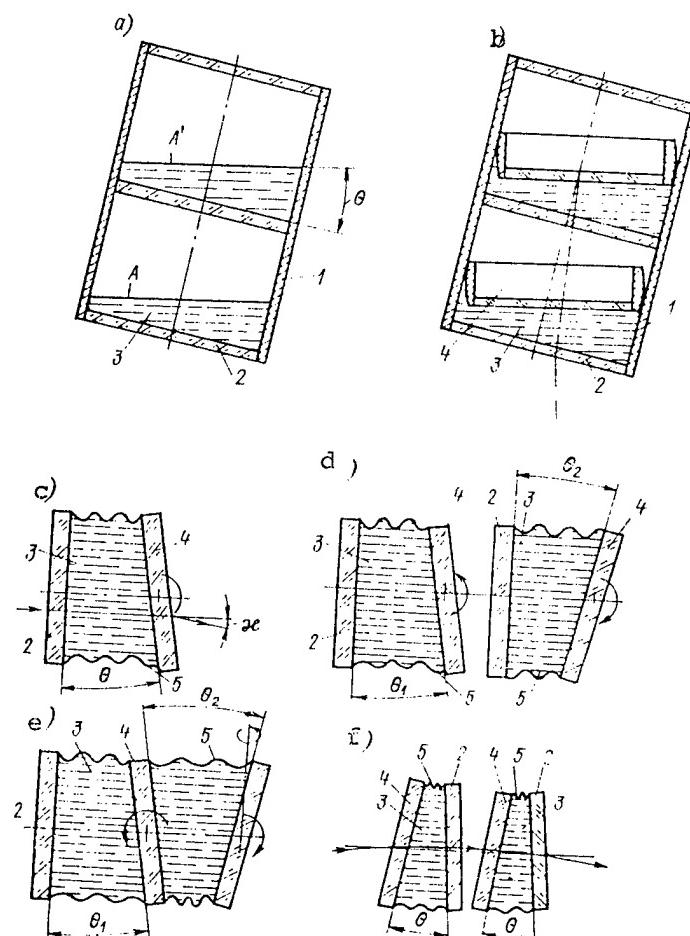

Figure 3.3. Layouts of Stabilization Devices With
Liquid Optical Devices:
a, b--liquid inertial wedges; c--single liquid wedge;
d, e, f--pair of liquid wedges; 1--cylindrical vessel
2--planoparallel glass plate; 3--liquid; 4--movable
planoparallel glass plate; 5--elastic corrugation

The condition of stabilization of an image by an achromatized wedge system of this type can be expressed in the form of changes of the deflection of a medium-wavelength beam in crown and flint pairs of optical compensator elements. It is necessary for reducerless stabilization of the image that the total deflection of the system of beams be equal to the angle of deflection of the body of the device

$$\sum_{i=1}^{m} \Theta_{\kappa i} - \sum_{l=1}^{p} \Theta_{\phi l} = \Theta, \qquad (3.11)$$

where $\theta_{\kappa i}$ and $\theta_{\phi 1}$ are deflection of the beams by crown and flint pairs, respectively.

Function (3.7) with regard to relations (3.11) then assumes the form

$$\sum_{i=1}^{m} (n_{\kappa i} - 1) - \sum_{l=1}^{p} (n_{\phi l} - 1) = 1. \qquad (3.12)$$

One of the possible layouts of the achromatic optical axis wedge stabilizer system, in which element 3 is an element of achromatization, is presented in Figure 3.2, f. It invludes four lenses, two of which are glued and are the movable component.

Stabilization devices with liquid optical wedges. Liquid wedge compensators (Figure 3.3) are equivalent in the effect of compensating for the rate of motion of the image or stabilization of the optical axis of the device in space to the above glass wedge compensators.

The first sighting axis stabilization systems using liquid wedges were inertial and had individual containers. The open surfaces of the liquids, enclosed in the containers, retained their position in space during all possible rotations of the container itself.

It is pointed out in [45] that liquid wedges were used successfully in levels by G. Yu. Stoldokeveich in 1946. N. A. Gusev developed the theory of liquid inertial wedges [26]. Liquid wedges, based on this principle, consist of a cylindrical vessel and two chambers, having three sequentially arranged planoparallel optical plates (Figure 3.3) [12]. The layers of liquid are of constant thickness in the neutral position, i.e., when the optical axis of the apparatus is perpendicular to the earth's surface, and the system is a planoparallel plate. The input planoparallel plates also rotate together with the cylinder upon rotation of the apparatus about axes x or y by angle θ. The surfaces of the liquid A and A', due to the earth's gravity, remain parallel to the earth's surface as before, i.e., optical wedges are formed between surfaces A and A' and between the corresponding inclined input windows.

67

If the sum of the refractive indices of the liquids are equal to 3, two chambers are sufficient for stabilization of the optical axis of the device according to condition (3.9). This type of compensators is used extensively in surveyor's instruments [12].

The main factors that reduce the accuracy of stabilizing the sighting beam of a compensator of given type are temperature variations of the refractive index of the liquid. The temperature range in which the liquid compensator provides the necessary stabilization accuracy upon inclination by angle θ is determined by the following formula:

$$\Delta t = \delta_i/(2\Theta \; \Delta n_t),$$

(3.13)

where δ_i is the permissible angular error of stabilizing the sighting beam and Δn_t is the temperature coefficient of the refractive index of the liquid.

Capillary phenomena will affect the accuracy of sighting in a liquid compensator with open surface. The surface of the liquid will assume the form of a lens rather than being flat. The radius of curvature R_K of the liquid surface in a cylindrical vessel is expressed by the function

$$R_{\kappa} = a^2/h_1,$$

(3.14)

where a is the capillary constant of the liquid and h_i is the capillary rise of the liquid along the axis of the vessel.

The value h_1 is found from the expression

$$h_1 = 4 \sqrt{2\pi} \; \text{tg} \, \frac{1}{2} \left(\frac{\pi}{4} - \frac{\Theta_{\kappa}}{2} \right) \frac{\sqrt{ar}}{\sqrt[4]{r_1}} \exp\left(-\frac{r_1\sqrt{2}}{a} \right),$$

(3.15)

where r_1 is the internal radius of the vessel and $r_1 = r + a\sqrt{2} - a\sqrt{1 - \sin\Theta_{\kappa}}$ and θ_K is the boundary angle of the liquid.
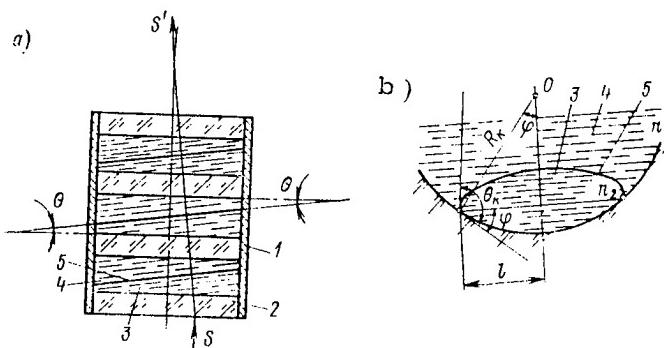
Figure 3.4. Diagrams of Stabilization Devices Using
Nonmiscible Liquids:
a--optical wedges with flat surfaces; b--optical
wedges formed by liquid lenses: 1--cylindrical
vessel; 2--planoparallel glass plate; 3, 4--
nonmiscible liquids with different refractive
indices; 5--interface of media

Thus, we find a radius of curvature of the surface of R_K = 67 mm for a
benzyl acetate-dimethyl phthlate mixture whose capillary constant is a =
= 2.53 mm in a glass tube 16 mm in diameter at θ_K = 24° by formulas
(3.14) and (3.15), i.e., the surface of the liquid has rather large
curvature and accordingly the lens formed by this surface also has high
optical intensity. To eliminate the effect of capillary phenomena on
the accuracy of stabilizing the axis without changing the design of the
compensator, either the diameter of the tube must be increased or a
correcting lens, which forms an afocal system in combination with the
liquid lens, must be introduced into the optical system [12, 24].

The stabilization errors can be reduced considerably without changing
the diameter of the tube if floating planoparallel glass plates are also
introduced into each chamber (Figure 3.3, b). (Footnote) (U.S. patent
3,655,274)

Some liquids are not miscible with each other. The use of these liquids
permitted one to develop essentially new designs of optical liquid
wedges for stabilization systems. Diagrams of these liquid compensators
are presented in Figure 3.4, a and b.

Nonmiscible liquids in a closed space were used in the first case [25,
45]. The compensator consists of three sections, each of which contains
two layers of liquid (Figure 3.4, a).

69

Based on condition (3.9), the difference of the refraction of the liquids (upper and lower) should be $n_B - n_H \approx 0.333$ for automatic stabilization of the sighting axis.

It is pointed out in [45] that this compensator can be realized when using liquids in the form of a mixture of α-methylnaphthaline and toluene for the top layer and perfluoroethylamine for the bottom layer. It is noted that perfluoroethylamine has greater density than a mixture of α-methylnaphthaline and toluene, while the refractive index of perfluoroethylamine is less. The latter means that a three-chamber compensator using these liquids will stabilize the beams when they pass in the bottom-upward direction.

A diagram of a two-liquid compensator, in which the liquids are separated by a sphere rather than through the plane, is presented in Figure 3.4, b [13]. The compensator consists of a tube, which has a spherical bottom. The tube is filled with liquid having refractive index n_1. A positive liquid lens, formed by capillary forces whose refractive index is equal to n_2, is located inside this liquid on the bottom of the tube.

Misalignment of the beam as a function of n_1 and n_2 without regard to the refractive index and radius of curvature of the tube R_a is determined by general formula (3.1).

It is shown in [13] with regard to these factors that the following relation must be fulfilled to stabilize the sighting axis of the device in space:

$$R_a = R_{\kappa} \frac{n_2 (n_{CT} - 1)}{n_{CT} (n_1 - n_2)}, \qquad (3.16)$$

where R_{κ} is the radius of curvature of the interface of the two liquids at point O--the middle of the liquid lens, n_1 and n_2 are the refractive indices of the liquids, and n_{CT} is the refractive index of glass.

The radius of curvature of the interface of the two liquids at point O is calculated by the formula

$$R_{\kappa} = \frac{a^2 \operatorname{ctg} \frac{\Theta_{\kappa}}{4}}{4 \sqrt{a l \pi \sqrt{2}}} \exp\left(\frac{l \sqrt{2}}{a} + 4 \sin^2 \frac{\Theta_{\kappa}}{4}\right), \qquad (3.17)$$

where a is the capillary constant at the interface of two liquids, 1 is the dimension of the positive liquid lens along the horizontal (see

70

Figure 3.4, b), and θ_K is the boundary angle of the interface of two liquids at the point of contact with the surface of the bottom of the tube.

The use of inertial liquid wedges in optical devices with large diameters of the entrance pupil of the system (up to 200 mm) results in an unsubstantiated increase of the overall dimensions and mass of the system; therefore, liquid wedges with forced variation of the refracting angle are of interest.

It follows from Figure 3.3, c that the wedge is two planoparallel glass plates attached by an elastic corrugation. The cavity of the corrugation is filled with liquid. (Footnote) (U.S. patent 3,212,420) One of the glass plates is rigidly attached to the body of the optical device, while the other plate is mounted in a gimbal suspension and can rotate in a small range, forming a wedge with variable angle at the vertex. The variation of the angle of the wedge (as well as of the azimuth of its edge) is monitored by a servo system, controlled from angular-rate sensors. Different design versions of liquid wedges are possible. Specifically, the functional diagrams of two liquid wedges are shown in Figure 3.3, d, e, and f. The design of the wedges shown in Figure 3.3, f was developed for stabilizing the position of a light beam in laser communication lines, but this design can also be used in imaging devices [25]. The operating principle of the given device follows from Figure 3.3, f. There are two liquid wedges, in each of which one planoparallel plate is directly attached to the device, while the other two plates, connected to each other, are mounted on the movable chassis of the device and are moved by the corresponding drives.

The azimuth of the variable angle can generally be changed by a simpler method, by rotating the planoparallel plates about mutually perpendicular axes, which in turn are perpendicular to the optical axis of the objective (Figure 3.3, e).

The range of application of wedge compensators is limited by the chromatic aberration, the permissible value of which for estimating calculations can be determined from the following expression:

$$d\varkappa = dn\theta \leqslant \frac{1}{2} \delta_{доп},$$

(3.18)

where $\delta_{доп}$ is the angular resolution of the system.

More complicated designs of wedge compensators, which envision the use of liquids having different refractive indices and variances, should be used to eliminate chromatism. It is known that an optical wedge consisting of two optical wedges will deflect the beams by angle æ and

does not have chromatic aberration if the following ratios are fulfilled:

$$\varkappa = (n_1 - 1)\,\Theta_1 + (n_2 - 1)\,\Theta_2; \qquad (3.19)$$

$$(n_1 - 1)\,\frac{\Theta_1}{v_1} + (n_2 - n_1)\,\frac{\Theta_2}{v_2} = 0. \qquad (3.20)$$

Solving system of equations (3.19) and (3.20) with respect to angles θ_1 and θ_2, we find:

$$\left.\begin{array}{l} \Theta_1 = \dfrac{1}{n_1 - 1}\dfrac{1}{v_1 - v_2}\varkappa; \\[2mm] \Theta_2 = -\dfrac{1}{n_2 - 1}\dfrac{v_2}{v_1 - v_2}\varkappa. \end{array}\right\} \qquad (3.21)$$

The given functions permit one to determine the corresponding operating logic of a liquid optical wedge system and to achieve dynamic correction of the chromatism of this system, which is impossible in a stabilization system in which glass wedges are used.

If the requirements on the chromatic aberration are low, these designs can be used to achieve rough and precise stabilization of the position of the beam.

Thus, liquid optical wedges with induced variation of the angle of refraction have a number of advantages over glass and inertial liquid wedges with respect to guaranteeing a variable angle of refraction of the wedge over time. The main advantages of liquid wedges is the fact that the refracting angle of these wedges is varied by rotation of a comparatively thin planoparallel plate. First, this permits one to provide a variable wedge at large luminous diameters of the optical system with small thickness of the wedge and, secondly, it permits a considerable reduction of the mass of the movable part, which in turn permits a reduction of the energy consumption of the entire system. Third, it permits one to reduce the overall dimensions of the entire optical compensator, since the rotational axis of the planoparallel plate essentially coincides with the plane of the plate itself. This advantage becomes obvious when compared to the design of a reductionless two-wedge compensator (see Figure 3.2, b), in which the lens module must be rotated about the combined center of curvature.

Although engineering realization of optical liquid wedges is undoubtedly more complicated than traditional glass compensators, their advantages in a number of cases are superior to the disadvantages; therefore,

72

optical liquid wedges have been used in devices of different designation, for example, in television, movie and still cameras, surveyor's instruments and so on.

The Dynasciences Corporation has achieved the greatest success in development of liquid wedge compensators. This company conducted careful studies during the period from 1962 through 1965 of the system of an optical liquid wedge and development of its design. (Footnote) (U.S. patent 3,910,693) Small control systems were developed as a result that achieve programmable rotation of planoparallel plates, where small high-speed gyroscopes were used as the information channel. Practically all modifications of the liquid wedges of this company operate with a stabilization time constant T_c of approximately 1 second.

The time constant is understood as the value determined by the expression $T_c = 1/(2\omega_c)$, where ω_c is the cutoff frequency of the system. This company has developed a number of modifications, which are distinguished by the diameter of the input aperture and by accuracy characteristics. Moreover, the price of the accessory fluctuates considerably as a function of these parameters.

Thus, the Vibra Stop Lens, having a mass of 1.2 kg, diameter of 120 mm, and thickness of 122 mm, was developed to stabilize the image in cameras and laser and IR systems. The light diameter of the accessory is 60 mm and light transmission is 95 percent [95].

The Dynalens So-38 accessory was developed for a camera mounted on helicopters and operates successfully with an objective having f′ up to 1,000 mm and aperture ratio of 1:11 at shutter speed of 1/125 s.

It should be noted that the company does not develop a universal system, suitable for all possible cases, but develops specific accessories based on one model. Thus, the XM-76 accessory has been developed for a vertical observation system, the SO-35 and SO-60 accessories have been developed for working with the objectives of variable focal distance of television cameras, and the P-060-01 accessory has been developed for nontopigraphic frame aerial cameras of the KA-45, KA-51, KA-53, and KS-72 type. (Footnote) (Prospectus of Dynasciences Corporation)

The specifications of two accessories, the T-030 and T-060, which permit one to judge the capabilities of these systems, are presented below.

Analyzing the applicability of image stabilization systems through the use of liquid wedges without introducing achromatization systems, one can conclude that the correction angle is in the range of $\pm 5°$.

Further studies in development of more improved designs of liquid compensators resulted in development of an inertial compensator, capable of operating with essentially various types of initial orientations of the device. (Footnote) (U.S. patent 3,941,451)

	T-030	T-060
Range of compensation angles, °	±3	+1.8
Effective aperture, mm	76.2	162.4
Band width for λ = 380-780 nm,		
percent	95	95
Readiness time to operation, min	2	2
Overall dimensions, mm:		
diameter	177	300
length	100	127
Dimensions of power module, mm	280 × 220 × 150	160 × 135 × 125
Mass of head, kg	1.64	6.35
Mass of power module, kg	1.72	3.26
Mass of charging battery, kg	2.05	2.05

This compensator consists of a closed liquid-filled vessel, in which there are two tubes formed of planoparallel plates, free of liquid. The design of the tubes ensures on the one hand that they are sealed and on the other hand that one of the plates can rotate in each tube. The rotary plates, due to the effect of the earth's gravity, will try to maintain their position in space and will thus create a pair of wedges, and will also guarantee fulfillment of the stabilization condition (3.9).

Stabilization devices with rotary optical wedges. Maintenance of the optical axis of the device in space with small evolutions of the device itself was envisioned in the previous cases. This design principle is suitable both for display devices and for image recording devices. However, the position of the optical axis in space need not be retained for image recording devices, but it is sufficient to eliminate the influence of misalignment of the image on its quality. One can talk about stabilization of the image recording quality rather than about image stabilization in the ordinary understanding. In other words, the motion of the image during the time of its recording must be eliminated. To do this, various types of image motion compensation devices and specifically optical wedges, which rotate about an axis coincident to the axis of the objective, can be used. However, the design of an optical wedge compensator is complicated due to an additional mechanism that supports rotation of the entire compensator with respect to the optical axis of the device to combine the vector of the compensation motion of the image with the vector of motion of the image, caused by vibrations of the device. One of the possible compensators is a Rochon-Herschel prism [23], which consists of two identical wedges, rotated about the optical axis at identical speeds, but in opposite directions. It is easy to show that the angle of deflection of this system for paraxial beams is equal to with sufficient degree of accuracy [76]

$$\varkappa = 2\Theta \, (n - 1) \sin \xi, \qquad\qquad (3.22)$$

74

where ζ is the angle of rotation of the wedge with respect to the position in which the two wedges form a planoparallel plate.

The angular velocity of the beam is determined from the equation

$$\dot{x} = 2\Theta\dot{\xi}\,(n-1)\cos\xi, \qquad (3.23)$$

where $\dot{\zeta}$ is the angular rotational velocity of the wedges.

The speed of the image with regard to the focal distance of the objective of the device, caused by a wedge compensator, will be equal to

$$v_{из} = 2f'\Theta\dot{\xi}\,(n-1)\cos\xi. \qquad (3.24)$$

It follows from formula (3.24) that the same speed of the image can be provided both by selecting the angle of refraction of the edge θ and by the corresponding rotational frequency of the wedges. This dependence shows that the position of the sighting axis in the space of objects is not tracked in all cases (as occurred in the previous versions).
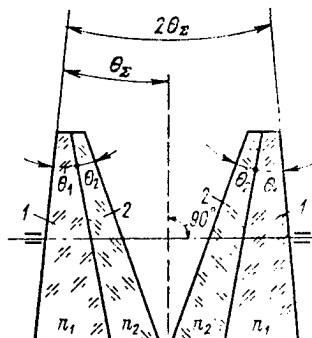

Figure 3.5. Design of Optical Wedge With Variable
Angle Without Lateral Misalignment of Axial Bundle
of Beams:
1, 2--optical wedges with different refractive indices

The problems related to the use of a Roshon-Herschel prism was studied in detail in different papers [23, 60, 76, 87] with regard to the use of it in monitoring devices, in aerial cameras, in television sets, in geodetic instruments, in rangefinders and in cameras. We note in this regard that the very first and the most important is H. Erfle's paper [87], which considered in detail the characteristic features of the

75

given prism and showed, specifically, the presence of lateral misalignment of the axial beam, which is determined by the expression

$$\varkappa_\perp = 2\Theta^3 (n - 1) \sin \xi \cos^2 \xi. \qquad (3.25)$$

The range of transverse misalignment will then be equal to

$$\dot{\varkappa}_\perp = 2\Theta^3 (n - 1) \cos \xi (1 - 3 \sin^2 \xi) \dot{\xi}. \qquad (3.26)$$

The function $\cos \xi (1 - 3 \sin^2 \xi)$ reaches extreme values at angles $\zeta = 0$, $\xi = \arccos \left(\pm \dfrac{\sqrt{2}}{3} \right)$ and $\zeta = \pi/2$. The value of $\dot{\varkappa}$ is maximum at $\zeta = 0$ and approaches zero upon rotations of the wedge by angles $\xi = \arccos \left(\pm \dfrac{\sqrt{2}}{3} \right)$ and $\zeta = p/2$.

Further analysis of the given system by N. V. Sheynis showed that lateral misalignment of the axial beam can be essentially reduced to zero, if one uses wedges of more complicated design, for example, in systems consisting of wedges having different refractive indices and glued as is shown in Figure 3.5 [80].

It is shown in [80] that the angle between the refracting input and output edges of the system also affects the lateral misalignment. The values of the angle of deflection and of the rate of deflection of the beam in the perpendicular direction will then be expressed by the following functions:

$$
\left.
\begin{aligned}
\varkappa &= 2 \sin \xi \cos^2 \xi \sum_{i=1}^{2} \Theta_i (n_\kappa - 1) \left[\Theta_\Sigma \sum_{i=1}^{2} \Theta_i \frac{n_\kappa^2 - 1}{n_\kappa} - \right. \\
&\quad \left. - \sum_{i=1}^{2} \Theta_i^2 \frac{n_\kappa - 1}{n_\kappa} - \Theta_1 \Theta_2 \frac{n_1 + n_2}{n_1 n_2} (n_2 - 1) \right]; \\
\dot{\varkappa} &= 2 \cos \xi (1 - 3 \sin^2 \xi) \dot{\xi} \sum_{i=1}^{2} \Theta_i (n_\kappa - 1) \times \\
&\quad \times \left[\Theta_\Sigma \sum_{i=1}^{2} \Theta_i \frac{n_\kappa^2 - 1}{n_\kappa} - \sum_{i=1}^{2} \Theta_i^2 \frac{n_\kappa - 1}{n_\kappa} - \right. \\
&\quad \left. - \Theta_1 \Theta_2 \frac{n_1 + n_2}{n_1 n_2} (n_2 - 1) \right],
\end{aligned}
\right\} \qquad (3.27)
$$

76

where θ_Σ is the angle at the vertex of one glued wedge.

It follows from analysis of the indicated functions that the minimal values of misalignment and velocity of an axial beam are reached if the input and output edges are perpendicular to the optical axis of the device.

3.2. Stabilization Devices With Flat Mirrors

Stabilization devices with reflecting elements are also based on flat mirrors. These devices have become widespread, since any system of flat mirrors is an aberrationless system at any path of the beams. Devices with a combination of no more than two mirrors are ordinarily used in parallel bundles of beams. Combinations of three-four mirrors are possible when using devices in rear segment. This is primarily related to the dimensions of the entrance pupil and to its angular field.

Stabilization devices with flat mirrors in parallel bundles of beams. The different versions of reflecting stabilizers are shown in Figure 3.6, a, b, and c.
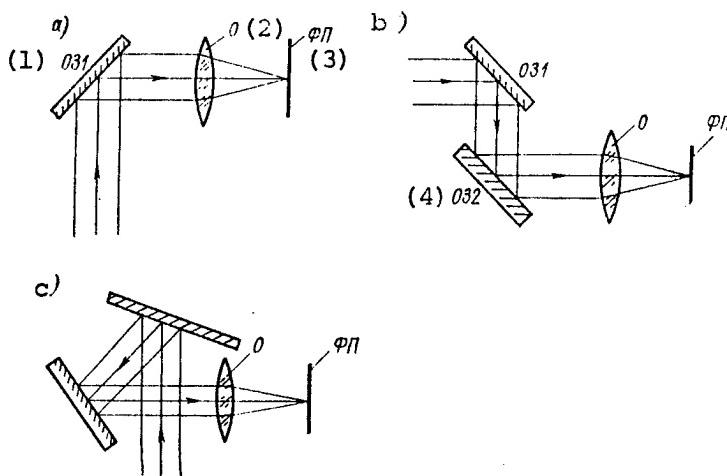

Figure 3.6. Diagrams of Stabilization Devices With Movable Flat Mirror:
a--with one movable mirror; b, c--with additional fixed mirror; OZ1--movable mirror; OZ2--fixed mirror; O--objective; FP--photodetector

KEY:
1. Movable mirror
2. Objective
3. Photodetector
4. Fixed mirror

77

Based on Chapter 1, let us consider some examples of stabilization devices that use one mirror. Let us determine for these examples, the condition of stabilization of the image field at different orientations of the apparatus, mounted on a movable base.

Example 1. The incident beam is perpendicular ot the axis of rotation of the mirror by angle α_1 (Figure 3.7). This example corresponds to the case presented in Figure 1.9, a and b at $\alpha_1 = 0$, $\alpha_2 = 45°$ and $\omega_\phi = \omega_0$.

According to equations (1.70) and (1.71), one can write:

$$\omega_{\delta x}^0 = \omega_{z0} + \dot{\alpha}_1; \quad \omega_{\delta y}^0 = \omega_{y0} + 2\dot{\alpha}_2; \quad \omega_{\delta z}^0 = \omega_{x0} + \alpha_1.$$

Hence, the condition of stabilization of the image (1.72) is written in the form:

$$\dot{\alpha}_2 = -\frac{1}{2}\,\omega_{y0}; \quad \dot{\alpha}_1 = -\omega_{x0}; \quad \dot{\alpha}_1 = -\omega_{z0}.$$

It follows from the last expressions that rotation of the mirror by angle α_1 can be used to stabilize the image only if ω_{x0} or ω_{z0} are equal to zero.
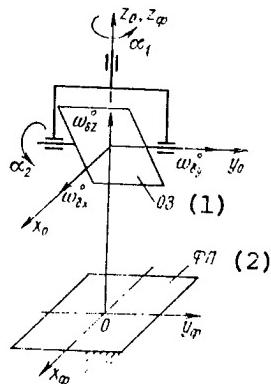

Figure 3.7. Stabilization Device With Flat Mirror
(Rotational Axis of Mirror Is Fixed)

KEY:
    1. Mirror   2. Photodetector
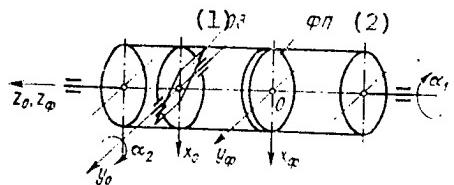
Figure 3.8. Stabilization Device With Flat Mirror
Having Additional Rotation of Axis of Mirror and
Photodetector

KEY:
1. Mirror   2. Photodetector

Example 2. Let the problem considered in example 1 be supplemented by simultaneous motion of the photodetector and mirror about axis OZ_0 by angle α_1 (Figure 3.8).

As before, if $\alpha_1 = 0$ and $\alpha_2 = 45°$, then

$$[\omega_{x\phi}\omega_{y\phi}\omega_{z\phi}]^T = [\omega_{x\pi}\omega_{y\pi}(\omega_{z\pi}+\dot{\alpha}_1)]^T.$$

Having substituted these conditions into expressions (1.70) and (1.71), we find:

$$\omega_{\delta x} = \omega_{z\pi} + \dot{\alpha}_1; \quad \omega_{\delta y} = \omega_{y\pi} + 2\dot{\alpha}_2; \quad \omega_{\delta z} = \omega_{x\pi}.$$

Hence follows the condition of stabilization of the image:

$$\dot{\alpha}_1 = -\omega_{z\pi}; \quad \dot{\alpha}_2 = -\frac{1}{2}\omega_{y\pi}.$$

To eliminate blurring of the image due to rotation of the object at angular velocity ω_{x0}, the possibility of angular misalignment of the photodetector about axis Oz_ϕ at angular velocity $\dot{\alpha}_3$ must be created;

$$\dot{\alpha}_3 = -\omega_{x\pi}.$$

Example 3. This case (Figure 3.9) corresponds to the version presented in Figure 1.10 with the following conditions: $\alpha_1 = 45°, \alpha_2 = 0, \omega_\phi = \omega_0$.

79

We find from expressions (1.72) and (1.73):

$$\omega_{\delta x} = \omega_{z\Pi} + \sqrt{2}\dot{\alpha}_2; \quad \omega_{\delta y} = \omega_{y\Pi} + 2\dot{\alpha}_1; \quad \omega_{\delta z} = \omega_{x\Pi} + \sqrt{2}\dot{\alpha}_2.$$

Thus, only the component $\omega_{y\Pi}$ can be totally compensated provided that $\dot{\alpha}_1 = -\frac{1}{2}\omega_{y\Pi}$; compensation of components $\omega_{z\Pi}$ and $\omega_{x\Pi}$ is possible (as in example 1) only if one of them is equal to zero.

On the other hand, if (as was considered above) angular displacements of the photodetector about axis Oz_ϕ at angular velocity $\dot{\alpha}_3 = -\omega_{x0} - \sqrt{2}\dot{\alpha}_2$, is introduced, the condition of total compensation of the misalignment of the image at $\dot{\alpha}_2 = 0.707\omega_{z\Pi}$ can be fulfilled.
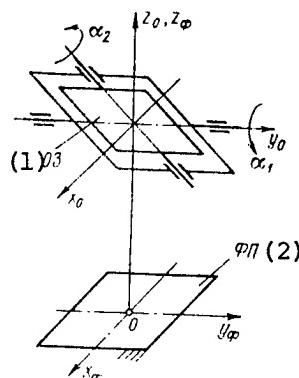

Figure 3.9. Stabilization Device With One Flat
Mirror Mounted in Gimbal

KEY:

    1. Mirror   2. Photodetector

Compared to the case considered in example 2, the mirror must be rotated by angle α_2 with somewhat lower relative velocity to fulfill the condition of compensation in the version under consideration, which may have specific advantages in design of a stabilization system.

If the possibility of angular misalignment of the photodetector about axis Oz_ϕ at angular velocity α_3 can be guaranteed, then $\omega_{\delta z} = \omega_{x\Pi} +$
$+ \dot{\alpha}_2\sqrt{2} - \alpha_3$.
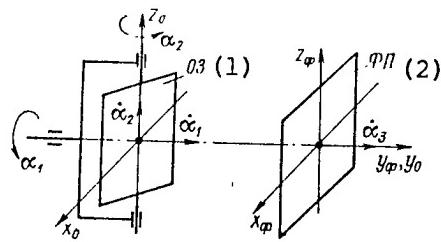
Figure 3.10. Stabilization Device With Flat Mirror
Mounted in Gimbal (Axis Oz Coincides With Plane of Mirror)

KEY:

1. Mirror   2. Photodetector

Let us assume that $\omega_{\delta x} = 0$. For this, let us assume that $\dot{\alpha}_2 = -\dfrac{1}{\sqrt{2}}\omega_{z\Pi}.$

Then to find $\omega_{\delta z} = 0$, the following should be guaranteed

$$\dot{\alpha}_3 = \omega_{x\Pi} + \sqrt{2}\,\dot{\alpha}_2 = \omega_{x\Pi} - \omega_{z\Pi}.$$

Thus, three drives must be developed for total stabilization of the image, and reduction to a gyro sensor with transfer factor 0.5 is required along axis Oy_3, while reduction $1/\sqrt{2}$ with the axis of sensitivity of the gyro sensor located along axis Oz_0 is required along axis Oz_3.

Example 4. In this case (Figure 3.10) for $\alpha_1 = 0$ and $\alpha_2 = 45°$ according to expression (1.73), we find:

$$\omega_{\delta x}^0 = -\omega_{y\Pi}\frac{\sqrt{2}}{2} - \dot{\alpha}_1\frac{\sqrt{2}}{2};$$

$$\omega_{\delta y}^0 = -\omega_{x\Pi} + \omega_{yo}\left(\frac{\sqrt{2}}{2} - 1\right) + \dot{\alpha}_1\frac{\sqrt{2}}{2};$$

$$\omega_{\delta z}^0 = \omega_{z\Pi} + 2\dot{\alpha}_2.$$

81
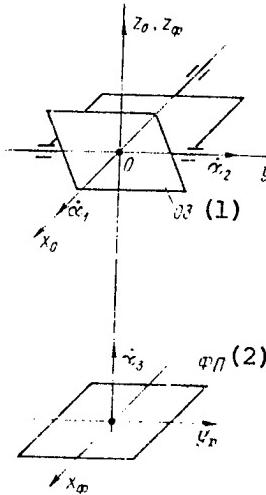
Figure 3.11. Stabilization Device With Flat
Mirror in Gimbal Suspension (Axis y
Coincides With Plane of Mirror)

KEY:

1. Mirror   2. Photodetector

Hence, we have:

$$\dot{\alpha}_2 = \frac{1}{2}\,\omega_{z\Pi}; \quad \dot{\alpha}_1 = -\,\omega_{y\Pi};$$

$$\omega_{\delta y}^0 - \omega_{x\Pi} + \omega_{y\Pi}\left(\frac{\sqrt{2}}{2} - 1\right) + \dot{\alpha}_1\,\frac{\sqrt{2}}{2} - \alpha_3 = 0,$$

at $\alpha_3 = -(\omega_{x\Pi} + \omega_{y\Pi})$.

Thus, reduction is required only along axis Oz and example 4 completely
coincides with example 2.

Example 5. We find according to expressions (1.74) with the
photodetector mounted on a base for $a_1 = 0$ and $a_2 = 45°$ in the case
presented in Figure 3.11:

$$\omega_{\delta x} = \omega_{z\Pi} + \dot{\alpha}_1; \quad \omega_{\delta y} = \omega_{y\Pi} + 2\dot{\alpha}_2; \quad \omega_{\delta z} = \omega_{x\Pi} + \dot{\alpha}_1 - \dot{\alpha}_3.$$

Hence: $\dot{\alpha}_1 = -\omega_{z\Pi}; \quad \dot{\alpha}_2 = -\frac{1}{2}\,\omega_{y\Pi}; \quad \dot{\alpha}_3 = \omega_{x\Pi} - \omega_{z\Pi}.$

Thus, versions 1 and 5 are equivalent in complexity of realization, but version 1 can be used both for stabilization and for scanning the image.

Example 6. Let us now consider the functional diagram of example 2 in the general case, i.e., when angle α_1 is arbitrary. This situation is created when using a drive with respect to angle α_1 to develop scanning displacements.

Let us arrange the sensitive axes of gyrosensors along axes Oz_0 and Oy_3. We then find from the output of ther second gyro unit:

$$\omega_{\text{r}2} = \omega_{x\text{п}} \sin \alpha_1 + \omega_{y\text{п}} \cos \alpha_1,$$

and we find from the output of the first gyro unit $\omega_{\text{r}1} = \omega_{z\text{п}} + \dot{\alpha}_1$.

Let there be provided $\omega_{\text{r}} = 0$, i.e., $= 0$, т. е. $\alpha_1 = -\omega_{\text{r}1} = -\omega_{z0}$; $\dot{\alpha}_2 = -\frac{1}{2}\omega_{\text{r}2} =$

$= \frac{1}{2}(\omega_{x\text{п}} \sin \alpha_1 - \omega_{y\text{п}} \cos \alpha_1)$. during operation of an image stabilization

system.

Having substituted these equalities into expression (1.70), we find

$$\omega^0_{\delta y} = -\omega_{x\text{п}} \frac{1}{2}\sin 2\alpha_1 + \omega_{y\text{п}}\cos^2 \alpha_1 + \omega_{z\text{п}}\sin \alpha_1 + \dot{\alpha}_1 \sin \alpha_1 + 2\dot{\alpha}_2 \cos \alpha_1 = 0;$$

$$\omega^0_{\delta z} = \omega_{x\text{п}}\cos \alpha_1 + \omega_{y\text{п}}\sin \alpha_1.$$

Thus, the photodetector must be rotated about axis Oz_ϕ at velocity

$\dot{\alpha}_3 = \omega_{x\text{п}}\cos \alpha_1 + \omega_{y\text{п}}\sin \alpha_1$ for total compensation of the image misalignment.

The instruction to rotate at this velocity can be obtained from the gyro sensor, the axis of which is perpendicular to axes $Oz_\text{п}$ and Oy_3.

Thus, the elements of the optical system (photodetector and mirror) must be provided with a total three degrees of freedom and must have information about all three values of $\omega_{x\text{п}}$, $\omega_{y\text{п}}$, and $\omega_{z\text{п}}$ --the current values of the projections of the angular velocities onto axes $Ox_\text{п}y_\text{п}z_\text{п}$ of an inertial coordinate system--for total stabilization of the image on the photodetector. Total compensation of the misalignment can be guaranteed only in the stabilization mode, while it is difficult to achieve total compensation in the scanning mode, when the rotational angles of the mirror vary over a wide range.

83

Stabilization devices with mirrors in convergent bundles of beams. Mounting the mirrors in front of the object was suggested in all the previous versions, and rotation of them permitted stabilization of the optical axis in the space of the objects. Mounting movable mirrors in the rear segment results in compensation of the effect of vibrations of the optical device, mounted on a movable base, on image quality, rather than in stabilization of the optical axis of the device in the space of objects, i.e., the movable mirrors in the rear segment are compensators of the motion of the image. The motion of the image will be dependent on the distance l between the image plane of the objective and the rotational axis of the mirror and is expressed by the function

$$v_{\text{и}} = l \, 2\dot{\varphi}_{\text{в}},$$

where $\dot{\varphi}_3$ is the angular rotational velocity of the mirror.

Since the image in the focal plane for point on the axis is shifted at velocity $v_{\text{и.п}} = f'\dot{\alpha}$ upon rotation of the entire instrument for angle α, the following condition must be fulfilled to eliminate the effect of angular displacements of the optical device on its image quality: $v_{\text{и.п}} - v_{\text{и}} = 0$. It follows from the foregoing that the rotational axis of the mirror should lag behind the focal plane by $f'/2$ at $\dot{\varphi} = \dot{\alpha}$. However, the image plane is rotated by the same angle (with is not always permissible) and the appropriate measures to eliminate the defocusing should be undertaken. A way out of this situation may consist in using angular ang corner mirrors of different designs. Angular mirrors are characterized by the following features [60]:

an angular mirror is equivalent in its action to a flat mirror, the normal of which is the bisector of a two-sided angle, while the edge of the two-sided angle lies on the plane of the mirror;

rotation of the angular mirror about the axis coinciding with the edge of the two-sided angle does not cause rotation or misalignment of the image, but causes displacement of the image along the optical axis by a value proportional to the square of the rotational angle, and this value is approximately equal to $l\varphi^2$, where l is the distance from the edge of the two-sided mirror to the image plane;

misalignment of the angular mirror in a direction perpendicular to the edge of the mirror causes double misalignment of the image.

Thus, if an angular mirror is rotated with respect to an axis, separated from the edge of the angular mirror by $f'/2$, the motion of the image, caused by angular displacement of the optical device, will be completely compensated and the image quality due to defocusing will essentially not

be worsened. If one assumes that the optical device is rotated by angle $\psi = 1°$ during the delay, the defocusing will comprise $0.017^2 f'/2$, which corresponds to approximately 0.02 percent. The defocusing will be approximately equal to 0.02 mm at $f' = 100$ mm. The effect of this value on the FPM can be evaluated by the following function [20]:

$$T(N') = \frac{\sin\left[\pi N' \Delta \left(2\sigma'_A - \lambda N'\right)\right]}{2\pi \Delta N' \sigma'_A},$$

where Δ is the amount of defocusing, N' is the working spatial frequency, and σ'_A is the aperture angle of the objective.

We have $T(N') \approx 1$ at $N' = 50$ lines/mm, $\sigma'_A = 0.1$, $\Delta = 0.02$, and $\lambda = 5 \cdot 10^{-4}$ mm, i.e., defocusing essentially does not affect image quality.

Let us consider the possible circuit solutions of these systems.

The design of a system for compensation of random vibrations, acting along the bank and pitch axes, using angular mirrors arranged so that their edges in projection onto the image plane are mutually perpendicular, is presented in Figure 3.12, a. (Footnote) (U.S. patent 3,437,395) Each of the angular mirrors 1 and 2 is stabilized inertially or by the gyroscopic method in space with respect to a point located on an axis, perpendicular to the edge of the mirror, at a distance equal to half the focal distance; as a result, one of the mirrors stabilizes the optical axis in bank and the other stabilizes it in pitch.

A somewhat different version of a stabilization device is possible, which is designed to compensate for the effect of random vibrations, but the angular mirrors are arranged so that their edges are parallel to each other. (Footnote) (U.S. patent 3,437,396) The mirrors are mounted on frictionless supports and are stabilized inertially or by another method with respect to the sighting line. Each of the mirrors has two degrees of freedom and is mounted in a universal suspension. The mirrors are balanced with respect to the points of the support and are linked to each other so that the unbalanced centrifugal forces do not induce deviations of the system, i.e., the system is completely balanced. The distance between the vertices of the mirrors is half the focal distance of the objective. The edges of the angular mirrors should lag behind the rotational axes by 1/4 the focal distance to achieve total compensation.
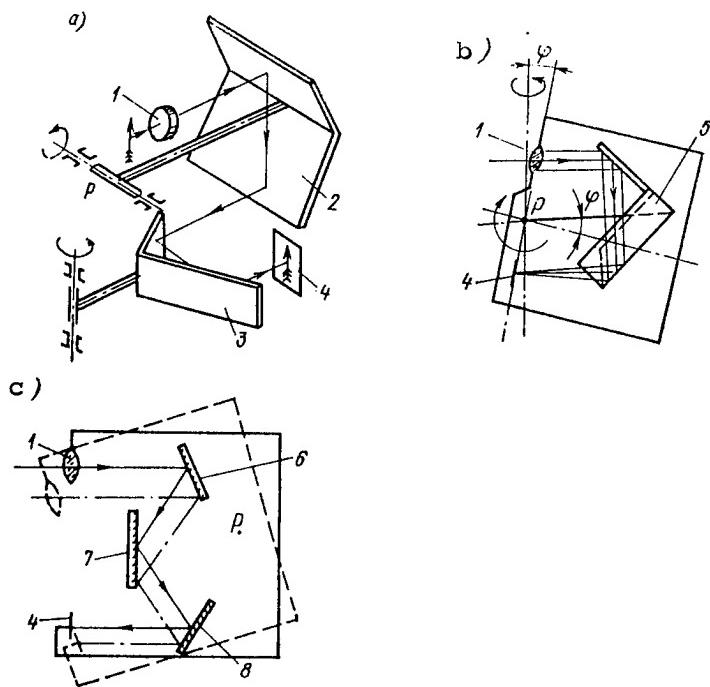
Figure 3.12. Diagrams of Stabilization Devices With
Mirrors in Convergent Bundles of Beams:
a--with two angular mirrors; b--with corner mirror;
c--with three flat mirrors; 1--objective; 2, 3--
angular reflectors; 4--detector; 5--corner mirror;
6, 7, 8--flat mirrors

The most common and universal is a system for compensating the effect of
random vibrations using a corner mirror (UZ)--a triple mirror, formed by
three mutually perpendicular mirrors. (Footnote) (U.S. patent
3,467,595) This mirror is equivalent to an angular mirror, but unlike
it, rotation of the corner mirror about any axes passing through its
vertex does not cause displacements of the image. Thus, unlike the
previous systems, total compensation of the effect of random vibrations
is provided by one element. The schematic solution of this system is
shown in Figure 3.12, b. The corner mirror is arranged between the
objective and its focal plane and causes a break of the optical axis by
$180°$ and misalignment of it. It is stabilized by gyroscopic methods in
space with respect to some reference point P, rigidly bound to the body
of the optical device. The point of support P lies on a line parallel
to the axis of the objective, passing through the vertex of the mirror,
and lags behind the image plane by a distance equal to half the focal
distance. The same as angular mirrors, displacement of the corner
mirror in space causes displacement of the image by twice as much.
Since the corner mirror is stabilized with respect to the support point,
one can assume that the body of the device is rotated by the same angle

86

φ with respect to the vertex of the corner mirror upon inclination of it by angle φ together with the objective. The image would be rotated by $f'\varphi$ if the triple mirror were rigidly attached to the device, but since the mirror retains a fixed position in space with respect to point p, it is rotated with respect to the image plane about its own vertex and will be misaligned in a plane parallel to the image plane by a value equal to double the product of the distance from the reference point to the vertex of the corner mirror by the rotational angle of the device, i.e., the misalignment of the image will be determined by the relation $\delta =$ $= 2l\varphi$. But since $l = 0.5f'$, $\delta = f'\varphi$. As a result, the two misalignments of the image compensate each other and the image in the focal plane remains stabilized at any rotations of the system about axes z and x. As in the previous cases, a system whose value is equal to $f\varphi^2$ will be defocused upon rotations of the system. Either the focal plane is displaced or a planoparallel plate with variable thickness is used in high-precision systems. A version of image stabilization using three mirrors, the main cross-sections of which lie in the same plane, is shown in Figure 3.12, c.

It was assumed that the above image misalignment mirror components are used in an optical device that records an image by using some detector. Situations that require the incoming and outgoing beams to be parallel may arise when using visual systems. Let us assume that the device consists of the following main components: objective 1, a rotating system 2 and eyepiece 3 (Figure 3.13, a). Let the device be rotated in space by some angle θ. The beams emerging from an infinitely remote object, which was initially located on the optical axis of the device, are then collected in the focal plane at point P. If the image of an infinitely remote object is returned from point P to point a, lying on the axis of the optical system, using a random vibration compensator, the beams at the output from the eyepiece will not be parallel to the incoming beams. Thus, the image at the focal plane of objective 1 must actually be shifted to some point A, located between points P and a. The beams emerging from the eyepiece will be parallel to the incoming beams if the condition $bB = f_{OK}\theta$, where f_{OK} is the focal distance of the eyepiece (Figure 3.13, a), is fulfilled. Since rotating system 2 transfers the image with magnification of -1 to the plane of the objective 1, then $bB = -aA$ and, accordingly, the misalignment in the focal plane of the eyepiece is the inverse misalignment of the focal plane of the objective. If the following condition is fulfilled

$$|aA| = |bB| = |f_{\text{ok}}\Theta|,$$

the random vibration compensator switches the image from point P to point A and thus compensates the effect of the misalignment of the device on the misalignment of the image. Based on these arguments, let us determine the compensation factor k_K, which is expressed in the form of the ratio of values of the required compensation of image

87

misalignment and of the total image misalignment in the focal plane of the objective 1, i.e.,

$$k_{\text{к}} = \frac{P\Lambda}{P_a} = \frac{P_a - A_a}{P_a}.$$

Since Pa = $f_{\text{OK}}\theta$ and Aa = $f_{\text{OK}}\theta$, then k_{K} = 1 - $f_{\text{OK}}/f_{\text{об}}$.
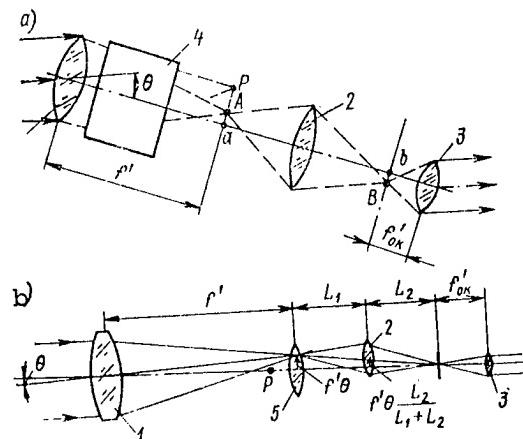

Figure 3.13. Diagrams of Systems for Stabilization of Parallel Incoming and Outgoing Beams in Visual Systems: a--with additional compensator; b--with motion of rotating system; 1--objective; 2--rotating system; 3--eyepiece; 4--compensator; 5--collecting lens

The value $\Gamma = f_{\text{OK}}/f_{\text{об}}$ is the magnification of the device and then the compensation factor is equal to $(1 - 1/\Gamma)$. Hence, it follows that the compensation factor k_{K} will be equal to $(1 + 1/\Gamma)$ or that the length of the lever on which an angular or corner mirror should be located should be equal to

$$l = \frac{l'}{2}\left(1 \pm \frac{1}{l'}\right).$$

(3.28)

for a telescopic system with rotation.

The plus sign is required in optical systems with inverted image, while the minus sign is required in systems with direct image.

88

A rotating system itself can generally be used for an image field stabilization system. (Footnote) (U.S. patent 3,504,957) The question also arises about which point the rotating system can rotate. Carrying on the discussion in similar fashion, it is easy to reach the following conclusion: if the system is rotated by angle θ (Figure 3.13, b), the rotating system should be rotated by the same angle with respect to point P, which lags behind the principal plane of the rotating system at distance

$$l_p = f' \frac{L_2}{L_1 + L_2} = f' \left(1 + \frac{1}{\Gamma} \right), \qquad (3.29)$$

where f′ is the focal distance of the object and Γ is the magnification of the inversion system.

One should naturally estimate a decrease of image quality due to defocusing of the entire optical system.

Prism stabilization devices. Reflecting prisms (provided their manufacture is ideal) are equivalent in their effect on the bundle of beams to a combination of a planoparallel plate with one, two or three mirrors. Combinations of prism elements permit one to develop image field stabilization systems which are similar to the above reflecting stabilization systems. For example, a stabilization system based on angular mirrors corresponds to one using two rectangular prisms (a Porro system of first kind), widely used in prismatic binoculars.

A similar system with BR-180° prism, which has become widespread [86], corresponds to a stabilization system with triple mirror. (Footnote) (French patent 2,203,567, British patent 1,235,175, U.S. patent 3,556,632, and U.S. patent 3,473,861) Specifically, this prism compensates for the random misalignments of the image in the binoculars by using gyroscopic devices (Figure 3.14). (Footnote) (Prospectus of Intra-World Sales Corporation)

The stabilization system of this binocular permits one to track targets at angular velocity up to 5°/s and stabilization by bank and pitch angles of ±5° and to observe with magnification of 10^x and 20^x.

Stabilization systems with the use of the well-known diagram of the Hertz panorama, containing a rectangular and a Dove prism, are considered in some patents (Figure 3.15). (Footnote) (U.S. patent 3,428,812, FRG patent 1,225,954) The rectangular prism is mounted with the possibility of rotation about the bank and pitch axes. It compensates for the motion of the image, which occurs due to forward displacement of the carrier and due to pitch stabilization errors, upon rotation with respect to the pitch axis. The prism is rotated at angular velocity equal to half the sum of the angular velocities of the uniform translational motion of the image and of the motion of the image

caused by errors in pitch axis. The errors in bank axis are compensated by rotation of this prism about the axis at angular velocity equal to the angular motion of the image, caused by bank errors. The Dove prism, mounted in front of the objective, compensates for rotation of the image.
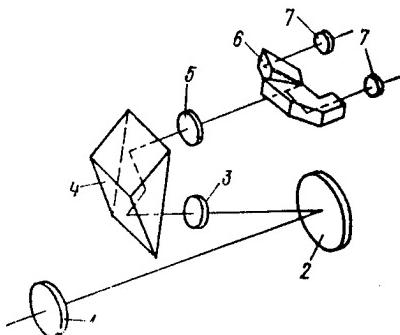

Figure 3.14. Optical Layout of Binoculars:
1--objective; 2--mirror; 3--inversion system;
4--stabilizing prism; 5--additional objective;
6--splitting prisms; 7--eyepieces

A cube prism (or a double Dove prism) is equivalent in its action to a flat mirror, but does not change the direction of the optical beams. The latter permits one to arrange a stabilization system based on two series-connected cube prisms. The cube prisms are mounted so that their rotational axes, coinciding with the reflecting surface, would be mutually perpendicular: the image is stabilized in bank by using one prism and stabilized in pitch by using the second prism.

Because of errors in manufacture of the prism, it becomes equivalent to a combination of three elements: flat mirrors, a planoparallel plate and a wedge with small refracting angle.

It is shown in [72] that prisms with wedge-like scanning cause a number of defects and namely: 1) misalignment of the image of the axial point of the object with respect to the center of the visual field and also rotation of the image, 2) transverse chromatism, and 3) aberration of the coma.

90
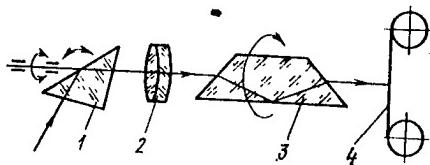
Figure 3.15. Layout of Camera With
Image Stabilization:
1--rectangular prism; 2--objective;
3--Dove prism; 4--photographic film

The indicated aberrations cause additional momentum of the image due to rotation of a weak optical wedge, mounted in the convergent beams, with respect to stabilization systems, and namely:

1) upon rotation of the prism about the axis parallel to the edge of the wedge by the value:

$$\Delta V = l\dot{\Theta}\,\frac{n^2-1}{2n}\,\mathrm{tg}^2\,i,$$

where 1 is the distance from the output edge of the prism to the image plane;

2) upon rotation of the prism about an axis perpendicular to the edge of the wedge and parallel to the principal cross-section by the value

$$\Delta V = l\left(-\dot{\Theta}\,\frac{n^2-1}{2n}\,\mathrm{tg}\,i\sin i - 2\dot{\Theta}\,(n-1)\sin^2\frac{i}{2}\right).$$

Compared to stabilization systems, developed on the basis of mirror elements, the use of reflecting prisms permits one to develop optical devices with smaller overall dimensions, but these systems have more sources of error. Moreover, advances in development of lightweight mirrors, for example, mirrors of beryllium or graphite-epoxide materials having low density, essentially permit one to develop stabilization systems based on them with smaller mass than prism systems.

3.3. Composite Stabilization Devices

Stabilization devices with optical wedge and flat mirror. The operator matrix of a stabilization device, consisting of an optical wedge and flat mirror, can be represented by the following expression:

$$M_{\text{эк}} = M_{\text{кл}}M_{\text{э}}M_{\text{кл}}.$$

Let us limit ourselves to consideration of paraxial beams (as in section 3.1) for the capabilities of the joint action of an optical wedge and reflecting surface, and by analogy with section (3.1), let us consider the design of an optical wedge compensator, consisting of two adjacent lenses, and one of the surfaces of the fixed lens has a reflective coating (Figure 3.16). The optical axis of the device does not coincide with that of the fixed lens of the optical compensator and forms some angle with it.
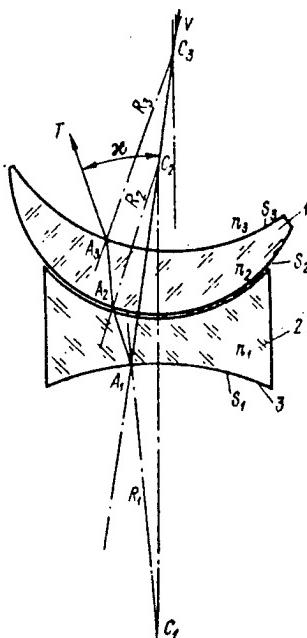

Figure 3.16. Optical Wedge Compensator:
1--movable lens; 2--fixed lens; 3--reflecting
surface; n_1, n_2, n_3--refractive indices of
corresponding media; R_1, R_2, R_3--radii of
curvature of surfaces of lenses

Using the same notations as in section 3.1, we find the angle of deflection of the beam from the initial position in the form

$$\varkappa = 2 \left(1 + \frac{R_2 d_1}{R_1} \right) \left\{ \left(\frac{n_2}{n_3} - 1 \right) \times \right.$$
$$\times \left[\frac{d_1}{R_3} + \frac{d_2 d_1}{R_3 R_2} \left(\frac{n_1}{n_2} - 1 \right) + \frac{d_2 n_1}{R_3 n_2} \right] + \tag{3.30}$$
$$\left. + \left[\frac{d_1}{R_2} \frac{(n_1 - n_2)}{n_3} + \frac{n_1}{n_3} \right] \right\} \Theta.$$

We find in the special case at $n_1 = n_2 = n$ and $n_3 = 1$, $R_1 = R_3 = \infty$ that

$$\varkappa = 2n\Theta. \qquad (3.31)$$

This device can be mounted both in parallel beams and in convergent beams in the rear segment. Realization of this principle in a reflecting-lens telescope is shown in some patents. (Footnote) (U.S. patent 3,761,157, U.S. patent 3,761,158, French patent 2,203,567) The layout of this system is shown in Figure 3.17, a. A flat mirror, which is placed in a closed container and is held in space by magnetic suspension, is provided in the optical system. When the entire device is rotated, the mirror is rotated by an angle, different from the rotation of the entire device, and a liquid wedge is formed between the mirror and the porthole of the container. It is obvious that the condition of stabilization is determined by the expression

$$2n\Theta L = \varphi f', \qquad (3.32)$$

where n is the refractive index of the liquid, Θ is the angle of rotation of the mirror, φ is the angle of rotation of the entire device, L is the distance from the surface of the mirror to the focal plane, and f' is the focal distance of the objective.

The following function should be fulfilled upon fulfillment of the condition of parallelism of the incoming and outgoing beams:

$$2n\Theta L = \varphi f' \left(1 \pm \frac{1}{\Gamma} \right), \qquad (3.33)$$

where (as in the previous systems) the "+" sign is related to systems without inversion, while the "−" sign is related to systems with inversion.

Stabilization devices with telescopic system and optical wedge. To determine the correlation between rotations of these two systems and the condition of image stabilization, let us assume that the afocal system is placed in a container, the inlet and outlet portholes of which are planoparallel plates (Figure 3.17, b). Let us consider different versions of the mutual motion of an ofocal system and a container with a liquid. Let us also assume that the entire container is rotated about some point, lying on the optical axis, by some angle, while the afocal system retains its position in space, i.e., an optical wedge with angle equal to Θ at the vertex was formed between the porthold and the primary surface of the afocal system (Figure 3.17, c). A parallel light beam, after refraction in this wedge, will arrive at the input of the afocal

system at angle $\theta - (\theta/n)$. Upon magnification of the afocal system Γ, the beams emerging from it are deflected by angle $\Gamma(\theta - \theta/n)$ with respect to the initial position.
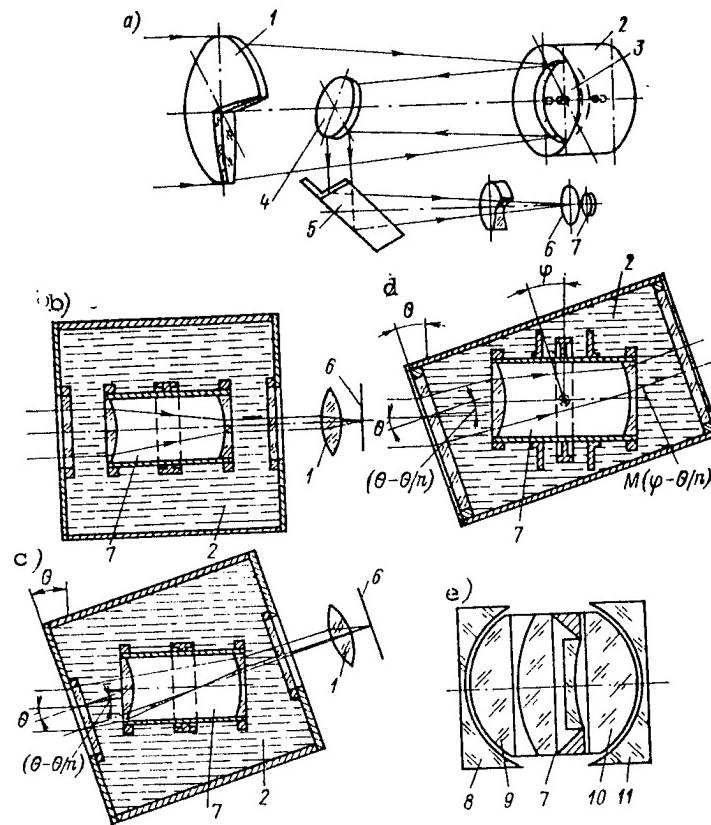
Figure 3.17. Layouts of Composite Stabilization Devices:
a--flat mirror and optical wedge; b, c, d--liquid optical
wedge and telescopic system; e--optical edge formed by
lenses and telescopic system; 1--objective; 2--container
and liquid; 3--movable mirror; 4--secondary flat mirror;
5--angular mirror; 6--image plane; 7--afocal adapter;
8, 11--fixed lenses; 9, 10--movable lenses

Hence, it follows that the condition of stabilization of a bundle of beams with respect to the following system assumes the form:

$$\Theta - \Gamma\,(\Theta - \Theta/n) = 0, \qquad\qquad (3.34)$$

i.e.,

$$(\Gamma - 1)(n - 1) = 1. \tag{3.35}$$

The afocal system $\Gamma = 4$ must be increased in this regard at refractive index of the liquid of $n = 1.33$.

Let us consider another case when the container and afocal system are rotated by angle θ about axis x (Figure 3.17, d). The beam to the telescopic system then enters at angle θ/n. If we rotate the telescopic system by angle φ in the opposite direction to stabilize the beam, the bundle of beams will enter the afocal system at angle $(\varphi - \theta/n)$ and will comprise $\Gamma(\varphi - \theta/n)$ at the output.

The condition of stabilization will assume the form

$$\varphi - \Gamma(\varphi - \Theta/n) = 0. \tag{3.36}$$

An optical system with magnification $\Gamma = 2$ is required at $\theta/\varphi = 1.5$ and $n = 1.33$, i.e., a system one-half as large as in the previous case.

By analogy with the foregoing, formula (3.36) for visual systems assumes the form

$$\varphi(\Gamma - 1) = \Theta(\Gamma/n)(1 \pm 1/\Gamma_f). \tag{3.37}$$

Here Γ is the magnification of the telescopic accessory, Γ_f is the total magnification of the system, and $\Gamma_f = \Gamma\Gamma_{OK}$, where Γ_{OK} is the magnification of the eyepiece.

Similar combinations are also possible using optical glass wedges. The use of wedge systems having different refractive indices is possible. One of the possible designs is presented as an example in Figure 3.17, e. The system contains three elements: two optical compensators, formed by spherical lenses with single center of curvature, and a telescopic system, which is located between the optical wedges. Lenses 8 and 11 are fixed, while the module containing lenses 9 and 10 and telescopic system 7 can be rotated in two planes about a point, coinciding with the center of curvature of the lenses of the optical wedges.

The condition of compensation will assume the form

$$(n_1 - 1)\Gamma - (n_2 - 1) = 1, \tag{3.38}$$

95

where n_1 and n_2 are the refractive indices of the marks of glass from which the first and second pair of lenses of the optical wedge compensators are made.

Expression (3.35) is valid at $n_1 = n_2$. And, for example, an identical effect with variant corresponding to Figure 3.17, e, can be achieved at refractive index of $n_1 = 2$ and $n_2 = 1.5$ using a telescopic system having magnification of only 1.5^x.

We note that the condition of total stabilization when using only the first pair of the wedge compensator alone is expressed by the relation

$$(n - 1)\, \Gamma \simeq 1. \tag{3.39}$$

With serial combination of two telescopic systems, between which the wedge compensator is located, the condition of stabilization assumes the form

$$\Gamma_2\,(n - \Gamma_1) = 1,$$

where Γ_1 and Γ_2 are the magnifications of the first and second telescopic system, respectively, and n is the refractive index of the wedge glass.
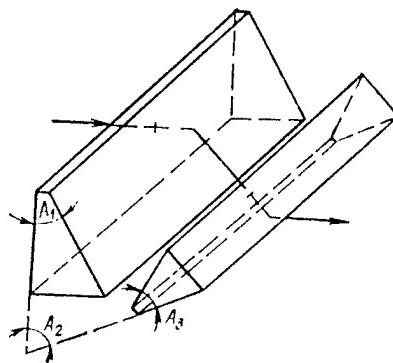
Figure 3.18.   Layout of Brewster-Amichi Prism:
A_1 and A_3--angles at vertex of prisms;
A_2--total angle

Stabilization devices with telescopic system and flat mirror. It was shown above that the output beam will be deflected by a value determined by the function $\theta\Gamma$ upon rotation of a telescopic system $\theta\Gamma$ upon rotation of a telescopic system with magnification Γ. On the other hand, a flat

mirror causes corresponding rotation of the incident beam by an angle equal to 2θ upon rotation about axis x and z. Thus, if an afocal system with magnification $\Gamma = 2^x$ is placed in front of a mirror, a stabilization system can be designed without resorting to a reducer. If the mirror is placed in a medium with refractive index n, it follows from the foregoing that the required magnification of the afocal attachment is selected from the expression $\Gamma = 2n\theta/\varphi$, where θ is the rotational angle of the mirror and φ is the rotational angle of the system. The mirror should naturally be rotated in the direction opposite the rotation of the system. Rotation of the entire system about the optical axis is compensated by rotation of the mirror about the same optical axis, but the image is rotated by the same angle. Rotation of the mirror and rotation of the entire system are correlated to each by the ratio 1:1. Rotation of the image can be eliminated by introducing a Dove or Pechan prism into the optical layout. Thus, anamorphotic telescopic systems, which would have magnification 2^x in one direction and -1^x in the perpendicular direction, are required for direct reducerless stabilization; the mirror can than be mounted directly on the gyroscope rotor. Anamorphote systems either using cylindrical lenses or Brewster-Amici prisms can be used for these purposes (Figure 3.18).

The latter system is the more technologically effective in manufacture and can be achieved in the following manner: the first prism with angle at vertex $A_1 = 33°$, second prism with angle at vertex $A_3 = 28°48'$. The edges of the prism are parallel and the angle between the input surface of the first prism and of the first and output surfaces of the second prism is equal to $A_2 = 53°$.

The dimensions of the prisms are determined by the dimensions and position of the pupil and visual field of the optical system.

Table 3.1

$\theta_{пд}$	$\theta_{отк}$	m_d	θ'_C	θ'_F
—6	—12°,42	2,213	—12°,35	—12°,56
—4	—8°,14	2,083	—8°,09	—8°,22
—2	4°,04	2,021	—4°,02	4°,08
0	0,02	2,008	—0°,01	—0°,02
2°	4°,02	2,038	—4°,01	+4°,06
4°	8°,17	2,118	—8°,15	+8°,24
6°	12°,54	2,267	—12°,50	+12°,65

The results of calculation for a real system are presented in Table 3.1 [86], in which $\theta_{пд}$ and $\theta_{отк}$ are the angles of incidence and deflection on the input and output edges of the prism, m_d is anamorphotic factor, and θ'_C and θ'_F are the angles of deflection for spectral lines C and F of the prism.

It follows from the data presented in Table 3.1 that the chromatic aberration is completely corrected within a visual field of approximately 12° and the anamorphotic factor essentially remains constant.

Measurement results, which were made on a series of anamorphotes of the Lux Color Company, manufactured from cylindrical lenses and used for movie projection, are presented in [86]. These measurements yielded the following results:

$\theta_{пд}$	$\theta_{отк}$
0	0
±2°	±3°,986
±4°	±8°,014
±6°	±12°,14

Comparing the above data, one can state that anamorphotic systems, designed on the basis of optical wedges, are quite suitable for mounting in optical devices to stabilize the image field.

3.4. Stabilization Devices With Fiber Optic Elements (VOE)

Image motion compensation devices, designed on the basis of fiber optic elements (VOE), unlike the above compensation devices based on the use of traditional optical elements, act on the integral bundle of beams and guarantee the effect of the motion of the image due to spatial displacement of the fiber light guides, each of which carries information about one element of the image. These devices are generally a single fiber optic element or several combined fiber optic elements (i.e., a stack), mounted in the image plane and having the capability of spatial displacement either with respect to each other or with respect to the focal plane of the objective.

A considerable number of layouts of these devices have now been developed, distinguished by the shape of the fiber optic, by their number, and by the direction of placement of the fibers. (Footnote) (U.S. patent 3,651,325, British patent 1,493,339, British patent 1,483,878, USSR inventor's certificate 853,599, USSR inventor's certificate 623,976, USSR inventor's certificate 731,412, USSR inventor's certificate 769,479, and USSR inventor's certificate 890,352) These designs of fiber optic compensators should correspond in the entire variety to some general requirements.

First, the input surface of the fiber optic element or stack should coincide with the image plane of the objective; second, the output surface should contact or be optically connected to the image detector. Third, the combined surfaces of the moving elements of the compensation system should provide at least one degree of freedom to them to guarantee spatial displacement. Fourth, contact between all the fiber optic elements must be maintained or the space between them of not more

than six-seven diameters of a single fiber must be provided. Flat,
cylindrical surfaces and also surfaces of revolution correspond to the
last condition. The main types of combination surfaces, by which the
separate fiber optic elements of the system can be limited and also the
number of degrees of freedom and nature of the possible displacements of
the fiber optic element can be provided, are presented in Table 3.2.
this table also gives an idea of the number of possible variants of the
system.

Table 3.2

Type of combination of surfaces	Number of degrees of freedom	Nature of displacements
Noncircular cylinder	1	Forward
Aspherical surface of revolution	1	Rotational
Circular cylinder	2	Forward--1; rotational--1
Sphere	3	Rotational--3
Plane	3	Forward--2; rotational--1

Table 3.2 permits one to design fiber optic elements, suitable for image
stabilization. The main versions of the stabilization devices are
considered below.

Stabilization devices with two combined fiber optic lenses. A
compensation device using a fiber optic element, which consists of two
combined lenses, is shown in Figure 3.19, a. The compensator contains
an objective 1, in the focal plane of which a stack of two fiber optic
elements that form a planoparallel plate in combination is mounted. The
fiber optic elements are lenses: planoconvex 2 and planoconcave 3, the
single light guides of which are parallel to the optical axis of the
objective in the neutral position. An image protector, for example,
photographic film, is combined with the output surface of the fiber
optic element 3; the fiber optic element 2 and objective 1 are rigidly
connected to each other into a single module having the capability of
being rotated about an axis perpendicular to the optical axis of the
objective and passing through the center of curvature O of the combined
surfaces of parts 2 and 3. The image is displaced along the output
surface when module 1 is rotated about this axis.
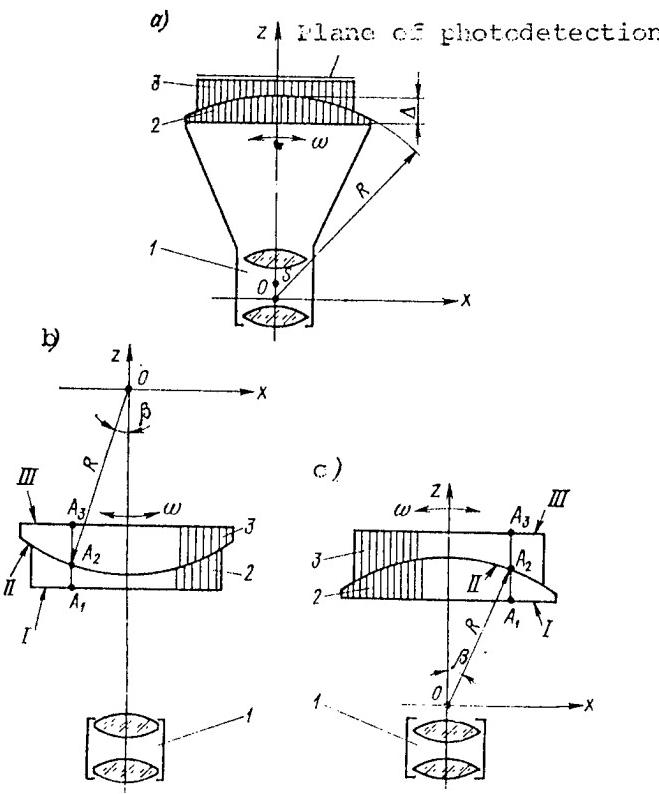
Figure 3.19.   Stabilization Devices With Two Combined
Fiber Optic Lenses:
a--with movable planoconvex lens and objective;
b--with movable planoconvex lens; c--with movable
planoconcave lens; 1--objective; 2, 3--fiber optic
lenses; I, II, III--surfaces of combined lenses

Based on the method of determining the motion of the image, outlined in
Chapter 1, it is easy to show with respect to compensation devices in
which fiber optic elements are used that the motion of the image is
determined with sufficient degree of accuracy by the following
expression:

$$v_{\text{из}} = f'\dot\varphi \left[\frac{1 + \text{tg}^2\,\omega'}{1 - \text{tg}\,\omega'\varphi} - \right.$$

$$\left. - \sqrt{ \left(1 + \frac{\Delta}{f'} + \frac{z_s}{f'}\right)^2 - \left(\frac{\varphi + \text{tg}\,\omega' + \frac{x_s}{f'} + \frac{x_s}{f'}\,q\,\text{tg}\,\omega'}{1 - \varphi\,\text{tg}\,\omega'}\right)^2 } \right], \tag{3.40}$$

100

where $\varphi = \dot{\varphi}t$ is the angle of rotation of the module during recording, $\dot{\varphi}$ is the angular velocity of rotation of the module, t is the exposure time, $2\omega'$ is the angle of the visual field of the objective, x_s and z_s are the coordinates of the rear nodal point of the objective with respect to the rotational axis, f′ is the focal distance of the objective to be used, and Δ is the thickness of the fiber optic 2 along the optical axis.

The distribution of the compensation rate with respect to the field will be different as a function of parameters x_s, z_s, and Δ.

Let us consider the different versions of the position of the rear nodal point with respect to the rotational axis of the module.

First case. Let $x = 0$ and $z_s \neq 0$, i.e., the rotational axis passes through the optical axis of the objective. The motion of the image will vary by field symmetrically with respect to the center of the field and these changes will approach zero at $\omega' \to 0$. Specifically, the variation of the motion of the image with respect to the field will be similar to variation of the motion of the image in the case of using a two-wedge compensator, mounted in front of the objective and rotated in different directions at identical velocities, at parameters $\Delta/f' = 0.2$, $z_s/f' = 1.5$, $\varphi = 0.01$ and $2\omega' = 40°$ (Table 3.3).

Table 3.3

(1) Вид компенсатора	(2) Значение нескомпенсированной скорости, %₀ при угле поля зрения ω′, °								
	−20	−15	−10	−5	0	5	10	15	20
(3) Волоконно-опти- ческий	9	4,5	2	0,5	0	0,5	2	5	10
Оптический кли- новой (4)	13	7	3	1	0	1	3	7	13

KEY:

1. Type of compensator
2. Value of uncompensated velocity, percent at angle of visual field ω', °
3. Fiber optic
4. Optical wedge

Second case. Let $x_s \neq 0$ and $z_s \neq 0$, i.e., the rotational axis of the module is shifted with respect to the optical axis. It is then easy to guarantee monotonic variation of the motion of the image at corresponding parameters of x_s, z_s and Δ. To do this, the following condition must be fulfilled:

$$\frac{1 + \mathrm{tg}^2\,\omega'}{(1 - \varphi\,\mathrm{tg}\,\omega')^2} \leqslant$$

$$\leqslant \sqrt{\left(1 + \frac{\Delta}{f'} + \frac{z_s}{f'}\right)^2 - \left(\frac{\varphi + \mathrm{tg}\,\omega' + \dfrac{x_s}{f'} + \dfrac{x_s}{f'}\varphi\,\mathrm{tg}\,\omega'}{1 - \varphi\,\mathrm{tg}\,\omega}\right)^2}\,.$$

It is known that monotonic variation of the motion of the image from one edge of the photograph to another occurs during forward frame prospective photography. Image velocity compensators (KSI), known up to the present, do not provide the required degree of compensation and, therefore, the effect of the motion of the image is achieved in equipment of this class only by using short delays. Data on the degree of compensation of image motion in equipment of this class, provided there is total compensation for the middle layout, are presented in Table 3.4 for illustration. If a fiber compensator, for example, with parameters $x_s/f' = 1.0$, $z_s/f = 0.7$, and $\Delta/f = 0.2$, is used, the degree of compensation is increased sharply (Table 3.4). The calculation was made for angle of inclination of the equipment $\alpha = 50°$ and for total angle of the visual field of the apparatus of $2\omega' = 40°$.

Table 3.4

(1) Вид компенсатора	(2) Значение нескомпенсированной скорости, %, при угле между надиром и направлением визирования, $(\alpha \pm \omega')°$								
	30	35	40	45	50	55	60	65	70
Волоконно-оптический (3)	47	32	23	10	0	9	18	16	12
Оптический клиновой (4)	57	43	32	18	0	25	60	116	215

KEY:
1. Type of compensator
2. Value of uncompensated velocity, percent, at angle between nadir and direction of sighting $(\alpha \pm \omega')°$
3. Fiber optic
4. Optical wedge

Third case. Let $x_s = 0$ and $z_s = -\Delta$, then formula (3.40) will assume the form

$$v_{\text{нз}} \approx f\dot\varphi \left(\frac{1 + \mathrm{tg}^2\,\omega'}{1 - \mathrm{tg}\,\omega'\varphi} - 1\right) \approx f\dot\varphi\,\mathrm{tg}^2\omega'. \qquad (3.41)$$

It follows from this formula that the motion of the image at any inclinations of the module is equal to zero in the center of their frame. The image whose velocity has quadratic dependence on angle

102

$-\mathrm{tg}^2 \omega'$ moves at points that do not coincide with the center of the frame. Specifically, this value comprises only 3 percent for $2\omega' = 20°$.

The given variant corresponds to the greatest degree to the operating conditions of a stabilization system and only the fiber optic part 3 and the image detector combined with it are stabilized.

A version of a fiber optic compensator, in which lens 3 is displaced jointly with the image detector, is presented in Figure 3.19, b. The radius of curvature of the lens can be arbitrary. The nature and value of the resulting motions of the image will differ from that considered above.

It follows from Figure 3.19, b that the motion of the image upon rotation of lens 3 at angular velocity $\dot{\varphi}$ is determined from the equation

$$v_{\text{из}} = -\dot{\varphi} R \, \frac{\sin \alpha_{II}}{\sin \alpha_{III}}, \qquad (3.42)$$

where R is the radius of the curvature of the combined parts, α_{II} is the angle betweent he surface II and the direction of the fibers, and α_{III} is the angle between surface III and the direction of the fibers.

It follows from the figure that $\sin \alpha_{II} = \sin(90° - \beta)$, where β is the angle between the optical axis Oz and the radius that joins point A_2 and O; $\sin \alpha_{III} = \sin 90° = 1$, i.e.,

$$v_{\text{из}} = -\dot{\varphi} R \cos \beta. \qquad (3.43)$$

It is more convenient for practical purposes to turn to the rate of compensation as functions of coordinates x of the depicted point on surface I, coinciding with the image plane of the objective. It follows from Figure 3.19, b that $\sin \beta = x/R$. Formula (3.43) then assumes the form:

$$v_{\text{из}} = -\dot{\varphi} \sqrt{R^2 - x^2}. \qquad (3.44)$$

A similar effect is achieved in the case of designing a system when a fiber optic lens 3 has a radius of curvature of opposite sign (Figure 3.19, c). It is easy to show that the function that determines the motion of the image coincides with function (3.44).

Thus, the sequence of arrangement in a system of convex and concave fiber elements has no effect on the value of the compensation rate. All the above mathematical calculations were made on the condition that the directions of the fibers of both elements were parallel at the moment of exposure, i.e., the recording (exposure) time was infinitely small. The exposure in real systems occurs within a specific time segment t. The rotating element of the system is rotated during this time by some angle and the directions of the light guides of both elements cease to be parallel, which results in variation of the motion and, accordingly, in the residual shifts of the image. The residual shift Δv for the considered design systems is determined by the following expression:

$$\Delta v = R \left(\dot{\varphi} t \cos \omega t - \sqrt{1 - \dot{\varphi}^2 t^2} \sin \omega t \right). \tag{3.45}$$

Stabilization devices with three combined fiber optic lenses. The stack consists of three elements, which in combination form a planoparallel plate (Figure 3.20). The central element 2 is made in the form of a sphere with radius R, while elements 1 and 3 are planoconcave lenses of the same radius, i.e., all the surfaces have a center of curvature that passes through point O.
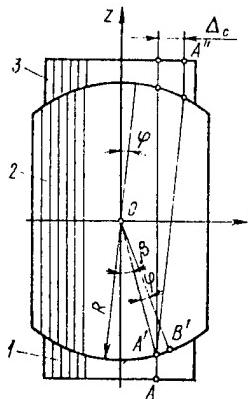
Figure 3.20. Stabilization Device With
Three Combined Fiber Optic Lenses:
1, 2, 3--fiber optic lenses

Let us consider the variation of motion of the image upon rotation of the spherical fiber element 2. It is obvious that the value of the image shift Δ_c will be different for different points on the output surface of lens 3 upon rotation of spherical lens 2 by angle φ; it is determined by the expression:

$$\Delta_c = d_{\text{в}} \sin \varphi, \qquad\qquad (3.47)$$

where d_{B} is the length of the fiber of the spherical lens 2, combined with the given point of the image.

Let us take arbitrary point A with coordinate x. Its image A′ on the input surface of rotary lens 2 lies at angle β toward axis Oz, and:

$$\sin \beta = \frac{x}{R}; \quad \cos \varphi = \frac{\sqrt{R^2 - x^2}}{R}. \qquad\qquad (3.48)$$

Point B′ on the input surface of lens 2, lying on arc $\varphi + \beta$, will be combined with the image after rotation of lens 2 by angle φ (clockwise). the coordinate of this point along axis Ox is equal to

$$x_{\text{в}} = R \sin (\varphi + \beta), \qquad\qquad (3.49)$$

and the length of the light diode at this point is

$$d_{\text{в}} = 2R \cos (\varphi + \beta). \qquad\qquad (3.50)$$

Function (3.50) with regard to formulas (3.48) will assume the form

$$d_{\text{в}} = 2\left(\sqrt{R^2 - x^2} \cos \varphi - x \sin \varphi\right), \qquad\qquad (3.51)$$

while the amount of shift of the image is

$$\Delta_c = d_{\text{в}} \sin \varphi = 2 \sin \varphi \left(\sqrt{R^2 - x^2} \cos \varphi - x \sin \varphi\right), \qquad\qquad (3.52)$$

or

$$\Delta_c = \sqrt{R^2 - x^2} \sin^2 \varphi - 2x \sin^2 \varphi.$$

It follows from this formula that the maximum shift of the image will occur near a point with coordinate x = -R sin φ and it is equal in value to $\Delta_{c\,\text{max}} = 2R \sin \varphi$.

The extent of the shift decreases as the distance from this point increases, since the length of the light guides decreases. For example, the shift for a point on the axis is equal to

$$\Delta_c = 2R \sin \varphi \cos \varphi = R \sin 2\varphi.$$

Accordingly, the image is not only shifted on the output surface of the stack, but there is some transformation of the image upon rotation of a movable fiber optic element. Thus, the left side of the image is extended somewhat, while the right side is contracted with respect to Figure 3.20. The entire image is shortened, since its outermost right point is displaced by a lesser value than the left point. However, the distortion is insignificant at small values of the angle of rotation φ and can be estimated by using the above expressions.

Let us consider the nature of variation of the motions of the image of points lying on axis Ox ($y \neq 0$). Let us split the spherical lens with plane parallel to plane xOz at distance y from the origin. We find in the cross-section a circle of radius

$$R' = \sqrt{R^2 - y^2}. \tag{3.53}$$

Having substituted the value R' into formulas (3.51)-(3.53), we find:

$$d_B = 2\sqrt{R^2 - x^2 - y^2} \cos \varphi - x \sin \varphi; \tag{3.54}$$

$$\Delta_c = 2 \sin \varphi \left(\sqrt{R^2 - x^2 - y^2} \cos \varphi - x \sin \varphi \right), \tag{3.55}$$

or

$$\Delta_c = \sqrt{R^2 - x^2 - y^2} \sin 2\varphi - 2x \sin^2 \varphi. \tag{3.55a}$$

Functions (3.54), (3.55) and (3.55a) permit one to determine the shifts of the image for any point on the input surface of lens 2. These formulas state that the shift decreases as the distance from the center increases.

A sample pattern of geometric distortions, introduced by a fiber system of given type, is shown in Figure 3.21.
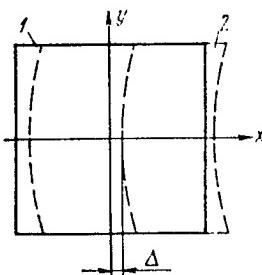
Figure 3.21. Pattern of Geometric
Distortions Introduced by Rotation of
Fiber Optic Element:
1--configuration of initial image;
2--configuration of image upon rotation
of fiber optic element

It also follows from expression (3.55a) that the motion of the image
will depend on the coordinates of the point and on the angle of
rotation, i.e.,

$$
\begin{aligned}
v_{\text{из}} = \dot{\Delta}_c = \\
= 2\dot{\phi}\left(\cos^2\phi\ \sqrt{R^2 - x^2 - y^2} - x\sin 2\phi\right).
\end{aligned}
\tag{3.56}
$$

The shift of the image in its absolute value is rather small during
exposure of the frame, and the compensation rotation will also be small.
Thus, the angle of rotation will comprise approximately $3°$ at the
required compensation shift of 0.5 mm and at diameter of the spherical
lens of 10 mm.

One can assume that the length of the fiber, combined with a given point
of the image, remains constant during the delay time. The shift of the
image for this point will then be determined only by the angle of

rotation of spherical lens 2, i.e., by $\Delta_c = d_B \sin\phi \approx d_B\phi$, while the

motion of the image will be proportional to the thickness of the movable

lens at a given point $v_{\text{из}} = \dot{\Delta}_c = \dot{\phi}d_B$.

This thickness is easy to determine as the difference of coordinates z_2
and z_1 of points lying on the surfaces of an inverted lens at the point
of intersection with the straight line, passing through a given point of
the image parallel to axis Oz, i.e.,

$$
d_B = 2\sqrt{R^2 - x^2 - y^2}.
\tag{3.57}
$$

107

Using this formula, one can easily determine the value $v_{\text{из}}$ for any point of the field and also the relative error of the rate of compensation on the edge of the field compared to the central point.

Example. Let R = 35 mm and let the frame be 20 × 20 mm. We then have for the most distant point with coordinates x = ±10, y = ±10 from formula (3.57):

$$d_{\text{в. кр}} = 2\sqrt{35^2 - 10^2 - 10^2} = 64 \text{ мм};$$

$$d_{\text{в0}} = 2 \cdot 35 = 70 \text{ мм} - \text{thickness along axis } Oy;$$

$$\delta = \frac{d_{\text{в. кр}} - d_{\text{в0}}}{d_{\text{в. кр}}} = 5{,}7\%.$$

The motion of the image on the edge of the visual field is 5.7 percent less than that in the center.

If the condition of automatic stabilization is given, it follows from formula (3.57) that the condition $\dot{\varphi}_1 d_{\text{в}} = f' \dot{\varphi}_{\text{ап}}$ should be fulfilled.

If the angular rates are equal, the focal distance of the objective should be equal to the diameter of spherical fiber lens, which limits very considerably the range of application of this device. A mechanism with transfer factor k > 1 is preferable, then $\dot{\varphi}_{\text{k}} d_{\text{в}} = f' \dot{\varphi}$, where $\dot{\varphi}_{\text{k}} = k\dot{\varphi}$.

For example, a spherical lens with one-half the diameter of the focal distance of the objective is required at k = 2.

Stabilization devices with planoparallel fiber optic elements. It was shown above that fiber optic elements, which are a planoparallel plate in which the individual light guides form an angle with the input and output surfaces differing from 90° upon rotation about the axis perpendicular to them, causes motion of the image in a circle; the image itself remains parallel to itself, i.e., the fiber optic element coincides in its effect to the single rotary optical wedge.

The combination of two similar fiber optic elements, rotating in different directions at identical angular rates w, leads to motion of the image at a rate whose amplitude is generally determined by the following expression:

$$v_{\text{из}} = \omega \sqrt{r_1^2 + r_2^2 + 2r_1 r_2 \cos \omega t}, \qquad (3.58)$$

while $r_1 = d_1/\text{tg}\,\alpha_1$; $r_2 = d_2/\text{tg}\,\alpha_2$, where d_1 and d_2 are the thicknesses of the corresponding fiber optic elements and a_1 and a_2 are the angles of inclination of the light guides in the corresponding fiber optic elements. The angle of rotation of the velocity vector with respect to zero position ϵ is determined by the expression

$$\epsilon = \text{arctg}\left(\frac{r_1 - r_2}{r_1 + r_2}\,\text{tg}\,\omega t\right).\tag{3.59}$$

It follows from expression (3.58) that the motion of the image will retain its direction at $d_1 = d_2$ and $r_1 = r_2$ and it will vary by harmonic law, i.e., $v_{\text{из}} = 2\omega r \cos \omega t$.
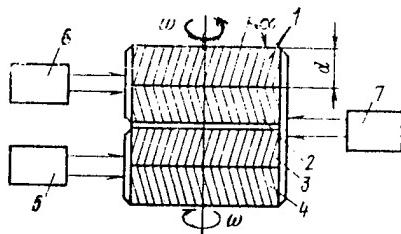

Figure 3.22. Layout of Stabilization Device
With Planoparallel Fiber Optic Elements:
1, 2, 3, 4--planoparallel fiber optic element;
5--drive for mutual rotation of elements 3 and
4; 6--drive for mutual rotation of elements 1
and 2; 7--drive of stabilization system

A variant of a combination of flat fiber optic elements is presented in Figure 3.22, which can be used as an actuating element in an image field stabilization system. The stack of fiber optic elements consists of four plates, which are combined in pairs such that there is no misalignment of the image with respect to the optical axis. Moreover, the plates of each pair have the capability of being rotated with respect to each other. Each of the pairs causes no additional displacements whatever upon rotation in the neutral position. If pairs of fiber optic elements are rotated about the optical axis in opposite directions and if additional rotation of the constituent parts is given in each pair, the amplitude will vary from 0 to $v_{\text{max}} = 4\omega r \cos \omega t$. at the same rotational velocity ω. The direction of motion of the image will also vary.

Flexible fiber optic elements find their application as the element of a stabilization device in optical mirror-lens systems. One of these solutions, developed by the Rank Organization with respect to wide-angle

109

observation systems (up to 120°), is presented in Figure 3.23.
(Footnote) (British patent 1,374,765) This system contains a
mirror-lens objective with spherical concave mirror 1, which focuses the
light impinging on it on the curvilinear surface of the image 4. The
center of curvature of the surface of the image coincides with that of
the spherical mirror, while the radius of curvature comprises half that
of the spherical mirror. Flexible fiber light guides 2 are used to
transmit the image to the output module. The fiber elements in the form
of a flat tape or strand are attached together with the mount of the
lens system in a gimbal suspension, upon rotation of which the image is
scanned with respect to the center of curvature and it is transmitted by
the fiber elements. Misalignment of the image due to vibrations is
eliminated and formation of a stable image is provided in the output
module of the device.
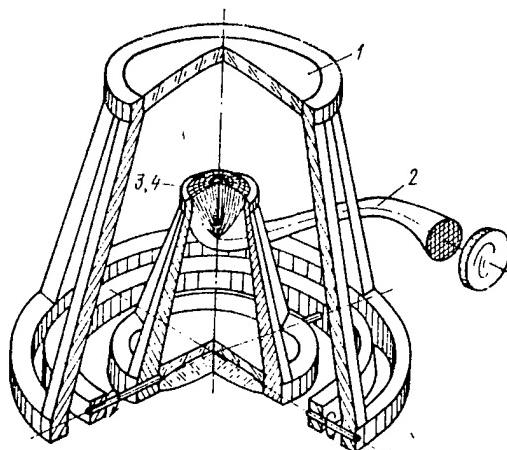
Figure 3.23. Stabilization Device With
Flexible Fiber Optic Elements:
1--mirror; 2--light guide; 3--surface
of light guide; 4--surface of image

3.5. Stabilization Devices Using Elements of Objective

Stabilization devices in mirror objectives. (Footnote) (This section
was written jointly with Yu. A. Stepin) A so-called "neutral point,"
located on the optical axis of the main mirror, exists for two-mirror
optical systems. Rotation of the secondary mirror with respect to it
does not worsen the quality of the image, but results only in
misalignment of the image. This mirror can generally be used as the
element of an image field stabilization system. The neutral point for
Cassegrain-type objective, for example, lies at the following distance
from the vertex of the secondary mirror (Figure 3.24) [51]

$$x_N = \pm \beta q f'_{\text{экв}} = \mp S_2, \qquad (3.60)$$

where $\beta = -S_2/S_2'$; $q = 1/\alpha$; $\alpha = f_1'/S_2$.
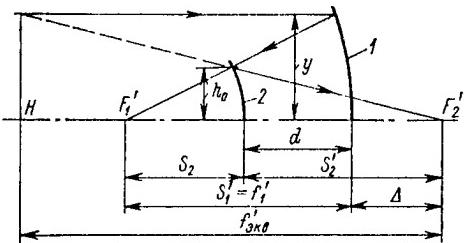
Figure 3.24. Diagram of Two-Mirror Objective:
1—main mirror of objective; 2—secondary mirror

It is pointed out in [51] that aplanatic two-mirror systems, for example, the two-mirror layout of a Ritchey-Chretien telescope, permit rotation of the secondary mirror with respect to a neutral point by a larger angle than non-aplanatic systems. The distance from the apex of the mirror to the neutral point is determined by the following expression:

$$x_N = \pm \frac{(1-\beta^2)(1-q)\beta q}{(1-\beta^2)(1-q)+\beta^2} f'_{\text{экв}} = \pm \frac{1}{1 + \frac{\beta^2}{(1-\beta^2)(1-q)}} \beta q f'_{\text{экв}}. \qquad (3.61)$$

It follows from comparison of formulas (3.60) and (3.61) that the distance of the vertex of the secondary mirror to the "neutral point" is less in aplanatic systems, which has a considerable effect on the design of the image field stabilization device. The calculations presented in [61] show that the neutral point lags behind the vertex of the mirror by $x_N = -0.646$ m for an aplanatic space telescope, made according to the layout of a Ritchey-Chretien telescope with mirror diameter of 2.4 m and $f'_{\text{екв}} = 57.5$ m.

Stabilization devices in lens objectives. Rather large decentering of optical systems without significant deterioration of the quality of the optical system is permissible in lens optical systems containing aplanatic surfaces. Compared to mirror systems, lens systems contain 8-12 and sometimes 20 individual lenses each and their combinations determine the enormous number of layouts of the objective and modifications of them; therefore, analytical determination of "neutral" points induces specific difficulties. However, this variety of layouts permits simultaneous decentering of several surfaces. A procedure that permits one to determine surfaces which can be decentered and can be used to design image field stabilization systems will be considered below. The method of mutual compensation of decentering, developed by

111

Yu. A. Stepin, is used extensively in design of high-quality optical objectives (especially in those cases when the required tolerances on decentering of individual lenses are extremely high and are essentially impossible to fulfill). Yu. A. Stepin demonstrated that there are surfaces in objectives of different classes which mostly form a quasi-aplanatic system in combination. This method was also applied to image field compensation systems.

It was established that the statement that there is a linear dependence between the increment of aberration and misalignment of the image due to decentering is valid with sufficient degree of accuracy for objectives with angles of the visual field of $2w' \leq 20°$ [72].

With this condition, the increment of aberrations and the misalignment of the image with decentered optical elements can be found from the following expressions to an ideally centered system:

$$
\left.
\begin{aligned}
\delta &= |\delta \Delta y'_k|_i - |\delta \Delta y'_n|_i \frac{\sum\limits_{i=1}^{p} |\delta \Delta y'_k|_i}{\sum\limits_{i=1}^{p} |\delta \Delta y'_n|_i} ; \\[2ex]
\Delta S &= \Delta y'_{c0k} + \Delta y'_{c0n} \frac{\sum\limits_{i=1}^{p} |\delta \Delta y'_k|_i}{\sum\limits_{i=1}^{p} |\delta \Delta y'_n|_i} ,
\end{aligned}
\right\}
\tag{3.62}
$$

where $|\delta \Delta y'_k|$, $|\delta \Delta y'_n|_i$ are the absolute increments of aberrations at the i-th point of the image field of the k-th and n-th elements of the objective, respectively, during identical decentering of them by b_k, $\Delta y'_{c0k}$, $\Delta y'_{c0n}$ are misalignments of the image with the same decentering b_k of the same elements of the objective, and $\sum\limits_{i=1}^{p} |\delta \Delta y'_k|_i \Big/ \left(\sum\limits_{i=1}^{p} |\delta \Delta y'_n|_i \right)$ is a coefficient that determines the relationship between decentering of the k-th and n-th elements, at which there is mutual compensation of the increments of aberrations of the objective caused by them.

It is easy to show that the values of decentering b_k for the k-th and b_n for the n-th elements of the objective are linked by the relation:

$$
b_n = b_k \frac{\sum\limits_{i=1}^{p} |\delta \Delta y'_k|_i}{\sum\limits_{i=1}^{p} |\delta \Delta y'_n|_i} .
\tag{3.63}
$$

One can write with regard to the above arguments and also using the dependence between the small scattering circle of the system, spatial frequency and FPM on this frequency [20]

$$\delta_{ocn} + \left(|\delta \Delta y_k'|_i - |\delta \Delta y_n'|_i \frac{\sum\limits_{i=1}^{p} |\delta \Delta y_k'|_i}{\sum\limits_{i=1}^{p} |\delta \Delta y_n'|_i} \right) \approx \frac{2}{\pi N} \sqrt{2.5(1-T)}.$$

Hence,

$$T = 1 - 0.1 \left[\delta_{ocn} + (|\delta \Delta y_k'|_i - |\delta \Delta y_n'|_i \frac{\sum\limits_{i=1}^{p} |\delta y_k'|_i}{\sum\limits_{i=1}^{p} |\delta y_n'|_i} \right]^2 \pi^2 N^2.$$

Taking into account that $T_{сл} = \exp(-2\pi^2 a_v^2 N^2)$, where $T_{сл}$ is the FPM of a random shift of the image and a_ν is the misalignment of the image during the delay, we find the criterion for estimating the suitability of selected optical elements for solution of the compensation problem

$$1 - 0.1 \left[\delta_{ocn} + \left(|\delta \Delta y_k'|_i - |\delta \Delta y_n'|_i \frac{\sum\limits_{i=1}^{p} |\delta \Delta y_k'|_i}{\sum\limits_{i=1}^{p} |\delta \Delta y_n'|_i} \right) \right] \pi^2 N^2 \gg \qquad (3.64)$$

$$\gg k_0 \exp \left(-2\pi^2 a_v^2 N_{раб}^2 \right).$$

Table 3.5, which is a summary of the effective of decentering of the surfaces of lenses of the objective on the position and quality of the image shaped by them with alternate decentering of each of the surfaces by the same value, can be used to determine the most suitable surfaces or elements of the objective, suitable for the role of image motion compensator. These tables are compiled in development of any objective according to known programs that guarantee calculation of the path of real rays.

113

Table 3.5

(1) Угол поля зрения объектива ω'	(2) Координаты в плоскости выходного зрачка, мм	(3) Аберрация исходной системы, мм	(4) Приращение аберраций для поверхностей		
			№ 3		№ 8
			(5) при $b = 0,2$ мм, $\Delta y'_{c0} = 0,476$ мм	при $b = 0,37$ мм, $\Delta y'_{c0} = 0,865$ мм	при $b = 0,2$ мм, $\Delta y'_{c0} = -0,531$ мм
0	33,3	0,001	0,015	0,028	—0,028
	23,56	—0,002	0,007	0,013	—0,013
	—23,56	0,002	0,007	0,013	—0,014
	—33,33	—0,001	0,014	0,026	—0,030
—3° 30'	31,14	0	0,027	0,050	—0,052
	16,00	—0,001	0,010	0,018	—0,018
	—16,00	0,001	—0,004	—0,007	0,005
	—30,8	0,002	—0,001	—0,002	0
7°	23,81	0	0,025	0,05	—0,054
	8,00	0	0,007	0,013	—0,014
	—8,00	0	—0,006	0,010	0,010
	—25,50	0,001	—0,014	—0,026	0,023

KEY:
1. Angle of visual field of objective ω'
2. Coordinates in plane of exit pupil, mm
3. Aberration of initial system, mm
4. Increment of aberrations for surfaces
5. at

The increments of aberrations of the initial value with respect to Octon-5 objective are presented in Table 3.5. In this table, b is the decentering of the surface and $\Delta y'_c$ is the misalignment of the image.

It follows from Table 3.5 that the increment of the aberrations, caused by decentering of the eighth optical surface by $b_8 = 0.2$ mm is essentially compensated completely for all angles ω' and points m of the working field of the increment of aberrations, caused by decentering of the third optical surface in the same direction by $b_3 = b_8 \cdot 1.85 = 0.37$ mm, where 1.85 is the coefficient of mutual compensation of aberrations. It also follows from this table that the image is misaligned by $\Delta y'_{c03} =$ = 0.468·1.85 = 0.865 mm (0.468 mm is the misalignment of the image upon decentering of the third surface by $b_3 = 0.2$ mm) upon decentering of the third surface by $b_3 = 0.37$ mm, while the image is misaligned in the

114

opposite direction by $\Delta y'_{c08}$ = -0.532 mm upon decentering of the eighth surface by b_8 = 0.2 mm. Thus, simultaneous decentering of the third and eighth surfaces in the same direction with transfer relation (1.85) causes misalignment of the image by $\Delta y_{c03,8}$ = 0.865 - 0.532 = 0.333 mm with the quality of the image created by the objective practically unchanged. Thus, the third and eighth surfaces form a quasi-aplanatic system in combination.
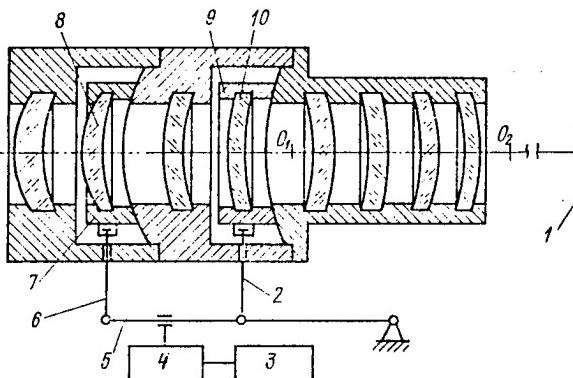

Figure 3.25. Arrangement of Objective With
Movable Lenses:
1--focal plane; 2, 6--articulated rods; 3--
sensor of rate of misalignment of image; 4--
processing system; 5--processing mechanism;
7, 9--movable mounts; 8, 10--lenses

One of the possible solutions of an objective with movable lenses is presented in Figure 3.25. The objective constructs an image of the objects to be observed on a surface combined with the image detector. The image is displaced in the focal plane 1 of the objective during photography from a moving base. The sensor of the rate of misalignment of the image 3 issues a signal to the image displacement development system 4. The development mechanism 5, using articulated rods 6 and 2, rotates mounts 7 and 9, respectively, about axes passing through the centers of curvature O_1 and O_2. As a result of these rotations, the second surface of lens 8 and the first surface of lens 10 remain centered, and the first and second surfaces of these lenses, respectively, are decentered by b_3 and b_8, providing mutual compensation of aberrations, which are caused by this decentering. The indicated displacement of the lenses (decentering of two surfaces) results in compensation of image misalignment, caused by motion of the base with the device attached to it.

There is sometimes the possibility of not rotating the lenses of the objective, but of shifting them parallel to the optical axis by the same value. This can be illustrated on an example of the Tair-3 objective,

115

widely used in amateur photography and having the following data: f' =
= 300 mm, aperture ratio of 1:4.5, and 2ω' = 8°.

Data obtained as a result of misalignment of individual lenses are
presented in Table 3.6.

Table 3.6

(1) Угол поля зрения объектива ω'	(2) Координаты в плоскости выходного зрачка, мм	(3) Аберрации исходной системы, мм	(4) Приращение аберраций для линз		
			I	II	III
			(5) при $b = 0,2$ мм		
			$\Delta y'_{c0} =$ $= 0,423$ мм	$\Delta y'_{c0} =$ $= -0,215$ мм	$\Delta y'_{c0} =$ $= -0,008$ мм
0	30	—0,026	0,044	—0,042	—0,001
	15	—0,005	0,010	—0,009	0
	—15	0,005	0,010	—0,01	—0,001
	—30	0,026	0,044	—0,043	—0,002
2°	30	—0,028	0,038	—0,033	—0,005
	15	—0,007	0,008	—0,005	—0,002
	—15	0,007	0,013	—0,015	0,001
	—30	0,014	0,053	—0,055	0,02
4°	30	0,059	0,041	—0,027	—0,015
	15	0,010	0,007	—0,002	—0,005
	—15	0,010	0,017	—0,020	0,003
	30	0,003	0,063	—0,07	0,005

KEY:

1. Angle of visual field of
   objective ω'
2. Coordinates in plane of
   exit pupil, mm
3. Aberrations of initial
   system, mm
4. Increment of aberrations for
   lenses
5. at

It follows from the table that misalignment of the first two lenses in a
direction perpendicular to the direction of the optical axis results in
misalignment of the image by approximately the same value essentially
without a deterioration of image quality.

Experimental results of changing the resolution of the Tair-3 objective
as a function of decentering, which confirm the correctness of this
approach in development of compensation systems, are presented in Figure
3.26. The given graphs show that the quality of a system for the center
of the visual field essentially remains unchanged even when the system
is decentered by ±2.5 mm. The permissible amount of decentering
decreases as the visual field increases, but it can be permitted up to 1
mm even with regard to the edge of the field.
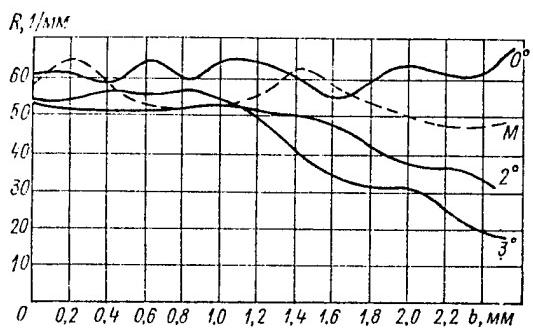
Figure 3.26. Measurement of Resolution of
Tair-3 Objective Upon Decentering of Pair
of Lenses

If one takes into account that photography is carried out using cameras
with exposure time of 0.01 s or less, this decentering permits one to
compensate for rates that reach values of 100 mm/s or more.

Stabilization devices in objectives with nonplanar image field. There
is a class of objectives in which the image is arranged along the
surface of the sphere or cylinder. Let us consider the possibilities of
developing apparatus in which these objectives are used. A working
diagram of such a system under vibration conditions is shown in Figure
3.27.

Let us assume that an optical device having an objective which
constructs an image along a cylindrical surface is rotated by some angle
about the axis passing through the rear nodal point. Point A, lying on
the optical axis at infinity, will be projected onto the same point of
the cylinder. If the image detector has the shape of a cylindrical
surface and is rigidly connected to the objective, blurring of the image
blurs. However, if the image detector is made movable and if it is
forced to maintain its initial position regardless of rotation of the
projecting objective, then (as follows from Figure 3.27) the image will
remain immobile. Thus, the image detector alone can be stabilized in a
camera in which an objective of the Spherogon type or panoramic
objectives developed by A. Bowers are used. (Footnote) (U.S. patent
2,923,220) Specifically, if the image detector is photographic film,
the leveling table with photographic film pressed against it must be
stabilized with the respect to the rear nodal point.
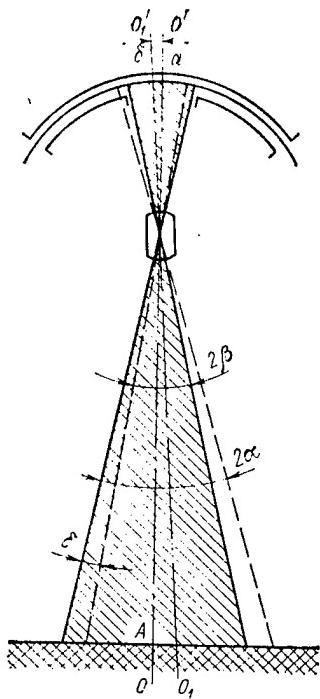
Figure 3.27. Layout of Stabilization Device,
in Which Objective With Nonplanar Field Is Used:
OO′, O₁O′₁ --optical axes of apparatus

One should note an important practical conclusion, since the effect of stabilization errors in the direction of scanning can be correcte by spatial stabilization of the leveling table containing the photographic film with respect to the rear nodal point of the objective to be used in panoramic cameras, designed according to layouts in which scanning by rotation of the objectives about the rear nodal point is provided.

One of the possible versions of this system is shown in Figure 3.28. The objective of the camera 1 constructs an image on a spherical or cylindrical surface, to which photographic film 3 is attached using leveling table 4. The carrier oscillates during aerial photography and all components of the AFA, rigidly connected to the body of the carrier, experience the same oscillations. Only the leveling table with the section of photographic film and the measuring roller 6 is stabilized in the AFA. Thus, all components of the chamber (except the leveling table and photographic film and measuring roller) are also rotated by angle α upon rotation of the platform, about its longitudinal axis by angle α. The image is not displaced with respect to the photographic film.
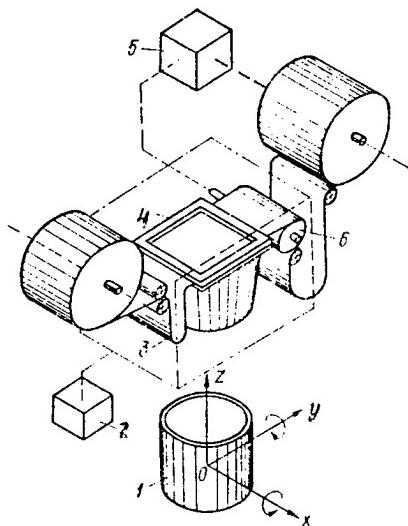
Figure 3.28. Layout of AFA in Which Objective
With Spherical Field Is Used:
1--objective; 2, 5--drives; 3--photographic film;
4--leveling table; 6--measuring roller

Another example of stabilizing the image field by using the main optical
components of the system is stabilization of the scanning devices
directly. There are a number of panoramic cameras in which the exposure
slot is fixed, while scanning is achieved either by reflecting or
prismatic elements, for example, by a cube prism. This prism, mounted
in front of the objective, is equivalent in its action to a flat mirror.
When this prism is rotated about an axis coinciding with the reflecting
edge and parallel to the exposure slot, the optical axis is deflected by
a double angle in the space of the objects. The motion of the image

caused by scanning is then determined by the relation $v_{H3} = 2f'\dot{\varphi}$.

On the other hand, rotation of the camera about an axis coinciding with
the scanning axis causes additional motion of the image for the center
of the photograph, equal to $v = f'\dot{\varphi}_K$, where $\dot{\varphi}_K$ is the angular rate of
rotation of the camera in bank angle. Comparing these expressions, it
is easy to conclude that regulated rotation of the scanning element is
feasible in the direction of scanning in panoramic AFA with fixed slot
for image stabilization, so that there is constant motion of the image
in the focal plane and the effect of an error of the stabilization
system on the quality of the recorded image is thus eliminated.

There is also a class of panoramic cameras in which rotation of the
optical system of the camera about an axis that does not pass through
the rear nodal point is used for scanning. The image is located on a

119

cylinder of radius R ≠ f', while the motion of the image is expressed by the function [44]

$$v_{из} = (R - f') \dot{\phi} = \dot{\phi}z, \qquad (3.65)$$

where z is the distance from the rotational axis to the rear nodal point.

It follows from formula (3.65) that the motion of the image at R < f' is directed in a direction opposite that of scanning, while the motion at R > f' coincides with the direction of scanning.

Thus, two stabilization devices must be introduced in these systems to stabilize the image field and namely: stabilization of the image detector with respect to the rotational axis of the scanning system to retain the position of the detector in space and simultaneous variation of the angular velocity of the scanning system.

Thus, panoramic AFA with rotation of the objective about an axis not passing through the rear nodal point are less advantageous than panoramic cameras, designed on other circuits, from the viewpoint of developing an image field stabilization system.

3.6. Stabilization Devices Using Mechanical Displacement of Image Detector

The image on a photodetector must be stabilized in some engineering problems only for a comparatively short time period. An example of these devices are cameras in which the quality of the image is determined by its misalignment during exposure. The misalignment of the image during such a short time is small and can be compensated by comparatively small displacements of the elements of the optical system. (Footnote) (For example, the misalignment of the image is only 1 mm at image motion of 100 mm/s and at delay of 0.01 s) Displacement of the objective in a plane perpendicular to the principle optical axis of the device or displacement of the photodetector (photographic film) is possible, besides the above versions. The section of film in the exposure zone in the latter case can be displaced linearly in two mutually perpendicular directions in the focal plane of the objective and, moreover, may have angular displacements about the principle optical of the device. This procedure permits one to obtain more complete compensation of image misalignment.

The design of an objective displacement mechanism or of an image detector should provide the necessary accuracy characteristics at minimal mass and overall dimensions. Detailed analysis of the alternative versions of using compensation is required in this regard. Devices that provide lateral displacement of the objective can be used efficiently only with comparatively small dimensions of the objective.

Otherwise, acceleration to the exposure time and subsequent deceleration of the mass of assembly result in the appearance of considerable reaction forces of the drives, acting on the base of the device, and as a result, oscillation of the device on shock absorbers.

Displacement of the film in the exposure zone to stabilize the image can be used more efficiently when it can be rigidly attached and for other reasons as well. This situation occurs, for example, in some designs of panoramic AFA, in which the panning motion of the scanning element should be accompanied by the corresponding misalignment of the photographic film. The film speed should be controlled with regard to the requirements of image stabilization along the frame. The film must be misaligned in this direction as well to compensate for projection of the rate of shift of the image perpendicular to the frame. A direct solution of the problem is the useof the assembly shown in Figure 3.29. The guide rollers 1 with clamping rollers 2 and with drive motors 3 are mounted on a carriage 4, having one degree of freedom of displacement in the transverse direction (toward the motion of the film). This linear motion can be provided by a cam mechanism 5 with drive 6. The use of two additional rollers 7, linked mechanically to the drive shafts, is provided to relieve the segment of film between the rollers of the fixed elements of the film transport mechanism. The film forms loops between rollers 1 and 7, which permit one to avoid deformation of the film in the exposure zone upon misalignment of the carriage. An obvious disadvantage of this device is the massive nature of the moving parts.

The design of a film displacement assembly (Figure 3.30), in which only the section of film to be exposed, having small mass, makes a reciprocating motion, while the moments of the response of the frames, oscillating toward each other, are mutually compensated and, accordingly, the dynamic moments acting on the base in this design are minimal, is suggested in one paper. (Footnote) (USSR inventor's certificate 1,151,913)

The film is moved along rollers 1, 2 and 8, 9, which rotate freely about their own axes in frames 3 and 10, forming a S-shaped line on the rollers. The presence of transverse misalignment of the image due to displacement of the base is compensated by rotation of the frames about their own axes due to the action of eccentric 5 on levers 4 and 7. Frames 3 and 10 are returned by spring 6 to their initial position during the exposure time. If the diameters of the rollers are equal to D_B, the film is misaligned by $S = \pi D_B \sin \beta$ upon rotation of the frames toward angle β.

121
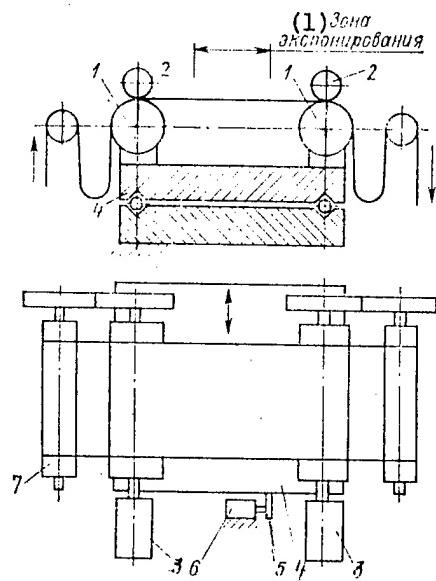
Figure 3.29. Image Stabilization Device by Displacement
of Photographic Film in Two Directions:
1--drive roller; 2--clamping rollers; 3--propulsive device;
4--carriage; 5--cam; 6--cam drive; 7--additional roller

KEY:

1. Exposure zone
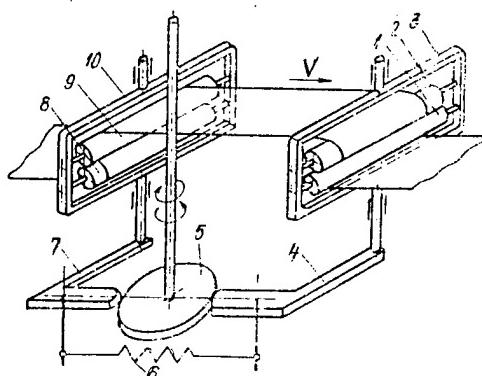
Figure 3.30. Film Displacement Assembly:
1, 2, 8, 9--rollers; 3, 10--frames;
4, 7--levers; 5--eccentric, 6--spring

The mass of the film is small; therefore, its linear displacement does
not result in the appearance of significant dynamic moments acting on
the base.

The layout of the rollers is presented in Figure 3.31, a. The lines of the beginning and end of contact of the film with the surface of the rollers are denoted by: AB, CD, EF, GH.

The position of the film is misaligned with respect to the rotors upon rotation of the rollers by angle β about axes OO and O_1O_1, located in the middle of their length (Figure 3.31, b).

The axes of the rollers occupy position $A'_1B'_1$ and $C'_1D'_1$, respectively (Figure 3.31, b). The film assumes the position shown in Figure 3.31, b by the dashed lines. It is obvious that the film is stretched. Component $F_{y.\pi}$ of elastic force F_y causes the film to slip along the roller to the position denoted by the solid line, provided that

$$(F_y + F_{\text{H}}) \sin \beta > (F_y + F_{\text{H}}) \xi,$$

where F_{H} is the force of the preliminary tension of the film and ξ is the friction of the film against the rollers.
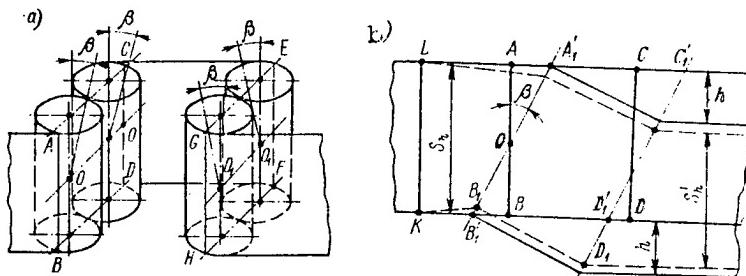

Figure 3.31. Diagram of Rotation of Guide Rollers (a) and Film Shifting Rollers (b)

This condition can be written in the form $\beta > \xi$ for small β; warping of the film in the exposure zone can then be estimated by the formula

$$\Delta S = S_n - S'_n = S_n (1 - \cos \beta) = 0{,}5 S_n \beta^2.$$

Hence, $\Delta S < 0{,}5 S_n \xi^2$. We find $\Delta S < 5 \cdot 10^{-6}$ m at $\xi = 0.005$ (lavsan on polished metal) and $S_n = 0.4$ m, which is quite permissible in most cases.

Thus, the use of different mechanisms to realize compensating movements of the film in the exposure zone is related to the need to solve a

123

number of design problems. Careful estimation of the different versions of compensators is necessary to make a decision about the efficiency of one or several degrees of freedom of the film instead of using other devices.

3.7. Electronic Image Field Stabilization Devices

There are additional capabilities of developing an image field stabilization system (or rather an organization of an image motion compensation system, caused by random rotations of the entire apparatus) in observation apparatus, in which image detectors of the television tube and image converter tube (EOP) type are used.

The essence of electronic stabilization systems is that misalignments of the image at the input (on the photocathode) of the EOP or of the television tube, caused by angular vibrations of the apparatus as a whole, are compensated by the corresponding misalignment of the electronic image when it is transported from the photocathode to the screen of the EOP or to the target of the television tube. Compensation misalignment of the electronic image is achieved by deflecting the electron beam by using electromagnetic or electrostatic deflecting systems. An electromagnetic deflecting system consists of two pairs of electromagnetic deflecting coils, mounted outside the tube. They permit deflection of the electron beam in two mutually perpendicular directions. The electrostatic deflecting system has two pairs of deflecting plates, mounted in two mutually perpendicular planes inside the tube after the anode cone. Special designs of the EOP or television tube are required for this system. Each pair of coils or plates is controlled by electric signals, fed from the angular position sensors of the camera in the same planes in which the deflecting coils or plates are mounted. As a result, the image on the EOP screen or on the target of the television tube is fixed.

It should be noted that the motion of the image can not be compensated electronically either on any image inverter tube or on any television tube. It follows from the foregoing that this compensation can be realized in a tube having an image transfer chamber. Moreover, the displacement of the electronic image may comprise fractions of a millimeter or several millimeters as a function of the design of the image tube. Otherwise, the quality of the image is reduced and the error in the rate of compensation on the edge of the image field increases.

Let us consider some engineering solutions of the electronic image field stabilization system for a night vision device, developed by the Itek Corporation (Figure 3.32). (Footnote) (U.S. patent 3,515,881)
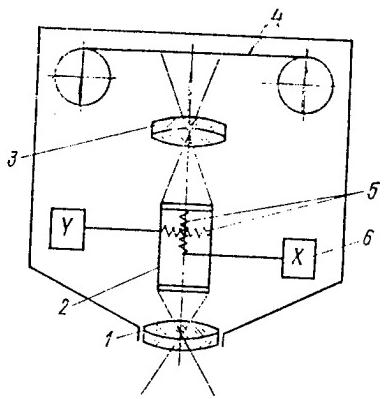
Figure 3.32.   Layout of Device With Electronic
Image Stabilization Systems:
1—objective; 2—image inverter tube; 3—projection
objective; 4—film; 5—electromagnetic coils; 6—gyroscope

The objective 1 constructs an image on the input screen of the image
inverter tube 2, from the output screen of which the image is
transferred to projection objective 3 to film 4 or is viewed in an
eyepiece.   Two electromagnetic coils 5, in the windings of which is fed
control voltage, proportional to the angular deflections of the optical
axis of the camera with respect to two mutually perpendicular axes x, y
of gyroscopes 6, are mounted inside the image converter tube.   The given
system can be used in a night vision aerial camera, in
high-magnification optical sighting devices and in other observation and
recording devices.   However, the use of gyroscopes and of special
integrated correcting circuits in the system results in a significant
increase of the cost of the camera.   The same company has developed a
more improved automatic stabilization system.   (Footnote) (U.S. patent
3,577,206)   The given device consists of an inner body, containing an
objective and image converter tube.   The inner body is in turn mounted
in the outer body such that they move with respect to each other.   The
inner body is arranged with respect to the outer body in a gimbal
suspension.   The angular vibrating motions of the outer body with
respect to the inner body induce electric current in the deflecting
coils of the EOP, which in turn create a counter motion of the electron
beam which stabilizes the image.   Inexpensive small potentiometers are
used to check the currents.

The Itek Company first developed those systems for astronomical
photography at which deterioration of image quality, caused by
vibrations of the telescope, must be prevented.   Systems with different
information channels were developed.   In some, information about
displacement of the object and about the corresponding variation of
current in the deflecting coils is provided by four photomultipliers.
In others, acceleration sensors in the horizontal and vertical planes

are used. If the moving object must be photographed with a moving camera (for which not one system has been adapted separately), both types of stabilizers are used, connecting them to each other.

This system permits one to obtain unblurred images of objects, vibrating at frequency up to 2,000 Hz. Specifically, this camera was used to photograph the valves of an operating internal combustion engine. An image motion compensation system during random vibrations of the camera can also be developed in optoelectronic devices, in which solid-state photosensitive charge-coupled devices (PZS) are used [54]. This device is an array (linear or two-dimensional) of single MOS components (metal + oxide + semiconductor), arranged on a chip as close as possible to each other, so that there is an electronic connection between adjacent components [54].

The operating principle of the CCD is as follows. If a negative voltage is applied to any one of the electrodes, a stripped region is formed in the surface zone of the semiconductor (the free electrons are repulsed into the inside of the chip), which is a potential well for holes. The effect of light induces generation of charge carriers inside the semiconductor, the formed holes are attracted to the dielectric-semiconductor interface, and are localized in this surface layer. The charge accumulated in the potential well is proportional to the illumination of the element.

If a high-amplitude negative voltage is applied to the electron (adjacent to that considered) at some moment, a deeper potential well is formed and the holes flow into it. Varying the control voltage on the electrodes in the necessary manner, one can direct transfer of the charge along the surface from structure to structure, up to exit of it from the chip, i.e., the spatial distribution of the light intensity in the CCD is converted to the relief of electric charges, localized in the surface region of the semiconductor. The charge packets flow from element to element, emerge to the outside, and yield a sequence of video pulses, adequate to the discernible specimen.

The motion of the image is compensated by synchronous displacement of all the charge packets in the array during accumulation (exposure).

A layout for designing a CCD array, in which the charge packets are stored and moved in the plane along two coordinates, was proposed in [79]. The device is formed by a two-dimensional block of MOS capacitors. Controlling the cadence voltages on the electrodes using external circuits, one can store and move the charge packets in any direction.

Although this CCD array was not used in real devices due to the complexity of addressing the two-dimensional electrode block, the direction itself in development of these CCD arrays is promising, especially with respect to a camera mounted on a moving base. The problem of compensating the random motion in one coordinate is most

simply solved for CCD detectors, operating in the time delay and storage (VZN) mode. The image detector consists of a number of MOS elements, which form columns extended in one direction. The image is scanned in the direction of the columns. The cadence frequency of this scanning is assigned by image motion sensors and the delay between separate inputs should be equal to the time of displacement of the image from one MOS element to another. Thus, storage occurs in the same charge packets, but in spatially different elements of the array. A long storage time can be achieved in the absence of blurring of the image by using the VZN mode. The motion of the image along the second coordinate should be compensated by one of the above methods.

If the rate of the charge packets differs somewhat from the rate of displacement of the image, image quality deteriorates. According to [6], the synchronization FPM is determined by the following function:

$$T_{\Delta v} = \frac{\sin\left[(\pi/2)(v/v_{\mathrm{H}})M(\Delta v/v)\right]}{(\pi/2)(v/v_{\mathrm{H}})M(\Delta v/v)},$$

where v_{N} is the Nyquist frequency for a CCD and $v_{\mathrm{N}} = 1/(2l_x)$; l_x is the size of the light-sensitive element in the direction of motion, Δv is the difference between the motions of the image and the rate of displacement of the charge packets, v is the rate of displacement of the charge packets, and M is the number of elements in the column.

It follows from this function that the permissible shift should not exceed one-third the size of the light-sensitive element; this shift comprises 5-10 μm under real conditions.

3.8. Comparative Analysis of Functional Image Stabilization Devices

The data presented in the previous paragraphs of the given chapter indicate the wide variety of image field stabilization devices. To determine the reasons for this variety, let us briefly consider the advantages and disadvantages of various image field stabilization devices.

Thus, image field stabilization systems based on optical wedge systems (OKS), used in devices with resolution of approximately 1 angular minute, permit the presence of an angle of variation of the wedge up to 5° (with regard to chromatic aberration of wedge compensators), i.e., a vibration amplitude of approximately ±3° can be provided in a single wedge.

Additional optical wedge systems must be introduced to correct the effect of chromatic aberration, which increases the overall dimensions and mass of the entire camera. However, selection of one or another layout of wedge compensator will also be largely determined by the

127

operating conditions of the camera. For example, an OKS using movable lenses is rather simple to combine with the main gyroscope stabilization element. One of the lenses of the optical wedge is attached to one rotor of the gyroscope and holds its position in space regardless of vibrations of the apparatus itself. This principle can be used in devices of any designation. It should be kept in mind that the diameter of the rotary lens is increased by approximately 17 percent of the radius of curvature of adjacent surfaces upon vibrations of the system in the range of ±5°, i.e., the increment is 51 mm with radius of curvature of 300 mm, which increases the size of the lens approximately 1.5-fold with an entrance pupil of 100 mm. This is not always permissible.

The range of application of liquid optical wedge systems (OKZhS) based on liquid wedges is determined as a function of their design. Thus, an OKZhS with open surface and also using nonmiscible liquids can operate successfully only in the absence of vibrations, which will cause deformation of the surfaces and thus worsen the quality of the image. It is for these reasons that liquid optical wedge systems have found their application in surveyor's instruments and specifically in levels. Liquid optical wedge systems using nonmiscible liquids and the line of the interface along a spherical surface are applicable in systems having entrance pupils of not more than 2-3 mm.

These systems, based on closed tubes with moving input windows, are free of essentially all the disadvantages of the previous liquid optical wedge systems, but they are inferior in simplicity of the design of optical wedge systems and namely: the diameter of the view port is increased considerably compared to the entrance pupil of the objective; dynamic achromatization of the system can be provided.

The use of stabilization devices that contain optical wedges, which rotate about the optical axis, also do not cause an increase of their diameter. But their disadvantage is the need to arrange a rather complex functional device that provide a nonlinear relationship between the rotation of the camera and rotation of the optical wedges. The wedges should not only be rotated, but should also be turned jointly about the optical axis of the camera.

Reflecting elements are preferable for use in stabilization systems, since these elements are essentially inertialless during the corresponding processing and providing the quality of manufacture. They can be mounted in both parallel and converging beams and can be used in practically all optical devices.

The corresponding designs of optical reflecting compensators (OZK) permit stabilization at larger vibration amplitudes. The disadvantages of these compensators should include an increase of their overall dimensions, since OZK operate on reflection and comprise a significatn angle with the optical axis of the system.

Fiber optic compensators (VOK) may find application in systems with large entrance pupils, at small dimensions of the image detectors, i.e., when the ratios of the detector and entrance pupil are approximately 1:10-1:1,000, which occurs when using CCD arrays.

Fiber optic compensators have yet another important advantage, and namely: the possibility of providing variable motion of the image along the entire image field simultaneously, which is necessary with different orientations of the camera. Moreover, the necessary law of variation of motion can be calculated and realized by the corresponding design of the VOK. However, it should be noted that stabilization can not be guaranteed by using VOK at large vibration amplitudes of the camera (greater than ±10°), while rates of not more than 50-100 mm/s are permissible for VOK operating in the image motion compensation mode due to random rotations of the system.

The use of the components themselves of the optical system, having optical intensity in image field stabilization devices, is very feasible, since the same optical elements perform various types of functions. The above examples indicate that these systems may not operate at large angular displacements and they should be recommended as additional circuit elements that perform fine stabilization of the image.

Thus, the following problems always arise before the developer of an optical device, mounted on a moving base.

1. Is it necessary or not to introduce an image field stabilization system into the device?

2. If "yes," then which type of stabilizer is used in development of one or another optical device?

Selection of one or another engineering solution, when the same problem can be solved by essentially all types of operating systems, is determined largely by the experience and skills of the developer, by the tooling of the enterprise that produces this type of instrument and so on.

However, one can formulate several principles by which one should be guided in selection of an operating system: 1) it is desirable to stabilize the image field by displacing the elements of the device itself, i.e., without introducing additional elements; 2) elements with the least mass should be selected from all the possible optical elements that permit image stabilization; and 3) preference should be given to reflecting elements if it is necessary to introduce an additional optical element into the system.

Chapter 4.   Information Systems for Checking Image Misalignment

4.1.   Information Systems for Checking Spatial Displacements of Moving
       Bases in Problems of Indirect Control of Image Misalignment

Open and closed image stabilization systems were considered in Chapter
2.   The presence of an information system for checking the current
parameters of spatial displacements of the base was suggested in the
first systems.   This information can be obtained only if a reference
coordinate system, developed by one or another method, is on a moving
base.   This method ordinarily consists in the use of gyroscopic devices,
combined into an information system.   If there is the possibility of
constant or periodic tie-in to some objects, the relative position of
which is known beforehand (astronavigation objects, radio beacons,
navigation satellites and others), this reference coordinate system can
be corrected.   Information about the position of the base with respect
to the earth can be used to create a reference coordinate system.   This
information is taken from sensors of the earth's physical fields
(pendulums, magnetic compasses, infrared vertical gyros and so on) and
is processed in a computer module or is used to correct onboard
gyroscopes.   A three-axis gyro-stabilized platform, which maintains a
fixed position in inertial space, can be used as the physical reference
coordinate system.   Information about the spatial angular displacements
of the base is fed to the coordinate converter from sensors of the
relative angular position of the axes of the platform and is used as an
assignment in the control system of the image stabilization device.
Besides sensors of the current value of the angular parameters of motion
of the base, linear velocity sensors with respect to displacement of the
base and of the surveying object (observations) and also sensors of the
distance to this object are used in image stabilization problems.   The
linear velocity of the base can be determined by using an inertial
navigation system or optical, radio engineering and any other devices.
The distance to the object of observation is measured by using
rangefinders, altimeters and other similar instruments.   These devices
are described in detail in the technical literature, for example, in
[39, 49]; therefore, they are not considered in this book.

A physical reference coordinate system can sometimes be replaced by a
mathematical model of it, which is constructed on a computer according
to the indicators of the sensors of angular spatial displacements of the
base.   An example of such a device is a gimballess system (BINS) [31].
Practically any gyroscope having sufficient accuracy can be used as the
sensors of this system.   The disadvantage of the BINS is the need to use
to use sensors with wide range of measured parameters, which is not
always compatible with high measurement accuracy.   At the same time,
sensors which are essentially null indicators of deviation of the
platform from the position fixed in inertial space, can be mounted on a

130

gyro-stabilized platform. It is obvious that these sensors can have characteristics with large curvature and high stability. The accuracy of the entire device is dependent on the accuracy of fulfillment of the gimbal suspension mechanism of the platform and on the operating accuracy of the platform drive control systems.

The problem of image stabilization is sometimes solved through synchronous operation of several local drives. The master signals can also be taken from gyroscopes, attached to the base or shifted with respect to the base together with the structural elements of the image stabilization device, in the feedback circuit of the control systems of these local drives. In the latter case, this local drive, with a gyroscope in the feedback circuit, forms a one-axis gyro stabilizer whose operation will be considered in detail below.

Methods of monitoring spatial displacements of moving bases in image shift control problems. Gyroscopic sensitive elements (ChE) are used to determine the parameters of spatial angular displacement of the base. Gyroscopes with two or three degrees of freedom having different methods of suspension of the rotor are used as the sensitive elements in image stabilization systems.

Gyroscopes on new physical principles, for example, vibratory and laser gyroscopes, having recently been developed intensively and introduced.

Gyroscopes with two degrees of freedom are used more frequently than others to solve stabilization and orientation problems with regard to their simplicity and reliability. The accuracy of gyroscopes with two degrees of freedom is improved by reducing the frictional moments in the supports of the suspension by different methods [42, 64]. Thus, purified gas is delivered to the narrow space between the cylindrical float and the inner surface of the float chamber of the instrument in floated gyroscopes with gas dynamic suspension. This suspension provides small frictional moments and insignificant drift rates (several angular seconds per second). The disadvantages of these instruments are the need for compressed air reserves or for an onboard compressor and high requirements on the precision of manufacture of parts of the device.

The most widely distributed type of gyroscope is the integrating floated gyroscope (PIG) [42]. The space between the cylindrical float and the body of this instrument is filled with liquid having high specific weight and large coefficient of viscosity. The weight of the float and the lifting force of the liquid are selected so that the supports of the suspension are completely relieved and so that they perform the roll of axial and radial displacement limiters of the float when loads act on the PIG. The drift of the PIG does not exceed fractions of angular seconds per second. An angle-data transmitter and torque sensor are mounted on the precession axis of the float. The simplified equation motion of the PIG can be represented in the form

$$H_\Gamma \dot{\alpha} - b\dot{\beta} = 0,$$

where α is the angle of rotation of the PIG about the axis of sensitivity, β is the angle of rotation of the float about the precession axis, b is the coefficient of the viscous friction moment about the precession axis, and H is the moment of momentum of the gyroscope.

Integrating this expression, we find

$$\beta = H_\Gamma \alpha / b + \beta_0,$$

where β_0 is the initial angle of rotation of the float.

Thus, the rotational angle β of the float about the precession axis, fixed by the angle-data transmitter, is directly proportional to the angle of rotation of the PIG about the axis of sensitivity. With more detailed consideration, the transfer function of the PIG by control action can be expressed in the form

$$W(p) = \frac{\beta(p)}{\alpha(p)} = \frac{k_\Gamma}{T_\Gamma p + 1},$$

where $k_\Gamma = H_\Gamma / b$ is the transfer factor of the PIG and T_Γ is a time constant.

For most serial instruments $k_\Gamma = 0.1-1$ and $T_\Gamma = 0.001-0.01$ s,

In the case of developing a restoring moment along the precession axis of a two-degree gyroscope in some manner, its deflection angle along this axis is proportional to the rotational velocity along the precession axis. This instrument is called a gyrotachometer and has a transfer function of type

$$W(p) = \frac{\beta(p)}{\alpha(p)} = \frac{k_{\Gamma T} p}{T_{\Gamma T}^2 p^2 + 2\xi T_{\Gamma T} p + 1},$$

where $k_{\Gamma T} = H_\Gamma / c$ is the transfer coefficient of the gyrotachometer, and c is the coefficient of the angular stiffness of the spring and $T_{\Gamma T}$ is the time constant of the gyrotachometer ($T_{\Gamma T} = 0.01-0.1$ s).

132

The restoring moment can be found in the simplest case by using springs, but a more promising direction from the viewpoint of improving the accuracy is development of feedback from the angle-data transmitter to the torque sensor (a so-called electric spring).

The range of velocities to be measured by the gyrotachometer is dependent on the angular stiffness of the springs and comprises 0.01-1.0 s^{-1}.

Laser gyroscopes. One of the promising sensitive elements in image stabilization systems is the laser gyroscope (LG) [18]. This is explained by the uniqueness of its characteristics. The most important of the following: wide range of velocities to be measured ($5 \cdot 10^{-8}$-100) 1/s, short readiness time to operation after switch-on (approximately 0.05 s), a practically unlimited number of starts, high reliability, stability to mechanical effects, insensitivity to linear accelerations, convenience in processing the frequency form of measurement results and in joining angular displacements to pulse sensors, and low power consumption.

The basis of the laser gyroscope is a ring laser, in which two waves are propagated in opposite directions. The difference frequency Δf of the opposite waves is dependent on the angular rotational velocity of the laser gyroscope in inertial space about the axis of sensitivity, perpendicular to the plane of the cavity.

The input characteristic of the laser gyroscope can be approximated by the expression [18]

$$\Delta f = \sqrt{(k_{\text{ЛГ}}\Omega + f_0)^2 - f_1^2},$$

where $k_{\text{ЛГ}}$ is the transfer factor of the laser gyroscope, f_0 is displacement of the center of the characteristic caused by the features of the laser gyroscope, and f_1 is the boundary frequency of the synchronization range of the counter waves.

According to the above expression, the characteristic of the laser gyroscope has a range of insensitivity and sections with considerable nonlinearity at small input signals. Beginning with angular velocities on the order of 0.3-0.4 s^{-1}, the input characteristic of the laser gyroscope is essentially linear, i.e., $\Delta f \approx k_{\text{ЛГ}}\Omega$.

The transfer factor of laser gyroscopes of acceptable overall dimensions is very high and comprises $k_{\text{ЛГ}} = (2 \cdot 10^5 - 2 \cdot 10^6)$ Hz·s. The input characteristic of the laser gyroscope is linearized by introducing the initial displacement of the working point by one or another method. Rotational or oscillatory motion about the axis of sensitivity is given

133

to the laser gyroscope for this purpose or elements having phase independence are placed in the optical circuit of the laser gyroscope. Measures should be adopted at the same time to eliminate that part of the output signal of the laser gyroscope which corresponds to the initial displacement or is related to introduction of this displacement. It should be noted that functional displacements of the optical element can be used in image stabilization systems for the initial shift of the laser gyroscope.

No fewer than three laser gyroscopes with mutually perpendicular axes of sensitivity must be installed to obtain complete information about the parameters of the motion of the base. Specific difficulties arise in introduction and subsequent elimination of the initial bias of the laser gyroscope. One of the methods [17] of solving this problem is to arrange these gyroscopes so that their axes of sensitivity comprise an orthogonal trihedron. Simultaneous rotation or oscillating motion about an axis not coinciding with any axis of sensitivity is imparted to all three gyroscopes (Figure 4.1). The array of laser gyroscopes 1 and the rotor of the relative angular position sensor (IU) 4 are set into rotation by drive 3. The signals from the outputs of the laser gyroscope and the relative angular position sensor are processed in computer module 2 and can also be used to control drive 3.
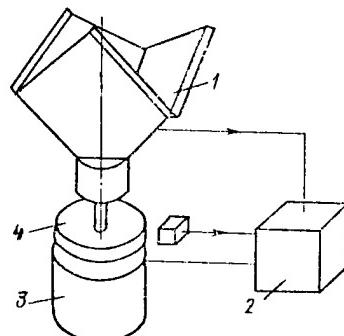
Figure 4.1. Diagram of Laser Gyroscope Array:
1--laser gyroscope array; 2--computer module;
3--drive; 4--relative angular position sensor

A coordinate system, bound to the base $Ox_1 y_1 z_1$, and coordinate system $Oxyz$, formed by the axes of sensitivity of the laser gyroscope, are presented in Figure 4.2. These systems are rotated with respect to each other by angles φ, ψ and ϵ.

It follows from Figure 4.2 that the angular velocity vector $\dot{\varphi}$ of the gyroscope array about axis Oy_1 is projected onto the axes of all the laser gyroscopes and can be used to create simultaneous initial bias of them.

There is the following correlation between the vector of the angular velocity of the base Ω_0 and that of the gyroscope Ω_r:

$$\Omega_r = A_\epsilon A_\psi (A_\eta \Omega_0 + \dot{\varphi}),$$

where A_ϵ, A_ψ, A_η are the matrices of the direction cosines, corresponding to rotations by angles ϵ, Ψ and φ, respectively.

The following conditions must be fulfilled to achieve equal misalignments of all the laser gyroscopes:

$$\sin \psi = 1/\sqrt{3}; \quad \sin \epsilon = \cos \epsilon = 1/\sqrt{2}.$$

One can find from expression (4.1):

$$\Omega_{x1} = \frac{1}{\sqrt{2}} A \sin \varphi + \frac{1}{\sqrt{6}} B \cos \varphi;$$

$$\Omega_{y1} = C/\sqrt{3} - \dot{\varphi};$$

$$\Omega_{z1} = \frac{1}{\sqrt{2}} A \cos \varphi - \frac{1}{\sqrt{6}} B \cos \varphi,$$

where $A = \Omega_x - \Omega_y$; $B = 2\Omega_x - \Omega_y - \Omega_z$; $C = \Omega_x + \Omega_y + \Omega_z$; Ω_x, Ω_y, Ω_z are the projections of the angular velocities onto the axes of sensitivity of the laser gyroscope and Ω_{x1}, Ω_{y1}, Ω_{z1} are the projections of the angular velocities onto the axes, bound to the base.

The relative velocity or relative angle of rotation of the gyro unit must be introduced from the measurement results to eliminate the signal, corresponding to the initial misalignment. A measuring algorithm with averaging at angular intervals can be realized in the latter case.

The mean value of the angular velocity during rotation t_i by angle φ_i is determined by the expression

$$\Omega_{ji} = \frac{1}{t_i \varphi_i} \int_t \int_\varphi \Omega_j \, dt \, d\varphi,$$

where $j = x$, y, z and i is the number of the measurement cycle.
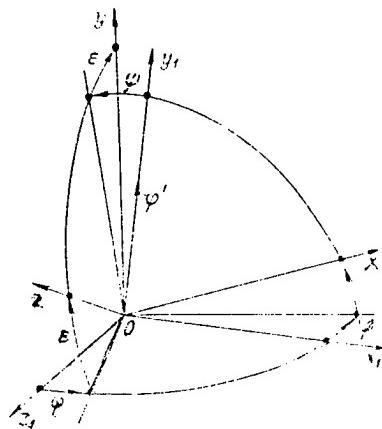
Figure 4.2. Coordinate Systems of Base and of
Axes of Sensitivity of Laser Gyroscopes

Harmonic oscillating motions of the gyro unit about axis Oy_1 according
to the law $\varphi = a \sin \omega t$, where a is amplitude and ω is the circular
vibration frequency, can be used instead of rotational motion.

The readings are taken from this gyro unit by integration of the beat
frequency of the laser gyroscope during one or a number of vibration
periods. The relative angular misalignment sensor of the gyro unit is
not required and the design of the computer module is simplified
somewhat.

4.2. Methods of Direct Check of Image Misalignment

Survey of methods of check image misalignment. Photoelectronic image
misalignment check systems (SKSI) permit one to determine directly the
extent, rate and direction of misalignment of the image. Direct check
information systems are in most cases considerably simpler indirect
check devices and are also distinguished by low inertia and rather high
accuracy. But certain deficiencies are also inherent to them as to any
other information systems. The most important of these deficiencies is
the possibility of operating failures in cases when the optical image of
the surface to be monitored has no sections of different illumination
(for example, there are no parts in images of the sea surface, of an
even section of desert, of a cloud layer that conceals the earth's
surface and so on).

The direct check system must be complicated with regard to this
deficiency, by introducing memories and other components into the data
processing channel, which guarantee operation of the automatic image
stabilization system (ASSI) over the time interval when no data are
issued from the SKSI sensor.

136

Optical image misalignment check systems (SKSI) are understood as optoelectronic information measuring systems that yield information in analog or digital form about the rate or absolute value of misalignment and also about the direction of misalignment of the optical image, created by the objective of the optical device, for example, by the objective of the AFA. All optoelectronic SKSI are based on analysis (by one or another physical method) of the law of distribution of the illumination of the image of the object, created by the optical system, and by the nature of its variation over time. Before turning to consideration of devices and the operation of various direct check SKSI, one must become familiar briefly with the classification of these information measuring devices. The features by which SKSI are classified can be the most diverse. Devices are distinguished by such a physical feature as the radiation spectrum for operation in the ultraviolet, in the visible and in the infrared regions of the spectrum.
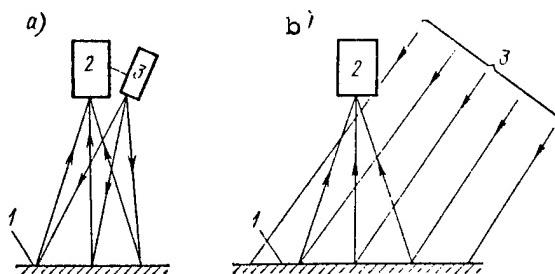

Figure 4.3. Varieties of SKSI:
a--active; b--passive; 1--object;
2--detector; 3--radiation source

Like other optoelectronic measuring devices, SKSI can be divided into active, semi-passive and passive. The object 1, an image of which is studied by system 2, is irradiated in active SKSI (Figure 4.3, a) by an electromagnetic radiation source 3, the characteristics of which can be controlled. In passive SKSI (Figure 4.3, b), the object 1, an image of which is also studied by system 2, has natural radiation or the radiation 3 of a natural light source (sun or moon) is used. Most modern SKSI are passive, while the use of active SKSI is limited by the power of the radiation sources and by a number of other factors. Passive SKSI can in turn be divided into a number of types, for example, into SKSI in which scanning and modulation of the light beam are used, into mosaic-type SKSI and so on. Only one detector is used in most SKSI of the first type. Different raster structures (fixed and movable raster arrays, switched strip photoelements and other devices) are used in these systems to modulate the luminous flux. A large number of detectors is used in mosaic-type SKSI. Scanners are used in some SKSI. The image can be scanned by displacement of the image with respect to a fixed analyzing diaphragm or by displacement of the diaphragm with respect to the image. Active and passive SKSI can be divided by operating principle into five types: time-pulse, frequency, phase,

137

amplitude and correlation (Figure 4.4). Time-pulse SKSI [32, 34, 65] are based on measurement of the pulse length of the signal at the output of the photoelectronic device or on determination of the distance between them if there is an error of position between the sighting line to the object and the optical axis of the SKSI.

Variations of the output signal frequency upon variation of the rate of misalignment of the image to be checked are used in frequency SKSI [32, 34, 85]. (Footnote) (USSR inventor's certificate 415,492, U.S. patent 3,511,150, British patent 1,391,779, British patent, 1,442,801)



```
                                                    ┌─────────────────┐
                                                ┌───│ Времяимпульсные │ (2)
                                                │   └─────────────────┘
                                                │   ┌─────────────────┐
                                                ├───│    Фазовые       │ (3)
                                                │   └─────────────────┘
      ┌──────────────────────────────────────┐ │   ┌─────────────────┐
(1)   │ Системы контроля смещения изображения │─┼───│   Амплитудные    │ (4)
      └──────────────────────────────────────┘ │   └─────────────────┘
                                                │   ┌─────────────────┐
                                                ├───│  Корреляционные  │ (5)
                                                │   └─────────────────┘
                                                │   ┌─────────────────┐
                                                └───│    Частотные     │ (6)
                                                    └─────────────────┘
```
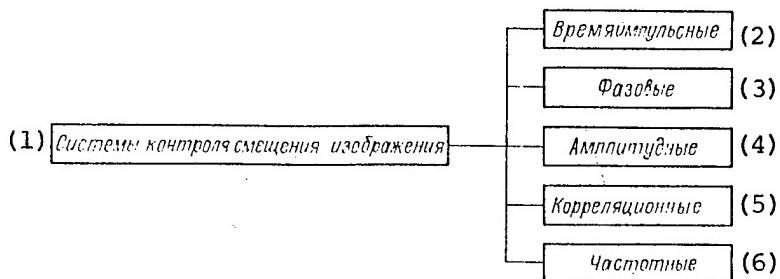
Figure 4.4. Classification of SKSI by Operating Principle

KEY:

1.	Image misalignment check systems	4.	Amplitude
2.	Time-pulse	5.	Correlation
3.	Phase	6.	Frequency

Phase SKSI [32, 34, 47, 50, 57, 82] are based on determining the extent of the phase shift between the signal from the image to be checked and the reference signal, introduced for the origin of reading.

The misalignments of the optical image with respect to the optical axis of the device are determined in amplitude SKSI [32, 33, 34, 42, 46, 52, 82, 83] by the signal amplitude at the output of the detector.

Correlation SKSI [8, 30, 32, 33, 34, 37] are designed on the basis of determining the time shift between signals, taken from the photodetectors, which are arranged along the direction of misalignment of the image, or on analysis of the shape of the autocorrelation function of the output signal of the photodetector, with respect to which the image is displaced. Correlation and frequency SKSI find application in practice; therefore, let us consider their operating and working principles.
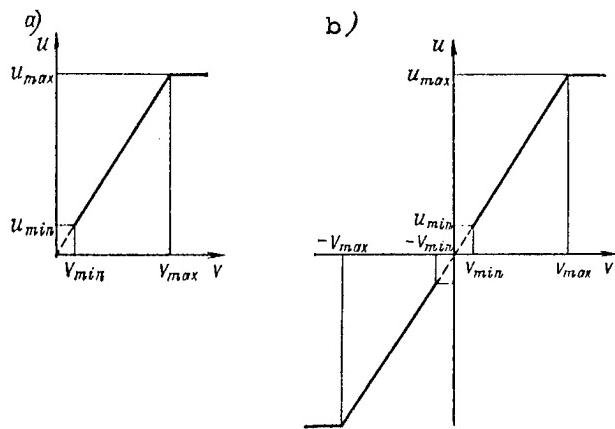
Figure 4.5. Static Characteristics of SKSI:
a--nonreversible; b--reversible

Requirements on SKSI as an ASSI component. The image motion check system is designed mainly for operation in an automatic image stabilization system. Its parameters with respect to this principle should satisfy the requirements determined by the stabilization system.

The image motion check system as an ASSI component are characterized by the main parameters presented below.

1. Output or in other words static characteristic. This is the dependence of the output value u on the motion v of the image, i.e., u = = f(v).

The working principle of a SKSI and its operating conditions determine the type of characteristic u = f(v). It can be nonreversible (Figure 4.5, a) and reversible (Figure 4.5, b) in this regard. The output characteristic should be linear, since the linearity of the characteristic may result in the need to consider the ASSI as a nonlinear system, and this makes calculation and adjustment of it difficult. The output parameter u can be analog (direct or alternating voltage or current), digital (pulse sequence), code (binary or other code) and so on as a function of the working principle of the SKSI and ASSI.

2. Static conversion factor. This coefficient is determined for the SKSI as the ratio of the output value u to the input parameter v when the SKSI is operating in the static mode $k_{CT} = u/v$.

The value of k_{CT} is determined by the parameters of the SKSI components and is selected with respect to a specific ASSI.

139

3. Dynamic conversion factor or sensitivity of SKSI. This coefficient is generally determined in the following manner: $k_{\text{дин}}$ = du/dv. It is used to determine the dynamic properties of the system and of its sensitivity mainly with small variations of the input parameter.

4. The transfer function W(p) determines the dynamics of variation of the input and output signals of the SKSI, and can be represented for some SKSI by an aperiodic link $W(p) = k_{\text{ст}}/(T_{\text{ск}}p + 1)$, where $T_{\text{ск}}$ is the time constant of the SKSI.

The time constant T_{c} is established according to the cutoff frequency of the entire ASSI, which is in turn determined from the required dynamics of image motion. The cutoff frequency ω_{c} should obviously be higher than the maximum frequency of the range of image motion, while the time constant $T_{\text{ск}}$ should be considerably less than the time constant T_{c} of the entire ASSI, determined from ω_{c}.

5. The threshold of sensitivity of the SKSI is the least input value, corresponding to the minimal velocity v_{min} (Figure 4.5, b), to which the system responds. The necessary threshold of sensitivity is determined by the parameters of the ASSI. For example, the threshold of sensitivity for a SKSI operating in the image stabilization system of an AFA should be less than the motion of the image, which results in a permissible shift of the image.

6. The range of measurement of the SKSI is the maximum input value (maximum velocity v_{max}), to which the system responds without distortions. The necessary range of measurement is determined by the parameters of a specific ASSI.

4.3. Operating Principle and Classification of Correlation SKSI

Main varieties of correlation SKSI. It was noted above that all correlation SKSI can be divided by operating principle into two large groups: cross-correlation and autocorrelation. Cross-correlation SKSI can be divided by working principle into continuous and sampling.

Autocorrelation SKSI are in turn divided into SKSI with fixed delay time and into spectral analyzing SKSI.

The classification layout of correlation SKSI is presented in Figure 4.6.

140

(1) Корреляционные СКСИ

(2) Взаимно-корреляционные

(3) Авто-корреляционные

(4) Непрерывные

(5) С дискретизацией по времени

(6) С фиксированным запаздыванием

(7) С регулируемым запаздыванием

(8) Спектро-анализирующие
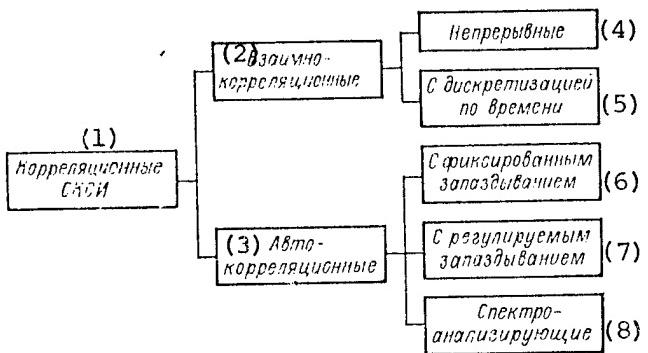
Figure 4.6. Classification of Correlation SKSI:

KEY:

1. Correlation SKSI
2. Cross-correlation
3. Autocorrelation
4. Continuous
5. Sampling
6. Fixed delay
7. Regulated delay
8. Spectral analyzing

Operating principle of correlation SKSI. Let us briefly consider the working and operating principles of the main types of correlation SKSI. A simplified layout of a continuous cross-correlation SKSI is shown in Figure 4.7, a.

The objective 1 of the optical system creates an image 2, located in plane xy, which is the image plane. Photoelements 3 and 4 are arranged one after the other in the image plane on axis x at distance L_ξ.

Photoelement 4 is connected to the regulated delay module 5, while photoelement 3 is connected to one of the inputs of the multiplication module 6. The multiplication module is in turn connected to integrator 7, while the output of the integrator is fed to the input of the extreme regulator 8, controlled by the delay time of module 5.

When the image moves at velocity v in the direction shown by the arrow in Figure 4.7, a, variable electric signals $u_1(t)$ and $u_2(t)$ occur at the outputs of the photoelements, and signal $u_2(t)$ will be the same as $u_1(t)$, but shifted by the transport delay time $\tau_T = L_\xi/v$. Thus, $u_2(t) = u_1(t - \tau_T)$.

The signal $u_1(t)$ is fed to the input of module 5, in which it is delayed by time τ. Modules 6 and 7 calculate the cross-correlation function $R(\tau)$ of signal $u_2(t)$ and of signal $u_1(t)$, delayed by time τ

$$R(\tau) = \frac{1}{T_\text{н}} \int_0^{T_\text{н}} u_1(t - \tau)\, u_2(t)\, dt = \frac{1}{T_\text{н}} \int_0^{T_\text{н}} u_1(t - \tau)\, u_1(t - \tau_\tau)\, dt,$$

141

where $T_\text{и}$ is the integration time.
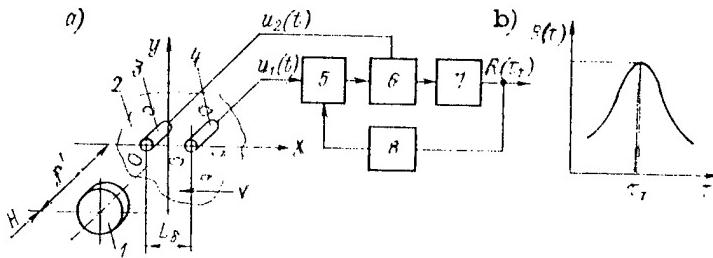
Figure 4.7. Continuous Cross-Correlation SKSI:
a--layout of device; b--type of correlation function;
1--objective; 2--image; 3, 4--photoelements;
5--regulated delay module; 6--multiplication module;
7--integrator; 8--extreme regulator

The extreme regulator 8 controls the delay time τ so that the maximum function $R(\tau)$, which occurs at $\tau = \tau_\text{T}$ (Figure 4.7, b), is always delayed at the output of integrator 5. The motion of the image can then be determined by the formula $v = L_\text{д}/\tau$.

The considered cross-correlation SKSI permits one to determine the speed upon motion of the image in only one direction. Analog SKSI are known, which can be used to vary the speed upon motion of the image both in the forward and opposite direction. (Footnote) (USSR inventor's certificate 822,037, USSR inventor's certificate 888,043) The operation of these SKSI is based either on use of the constant delay module of the signal from one of the photodetectors (Footnote) (USSR inventor's certificate 888,043), or is based on analysis of signals from photodetectors in two correlators, one of which operates upon motion of the image in one direction and the other of which operates during motion of the image in the other direction. (Footnote) (USSR inventor's certificate 822,037)

Continuous cross-correlation SKSI can in turn be divided into search and differential. The maximum cross-correlation function is found in search devices by using an extreme regulator through search oscillations in the region of the maximum cross-correlation function $R(\tau)$. The maximum cross-correlation $R(\tau)$ is determined in differential devices by taking the derivative $\partial R(\tau)/\partial \tau$ and by determining the point when this derivative becomes equal to zero.

Sampling cross-correlation SKSI are based on establishing the correlation between the signals which characterize the images to be checked, when these signals are found at different moments of time. These SKSI can be scanning (Footnote) (USSR inventor's certificate 824,055), with correction on the photoelement [33], and with sequential

photography of sections of the surface and with subsequent comparison of these photographs [94] on CCD structures (Footnote) (USSR inventor's certificate 718,786) [88] and television [8] by the signal processing method.
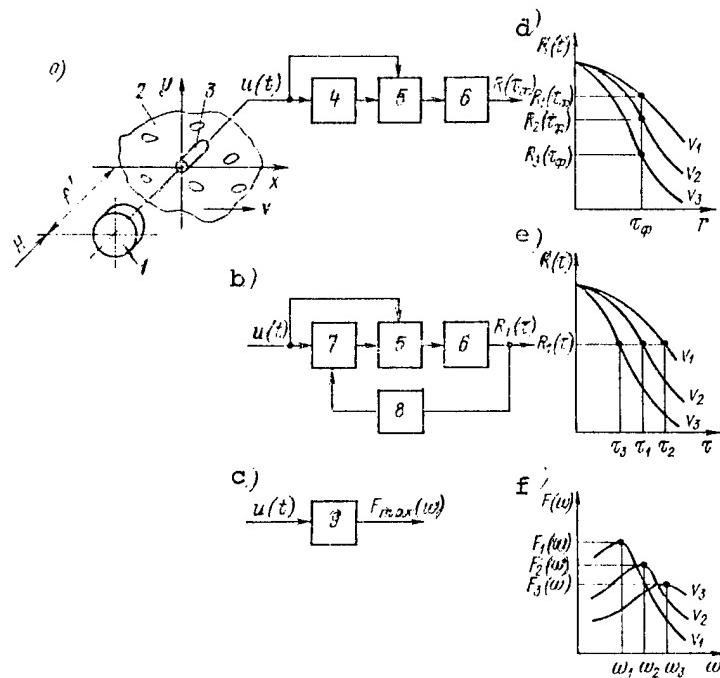
Figure 4.8. Autocorrelation SKSI:
a--fixed delay; b--regulated delay; c--spectral analyzing;
d, e, f--form of autocorrelation functions; 1--objective;
2--image; 3--photoelement; 4--constant delay module; 5--
multiplication module; 6--integrator; 7--regulated delay
module; 8--regulator; 9--frequency spectrum analyzer

The characteristic feature of cross-correlation SKSI is their comparatively small error, which can reach values on the order of 0.1 percent.

Let us also consider the working and operating principles of the main types of autocorrelation SKSI. Simplified layouts of autocorrelation SKSI are presented in Figure 4.8. The objective 1 in each of these systems creates an image 2, located in plane xy, which is the image plane. Photoelement 3 is also located in plane xy, and a small section of the image 2 is observed by using it. The illumination of the photoelement varies upon motion of the image at speed v in the direction of axis x, and a variable electric signal u(t) is shaped at its output. The type of autocorrelation function R(τ) of signal u(t) varies upon variation of the speed v of the image, and this permits one to determine the speed v by the parameters of the autocorrelation function

143

$$R(\tau) = \frac{1}{T_u} \int_0^{T_u} u(t)\, u(t - \tau)\, dt,$$

where τ is the delay time of the signal u(t).

The signal u(t) from the output of photoelement 3 is delivered to the constant delay module 4 and to multiplication module 5 in the layout of a fixed delay SKSI (Figure 4.8, a). The signal u(t) is delayed in module 4 for a fixed delay time τ_ϕ. The product u(t)u(t - τ) is calcualted in module 5. The signal is fed from module 5 to integrator 6, at the output of which the signal of autocorrelation function R(τ_ϕ) is shaped. The form of the autocorrelation functions of the signal u(t) for different speeds v of image motion is shown in Figure 4.8, d. Thus, the speed v can be determined from signal R(τ_ϕ) at known value of τ_ϕ.

The signal u(t) is fed from the output of photoelement 3 to the regulated delay module 7 and to multiplication module 5 in the layout of a regulated delay SKSI (Figure 4.8, b). A constant value of the autocorrelation function $R_1(\tau)$ is maintained at the output of the integrator 6 in this device. This is achieved through regulator 8, which controls the delay time τ of signal u(t) in module 7. The speed v of image motion can be determined by the delay time (Figure 4.8, e).

Signal u(t) is fed from the output of photoelement 3 to the analyzer 9 of frequency spectrum ω of the electric signal in a spectral analyzing SKSI (Figure 4.8, c).

The form of spectra F(ω) of signal u(t) for different speeds v of image motion is shown in Figure 4.8, f. The speed v of image motion is judged in devices of this type by the maximum of spectrum F(ω) or by frequency ω, corresponding to this maximum.

Autocorrelation SKSI are considerably inferior in accuracy to cross-correlation SKSI. The error of autocorrelation devices can reach values on the order of 5 percent and it increases sharply as the speed of image motion decreases. A considerable disadvantage of autocorrelation SKSI is the lack of possibility of determining the direction of motion of the image. All correlation SKSI have a number of significant common deficiences that sharply limit their application. The main ones of them are considerable complexity, the presence of a time delay during measurement, and the effect of transverse misalignment of the image on the measurement result.

4.4. Operating Principle and Classification of Frequency SKSI

Operating principle of frequency SKSI. The operating principle of this type of SKSI includes spatial filtration of the elements of the optical image using special optical filters (modulators) and in determination of the electric signal, the frequency of which is proportional to the motion speed of the image.
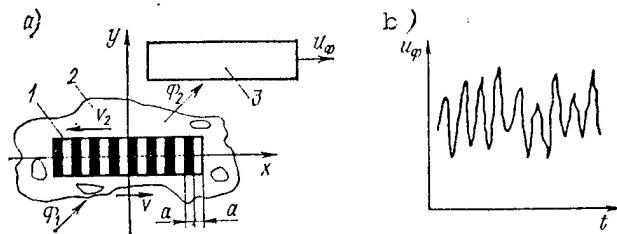
Figure 4.9. Working Principle of Receiving Part of SKSI: a--composition of receiving part; b--sample form of signal at output of photoelement; 1--spatial filter (modulator); 2--optical image of object; 3--photoelement

The main elements of this SKSI (Figure 4.9, a) are a modulator 1 and a photoelement 3, located behind the modulator. The optical system shapes an image 2 of the object in the image plane xy. The image 2 can be moved with respect to coordinates xy at some speed v_1. Modulator 1 is (generally) an optical structure, consisting of parallel transparent and opaque sections, of equal width, located in plane xy. The modulator can be fixed or can be moved with respect to coordinates xy at speed v_2. A luminous flux Φ_1, which shapes image 2, is fed from the optical system. The luminous flux Φ_2, traveling through modulator 1, impinges on photoelement 3. Signal u_ϕ at the output of photoelement 3 carries information about the relative speed v of image motion 2 and of modulator 1. Let us briefly consider the physical principles that are the basis of operation of this SKSI. It is known that the brightness function $B(q_\pi)$ of the space of objects is reflected and diffuse-scattered emission of the surface of the object. Brightness functions $B(q_\pi)$ of the object corresponds to the field of illumination $E(q_\pi)$, joined with it, in the image space of the optical system. The function $E(q_\pi)$, random in nature, is frequently considered stationary [43, 69, 90] to simplify the mathematical representation and it can then be represented in the form of function $E(x, y)$.

This stationary field of illumination or in other words the field of signals for the image plane can be described most fully by a correlation function of the following type [14, 48, 69]:

145

$$K_E(\Delta x, \Delta y) = \lim_{y, x \to \infty} \frac{1}{2x2y} \int_{-x}^{+x} \int_{-y}^{+y} E(x, y) E(x + \Delta x, y + \Delta y) \, dx \, dy,$$

where x, y, Δx, and Δy are the maximum values and increments of the coordinates of a square-wave frame, to the center of which the coordinate system is bound.

The following integral Fourier transform is used to describe the statistical properties of the signal field $E(q_\Pi)$ in the frequency range to the correlation function

$$S_E(\omega_x, \omega_y) = \int_{-\infty}^{+\infty} \int K_E(\Delta x, \Delta y) e^{-j(\omega_x x + \omega_y y)} d(\Delta x) d(\Delta y),$$

where $\omega_x = 2\pi v_x$; $\omega_y = 2\pi v_y$, and v_x and v_y are the spatial frequencies that determine the distribution of parameters in directions x and y.

Function $S_E(\omega_x, \omega_y)$ is the spectral density of dispersion of the signal field in the image plane, created by the optical system. This function is also called the spectral power density of the signal or the Hinchin-Wiener spectrum.

The relations and graphs of the Hinchin-Wiener spectra for different physical objects: the sky background, urban, rural, and forest landscapes and so on, have been presented in a number of papers [48, 84, 91]. The modulator 1 in the layout presented in Figure 4.9, a is essentially a spatial filter for the radiation passing through it and impinging on photoelement 3. It is known that the SKSI is intended to check the parameters of motion of the image and, therefore, the signal field $E(q_\Pi)$ can be represented at E(x, y, t).

The spatial filter has the weight function W(x, y, t) and can be represented by a direct Fourier transform

$$W(j\omega_x, j\omega_y, j\omega_t) = \int_{-\infty}^{+\infty} \int \int W(x, y, t) e^{-j(\omega_x x + \omega_y y + \omega_t t)} dx \, dy \, dt,$$

146

where $W\,(j\omega_x,\ j\omega_y,\ j\omega_t)$ is the frequency characteristic of a multidimensional frequency or, in other words, a frequency transfer function.

The luminous flux Φ_2, passing through modulator 1, impinges on photoelement 3 and generates an electric signal u_ϕ. The following relation can be written with regard to the fact that the parameters of the system are dependent on time t: $u_\phi\,(t) = k_\phi\Phi\,(t).$

The luminous flux at the output of the photoelement can generally be represented by the expression

$$\Phi\,(t) = \int\!\!\!\int\limits_{-\infty}^{+\infty} E\,(x,\ y,\ t)\,W\,(x,\ y,\ t)\,dx\,dy.$$

The luminous flux at the input of the photoelement and the corresponding signal at the output, after the corresponding transformations which are not presented here, can be represented in frequency form by the following expressions:

$$\Phi\,(j\omega_t) =$$
$$= \frac{1}{(2\pi)^2}\int\!\!\!\int\!\!\!\int\limits_{-\infty}^{+\infty} \tilde{E}\,(j\omega_x,\ j\omega_y)\,W\,(j\omega_x,\ j\omega_y)\,e^{-j\,[\omega_t-\omega_x\,(v_1-v_2)]\,t}\,d\omega_x\,d\omega_y\,d\omega_t; \qquad (4.2)$$

$$u_\phi\,(j\omega_t) =$$
$$= \frac{k_\phi}{(2\pi)^2}\int\!\!\!\int\!\!\!\int\limits_{-\infty}^{+\infty} \tilde{E}\,(j\omega_x,\ j\omega_y)\,W\,(j\omega_x,\ j\omega_y)\,e^{-j\,[\omega_t-\omega_x\,(V_1-V_2)]\,t}\,d\omega_x\,d\omega_y\,d\omega_t. \qquad (4.3)$$

Expression (4.3) indicates that the spectrum of the light signal at the output of the modulator and the spectrum of the electric signal at the output of the photoelement are essentially determined by multiplication of the independent spectra of complex conjugate spatial-frequency spectrum of the image $\tilde{E}\,(j\omega_x,\ j\omega_y)$ and of the spatial-frequency spectrum of the modulator $W\,(j\omega_x,\ j\omega_y)$ and are dependent on the relative motion speed of the image and modulator $(\bar{v}_1 - \bar{v}_2)$. Thus, one can judge the motion speed of the image by the frequency of the electric signal at the output of photoelement 3 (Figure 4.9, b), located behind modulator 1. An ordinarily raster optical element, having brightly marked flash of the spatial-frequency spectrum at frequency that creates optimal

147

conditions for modulation of the luminous flux, is ordinarily used as a
modulator.

(1) Частотные СКСИ

(2) С пространственно-неподвижным модулятором

(3) С оптическим модулятором

(4) Со ступенчатой функцией веса модулятора

(5) С гармонической функцией веса модулятора

(6) С модулятором на фотоэлектрической некоммутируемой матрице

(7) С модулятором на оптических волокнах и некоммутируемых фотоэлементах

(8) С пространственно-подвижным модулятором

(9) С оптико-механическим модулятором

(4) Со ступенчатой функцией веса модулятора

(5) С гармонической функцией веса модулятора

(10) С модулятором на фотоэлектрической коммутируемой матрице

(11) С модулятором на оптических волокнах и с коммутируемыми фотоэлементами

Figure 4.10. Classification Frequency SKSI

KEY:
1. Frequency SKSI
2. With spatially fixed modulator
3. With optical modulator
4. With stepped weight function of modulator
5. With harmonic weight function of modulator
6. With modulator on photoelectric nonswitchable matrix
7. With fiber optic modulator and with nonswitchable
   photoelements
8. With spatially fixed modulator
9. With optomechanical modulator
10. With modulator on photoelectric switched array
11. With modulator on optical fibers and with switched
    photoelements

Raster arrays of different configuration are used as fixed and moving
modulators [85]. (Footnote) (USSR inventor's certificate 415,492, U.S.
patent 3,511,150, British patent 1,391,779, British patent 1,442,801)
Modulators can be conditionally divided into those with stepped weight
function, the arrays of which are made with transparent or opaque zones
of equal width [85], and into modulators with harmonic weight functions,

148

the arrays of which have harmonic distribution of transparency [14] as a function of the nature of the ratio of transparent and opaque sections of modulators.

Fixed and moving modulators are mostly made in the form of an optical element, independent of the photodetector—of a transparent plate or disk with raster elements applied to the surface. Devices have appeared recently that combine the raster and photodetector in their design. These are usually a special photo array, containing a specific number of identical strip photoelement. (Footnote) (USSR inventor's certificate 1,037,178) A specific combination of fiber light guides [90] and other devices can also be used as the raster.

4.5. Working and Operating Principles of Frequency SKSI

System with spatially fixed optical modulator. The functional diagram of the simplest SKSI of this type is shown in Figure 4.11, a. The objective 1 creates an image 2 of the object in plane xy, which is the image plane in the given case. A modulator 3, which is a raster array, consisting of transparent and opaque strips of identical width a, is also located in image plane xy. The transparent and opaque strips of the raster form the so-called spatial period of the array $l_p = 2a$.

A fixed modulator with stepped weight function or, in other words, a fixed spatial filter is used in the given layout. A converging lens 4 is located behind the modulator, while a photoelement 5, connected to the input of the filter 6, is located behind it. The filter 6 is connected to an amplification-shaping section 7 and it is in turn connected to measuring section 8, as which a frequency meter can be used.

The image 2 of the object moves with respect to the array 3 at speed $v = v_{o6}f'/H$, where v_{o6} is the motion speed of the object with respect to the objective and H is the distance from the objective to the object.

Light is modulated by the structural elements of the image 2 when the image 2 moved with respect to the modulator array 3. The modulated light is collected by a lens 4 and is sent to photoelement 5. The modulation frequency is generally equal to $\nu = 1/T$, where T is the period of variation of the illumination on the photoelement, and T = $= l_p/v$.
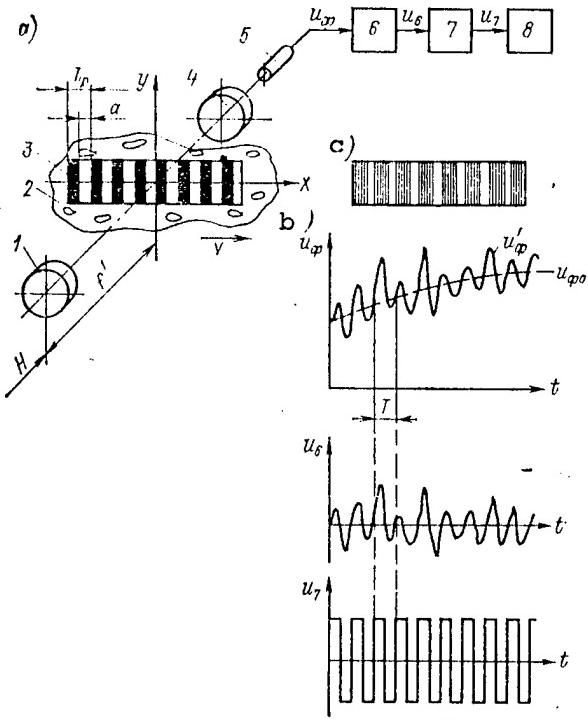
Figure 4.11. System With Fixed Optical Modulator:
a--SKSI with modulator having stepped weight function;
b--shape of signals; c--modulator with harmonic weight
function; 1--objective; 2--image; 3--modulator;. 4--
converging lens; 5--photoelement; 6--filter; 7--
amplification-forming link; 8--measuring link

Thus, $v = l_\text{p}/T = l_\text{p}\nu$, i.e., the motion speed of the image is proportional to the spatial period or step l_p of the raster (of the spatial filter or modulator) and to the frequency ν of variation of the signal u_ϕ at the output of photoelement 5. The shape of the signal u_ϕ generally is complicated, similar to that presented in Figure 4.11, b. The signal contains a constant or slowly variable component $u_{\phi 0}$ of background noise and a variable component u'_ϕ, containing frequency ν, proportional to the speed v of the image. Besides the fundamental frequency ν, signal u'_ϕ also contains other higher frequencies, which are noise in the given case. The constant component $u_{\phi 0}$ and the high frequencies are cut off by filter 6, and signal u_6 with frequency ν is formed at its output. The amplification shaping section 7 converts signal u_6 to signal u_7, having the shape of a square wave of constant amplitude. Measuring

150

section 8 measures the frequency ν or phase shift of the signal u_7, proportional to the motion speed v of the image.

A modulator with harmonic weight function of the array, i.e., with harmonic distribution of the transparency of the array along its length, is shown in Figure 4.11, c [14]. The use of this modulator permits one to obtain a signal u_ϕ with somewhat smaller noise spectrum at the output of photoelement 5. However, the complexity of manufacturing these modulators in the presence of filter 6 frequently makes their use unfeasible.
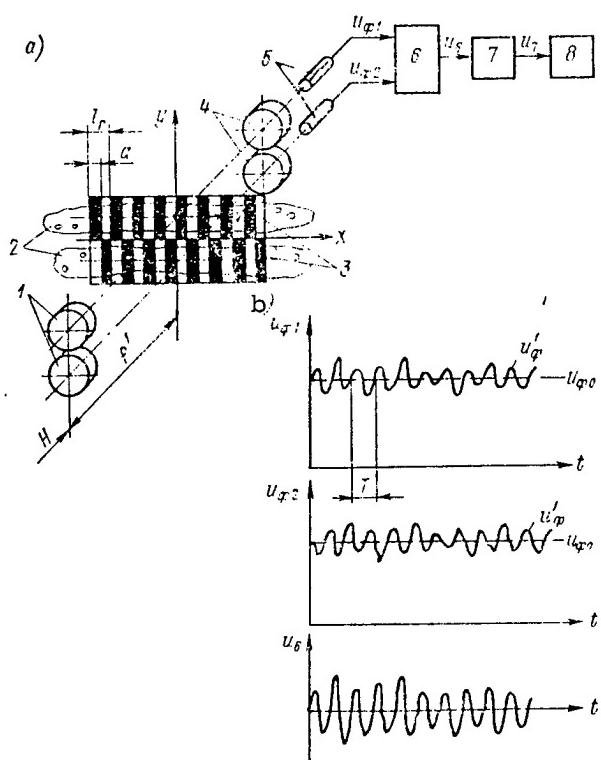
Figure 4.12. System With Fixed Optical Modulator
and With Compensation of Background Noise:
a--SKSI device; b--shape of signal; 1--objectives;
2--image; 3--modulators; 4--converging lenses;
5--photoelements; 6--differential amplifier;
7--former; 8--measuring section

Rather many SKSI and other devices, similar or close to that considered, are known [34, 35, 77, 81, 84, 85]. (Footnote) (USSR inventor's certificate 415,492, British patent 1,442,801) A significant disadvantage of most of these devices is the effect of rather significant constant or slowly variable brightness background of the

object or, in other words of background noise on their operation. This effect can be eliminated by some complication of the above SKSI. An example of this device is shown in Figure 4.12, a. Two identical images 2 of the object are projected to plane xy. This is achieved by using two identical objectives 1 or one objective with semitransparent mirror at the output. Two identical SKSI, similar to that shown in Figure 4.11, a, are essentially used, but the arrays of the modulators 3 are shifted one with respect to the other by half their spatial period l_p, i.e., by value a in the direction of axis x. Signals are fed from the outputs of photoelements 5 to the inputs of differential amplifier 6. When both images move at speed v, signals $u_{\phi 1}$ and $u_{\phi 2}$, containing a constant or slowly variable component u_ϕ, of the background noise, and variable components $u'_{\phi 1}$ and $u'_{\phi 2}$, identical in shape, but shifted one with respect to the other by half their period T (Figure 4.12, b), occur at the output of the photoelements. The components $u_{\phi 0}$ are mutually compensated, while components $u'_{\phi 1}$ and $u_{\phi 2}$ are added in the differential amplifier 6, yielding the resulting signal u_6, whose frequency is proportional to the motion speed v of the image, at the output of amplifier 6. Signal u_6 is then transformed in former 7 (as in the case of the SKSI shown in Figure 4.11) and is fed to the input of measuring section 8.

A variety of the previous SKSI, designed for determination of the angle of rotation ψ of the vector of the motion speed v′ of the image upon relative angular misalignment of the axis x of the image plane of the device toward the direction of motion of the object, is shown in Figure 4.13. Modulator 3 consists of two identical patterns, inclined at angle γ ot axis y and placed in the image plane xy. If the direction of misalignment of the image 2 coincides with axis x, then $\psi = 0$ and frequencies ν_1 and ν_2 of signals $u_{\phi 1}$ and $u_{\phi 2}$, generated by photoelements 5, will be equal to

$$\nu_1 = \nu_2 = v \cos \gamma / l_p.$$

If $\psi \neq 0$, then

$$\nu_1 = v' \cos (\gamma + \psi)/l_p;$$
$$\nu_2 = v' \cos (\gamma - \psi)/l_p.$$

It is not obligatory that $\nu_1 = v'$. Signals u_6 and u'_6 carry frequencies ν_1 and ν_2 from the outputs of amplifier-forming modules 6 and are fed to the inputs of the frequency comparison module 7. This module performs the operation of frequency comparison and signal u_7 from its output is

fed to the input of measuring section 8, where the following rotational angle is determined

$$\psi = \operatorname{arctg} \frac{v_1 - v_2}{(v_1 + v_2)\,\operatorname{tg}\gamma}.$$
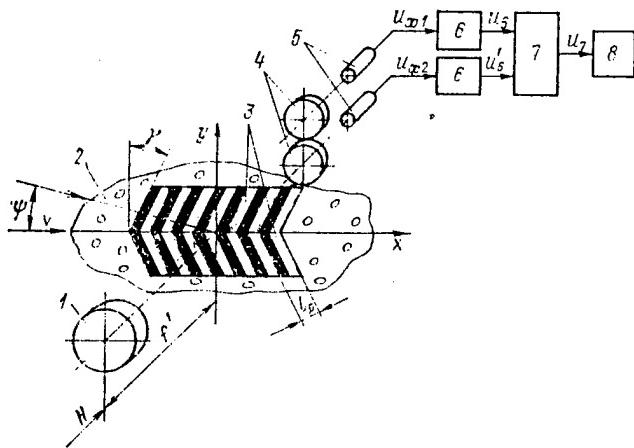

Figure 4.13. SKSI With Fixed Optical Modulator:
1--objective; 2--image; 3--modulators; 4--converging
lenses; 5--photoelements; 6--amplification-forming
modules; 7--frequency comparison module; 8--measuring
section

System with spatially fixed modulator on photoelectric unswitched array. The main disadvantages of the SKSI with optical modulators are their large overall dimensions and mass and also the inability to determine the direction of misalignment of the image. The use of modern photoelectronics and microelectronic technology permit one to develop SKSI with small dimensions and mass. Combining the modulator and photoelement in one assembly--a photoelectric array, which is a combination of a large number of identical narrow and parallel photoelements on a single flat substrate--yields especially effective results. A simplified functional diagram of a SKSI, based on the use of this photoarray, is presented in Figure 4.14, a. The objective 1 forms the image 2 in plane xy. Photoelectric array 3, which is a special photoelement that consists of a large number of N identical strip elements, is located in this same plane; each element has width 3 and length B. The length ofthe photoarray is A = Nd. These strip photoelements are generally combined in four groups as is shown in Figure 4.14, a. Leads a, b, c, and d of the groups of strip photoelements are joined to the inputs of four identical adders 4-7. The outputs of the adders are connected to the inputs of differential amplifiers 8 and 9. The outputs of amplifiers 8 and 9 are connected to

153
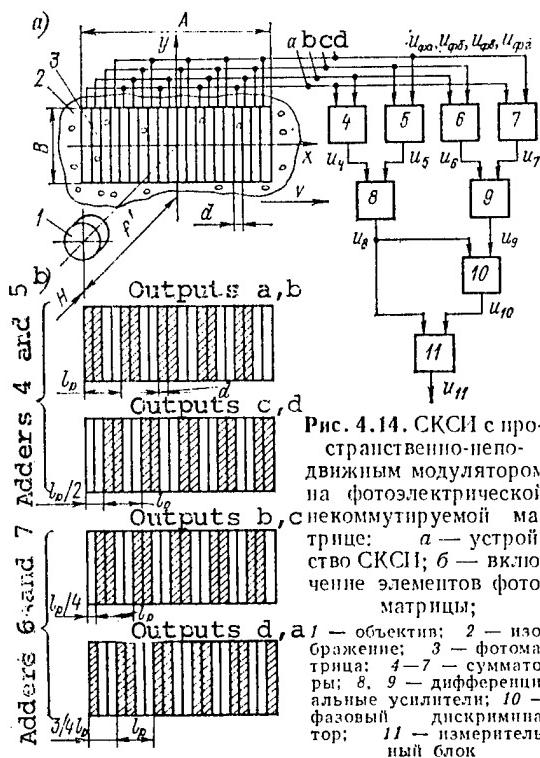
Рис. 4.14. СКСИ с пространственно-неподвижным модулятором на фотоэлектрической некоммутируемой матрице: a — устройство СКСИ; б — включение элементов фотоматрицы; 1 — объектив; 2 — изображение; 3 — фотоматрица; 4—7 — сумматоры; 8, 9 — дифференциальные усилители; 10 — фазовый дискриминатор; 11 — измерительный блок

Figure 4.14. SKSI With Spatially Fixed Modulator on Unswitched Photoelectric Array: a--SKSI device; b-- connection of photoarray components; 1--objective; 2--image; 3--photoarray; 4-7--address; 8, 9--differential amplifiers; 10--phase discriminator; 11--measurement module

154

the two inputs of measuring module 11, and the output of amplifier 8 is connected directly to the first input of module 11, while a signal is fed to its second input from amplifiers 8 and 9 through phase discriminator 10. Joining photoarray 3 to adders 4-7, shown in Figure 4.14, a, is equivalent to simultaneous use of four identical fixed optical pattern arrays, having spatial period 1_p and specifically misaligned one with respect to the other in the direction of axis x. The form of the equivalent arrays and their mutual shift are shown in Figure 4.14, b. Leads a and b of photoarray 3 are connected to adder 4 and leads c and d are connected to adder 5. Two identical pattern arrays, shifted one with respect to the other by half their spatial period 1_p, are created from the elements of the photoarray. These equivalent arrays are shown by the cross-hatched sections of the array in the first two diagrams (Figure 4.14, b). Leads b and c of photoarray 3 are connected to adder 6, while leads d and a are connected to adder 7. Two additional arrays, shifted one with respect to the other by half the period 1_p and with respect to the first pair of arrays by one-fourth the period 1_p, are formed from the elements of the photoarray. These equivalent arrays are shown by the last two diagrams in Figure 4.14, b.

The SKSI operates in the following manner. When the image 2 moves at speed v along axis x, the elements of the image are modulated by the connected elements of the equivalent pattern arrays of photoarray 3 and signals $u_{\phi a}$, $u_{\phi 6}$, $u_{\phi n}$, $u_{\phi r}$ occur at outputs a, b, c and d. These signals are added by adders 4-7 and signals u_1-u_7, which contain the constant component of the background noise and the variable component with frequency proportional to speed v, occur at the outputs of the adders. The same as in the case of the SKSI presented in Figure 4.12, the constant components are mutually compensated in differential amplifiers 8 and 9, while the variable components are added, yielding signals u_8 and u_9 at the outputs of the amplifiers. The phase discriminator 10 permits one to determine the mutual variation of the phase of signals u_8 and u_9 upon variation of the direction of motion of the image, making the SKSI sensitive to the direction of motion of the image. Signals u_8 and u_{10} are fed to the inputs of measuring module 11, the value of the output signal u_{11} of which is proportional to speed v, while the sign is proportional to the direction of misalignment of the image.

A pattern of the same design having constant step, or in other words spatial period 1_p is used as the modulator in the above SKSI. This pattern is a narrow-tuned spatial filter. The optimal modulation conditions of the image elements by this pattern occurs when half the step of the array is equal to or close to the mean dimensions of the most frequently encountered parts of the image. The modulation conditions deteriorate considerably and the useful signal at the output of the photoelement decreases sharply or disappears altogether if there are no image parts with these dimensions. The strip photoelement arrays

155

permit one to develop a SKSI free of this deficiency. Let us consider the working and operating principles of one of these SKSI. A simplified diagram of the SKSI is presented in Figure 4.15. Objective 1 forms an image 2 in the image plane, coinciding with the axes of coordinates xy.
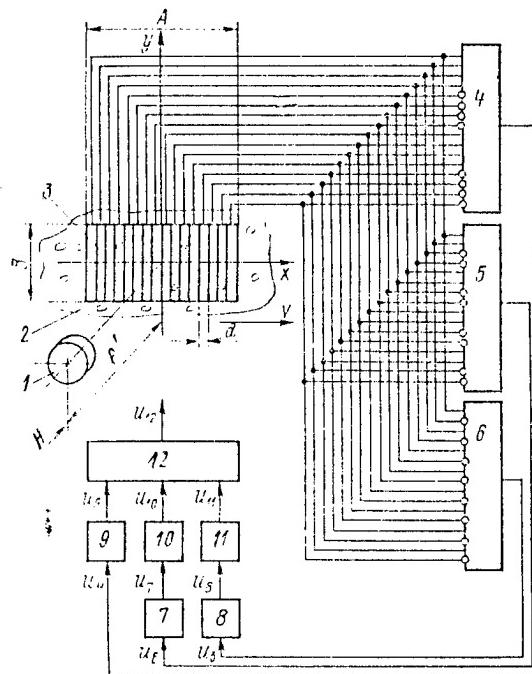

Figure 4.15. SKSI With Spatially Fixed Multifrequency Modulator on Unswitched Photoelectric Array: 1--objective; 2--image; 3--photoarray; 4, 5, 6-- differential amplifiers; 7, 8--frequency dividers; 9, 10, 11--frequency-to-voltage conversion modules; 12--maximum voltage separation module

Photoelectric array 3, which is a special photoelement which consists of a large number of N identical strip photoelements, is located in the same plane. The outputs of these photoelements are connected to the direct and inverse inputs of differential amplifiers 4, 5 and 6. The number of m_y differential amplifiers should generally be $m_y \leq \log_2 N$, but $m_y = 3$ for simplification of the diagram in Figure 4.15. The outputs of differential amplifiers 4, 5, and 6 are directly connected to the frequency-to-voltage conversion modules 9, 10, and 11 (amplifier 4) or through frequency dividers 7 and 8 (amplifiers 5 and 6). Thus, the number of $m_д$ frequency dividers is equal to $m_д = m_y - 1$. The outputs of modules 9, 10, and 11 are connected to the maximum voltage determination module 12. Moreover, the SKSI operates in the following manner. The signal determined by the background noise of this photoelement will

156

occur at the output of each strip photoelement upon motion of image 2 along photoarray 3. The outputs of the strip photoelements are connected to the inputs of differential amplifiers 4, 5, and 6. Moreover, photoelements with odd ordinal number are connected to the direct inputs of amplifier 6, while photoelements with even ordinal number are connected to the inverse inputs of this amplifier. If the total signal through the direct inputs of this differential amplifier is considered upon motion of the image along axis x, the signal will contain a smoothly variable component, determined by the background noise, and a variable component of frequency ν_1, determined by modulation of image elements 2 of the equivalent pattern array, which is organized by connection of photoelements with odd ordinal numbers to direct inputs of amplifier 6. The spacing l_{p1} of the equivalent pattern array is determined as $l_{p1} = 2d$.

The frequency of the variable component of the signal is then found by the formula $\nu_1 = v/l_{p1} = v/(2d)$.

The total signal along the inverse inputs of this differential amplifier will also contain a smoothly variable component, determined by the background noise, which is identical to the same signal component along the direct inputs, and a variable frequency component ν_1, caused by modulation of the image elements by elements of the equivalent pattern array, which is arranged by connecting the photoelements with even ordinal number to the inverse inputs of amplifier 6. The variable components of the total signals along the direct and inverse input of differential amplifier 6 will be shifted by half the period with respect to each other, since the equivalent pattern arrays are shifted by half the spatial period l_{p1}. The constant component is destroyed and the amplitude of the variable signal component is doubled in the differential amplifier.

Let us now consider differential amplifier 5. Photoelements with ordinal numbers 1, 2, 5, 6, 9, 10 and so on are connected to its direct inputs, while photoelements with ordinal numbers 3, 4, 7, 8, 11, 12 and so on are connected to the inverse inputs. The spacing of the equivalent raster arrays for amplifier 5 will be equal to $l_{p2} = 4d = 2l_{p1}$.

The image elements will also be modulated by elements of the equivalent pattern arrays, created by the above connection of photoelements to the inputs of amplifier 5, upon motion of the image 2 along photo array 3. The constant signal component will also be compensated and the amplitudes of the variable component will be added, and the frequency signal u_5 will exist at the output of this amplifier

$$v_2 = \frac{v}{l_{p2}} = \frac{v}{4d} = \frac{v}{2l_{p1}} = \frac{\nu_1}{2}.$$

157

Let us consider the action of differential amplifier 4. Photoelements with ordinal numbers 1, 2, 3, 4, 9, 10, 11, 12, 17, 18, 19, 20 and so on are connected to its direct inputs, while photoelements with ordinal numbers 5, 6, 7, 8, 13, 14, 15, 16, 21, 22, 23, 24 and so on are connected to the inverse inputs. The spacing of the equivalent arrays will then be equal to $l_{p3} = 8d = 4l_{p1}$ and the following signal frequency signal u_4 will exist at the output of amplifier 4 upon motion of the image 2 along photoarray 3

$$\nu_3 = \frac{v}{l_{p3}} = \frac{v}{8d} = \frac{v}{4l_{p1}} = \frac{\nu_1}{4}.$$

The frequency dividers are connected to the outputs of all the differential amplifiers (except the first). The division factor p of each frequency divider is determined by the ordinal number of the differential amplifier to which it is connected and is equal to

$$p_i = 2^{m-i},$$

where i is the ordinal number of the frequency divider, equal to the ordinal number of amplifier.

If the harmonic signals existed at the outputs of all the differential amplifiers, frequency signals ν_m would have existed at the outputs of the frequency dividers. The optimal modulation conditions of the image elements by elements of equivalent pattern arrays are observed when half the spacing of the array is equal to or close to the main dimensions of the most frequently encountered parts of the image. Thus, the qualitative harmonic signal whose frequency is determined by the motion speed of the image will exist at a specific moment of time at the output of the differential amplifer, on the basis of which the equivalent pattern array with spacing optimal for a given image is created. A harmonic signal of lesser amplitude will exist at the output of the other differential amplifiers, and the signal will even possibly disappear at individual moments of time. Upon motion of the image, its structure within the photoarray varies continuously, the optimal modulation conditions will be created alternately for different equivalent pattern arrays, and the stable harmonic signal will exist at the outputs of the different amplifiers. Frequency signal ν_m will exist at the output of the frequency divider, connected to the differential amplifier with spacing of the array, optimal for the given moment. Unstable frequency signals, the mean value of which is less than or equal to frequency ν_m, will occur at this moment of time at the outputs of the other frequency dividers. A voltage proportional to ν_m and accordingly proportional to the motion speed v of the image will then exist at the output of the frequency-to-voltage conversion module,

connected to the frequency divider, at the output of which frequency signal ν_m exists. Smaller voltages will occur at the outputs of the other frequency-to-voltage conversion modules. The signal u_{12}, proportional to frequency ν_m and to speed v, will then exist at the output of the maximum voltage determination module 12.
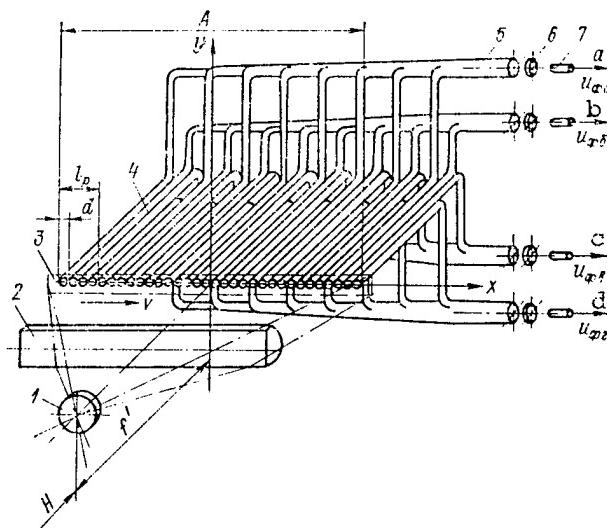

Figure 4.16. Working Principle of Detecting Part of SKSI on Fiber Optic Light Guides: 1--objective; 2--cylindrical lens; 3--image; 4--fiber light guides; 5--bundle of light guides; 6--collecting lens; 7--photoelement

System with spatially fixed modulator on optical fibers and unswitched photoelements. It is sometimes convenient for practical application of the SKSI to use a photodetector based on fiber light guides. Besides the purely structural advantages, this device may have greater sensitivity compared to a SKSI, based on the use of photoelectric strip arrays, since photoelements of very high sensitivity (photoelectronic amplifiers, cooled photodiodes and so on) can be used in it.

Such a photodetector, which operates in combination with the electric circuit presented in Figure 4.14, a, is shown in Figure 4.16. The objective 1 forms an image 3 in plane xy. Cylindrical lens 2 compresses the image along axis y. The ends of fiber light guides 4, each of which has diameter d, are arranged in one row along axis x in plane xy. The opposite ends of the light guides are collected into four identical bundles 5. Collecting lenses 6, which collect the luminous fluxes emerging from the ends 5 to photoelements 7, are located near the ends of the bundles.

159

The considered photodetector is connected to the circuit presented in Figure 4.14, a, to points, a, b, c, and d instead of photoarrays 3. The action of this SKSI is similar to that of the SKSI presented in Figure 4.14.
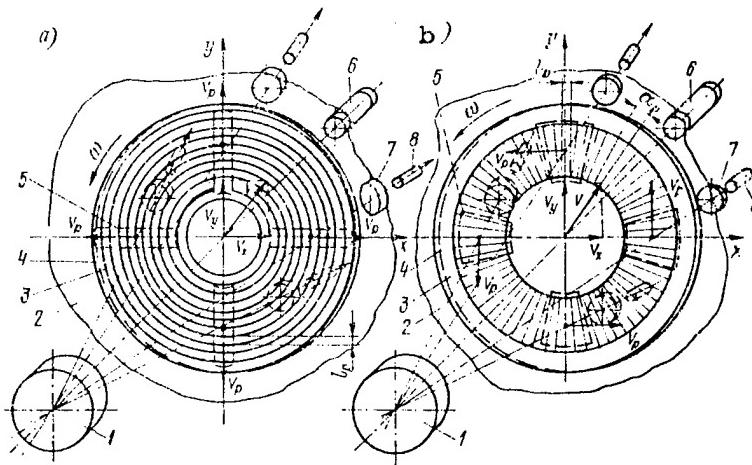

Figure 4.17. Working Principle of Photodetector Part of
SKSI With Spatially Fixed Optical-Mechanical Modulator:
a--with helical pattern array; b--with radial pattern array;
1--objective; 2--image; 3--modulator disk; 4--diaphragm;
5--diaphragm window; 6--electric motor; 7--collecting lens;
8--photoelement

System with spatially movable optical modulator. Systems with spatial movable filters or, as they are also called, with spatially movable modulators, are a further development of the SKSI considered earlier with spatially fixed modulators. Their advantages are increased sensitivity and the capability of determining the direction of misalignment of the image.

A number of these SKSI is known |34, 41, 77|, which differ by the modulator and by the signal processing circuit. (Footnote) (British patent 1,391,779, U.S. patent 3,511,150) Let us consider the working and operating principles of one of these SKSI, which permit one to measure the motion speed of the optical image upon displacement of it along two mutually perpendicular axes xy in both directions along each axis. Before turning to consideration of the SKSI, let us become familiar with the working principle of its photodetector part, which contains a moving optical-mechanical modulator.

Two variants of the photodetector of the SKSI with spatially movable optical disk modulator having spiral (a) and radial (b) pattern are shown in Figure 4.17. Each of these varieties of these photodetecting part has the following common elements: objective 1, which creates the image 2 of the object in image plane xy, a modulator disk 3 with spiral

160

or radial pattern pattern applied to it, fixed diaphragm 4 with windows 5 of the corresponding shape located on it, motor 6, which sets modulator disk 3 into rotation at constant velocity ω, collecting lenses 7 that collect the light passing through modulator 3 and windows 5 of diaphragm 4, on the sensitive surface of photoelements 8. The image plane 2 is combined with the pattern plane of modulator 3. The spatial period or, in other words the spacing of the pattern array is denoted by l_p. Parameter l'_p is the length of the arc encompassing the transparent and opaque sections of the pattern along the average length of window 5 in the case of a radial pattern. The vector v shows the speed and direction of motion of the image 2 with respect to the origin xy, while the values v_x and v_y are speed components v along axes x and y. When the modulator disk 3 rotates at constant velocity ω, its pattern lines move with respect to the fixed apertures 5 of diaphragm 4 and the effect of motion of the pattern array in the direction of axes x and y is created with a helical pattern (Figure 4.17, a) and perpendicular to the same axes with a radial pattern (Figure 4.17, b).

The motion speed of the pattern array is shown by vectors v_p with respect to axes x and y.

The pattern array of the modulator 3, moving with respect to image elements 2, modulates the luminous flux arriving through windows 5 and lenses 7 to photoelements 8.

If the image if fixed, the light impinging on photoelements 8 will be modulated by the following frequencies: $\nu_p = nk$ in the case of a modulator with spiral pattern and $\nu_p = nN$ in the case of a modulator with radial pattern. In these expressions, n is the rotational frequency of the modulator disk, k is the number of passes of the spiral, and N is the number of divisions of the radial pattern.

When the image moves at speeds v_x and v_y along axes x and y in modulated light impinging on photoelements 8, the following additional components appear

$$v_x = v_x'/l_p \quad \text{and} \quad v_y = v_y'/l_p.$$

Thus, if the motion moves at speed v, the photoelements will receive luminous fluxes modulasted by frequencies:

$$
\begin{aligned}
v_{x1} &= v_p - v_x; \\
v_{x1} &= v_p + v_x;
\end{aligned}
\tag{4.4}
$$

161

$$\left.\begin{aligned} \nu_{y1} &= \nu_p - \nu_y \\ \nu'_{y1} &= \nu_p + \nu_y \end{aligned}\right\} \tag{4.5}$$

Expressions (4.4) determine the frequencies ν_{x1} and ν'_{x1} for photoelements located in the plane passing through axis x in the case of using a photodetector with helical pattern of the modulator, and in the plane passing through axis y in the case of using a photodetector with radial pattern.
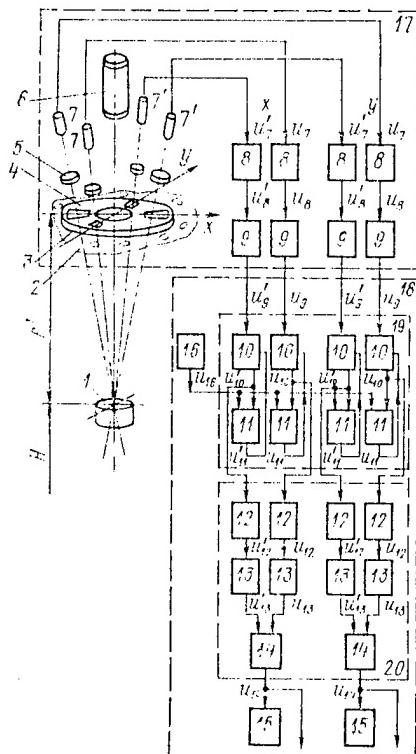

Figure 4.18.   SKSI With Spatially Movable Optical Modulator:
1--objective; 2--image; 3--modulator disk; 4--diaphragm;
5--collecting lenses; 6--electric motor; 7--photoelements;
8--filters; 9--comparators; 10--forward pulse front former;
11--rear pulse front former; 12--pulse level formers;
13--filters; 14--amplifiers; 15--indicators; 16--generators;
17--sensor; 18, 19, 20--measuring modules

Expressions (4.5) determine the frequencies ν_{y1} and ν'_{y1}, respectively, for the photoelements located in the plane which passes through axis y when using a photodetector with helical pattern of the modulator, and in the plane passing through axis x when using a photodetector with radial pattern.   The sign in front of the second term of expressions (4.4) and

162

(4.5) is dependent on the direction of motion of the image and corresponds in the given case to the directions of the speed vectors, shown in Figure 4.17.

It follows from expressions (4.4) and (4.5) that the speeds v_x and v_y correspond to double the variations of frequency:

$$\left. \begin{array}{l} \Delta v_{x1} = v'_{x1} - v_{x1}; \\ \Delta v_{y1} = v'_{y1} - v_{y1}. \end{array} \right\}$$

(4.6)

The above photodetector and the given relations indicate the possibility of using the different method of measurement with an increase of sensitivity characteristic for it. These types of SKSI are described in [36, 77]. There are also varieties of this device in which two photodetectors, arranged along axes x and y, are used instead of four windows in the fixed diaphragm 4. The signal coming from the additional photoelement, which is located in front of the aperture in the diaphragm and is illuminated from the opposite direction of the disk by a special illuminator, is used as the reference frequency. (Footnote) (U.S. patent 3,511,150)

A functional diagram of a two-coordinate SKSI with the above optical-mechanical modulator, which has a radial pattern array, is presented in Figure 4.18, while the type of processes occurring in this system is shown in Figure 4.19. The objective 1 (Figure 4.18) that does not include sensor 17 forms the image 2 of the object in the plane of the modulator disk 3, combined with plane xy. A fixed diaphragm, having four identical apertures, is located in the immediate vicinity of modulator 3. The modulator disk 3 is set into rotation by electric motor 6. The light that is passed from objective 1 through modulator 2 and the windows of diaphragm 4 is collected by collecting lenses 5 on photoelements 7. Filters 8 and comparators 9 are also included in the sensor.

The remaining part of the measuring channel of the SKSI is located in the measuring module 18 and contains a pulse former module 19, consisting of forward 10 and rear 11 pulse front formers, conversion module 20, having level formers 12, and amplifiers of different levels 14. A generator 16 and output indicators 15 are located in module 18, besides these assemblies.

Since the considered SKSI is two-coordinate, it contains two identical measuring channels, related to coordinates x and y. Let us consider the action of the system on the example of operation of one of the measuring channels, for example, of channel x.
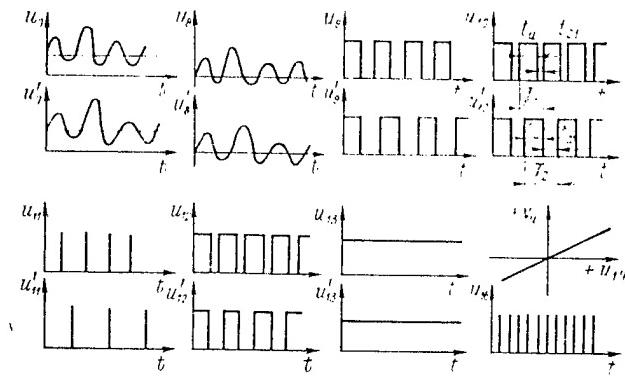
Figure 4.19. Type of Processes Occurring in SKSI With
Spatially Movable Optical Modulator

Electric signals of complex shape u_7 and u'_7, containing harmonics with

frequencies $v_{x1} = v_p - v_x$ and $v'_{x1} = v_p + v_x$, are fed from photoelements

7 and 7' to filters 8, which distinguish signals u_8 and u'_8 with
frequencies v_{x1} and v'_{x1}. Comparators 9 convert harmonic signals u_8 and
u'_8 to pulsed signals u_9 and u'_9 at the same frequency v_{x1} and v'_{x1};
these signals are fed to the inputs of module 18. Module 18 is designed
to find the difference of frequencies v_x and v'_x and to convert it to an
analog output signal u_{14}, proportional to the rate of displacement v_x of
image 2 along coordinate x. The action of module 18 is based on shaping
of square-wave pulses u_{10} and u'_{10} of stable length $t_{\text{и}}$, which follow at

frequencies v_{x1} and v'_{x1}, and on measuring the difference of the mean
values of potentials u_{13} and u'_{13}, corresponding to these pulses.

Pulsed signals u_9 and u'_9 are fed in the operating mode to the cell of
pulse former 19 to the inputs of the forward pulse front formers 10.
The positive potentials, by which the rear pulse front shapers 11 are
started, the output signals u_{11} and u'_{11} of which, arriving at the
second inputs of shapers 10, establish a zero potential at their
outputs, are established at the outputs of these formers after shaping
of the forward fronts.

thus, sequences of square-wave pulses u_{10} and u'_{10} of stable length t
with intervals t_{01} at t_{02} between them are formed at the outputs of the
cell of pulse shaper 19. The rear front shaper 11 is a time delay
element and is controlled by pulsed signals u_{16} of the stable frequency
of generator 16. The length $t_{\text{и}}$ is independent of frequency v_{x1} and v'_{x1}

of signals u_9 and u'_9; it is assumed identical for both channels and
should be close to period T of signals u_9 and u'_9 of the maximum
possible frequency $v_{x1\max}$ and $v'_{x1\max}$, but should not exceed it. The
length of intervals t_{01} abd t_{02} between pulsed signals u_{10} and u'_{10} is
inversely proportional to frequencies v_{x1} and v'_{x1}.

164

The level difference amplifier 14 subtracts the levels of signals u_{13} and u'_{13} and amplifies their difference. Thus, the output voltage u_{14} will be proportional to $2\nu_{x1}$ and, accordingly, it will be proportional to speed v_x of the motion of the image along coordinate x. The polarity of the output voltage u_{14} determines the direction of motion of the image. Signal u_{14} is fed to the input of the image stabilization system and to indicator 15.

SKSI with spatially movable modulator on photoelectric switched array. The main disadvantages of the above SKSI and other similar systems are the large overall dimensions of the moving optical-mechanical assemblies. SKSI based on the use of photoelectric switched arrays are devoid of these deficiencies. (Footnote) (USSR inventor's certificate 1,037,178) These devices can be made incomparably small in dimensions and mass, especially when using modern microelectronic technology, with the same sensitivity (as in SKSI with optical-mechanical modulator). Let us briefly consider the working and operating principles of one of these SKSI. A simplified functional diagram of the SKSI is presented in Figure 4.20, a. Objective 1 forms an image 2, lying in plane xy. A photoelectric array 3, which is a special photoelement that consists of N identical strip photoelements is located in the same plane. In the simplest case, these strip elements are combined into four groups (Figure 4.20, a). Leads a, b, c, and d of groups of strip photoelements are connected to the inputs of four identical switch modules 4-7. The control inputs of the switch modules are connected to the outputs of circular shift register 8, which controls master oscillator 9. The outputs of switch modules 4-7 are connected to the inputs of differential amplifiers 10 and 11, while the outputs of these amplifiers are connected to the inputs of the frequency comparator 12.

A sequential series of logic ones is written in the first half of the register digits 8 in the initial state of the circuit, while a sequential series of logic zeros is written in the other half. The direct outputs of register bits 8 are connected to the control inputs of switch modules 4 and 6, while the inverse outputs are connected to the control inputs of switch modules 5 and 7. The keys, to the inputs of which signals of a logic one from register 8 will be fed, will be opened and the keys, to the inputs of which signals of the logic zero will be fed, will be closed at each moment of time in the switch modules.

The system operates in the following manner. Frequency pulses ν_r are fed from master oscillator 9 to the input of register 8. Each of these pulses leads to an annular shift by one bit of the binary number written in register 8, which contains an even number of bits. The switches in modules 4-7 will be switched upon a circular shift of the number written in the register. Signals $u_{\phi4}-u_{\phi7}$ from photoarray 3 are the same at the outputs of the switch modules which would exist if four optically unconnected equivalent pattern arrays were applied to the image 2 to be checked; two of them, shifted by half a period l_p, would move in one

165

direction along axis x (vectors v_{p1} and v'_{p1}), while the two others (also shifted by half a period l_p) would move in the opposite directions (vectors v_{p2} and v'_{p2}). The following relation would occur

$$|v_{p1}| = |v'_{p1}| = |v_{p2}| = |v'_{p2}|.$$
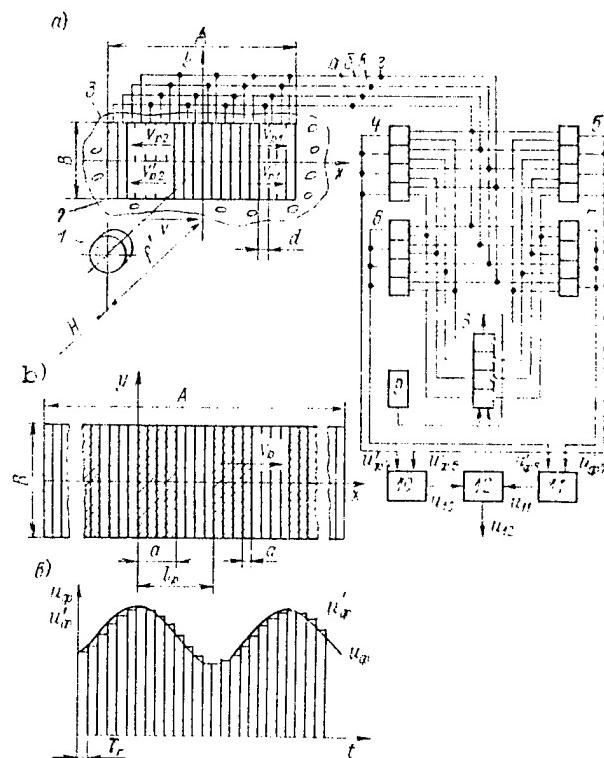
Figure 4.20. System With Spatial Movable Modulator on
Photoelectric Switched Array:
a--SKSI device; b--switching of photoarray; c--nature
of signals; 1--objective; 2--image; 3--photoarray;
4-7--switch modules; 8--circular shift register;
9--master oscillator; 10, 11--differential amplifiers;
12--frequency comparator

The given SKSI can be conditionally related to devices with spatially movable modulator with regard to this operating feature of the photoarray, which simultaneously performs the role of modulator. If there is no motion of image 2, i.e., at v = 0, signals $u_{\phi 4}$-$u_{\phi 7}$, containing variable frequency component $\nu_0 = \nu_p/l_p$, will exist at the

166

outputs of switch modules 4-7. The values of l_p and v_p are related to the number of m_p bits of register 8 and to the width d of strip photoelements by the following relations: $l_p = m_p d; \ v_p = dv_2$.

Then $v_p = v_r/m_p$.

The frequency ν_0 varies by value $\Delta\nu = v/l_p$ when the image moves along axis x at speed v in signals $u_{\phi4}-u_{\phi7}$ at the outputs of the switch modules. If the direction of the motion of the image and the direction of the equivalent pattern array coincide, frequency ν_0 is reduced by $\Delta\nu$. If these directions are opposite, the frequency ν_0 is increased by $\Delta\nu$. Thus, signals $u_{\phi4}$ and $u_{\phi5}$, containing frequencies $\nu_0 \pm \Delta\nu$, will occur at the outputs of key modules 4 and 5 and signals $u_{\phi6}$ and $u_{\phi7}$, containing frequencies $\nu_0 \mp \Delta\nu$, will occur at the outputs of switch modules 6 and 7. Besides the variable components, signals $u_{\phi4}-u_{\phi7}$ also have constant components, determined by the background noise from the object. The outputs of modules 4-7 are connected in pairs to differential amplifiers 10 and 11, in which the constant components of signals $u_{\phi4}-u_{\phi7}$ are mutually compensated, and the variable components containing frequencies $\nu_0 \pm \Delta\nu$ and $\nu_0 \mp \Delta\nu$ are separated. Signals u_{10} and u_{11} are fed from the outputs of amplifiers 10 and 11 to the frequency comparator 12, at the output of which there is a signal u_{12}, proportional to the frequency

difference   eq

The value of this signal is proportional to the motion speed v of the image, while the sign indicates the direction of motion. The number of bits of the register is $m_p = 4$ in the SKSI layout presented in Figure 4.20, a. The number of the keys in each of modules 4-7 is also equal to the number of bits of the register. The spatial period of the photoarray can be determined from the relation $l_p = 4d$, since here a =

= 2d. $\pm 2\Delta v = (v_0 \pm \Delta v) - (v_0 \mp \Delta v)$.

Upon operation of this SKSI, the motion of the equivalent arrays is discrete. The number of bits m_p of the register must be increased and the number of keys in modules 4-7 must accordingly be increased, and also the number of strip photoelements of photoarray 3 must be increased to reduce the discreteness of motion. Switching of photoarray at $m_p = 8$ is shown in Figure 4.20, b. The photoelements connected at a given moment of time and related to one of four equivalent arrays are denoted by the cross-hatching. The discrete shift of the array by d, equal to the width of one strip photoelement, occurs for each frequency pulse ν_r if master oscillator 9. There is a stepped signal u'_{ϕ}, shown in Figure 4.20, c, at the output of the switch module. The value of the time

167

interval T_r of each element of the stepped signal u'_ϕ can be determined from the expression $T_r = 1/\nu_r$.

The shape of the signal u_ϕ, which would exist if the motion of the array, superimposed on the image, would exist continuously, rather than discretely, is shown by the smooth curve in Figure 4.20, c. It is obvious that the greater the value of m_p, the closer the shape of the signal u'_ϕ approaches that of signal u_ϕ.

System with spatially movable modulator on optical fibers and switchable photoelements. It is sometimes convenient to have the photodetector of the system on fiber light guides for practical application of SKSI with spatially movable modulator. Besides design advantages, this device may provide higher sensitivity compared to SKSI in which strip photoelectric arrays are used. The photodetector part of this SKSI is similar to that shown in Figure 4.16, while the electric circuit differs in no way from that presented in Figure 4.20, a. Discrete photoelements of the photodetector part on fiber light guides are connected to points a, b, c, and d of the inputs of switch modules 4-7 (item 7 in Figure 4.16).

The operating principle of this SKSI is similar to that of the above SKSI on a photoelectric switched array.

4.6. Types of Image Motion and Their Influence on Operation of SKSI

Motion of image and its components. The approximate form and direction of misalignment of the image, which occurs in the image plane of an optical instrument (for example, an AFA), mounted on a movable base, are shown in Figure 4.21. Let us assume that axis s of the image plane is joined to the longitudinal axis of the platform on which the AFA is mounted and that it coincides with the direction of its translational motion. The value v_{Hx} will then represent the so-called ground or longitudinal component of the motion speed of the image, while v_{Hy} will represent the transverse component, determined, by the lateral misalignment or drift of the platform containing the AFA. Component v_{Kx} is determined by the longitudinal or pitching motion of the platform containing the AFA, while component v_{Ky} is determined by the rolling motion of the platform. Yawing of the platform containing the AFA is estimated by the angular rate of turn ω_{pK} of the image with respect to the origin of coordinate system Oxy. This rotation of the image results in the appearance of tangential components of the linear rotational speed of the points of the image v_{pKi}, the values of which are proportional to the angular velocity ω_{pK} and radius R_i, i.e., $v_{pKi} = \omega_{pK}R_i$. Misalignment of the platform and AFA along axis z in the

direction toward the object or from it results in the appearance of image speed components v_M', which occur due to variation of the image scale. The value of this speed is also dependent on radius R_i and the point of the origin of radius R_i does not always coincide with the origin of coordinate system Oxy.
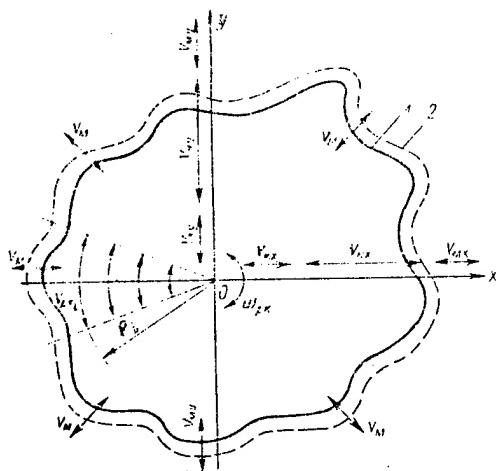

Figure 4.21. Nature and Types of Misalignment
of Optical Image:
1--image of object at specific distance H from
objective to object; 2--image of same object
upon decrease of H

In practice all these component speeds exist upon motion of the platform and AFA and, therefore, the motion of the image is rather complicated in nature. Calculated functions that permit one to determine the value of each of the considered components of the motion speed of the image were presented in Chapter 1.

Operating modes of SKSI and effect of type of image motion on its functioning. Depending on the designation and operating conditions of the optical instrument, which includes the SKSI, it can operate in two modes: 1) information measuring and 2) as an error sensor in the ASSI.

In the first case, the SKSI is a device that measures the absolute motion speed of the optical image.

For example, it is convenient to use the absolute values of the total speeds $v_{\Sigma x}$ and $v_{\Sigma y}$ along axes x and y for the general type of image motion of the SKSI, presented in Figure 4.21:

$$v_{\Sigma x} = v_{\text{п}x} + v_{\text{к}x} + v_{\text{м}x}; \quad v_{\Sigma y} = v_{\text{п}y} + v_{\text{к}y} + v_{\text{м}y}.$$

It is obvious that the value and direction of the resultant motion speed of the image can be determined from the values of $v_{\Sigma x}$ and $v_{\Sigma y}$. SKSI operating in the information measuring mode may have switchable limits of measurement along both axes, while the measurement error is determined by the type and working principle of the SKSI. In the second case, the SKSI essentially measures the difference of the motion speeds $v_{\Sigma x}$ and $v_{\Sigma y}$ of the image along the corresponding coordinates and the motion speeds $v_{\text{п}x}$ and $v_{\text{п}y}$ of the detector of the optical device, located in the image plane, for example, of the photographic film in an AFA.

In this case:

$$v_x = v_{\Sigma x} - v_{\text{п}x}; \quad v_y = v_{\Sigma y} - v_{\text{п}y}.$$

The static characteristics of a SKSI operating in this mode are similar to those shown in Figure 4.5, b. As in the case of using other sensors, the static characteristic of this SKSI has a range of measurement, zone of insensitivity and saturation region. Its sensitivity is generally determined by the formulas:

$$S_x = \frac{du_x}{dv_x}; \quad S_y = \frac{du_y}{dv_y}.$$

Signals u_x and u_y are fed from the outputs of the SKSI to the inputs of the image stabilization system, where they are converted to displacements of the compensating elements of the ASSI, which result in a decrease of the resulting speeds v_x and v_y to permissible limits.

The main requirements on the SKSI (as on the element of the ASSI) were outlined in section 4.2; let us additionally note the following.

When a number of optical instruments are operating, the value of the component speed $v_{\text{п}x}$ (Figure 4.21) may be considerably greater than that of $v_{\text{п}y}$ and of the other components $v_{\text{к}}$ and $v_{\text{м}}$. An additional compensating element (rotary mirror, or prism, or something else), which operates as a function of the ground speed component of the motion of the optical instrument with respect to the object, must be introduced into the instrument to provide the given stabilization accuracy of image motion and also to permit the use of a SKSI having high sensitivity and narrow measurement range. Information about the ground speed component

170

of the motion of the instrument can be obtained from various types of
sensors, including those from the SKSI operating in the information
measuring mode.

4.7. Errors of SKSI

Types of errors of SKSI. Real SKSI have finite accuracy
characteristics, determined by the errors of the system. The errors
that occur during operation of the system, according to the
classification of errors of systems [15, 16], can be divided with
respect to their features into absolute and relative, additive,
multiplicative, exponential, periodic, systematic and random, methodical
and instrumental, and static and dynamic. Based on the physical nature
of the origin of errors of the SKSI, they can be divided into
methodical, engineering design, dynamic and noise [15]. The methodical
errors Δ_M are determined by the adopted method of checking, by the
inaccuracy of determining the parameters of the physical processes
occurring in the system, and are ordinarily random in nature, mostly
approximated by normal distribution law.

The engineering design errors Δ_K are divided into systematic and random.
Systematic errors can be compensated or taken into account during
operation of the system. Random errors are static in nature and their
laws of distribution can be different.

Dynamic errors $\Delta_\text{Д}$ are determined mainly by the inertia of the elements
of the system and of the entire system as a whole. To reduce this
error, it is desirable to reduce the inertia of the system if possible,
but this may result in an increase of the noise error.

Noise errors $\Delta_\text{Ш}$ are caused by variation of the parameters of the system
due to the effect of different perturbing actions, which are random in
nature. These actions are temperature, voltage and current fluctuations
of the electric circuits and so on. It follows from the above
classification of errors of the SKSI that all the errors (except those
compensated by the systematic engineering design error) are random in
nature and they can be mostly considered independent [16]. The total
error Δ_Σ of the SKSI can be represented in the following manner:

$$\Delta_\Sigma = \sqrt{\Delta_\text{м}^2 + \Delta_\text{к}^2 + \Delta_\text{д}^2 + \Delta_\text{ш}^2}.$$

It is obvious that the parameters of the SKSI must be optimized
according to the criterion of the minimum error. Determination of the
effective errors of real SKSI is very difficult and is considerably
dependent on the working and operating principles of the system. The
limited scope of the book does not permit detailed consideration of the

171

determination of all errors of SKSI, different in working principle.
Let us dwell in this section on the main components of the total error
that determine the operating accuracy of the SKSI.
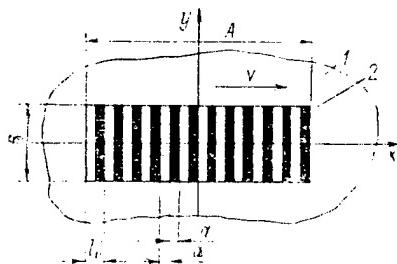
Figure 4.22. Working Section of Linear Modulator:
1--fixed diaphragm; 2--working segment of modulator
pattern in window of diaphragm

Methodical error of SKSI. The main error component of frequency SKSI,
determined by the method of issuing information about the motion speed
of the image, is the methodical error of the modulator in the measuring
channel of the system.

Fixed and movable optical modulators are mainly used in the above SKSI.
A fixed modulator on an unswitched photoelectric array is essentially a
variety of a fixed optical modulator, while a modulator on a switched
photoelectric array is a unique movable modulator with discrete, stepped
displacement.

The main geometric parameters of the working segment of a modulator with
linear pattern, used in some of the above SKSI, are presented in general
form in Figure 4.22. In this figure, A and B are the length and width
of the window of the diaphragm 1, through which a segment of pattern 2
is visible. A frequency system, operating in the information measuring
mode, is described in [89] and the determination of the methodical error
of the system is presented. A self-adjusting filter is used in the
electric circuit of the system. The frequency SKSI may have an electric
filter that is not self-adjusted to the center of the spectrum of the
electric signal from the photoelement when operating in a closed ASSI,
since this adjustment is essentially performed by the ASSI, which tries
to keep the image fixed in the working zone of the instrument and this
means in the plane of the SKSI modulator located in this zone, when
operating in a closed ASSI. But the center of the spectrum of the
electric signal from the photoelement is maintained at one frequency, to
which the electric filter of the measuring channel of the SKSI is
turned. Thus, the nature of the methodical error of the system
described in [89] and of the considered frequency SKSI is the same.

Based on mathematical analysis of the principles of modulation and
subsequent electric filtration of the signal from the photoelement, the

172

formula of the mean square error in frequency, estimated in hertz, which can be written in the following form for our case, was found in [89]:

$$\Delta_f = \sqrt{\frac{v v_{\phi\pi}}{24A}},$$

where v is the motion speed of the image, $mm \cdot s^{-1}$, $v_{\phi\pi}$ is the frequency band of the electric filter, Hz, and A is the length of the modulator, mm.

In turn, according to Figure 4.22, we have

$$A = l_p N',$$

where l_p is the spacing of the pattern array of the modulator, mm, and N' is the number of spaces of the working segment of the modulator pattern.

The mean square error in speed can then be determined from the expression

$$\Delta_v = l_p \sqrt{\frac{v v_{\phi\pi}}{24 l_p N'}} = \sqrt{\frac{v l_p v_{\phi\pi}}{24 N'}}. \tag{4.7}$$

The considered error is essentially the methodical error of a frequency SKSI with fixed linear modulator, and its distribution is subordinate to normal law [89]. Glass disks with spiral or radial patterns applied to them (see Figure 4.17) are used as the modulator in SKSI with spatially movable optical-mechanical modulator.

These SKSI (besides the methodical error described above) have an additional error, determined by the characteristics of the modulator pattern device, for example, by the nonlinearity of the strips of the spiral pattern and by the aparallelism of the strips of the radial pattern. This error is also related to the methodical error and is independent with respect to the above error.

A working segment of a modulator having spiral pattern is shown in Figure 4.23, a. The modulator is made in the form of a glass disk 1, on which the figure of a pattern 2, which is an Archimedean spiral, is applied. A fixed diaphragm 3 with windows in the form of narrow slits, oriented along axes x and y, is located in front of the modulator disk.
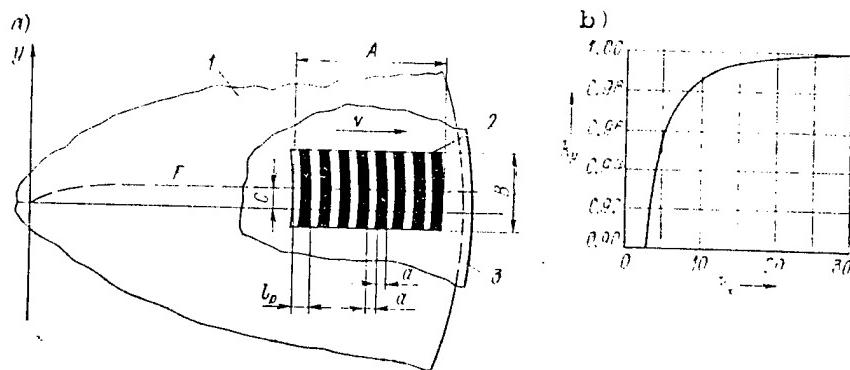
Figure 4.23. Working Segment of Modulator With Spiral Pattern:
a--shape and arrangement of working segment; b--graph of function
that determines position of line Γ; 1--modulator disk; 2--working
segment of pattern in diaphragm window; 3--fixed diaphragm

To eliminate the additional methodical error that occurs due to the
spiral pattern 2, which is visible in the diaphragm window 1, the middle
line F of the window should be shifted with respect to the corresponding
axis x or y such that the pattern lines, visible in the diaphragm
window, are perpendicular to this line, while the line itself is
parallel to axis x or y. The error of the modulator can then be
determined by the above formula (4.7). To determine the position of
line F, one can use the auxiliary graph presented in Figure 4.23, b.
Here:

$$
\left.
\begin{aligned}
x &= bk_x; \\
y &= bk_y.
\end{aligned}
\right\}
$$

(4.8)

The values of x and y in expressions (4.8) are the current values of the
coordinates of the points of curve F, while coefficient b is the
constant in the equation that describes the Archimedean spiral $\rho = b\varphi$,
and ρ is the length of the radius vector that describes the spiral and φ
is the angle between the radius vector and the axis.

The radius vector is elongated by the spacing l_p of the pattern during a
complete revolution, i.e., by $l_p = 2\pi b$. Expressions (4.8) can then be
written in the form:

$$
\left.
\begin{aligned}
x &= \frac{l_p}{2\pi} k_x; \\
y &= \frac{l_p}{2\pi} k_y.
\end{aligned}
\right\}
$$

(4.9)

174

Knowing the value of 1_p and being given the values k_x, for which we determine the corresponding values k_y from the given graph, using expressions (4.9), we find the coordinates x and y of the points of curve F.

It follows from expressions (4.9) and graph $k_y = f(k_x)$ that curve F passes approximately to axis x at distance $c = 1_p/(2\pi)$ from it at approximately $x = 41_p$. This also means that the middle line F of the diaphragm window can be made coincident with the corresponding coordinate axis x or y for small values of 1_p. The number of the spacing of the pattern should be added within the length A of the diaphragm window, i.e., $A = 1_pN'$. Violation of this condition causes the appearance of fluctuations of the luminous flux passing through the diaphragm window upon rotation of the modulator disk, i.e., it results in the occurrence of one of the components of the noise error Δ_{III}.

Modulators based on an unswitched photoelectric array can essentially be considered as fixed optical spatial filters. A working segment of this modulator is similar to that shown in Figure 4.22 and the mean square error in speed can also be determined from expression (4.7).

Matters are somewhat more complicated in the case of using a switched photoelectric array in a SKSI, similar to that considered in section 4.5. Discrete displacement of the equivalent pattern arrays occurs in this SKSI, which results in the occurrence of stepped signals at the output of the photoelements of the array. Therefore, besides the main methodical error of determining the motion speed of the image, related to the frequency method of measurement itself, there will exist an additional methodical error, caused by the discrete nature of the motion of the pattern.

The error in determination of the variation of signal frequency $\Delta(\Delta\nu)$ is caused by the quantum nature of the signal in the given SKSI and is determined by the formula $\Delta (\Delta v) = dv_0/l_p$, where ν_0 is the frequency of the electric signal in the check system, determined by the motion of the equivalent pattern with a fixed image.

It is known from description of the working and operating principles of the SKSI presented in Figure 4.20 that $v_n = v_r/m_p$, $l_p = m_p d$. The error can then be determined by the formula $\Delta (\Delta v) = v_r/m_p^2$.

The additional error in determination of the motion speed of the image, caused by the discrete motion of the pattern, is found from the expression

$$\Delta_v' = l_p \Lambda (\Delta v) = l_p v_r / m_p^2. \qquad (4.10)$$

Based on expressions (4.7) and (4.10), one can then write the following relation for the total methodical error of determining the motion speed of the image of a SKSI with single equivalent array:

$$\Delta_y = \sqrt{\frac{v l_p v_{\phi \Lambda}}{24 N''} + \frac{l_p^2 v_r^2}{m_p'}} .$$

It is obvious from this expression that an increase of the number of bits of the circular shift register (see Figure 4.20, a) and a decrease of the values of l_p and ν_r results in a decrease of the total methodical error. An increase of the number m_p may be reasonable only up to a limit at which the value of d assumes a value d = 1/(2R$_p$), where R$_p$ is the resulting resolution of the optical system of the device.

Chapter 5. Electromechanical Subsystems of Image Stabilization Systems

5.1. Design Principles and Problems of Design of Electromechanical
     Subsystems

Design principles of precision electric drives. Precision movements of
mechanisms can be achieved by using reducerless electric drives in open
and closed control systems. Control is primarily exercised in open
systems on the basis of electric step motors. Various types of electric
motors are used in closed systems and one can essentially achieve high
accuracy of motion of mechanisms. A complex control system can be
effectively broken down for interconnected electric drive systems by
creating separate closed systems.

Studies show that the motions of the mechanisms of functional devices of
image stabilization systems should proceed with current errors in
position that do not exceed units of angular seconds for angular
displacements and units of a micron for linear displacements. Errors of
motion by speed, estimated in percent of current speed, are in the range
of values less than 0.01 percent. The accuracy of these systems is
determined to a considerable degree by the indicators of dynamic
accuracy. The indicators of static accuracy are insignificant with
regard to the fact that integrals must also be introduced into control
laws when designing control systems to compensate for the constant
components of perturbations and this predetermines the receipt of as
small static errors as desired in control systems. Dynamic accuracy is
determined to a significant degree by both the dynamic characteristics
of perturbing actions and by the dynamic characteristics of measurement
noise, which is represented in the form of complex deterministic and
stochastic processes.

Stabilizing, follow-up and programmed precision motions of mechanisms
are realized by control systems in image stabilization problems.
Follow-up modes in precision electromechanical systems are performed so
that the spectral band of the control system is greater than the
spectrum of the master signal and that it be reproduced without
distortions. Follow-up modes are similar to stabilizing modes in this
regard. If follow-up is achieved in different regions of the motion
speeds of mechanisms, transition of the system from one region to
another occurs by switching the structure of the control system. This
trajectory mode is realized with limitations of the torques of electric
drives at the level of permissible values.

The general design principles and principles of calculation of electric
drive control systems are outlined in detail in [7]. Modern electric
drive control systems are constructed primarily on the principles of
subordinate (cascade) control. This principle guarantees maximum

177

simplicity of design and adjustment of electric drive systems, low
sensitivity of the systems to variations of parameters, and the
possibility of using standardized tunings of the control circuits and of
standardized components for realization of them.

The principle of control by the vector of state of the object is
widespread, along with the principle of subordinate control. This
control is used primarily in design of local electric drive systems with
flexible couplings between the motor and mechanism.

An important aspect in development of precision electric drives is
selection of the position or velocity sensors and of the comparators.
Several different methods of organizing control systems ensues from
analysis of the methods of formation of precision motions according to
the type of comparators. Technical descriptions of these systems are
given in more general form in |21|. The highest dynamic accuracies of
motion can be achieved in pulse phase systems with separation of the
formation of short-periodic and trajectory motions of electric drives.

The following characteristics, which distinguish them from other
electric drive systems, are typical for precision electric drive control
systems:

1. The high degree of organization of control of the electric drive
itself (converter-motor controlled systems) to achieve rigid mechanical
characteristics in open systems.

2. The need for detailed consideration of the combination of all the
determinant and random processes that influence the dynamic accuracy (in
the electric drive itself, in the information system, in the comparator
and in the control channels).

3. The need to achieve wide bandwidths of signals in closed control
systems, which determines the consideration of the flexible properties
of the electric drives and mechanisms over a wide frequency band.

Coupled electric drives as electromechanical subsystem of image
stabilization system. It follows from Chapters 1-3 that simultaneous
displacement of several optical elements or of one element in two-three
coordinates must be used to stabilize the image upon spatial
displacements of the base. Part of the functional devices of
stabilization systems can be related to each other by mechanical
assemblies and design elements. Moreover, cushioning devices, through
the flexible couplings of which there is mechanical coupling of the
coordinates of motion of the functional devices, are used in optical
instruments.

Electric drives are coupled with regard to these circumstances and,
together with the structural elements of actuating and cushioning
devices, are a very complicated electromechanical subsystem (VEMP) of
the image stabilization systems. The control object must be regarded as

variable jointly with the regulators for solution of the main task--
achieving the necessary accuracies of motion--rather than as the given
object in design of precision local and coupled electric drive systems
from the viewpoint of achieving given or maximum dynamic accuracies.
Both the coefficients of inertia and the parameters of flexible
mechanical couplings of the object are variable parameters during
design. On this basis, let us determine the generalized criterion of
quality for design of the system and let us formulate the condition of
decomposition of the control system.

Decomposition of a coupled system, which results in the possibility of
considering it in the form of separate individual systems similar to
self-contained systems, is always used in one or another form in design
of complex systems. This permits considerable simplification of a
complex control system both in the design phase and in the phase of
technical realization of it.

Considering r output variables of the control VEMP with regard to their
contribution to formation of the index of quality of the technical
object, let us define the generalized criterion of quality by special
criteria with regard to the standard of the estimation vector, of the
vector of variable parameters α, and of the constraints of variables in
the following form:

$$Q = \sum_{i=1}^{g} b_i \sum_{j=1}^{r} Q_{ij}(\alpha),$$ (5.1)

at $Q_{ij}(\alpha) \leqslant c_i, i = \overline{g + 1, r}; \alpha \in M_\alpha.$ Here b_i are weight coefficients of the

output variables, c_i are the values of constraints on estimates of

special criteria of quality, $Q_{ij}(\alpha)$ are elements of matrix $Q'(\alpha) = |Q_{ij}(\alpha)|,$

i, j = $\overline{1, n}$, and M_α is a closed set of permissible values of α.

The conditions of the diagonal dominance of the matrix of estimates, at
which

$$Q_{ii}(\alpha) \geqslant \beta \sum_{\substack{j=1 \\ j \neq i}}^{r} Q_{ij}(\alpha),$$ (5.2)

also determine the condition of decomposition of the coupled control
system. One can assume approximately in formula (5.1)

$$\sum_{j=1}^{r} Q_{ij}(\alpha) \approx Q_{ii}(\alpha) \text{ и } Q \approx \sum_{i=1}^{g} b_i Q_{ii}(\alpha). \qquad (5.3)$$

Accordingly, the estimate of the generalized criterion of quality Q must be minimized with regard to constraints of coordinates of the system by changing the vectors of parameters α and one must guarantee fulfillment of condition (5.2). The given principle of decomposition of a coupled system can be defined as the principle of dynamic decomposition. It is distinguished from the principle of separation of motions of separate systems by the fact that all separate systems when using it may have similar dynamics, which in good agreement with minization of the quadratic functionals of the qualities.

The principle of dynamic decomposition guarantees synthesis of control primarily without resorting to cross-correcting correlations between the main separate systems. This guarantees a comparatively simple structure of the control VEMP, similicity of the estimates of errors of separate control systems, and reliable realization of systems using microprocessors.

The high complexity of mathematical description of precision control VEMP and the requirements of considering a large number of factors that influence the accuracy of motion of electric drives result in the need to use the systems approach in formulation of design methodology. Indeed, there may be several coupled electromagnetic variables in local electromechanical systems in circuits of shaping the electromagnetic moment alone. This is especially manifested in electric AC systems. Strong couplings are formed in multimass mechanical subsystems with flexible couplings. It should be noted that high speed at all levels of couplings is typical for VEMP, which places them among specific objects in which the dynamic processes are simultaneously determined by a large number of variables.

Systems approaches to design of control VEMP can be used under these conditions.

The specifics of the systems approach [27] is that a complex system is divided into individual subsystems. The individual subsystems are described and their properties are studied with regard to the properties of the system as a whole. Alternative versions of individual subsystems and of the system as a whole are considered. The problem of determining the set of design versions of an electromechanical control subsystem is related to problems of structural analysis. It is necessary in this case: 1) to establish the levels in the system structure and to determine their correlation, 2) to perform topological decomposition with separation of subsystems having strong internal couplings and weak intersubsystem couplings, and 3) to determine separate control systems. The process of study is iterative in nature and ends in selection of a compromise version.

180
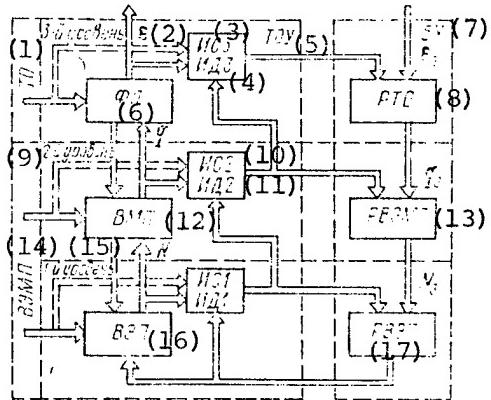
Figure 5.1. Diagram of Hierarchical Control System

KEY:

1.	Technical object	12.	Coupled mechanical subsystem
2.	Third level	13.	Regulator very complex
3.	Information system 3		electromechanical subsystem
4.	Identifier 3	14.	Very complex
5.	Technical control object		electromechanical subsystem
6.	Functional subsystem	15.	First level
7.	Control module	16.	Coupled electromechanical
8.	Not further identified		subsystem
9.	Second level	17.	Regulator coupled
10.	Information system 2		electromechanical subsystem
11.	Identifier 2		

Let us determine the problems of design of precision control VEMP from the aspect of the systems approach. But let us first consider the generalized layout of the structural organization of the control system of coupled electric drives of the technical object (TO), represented as the diagram of the hierarchical system having three levels (Figure 5.1). The first low level contains a coupled electromechanical subsystem (VEP), the input variables of which are control signals of different semiconductor converters, while the output variables of which are electromagnetic moments (forces) of the electric motor N. The second level has a coupled mechanical subsystem (VMP), which has feedback with the VEP through electromagnetic induction circuits. The output variables of the coupled mechanical subsystem q are variables that characterize the motion of the mechanisms (linear and angular displacements, velocities, and elastic forces and moments). VMP and VEP subsystems, considered jointly, form VEMP. The third level contains a functional subsystem (FP), which guarantees formation of the index of quality of image stabilization ϵ and which includes optical elements that are combined into a single optical system. One can consider the corresponding regulators--RVEP, RVEMP, and RTO, which are a coupled system in interlevel subordination in the control module (BU), similar to how this occurs in the technical control object (TOU). The

subsystems of each level contain information systems (IS) and identifiers (ID) that form the necessary information for the control process at each level and in the control system as a whole. The given sets of regulators are determined by the values of signals ϵ_3, q_3, and N_3.

The possibility of topological decomposition of a complex structure into individual subsystems, each of which has strong internal couplings and weak correlations and feedback, is provided in the given generalized structure of the control system. This type of decomposition is "horizontal decomposition." Moreover, "vertical" topological decomposition, which includes dynamic decomposition of correlated separated system included in the considered level subsystems, is possible.

Problems of design of electromechanical subsystems from aspect of systems approach. The resulting dynamic error of the electric drive control system is generally dependent on the regular and random components of actions. The regulator components of the actions include: rotary and gear changes of the flow of the engine and (related to this) variations of the torque, rotary changes of the moment of resistance of the mechanism and of the kinematic gearing and also changes of the electromagnetic moment in DC motors, caused by commutation in the brush-collector assembly, and changes of the electromagnetic moment in AC motors with regard to deviation of the shape of stator voltages and currents from harmonic shape, and wave, periodic and other types of changes of the moment of resistance, related to functioning of the technical object. The random components of the actions include random variations of the moment of resistance and of the network voltage, and noise in the channels for measuring the coordinates of motion.

The component of the resulting error, caused by variations of network motion if internal subordinate current or voltage subordinate control circuits of the controlled converter are used, is effectively reduced in the control systems. Changes of the moment of resistance and noise in the system for processing information about the coordinates of motion of the electric drive have the greatest effect on the dynamic error of the system. Optimization of the system, based on the minimum total dynamic error, is related to satisfaction of contradictory requirements of optimal filtration of measurement noise and of error components due to variations of the moment of load.

Experimental studies of precision electric drive systems show that random processes are subordinate to steady-state and ergodicity conditions and have probability density distribution according to normal law.

The perturbing effects and noise of measuring the coordinates of motion may have the most diverse form in practical situations and, accordingly, the form of a description. Specifically, descriptions in the following

182

form may be an adequate description of them: individual harmonic

components, Fourier series $f(t) = f_0 + \sum_{k=1}^{\infty} A_k \times \sin(\omega_k t + \varphi_k)$ with spectral

densities $S(\omega) = 2\pi \left\{ f_0^2 \delta(\omega) + \sum_{k=1}^{\infty} (A_k^2/4)[\delta(\omega - \omega_k) + \delta(\omega + \omega_k)] \right\}$, white or

color noise, wave processes, and also different combinations of them.
The structureof the control system can be different in this regard and
can be more or less adaptable to a specific practical situation. Design
of a control VEMP in a quasi-stabilizing mode reduces to design of a
system which, being a closed regulator, would correspond to the minimum
given functional of quality. The problem of designing a control VEMP
from the aspect of the systems approach reduces to one of making a
decision about selection of one alternative from a set of alternatives
according to generalized criterion of quality (5.1), which reflects
quantitatively the properties of the system. The problem of making an
optimal decision in selecting the alternative is one of mathematical
programming, which guarantees determination $Q* = \min Q$ among a set of
estimates.

Based on the foregoing, the general procedure of dynamic design of a
precision control VEMP can be performed by using a computer in three
steps: 1) design of a quasi-optimal structure of the system, 2) design
of the main VEM and VMP subsystems, and 3) parametric design within a
quasi-optimal technical realizable structure. The basis for solution of
problems of the first step is use of a comparatively limited number of
structures of control systems with approximately equal dynamic
capabilities, which permits one to select a quasi-optimal structure by
approximate dynamic synthesis with regard to the real actions and main
constraints.

Complications of the structure of a control system, related to
measurement of additional coordinates (accelerations, velocities,
dynamic moment) are justified only if the measurement noise is small
compared to dynamic fluctuations of the coordinates of the excited
system. The feasibility of introducing a new coordinate can first be
estimated on the basis of the inequality

$$D_{\text{и}i} < \frac{1}{2\pi} \int_{-\infty}^{\infty} S_i^y(\omega)\, d\omega,$$

where $D_{\text{и}i}$ is the error in measurement of coordinate y_i and S^y_i is the
approximate estimate of the spectral plane of the coordinate in an
excited system.

183

Not only the noise of measuring the coordinates of the system and perturbations by load, but also the parametric perturbations in the motors, related to formation of electromagnetic moments, and other effects must generally be taken into account in design of precision control VEMP. Moreover, the constraints of the output voltages of the regulators, coordinate error meters, converters and constraints on permissible currents of the motors must be taken into account. Let us assume that the effects on the system is the k-vector ρ ($\rho \in R^k$), while the checked coordinates are k-vector y ($y \in R^t$). Let us assume that the index of quality of the technical object is determined from r coordinates of vector y of g coordinates, while the remaining indices of the (r - g) coordinates should be in the range of the given constraints.

Considering the effect on the system in the form of superposition of determinant and stochastic processes and assuming that it is possible to represent determinant processes in the form of a Fourier series, let us write the elements of vector ρ in the form $\rho_j = q_j + A_j \times \sin \omega_j t$, $j = \overline{1, k}$, where q_j is the random component of the effect.

Having expressed the spectral density $S_{qj}(\omega)$ of the random component q_j by the intensity of white noise N_j and by the characteristics of the shaping filter $S_{qj}(\omega) = N_j \,|\, W_{\phi j}(j\omega)|^2$, where $W_{\phi j} \cdot (j\omega)$ is the transfer frequency function of the shaping filter, and having expressed the spectral density of the harmonic component of the effect in the form $S_{Aj}(\omega) = 2\pi A_j/4 \,[\delta(\omega - \omega_j) + \delta(\omega + \omega_j)]$ and relating the transfer function of the filter to that of the control system from the j-th effect on the i-th coordinate $W_{ij}(\omega)$, one can write the mean square dynamic deviations of the i-th coordinate in the following form:

$$\overline{y_i^2} = \sum_{j=1}^{k} \left[\frac{N_j}{2\pi} \int_{-\infty}^{\infty} |\, W_{\phi j}(j\omega)\, W_{ij}(j\omega)|^2 \, d\omega + 0.5 A_j^2 |\, W_{ij}(j\omega_j)|^2 \right].$$

Or, taking into account that the expression $1/2\pi \int_{-\infty}^{\infty} |\, W_{\phi j}(j\omega) \times W_{ij}(j\omega)^2 |\, d\omega = w_{ij}$ is the effective bandwidth of the system [9], and having denoted $0.5A^2_j = A'^2_j$, we find

$$\overline{y_i^2} = \sum_{j=1}^{k} [N_j w_{ij} + A'^2_j |\, W_{ij}(j\omega_j)|^2]. \tag{5.4}$$

184

If the random effects are presented in the form of the k-dimensional vector of white noise intensities $N = [N_1 N_2 \ldots N_h]^T$, the regular effects in the form of the k-dimensional vector of squares of amplitudes $A = [A_1^{'*} A_2^{'*} \ldots A_k^{'*}]^T$ and of dynamic deviations of the coordinates in the form of the r-dimensional vector of the mean squares of deviations $y = [y_1^2 y_2^2 \ldots y_r^2]^T$, the equation that characterizes the dynamic processe sin the system can be written in vector matrix form in the form

$$y = WN + KA, \tag{5.5}$$

where W is a $r \times k$ matrix of the effective bandwidths of the system, and $W = |w_{ij}|$, $i = \overline{1, r}$, $j = \overline{1, k}$, and K is a $r \times k$ matrix of the squares of the moduli of the transfer frequency functions, and $K = ||W_{ij}(j\omega_j)|^2|$, $i = \overline{1, r}$, $j = \overline{1, k}$.

The integrals of the elements of the matrix of the effective bandwidths W can be reduced to typical form and the tabular values of the integrals can be used in the calculations [9].

The parameters of the regulators, at which minimum total variation or mean square deviations of the output coordinates is provided when taking into account the main constraints in the system and the flexible mechanical couplings of the electric drives, are found within the quasi-optimal structure during parametric optimization of the system. The transfer frequency functions $W_{ij}(j\omega)$ are formulated on the basis of standardized dynamic characteristics of the control circuits of separate systems upon variation of a number of parameters. Having denoted the vector of the variable parameters $\alpha = |\alpha_1 \alpha_2, \ldots, \alpha_l|^T$, one can write the generalized criterion of quality in the following form:

$$Q = \sum_{i=1}^{g} b_i y_i^2(\alpha), \quad \alpha \in M_\alpha. \tag{5.6}$$

The constraints of the remaining $r - g$ coordinates, written in the form of inequalities $\overline{y_i^2}(\alpha) \leqslant C_i$ at $i = \overline{g + 1, r}$, can be established in the following manner. The value $A_{i\,max} \approx 3\sigma_{yi}$, $i = \overline{g + 1, r}$, where $\sigma_{yi} = \sqrt{\overline{y_i^2}(\alpha)}$ is the mean square deviation of coordinate y_i, can be taken as the maximum deviation with normal law of distribution of the dynamic deviations of the coordinates of systems.

185

The conditions for taking into account the constraints during design of the system can be written in the form $\sigma_{yi} \leqslant (1/3)\, C_i$, $i = \overline{g+1,\, r}$ or $\overline{y_i^2} \leqslant (1/9)\, C_i$, $i = \overline{g+1,\, r}$.

If each of the vectors y, N, A and α are represented in the form of composite vectors $y = [y_1^T \vdots y_2^T \vdots ... \vdots y_g^T]^T$; $N = [N_1^T \vdots N_2^T \vdots ... \vdots N_g^T]^T$; $A = [A_1^T \vdots A_2^T \vdots ... \vdots A_g^T]^T$ and $\alpha = [\alpha_1^T \vdots \alpha_2^T \vdots ... \vdots \alpha_g^T]^T$ according to the number of coordinates contained in the generalized criterion of quality, equation (5.5) can be represented in block matrix form

$$
\begin{bmatrix} y_1(\alpha) \\ \hline y_2(\alpha) \\ \hline \vdots \\ \hline y_g(\alpha) \end{bmatrix}
=
\begin{bmatrix} W_{11}(\alpha) & W_{12}(\alpha) & \cdots & W_{1g}(\alpha) \\ \hline W_{21}(\alpha) & W_{22}(\alpha) & \cdots & W_{2g}(\alpha) \\ \hline \vdots & \vdots & \ddots & \vdots \\ \hline W_{g1}(\alpha) & W_{g2}(\alpha) & \cdots & W_{gg}(\alpha) \end{bmatrix}
\times
$$

$$
\times
\begin{bmatrix} N_1 \\ \hline N_2 \\ \hline \vdots \\ \hline N_g \end{bmatrix}
+
\begin{bmatrix} K_{11}(\alpha) & K_{12}(\alpha) & \cdots & K_{1g}(\alpha) \\ \hline K_{21}(\alpha) & K_{22}(\alpha) & \cdots & K_{2g}(\alpha) \\ \hline \vdots & \vdots & \ddots & \vdots \\ \hline K_{g1}(\alpha) & K_{g2}(\alpha) & \cdots & K_{gg}(\alpha) \end{bmatrix}
\begin{bmatrix} A_1 \\ \hline A_2 \\ \hline \vdots \\ \hline A_g \end{bmatrix}
. \tag{5.7}
$$

If the dynamic decomposition conditions are implemented, the quadratic block matrices can be represented in the form of diagonal block matrices and equation (5.7) can be written in the form of g matrix equations

$$
y_i(\alpha_i) = W_{ii}(\alpha_i)\,N_i + K_{ii}(\alpha_i)\,A_i, \quad i = \overline{1,\,g}, \tag{5.8}
$$

which contain components of vectors y_i, N_i, A_i, and α_i, the elements of which are related only to the natural main separate systems. This representation considerably simplifies design of the control VEMF.
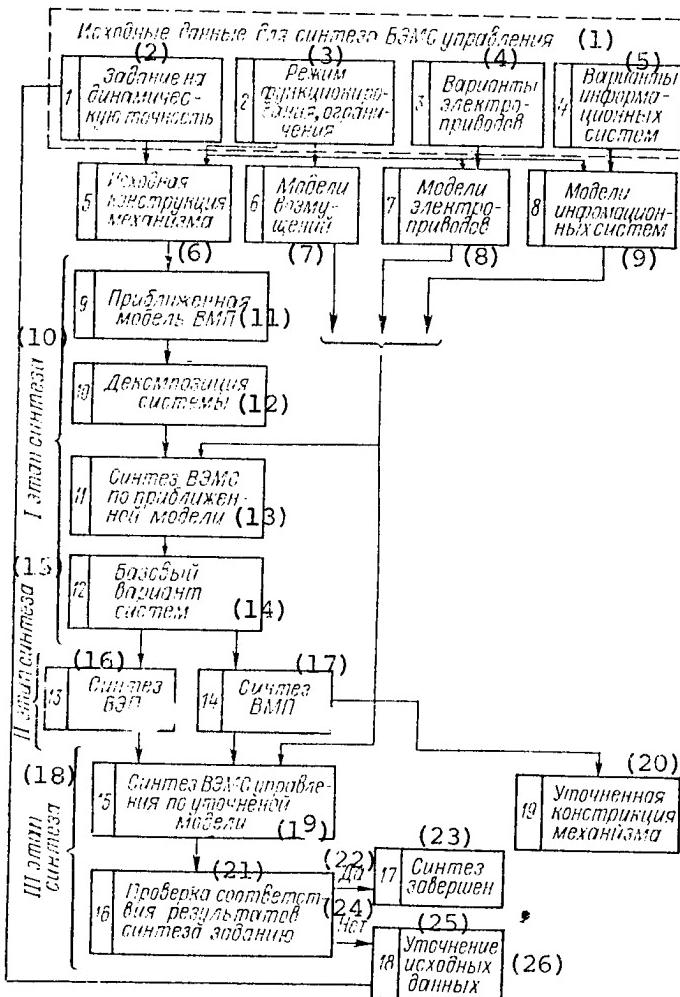
Figure 5.2. Diagram of Algorithm for Design of VEMP

KEY:

1. Input data for design of control VEMS
2. Program for dynamic accuracy
3. Functional and constraint mode
4. Variants of electric drives
5. Variants of information systems
6. Initial design of mechanism
7. Models of perturbations
8. Models of electric drives
9. Models of information systems
10. First stage of design
11. Approximate model of VMP
12. Decomposition of system

(Key continued on following page)

13. Design of VEMS by approximation model
14. Basic version of system
15. Second step of design
16. Design of VEP
17. Design of VMP
18. Third step of design
19. Design of control VEMS according to refined model
20. Refined design of mechanism
21. Check of conformity of results of design to program
22. Yes
23. Design completed
24. No
25. Refinement of input data

Thus, a solution for which

$$Q^* = \min \left[Q = \sum_{i=1}^{\ell} b_i \overline{\overline{y_i}}(\alpha) \right], \quad \text{at}$$
$$\overline{\overline{y_i}}(\alpha) \leqslant \frac{1}{9} C_i, \quad i = \overline{g+1, r}, \quad \alpha \in M_\alpha. \qquad (5.9)$$

must be found with regard to the adopted alternatives of design of a control VEMP.

The elements of vector α are: the coefficients of inertia and the parameters of the flexible couplings of the electric drives, the parameters of the regulators, the cutoff frequencies and the coefficients of the ratio of adjacent frequencies of amplitude-frequency characteristics of the system, corresponding to the transfer functions of the given type for separate control systems. The value of α^*, which satisfies formula (5.9) and which establishes the basic version of the control system among the adopted alternatives of the structures and elements during the first step of design, the bandwidths of the separate systems, and the coefficients of inertia of the drive elements of the mechanism; it establishes the refined versions of the electromagnetic and mechanical subsystems during the second step of design; and it is establishes the parameters of the regulators of the separate systems and the estimates of the achievable indicators of the criterion of equality with regard to refined models of electromagnetic and mechanical subsystems during the third step. The problem of design is solved on a computer by nonlinear programming methods. Dynamic decomposition of the system is guaranteed at each level and in the entire system as a whole. The algorithm for design of a control VEMP is explained by a diagram (Figure 5.2).

5.2. Dynamic Characteristics of Electromechanical Subsystems

Dynamic models of electromechanical subsystems. Electric torque motors can be used in precision movement control systems. The known condition

188

of disregard of feedback according to the emf of the electric motors is almost always fulfilled in precision electric drives if there are no reduction gears and if there are large moments of inertia of the driving devices of the mechanisms [7]. The electric motor can be regarded as an electromagnetic moment shaping device, and its moving mechanical parts can be regarded as elements of a mechanical subsystem. This is even more valid if the electric motor is built into the mechanism.

There are no principal complexities in development of highly efficient DC and AC electric drives with the modern development of semiconductor technology and control devices. Selection of the type of electric drive is determined as a result of design of the control system as a whole with regard to its characteristic features. The problem of independent control of the electromagnetic moment and flux of the motor ordinarily arises upon control of DC and AC electric drives. This problem is easy to solve due to the design features of electric motors in DC electric drives. Electromagnetic subsystems of DC electric drives have been thoroughly studied and have been widely illuminated in the technical literature. AC electric drives occupy a different position. Despite the large number of papers on AC electric drives, they are considered in control systems with regard to surplus parts, which make it development of simple algorithms for control and design of electric control systems difficult. Advances in this problem, which have been noted during the past few years, determine the appearance of prerequisites on the use of those methods for design of AC electric drive control systems, which are used for DC electric drive control systems.

If there are no links with distributed parameters in explicit form in a multimass flexible mechanical subsystem, which is controlled by multimotor electric drives, the mechanical subsystem can be represented in the form of many elements with concentrated masses, connected to each other by massless flexible couplings. The main motion and oscillatory motions with respect to the main motion will be completed under the effect of several input variables of the VMP. Oscillations of the VMP are always attenuating due to the effect of the restoring forces of the system; therefore, mathematical description of the VMP should be carried out with regard to these forces. However, this can be done only for simple cases or after simplification of the initial model of the system. This is explained by the fact that the total mathematical model of the VMP may be complicated and access to it in problems of analysis and design of coupled control systems essentially becomes impossible. A detailed mathematical description of the VMP can initially be compiled without regard to damping forces, it can be simplified such that the dynamic properties of the system can be rather accurately reflected in the given frequency bands of separate subsystems, and the damping forces can then be taken into account in the simplified models.

Systems with distributed parameters can also be reduced to mechanical systems with concentrated parameters.

The following problems occur during study of VMP: 1) determination of the structure of the mechanical model of the VMP that guarantees optimal solution of the problem of control of the VEMP at m input and r output variables, and 2) analysis and design of a VMP, according to which those combinations of inertial stiffness and damping parameters are in the design stage, which would guarantee low intensities of the vibrations of the mechanism in given frequency bands of separate control subsystems.

Let us consider the more general version of a VMP, in which the individual elements of the system have several degrees of freedom. The differential equations that characterize the free vibrations of this VMP can be found from Lagrange equations:

$$
\begin{gathered}
\frac{d}{dt}\left(\frac{\partial T}{\partial \dot{q}_j}\right) - \frac{\partial T}{\partial q_j} = -\frac{\partial \Pi}{\partial q_j}; \\
T = \frac{1}{2}\sum_{i=1}^{k}\sum_{j=1}^{k} \mu_{ij}\dot{q}_i\dot{q}_j, \quad j, \, i = \overline{1, \, k}; \\
\Pi = \frac{1}{2}\sum_{i=1}^{k}\sum_{j=1}^{k} c_{ij}q_i q_j.
\end{gathered}
\tag{5.10}
$$

Multiplying out equation (5.10) with respect to T and Π results in a system of second-order linear homogeneous differential equations

$$
M\ddot{q} + Cq = 0,
\tag{5.11}
$$

where q is the k-vector of generalized coordinates M, C is the symmetrical quadratic k × k matrices of the coefficients of inertia and stiffness coefficients, respectively $(\mu_{ij} = \mu_{ji}, \; c_{ij} = c_{ji})$.

The structure of a mechanical model, which can subsequently be used to analyze and design the VMP, can be compiled from the differential equations found in this manner.

Substituting the partial solutions into equation (5.11), we find

$$
-\lambda M\bar{q}_0 + C\bar{q}_0 = 0,
$$

where q_0 is the k-vector of the relative amplitudes of free vibrations and $\lambda = \omega^2 y$. (Footnote) (Here and further the bar on top denotes the relative values)

190

Having rewritten this equation in the form

$$(M^{-1}C - \lambda I)\,\bar{q}_0 = 0, \qquad\qquad (5.12)$$

where I is a unit matrix, we can determine vector $\bar{q}_0$ as the eigenvector of matrix $M^{-1}C$, and we can determine λ as its eigenvalues.

Equation (5.12) can be written for many versions of mechanisms in simpler form

$$(G - \Lambda I)\,\bar{q}_0 = 0, \qquad\qquad (5.13)$$

where

$$G = M^{-1}C = \begin{bmatrix} c_{11}/\mu_{11} & c_{12}/\mu_{11} & \cdots & c_{1h}/\mu_{11} \\ c_{21}/\mu_{22} & c_{22}/\mu_{22} & \cdots & c_{2h}/\mu_{22} \\ \cdot & \cdot & \cdot & \cdot \\ \cdot & \cdot & \cdot & \cdot \\ \cdot & \cdot & \cdot & \cdot \\ c_{h1}/\mu_{hh} & c_{h2}/\mu_{hh} & & c_{hh}/\mu_{hh} \end{bmatrix} = $$

$$= \begin{bmatrix} c'_{11} & c'_{12} & \cdots & c'_{1k} \\ c'_{21} & c'_{22} & \cdots & c'_{2k} \\ \cdot & \cdot & & \cdot \\ \cdot & \cdot & & \cdot \\ \cdot & \cdot & & \cdot \\ c'_{k1} & c'_{k2} & \cdots & c'_{kk} \end{bmatrix}.$$

The eigenvalues λ_1, λ_2, ..., λ_k of matrix G determine the natural vibration frequencies of the mechanical subsystem $\omega_{y1} = \sqrt{\lambda_1}$, $\omega_{y2} = \sqrt{\lambda_2}$, ..., $\omega_{yk} = \sqrt{\lambda_k}$. Solution of equation (5.13) for each of the derived λ_r yields the eigenvectors of matrix G, of important significance in study of the dynamics of the VMP.

The ratio of the relative vibration amplitudes of the elements of a mechanical system is illustrated graphically in theoretical mechanics in the form of the types of vibrations. However, they do not yield a clear answer about the preferred affiliation of the vibration frequency of interest to one or another element of the VMP. This information can be found if the distribution of the relative values of the potential energy, stored in the flexible couplings $\bar{\Pi}_{ij\,(r)} = c_{ij}\,(\bar{q}_{0\,ir} - \bar{q}_{0\,jr})^2$, where

191

$\Pi_{ij(r)}$ is the relative value of the potential energy stored in the flexible link c_{ij} at $\lambda = \lambda_r$, and $\overline{q}_{0ir}$ and $\overline{q}_{0jr}$ are the relative vibration amplitudes of the i-th and j-th inertial links, is considered jointly with the forms of vibration for each ω_{vr}.

One can then establish the affiliation of each vibration frequency to elements of the VMP, which is important in problems of design upon variation of the inertial stiffness parameters to find given vibration frequencies.

The transfer matrix, which links the output and input variables, must be known for mathematical description of the mechanical system in the control system. This matrix can be determined either by the equation of state or directly by differential equations, compiled for the known structure of the mechanical model in the form

$$W(p) = \frac{1}{\det(p\mathbf{I} - \mathbf{A})} \mathbf{C} \, \mathrm{adj}\,(p\mathbf{I} - \mathbf{A})\, \mathbf{B}. \qquad (5.14)$$

The resolvent $(pI - A)^{-1}$ of matrix A can be determined if one writes:

$$\det(p\mathbf{I} - \mathbf{A}) = \Delta(p) = p^n + \alpha_1 p^{n-1} + \alpha_2 p^{n-2} + \cdots + \alpha_n;$$
$$\mathrm{adj}\,(p\mathbf{I} - \mathbf{A}) = \mathbf{P}(p) = \mathbf{I}p^{n-1} + \mathbf{P}_1 p^{n-2} + \cdots + \mathbf{P}_{n-1},$$

where $\Delta(p)$ is the characteristic polynomial of the system and P(p) is the reduced matrix.

Coefficients α_i and matrices P_i are calculated according to the Fadeyev-Leverier algorithm [75].

Having made the substitutions of $\Delta(p)$ and P(p) in expression (5.14), we find

$$W(p) = \Delta^{-1}(p) \sum_{i=0}^{n-1} \mathbf{M}_i p^{n-1-i},$$

where $\mathbf{M}_i = \mathbf{C}\mathbf{P}_i\mathbf{B}; \quad \mathbf{P}_0 = \mathbf{I}.$

The transfer matrix W(p) is a polynomial matrix whose elements are transfer functions $W_{js}(p)$ between the j-th output y_j and the s-m input u_s

192

$$W_{js}(p) = \Delta^{-1}(p) \sum_{i=0}^{n-1} C^{[j]} P_i B_{[s]},$$

where $C^{[j]}$ is the j-th row of matrix C and $B_{[s]}$ is the s-th column of matrix B.

The algorithms for calculation of the transfer functions for specific numerical values are realized on the computer.

Matrix A contains coefficients which can be determined from the system of equations written on the basis of equations (5.13) with regard to additional variables and adopted notations

$$A = \begin{bmatrix} 0 & | & I \\ \text{---} & | & \text{---} \\ -G & | & 0 \end{bmatrix}.$$

Matrix B is determined by the right side of equations (5.13) if they are written for induced motions of a specific mechanical system. Specifically, if one assumes that the generalized force (considered as an input variable) acts on each element of the mechanical system and if there are no moments of resistance, matrix B can be written in the following form:

$$B = \begin{bmatrix} 0 & | & 0 \\ \text{--} & | & \text{---} \\ 0 & | & B_{22} \end{bmatrix}, \text{ где } B_{22} = \begin{bmatrix} 1/\mu_{11} & 0 & \ldots & 0 \\ 0 & 1/\mu_{22} & \ldots & 0 \\ \cdot & \cdot & & \cdot \\ \cdot & \cdot & \cdot & \cdot \\ \cdot & \cdot & & \cdot \\ 0 & 0 & \ldots & 1/\mu_{hh} \end{bmatrix}.$$

Writing the transfer matrices in the form of (5.14) is more general. However, this can be done in analytical form only for the simplest cases. The calculations for specific numerical values of the elements of the matrices of the equation of state must primarily be made and transfer matrices with numerical values of the coefficients must be found, which causes difficulties in analysis and design of control systems with VMP.

Design of electromechanical subsystems. Problems of design of electromagnetic and mechanical subsystems can be formulated separately according to the tasks and the general algorithm for design of electromechanical subsystems.

193

The problem of design of an electromagnetic subsystem is formulated from the condition of finding the minimum dynamic errors of reproduction of control actions. Design of electromagnetic subsystems from this condition can most frequently be reduced to design of a controlled semiconductor transducer with given bandwidth of the control actions, since it is the constraints on this frequency band that are an obstable in realization of control circuits with given frequency bands that reproduce the range of control actions essentially without distortions.

The problem of designing flexible multimass mechanical subsystems is formulated from the condition of finding the given dynamic characteristics of the subsystems in the frequency bands essential for motion control systems.

The problem of design of a VMP is formulated from the results of design of electromechanical control systems from the condition of finding the given bandwidth of the system and, accordingly, of the minimal frequencies of elastic vibrations of the VMP.

The problem of determining the structure of the mechanical model of the VMP and of the inertial stiffness and damping parameters that guarantee low intensity of elastic vibrations of the mechanism within given frequency bands is solved for the initial design of the mechanism. According to this, the design parameters of the mechanism are refined.

The parameters of the VMP must generally be selected such that the spectrum of matrix G is in a given ratio with the bandwidth of the control system, while the relative amplitudes of the vibrations assume given values. It is sufficient during design of VMP to limit oneself in the makeup of the control system to the lower part of the spectrum and to consider two-three minimal values λ_r, which have the most influence on the dynamics of the control system. Assuming that, besides the vibration elements of the elements of the VMP, it can move as a unit whole and, accordingly, $\lambda_1 = 0$ and λ_2 will be the minimal value that characterizes the vibration motions of the VMP. The problem of design of the VMP will then reduce to synthesis of the values of the inertial stiffness parameters, at which:

$$\lambda_2 \geqslant \lambda_{2\text{ зад}}; \quad \lambda_3 \geqslant a_1 \lambda_2; \quad \lambda_4 \geqslant a_2 \lambda_3; \left.\right\}$$
$$\mu'_{ij} \leqslant \mu_{ij} \leqslant \mu''_{ij}; \quad c'_{ij} \leqslant c_{ij} \leqslant c''_{ij}, \left.\right\} \tag{5.15}$$

where a_1 and a_2 are the coefficients of the ratio of the eigenvalues of matrix G, and $\lambda_{2\text{ зад}}$ is the given eigenvalue established according to the minimum permissible for the control system of the elastic vibration frequency $\omega_{y2\text{ зад}} = \sqrt{\lambda_{2\text{ зад}}}$; μ'_{ij}, μ''_{ij}, c'_{ij}, c''_{ij} are the given range of variation of the coefficients.

194

Coefficients a_1 and a_2 can be selected on the basis of the two following conditions. The first condition is: the need to eliminate beating in the VMP, which occurs at similar values of the minimum free vibration frequencies. The spectrum of matrix G for this case is considered as having no bearing on the bandwidth of the control system. The second condition is: the need to guarantee the ratios $\lambda_3 \gg \lambda_2$; $\lambda_4 \gg \lambda_2$; $\lambda_4 = a\lambda_3$, with respect to λ_2, at which elastic vibrations at frequency ω_{y2} can be compensated by the control devices.

The problem of design of a VMP according to condition (5.15) can be expanded so that, besides synthesis of the given values of λ_r, the values of the relative free vibration amplitudes are also synthesized. Specifically, one can set up the condition

$$\bar{q}_{0jr} \to 0, \tag{5.16}$$

where $\bar{q}_{0jr}$ is the relative amplitude of the free vibrations of the j-th element of the VMP at r-th frequency, which results in partial reduction of the zeros and poles of the transfer functions and improves the dynamic properties of the properties of the VMP.

Problems of analysis and design of mechanisms, according to which combinations of inertial stiffness parameters that guarantee the operation of the mechanism outside the range of resonance vibrations are found in the design stage, are considered in machine-building theory [56, 68]. A widespread problem of design of mechanisms is that of separation of the resonant frequencies of the mechanism from the frequencies of the perturbations acting on it. Equations (5.11) fulfill the design of the mechanism for this purpose on the basis of variation of the coefficients of matrices M and C primarily by search methods in different modifications with the use of experiment planning methods and dispersion analysis of the natural vibration frequencies for all the variable coefficients. A large volume of studies must be carried out to obtain reliable information about the parameters to be synthesized from dispersion analysis. If one also considers the relative vibration amplitudes, besides the natural vibration frequencies, solution of the problem of design is complicated considerably.

Development of methods that permit direct solution of the problem of design and the search for forms of mathematical description of VMP, at which the relationships of the values of the natural frequencies and the relative amplitudes of free vibrations to the coefficients of differential equations are determined directly, becomes timely with regard to the foregoing.

The method of design of a VMP, which is based on transition from differential equations (5.11) in generalized coordinates to differential

equtions in principal coordinates, is convenient in postulation of the above problem [74]

$$M^* \ddot{\eta} + C^* \eta = 0, \qquad (5.17)$$

where $\eta = |\eta_1 \eta_2, ..., \eta_h|^T$ is the vector of the principal coordinates, $\eta = Q^{-1} q$, and $Q = [\bar{q}_{0jr}]$ is a matrix of the relative vibration amplitudes, and M* and C* are diagonal k × k matrices of the reduced coefficients of inertia and of the stiffness coefficients.

This approach is essentially decomposition at the level of the mathematical model of the VMP, since each principal coordinate performs only monoharmonic vibrational motion, described by the equation

$$\eta_j = \eta_{j0} \sin (\omega_{yj} t + \Theta),$$

where η_{j0} is the vibration amplitude of the j-th principal coordinate.

Since matrices M* and C* are diagonal, the eigenvalues of the matrix are found by the formula $\lambda_r = c_{ii}^* / \mu_{ii}^*$, $r = i$.

The elements of diagonal matrices M* and C* are determined from the equations:

$$\mu_{ii}^* = \sum_{i=1}^{k} \sum_{j=1}^{k} \mu_{ij} \bar{q}_{0il} \bar{q}_{0jl}; \qquad (5.18)$$

$$c_{ii}^* = \sum_{i=1}^{k} \sum_{j=1}^{k} c_{ij} \bar{q}_{0il} \bar{q}_{0jl}. \qquad (5.19)$$

Moreover, the parameters of the VMP are related to the condition of orthogonality of the principal coordinates, which are written in the form:

$$\sum_{i=1}^{k} \sum_{j=1}^{k} \mu_{ij} \bar{q}_{0il} \bar{q}_{0jl} = 0, \quad l, l = \overline{1, k}; \ l \neq l; \qquad (5.20)$$

$$\sum_{i=1}^{k} \sum_{j=1}^{k} c_{ij} \bar{q}_{0il} \bar{q}_{0jl} = 0, \quad l, l = \overline{1, k}; \ l \neq l. \qquad (5.21)$$

196

A mathematical description of the VMP can be compiled on the basis of equations (5.18)-(5.21) for solution of the problem of design by conditions (5.15) and (5.16). This can be done in the form of normalized equations, having taken as the basic values the coefficients of μ_6 and c_6. Turning to the relative coefficients and having made the transformations, we find

$$
\left.
\begin{aligned}
&\sum_{i=1}^{k}\sum_{j=1}^{k} \bar{\mu}_{ij}\bar{q}_{0il}\bar{q}_{0jl} - \bar{\mu}_{ll}^{*} = 0; \\
&\sum_{i=1}^{k}\sum_{j=1}^{k} \bar{c}_{ij}\bar{q}_{0il}\bar{q}_{0jl} - \bar{c}_{ll}^{*} = 0; \\
&\sum_{i=1}^{k}\sum_{j=1}^{k} \bar{\mu}_{ij}\bar{q}_{0il}\bar{q}_{0jf} = 0; \quad l, f = \overline{1, k}, \; l \neq f; \\
&\sum_{i=1}^{k}\sum_{j=1}^{k} \bar{c}_{ij}\bar{q}_{0il}\bar{q}_{0jf} = 0; \quad l, f = \overline{1, k}, \; l \neq f; \\
&(\mu_{li}^{*}/\bar{c}_6)\lambda_i - \bar{c}_{li}^{*} = 0;
\end{aligned}
\right\}
\tag{5.22}
$$

$$
\left.
\begin{aligned}
&\bar{\mu}_{ij}^{'} \leqslant \bar{\mu}_{ij} \leqslant \mu_{ij}^{''}; \\
&c_{ij}^{'} \leqslant c_{ij} \leqslant c_{ij}^{''}; \\
&\lambda_2 \geqslant \lambda_{2\text{зад}}; \\
&\lambda_r \geqslant a_{r-2}\lambda_{r-1}; \quad r = 3, 4; \\
&\bar{q}_{0jr} \leqslant \varepsilon_{hj},
\end{aligned}
\right\}
\tag{5.23}
$$

where ε_{kj} is a small value, distinct from zero and which determines the boundary in values $\bar{q}_{0jr}$ upon its approach to zero and which determines the significance of the system of equations with respect to $\bar{q}_{0jr}$.

Solution of system of nonlinear equations (5.22), which satisfy inequalities (5.23), is possible by nonlinear programming methods with constraints oriented toward the use of a computer. Having denoted the square of the left side of the s-th equation of system (5.22) as

$f_{cs}, s = \overline{1, m}$ and having used the method of penalty functions to solve the nonlinear programming problem with constraints [78], let us write the specific function in the form

$$
F_{\text{п}} = \sum_{s=1}^{m} f_{cs} + \sum_{g=1}^{h} f_{\text{ш}g},
\tag{5.24}
$$

where $f_{\text{ш}g}$ is the penalty function with respect to the g-th variable parameter, introduced as a constraint function, and h is the number of variable parameters.

The penalty function for each variable parameter b_g, which is the coefficient of inertia or stiffness and which has constraints in the form of inequalities $b_g' \leqslant b_g \leqslant b_g''$, can be formed from the condition

$$
\begin{aligned}
f_{\text{ш}g} &= 0, \text{ at } \quad |\Delta b_g' - \Delta b_g(k)| < \Delta b_g'; \\
f_{\text{ш}g} &= r_{\text{ш}g} [\Delta b_g(k)]^2, \text{ if } \quad |\Delta b_g' - \Delta b_g(k)| \geqslant \Delta b_g',
\end{aligned} \right\}
\tag{5.25}
$$

where $\Delta b_g(k) = |b_g(k) - b_{g0}|$; $\Delta b_g' = b_g'' - b_{g0}$; $b_g(k)$ is the value of the variable parameter on the k-th variation step, b_{g0} is the mean variable parameter, $b_{g0} = 0.5(b_g' + b_g'')$ and $r_{\text{ш}g}$ is a weight coefficient.

The initial vector of variable parameters $b_{\text{нач}}$ is determined by given VMP, corresponding to the initial design of the mechanism. The design algorithm is based on the iteration procedure of maximizing the value of λ_2 within condition (5.15). The specific function $F_{\text{п}}$ is minimized at each iteration step. Situations may arise at which condition (5.15) is not satisfied due to the small boundaries of the variable parameters. Condition (5.15) then essentially reduces to the condition:

$$
\begin{aligned}
\lambda_2 &= \lambda_{2\max}; \quad \lambda_3 \geqslant a_1 \lambda_2; \quad \lambda_4 \geqslant a_2 \lambda_3; \\
\mu_{ij}' &\leqslant \mu_{ij} \leqslant \mu_{ij}''; \quad c_{ij}' \leqslant c_{ij} \leqslant c_{ij}''.
\end{aligned} \right\}
\tag{5.26}
$$

Otherwise, the design for $\lambda_2 = \lambda_{2\text{зад}}$ with expansion of the boundaries of the variable parameters can be carried out. The design algorithm of the VMP is based on iteration procedures of maximization of λ_2 up to values of $\lambda_{2\text{зад}}$ with an estimate of sensitivity $\partial\lambda_2(k)/\partial b_g(k)$ and on sequential expansion of the boundaries of the parameters by which the estimates of sensitivity are maximum.

The outlined method of design is easily used in design problems of multimass mechanical subsystems, contained in electromechanical control systems. All the correlations of the variables are clearly determined to the maximum extent when it is used and the physical interpretation of the intermediate and final results of design is maintained.
Difficulties of using the method may arise at large size of the VMP due to the increase of the number of nonlinear equations. These difficulties can be overcome by simplification of a complex VMP. To do this, one can use the known methods or, using the description of the VMP

198

in the principal coordinates (as in the problem fo design), it can be simplified by solving a system of nonlinear equations of smaller dimension with retention of the low spectrum of free vibration frequencies.

5.3. Electromechanical Subsystems Based on Two-Channel Precision Electric Drives

Increase of electric drive accuracy and of their functional capabilities by creation of two-channel control. A characteristic feature of image stabilization systems is the need to achieve low motion speeds of the optical elements with high dynamic accuracies. These motions are realized most successfully in two-channel electric drive systems.

Papers [29, 53, 55, 71] are devoted to study of two-channel motion control systems. Precise motions are guaranteed in these systems in differential circuits for connection of electric drives with combination, iterative, or hierarchical control structure. A qualitative survey of two-channel (multichannel) systems is given in [29].

Let us consider the operating principles and dynamic models of two-channel phase electric drive systems, which form angular and linear precision motions of mechanisms. The characteristic feature of these systems is that, besides helical gears to form linear displacements, different mechanical gears are eliminated in them, in the presence of which the accuracy indicators of the drives are considerably deteriorated due to the appearance of elastic vibrations of the gear elements. And this results in limitation of the bandwidths of the control systems. Kinematic errors, studies of which have been extensively outlined in the technical literature, for example, in [67], are reflected in the dynamics of electric drives. The noted factors have considerably less manifestation in screw gears. Thus, studies of many of the most diverse mechanisms of linear displacements--hydraulic, pneumatic, piezoelectric, levers, screw and other hybrid systems--are presented in [22]. The greatest accuracies were achieved in a drive with a planetary roller screw.

According to the foregoing, two-channel control can be developed with respect to image stabilization systems using combination information systems, on the basis of which phase control is achieved.

Two-channel phase control is achieved in the simplest version when using rough and precise channels. The signals can be added both in the moving moment (force) formation assembly and directly by the coordinates of motion. Specifically, one can use control systems with separation of channels by speed through the use of low- and high-frequency filters and also level restrictions of signals. (Footnote) (USSR inventor's certificate 779,772) These systems can be regarded as quasi-autonomous in study of the dynamics. Design of systems according to integrated quadratic criteria of quality essentially reduces to design of a precise

199

channel, while the course channel is regarded as a source of perturbations for the precise channel. Ball-and-screw gears together with piezoelectric transducers or electromechanical transducers are used as the coordinate summation assemblies of the electric drive system.

A different principle of organizing phase systems is used when two-channel connection of electric drives is carried out with given initial rotational frequency--the carrier frequency ω_0. (Footnote) (USSR inventor's certificate 635,587, USSR inventor's certificate 1,035,762) Both channels of this system are precision. Selection of frequency ω_0 is determined by the characteristics of the information channels and drives and guarantees minimal dynamic errors in control of the output coordinate. Variations of ω_0 essentially correspond to variation of the noise spectra of the information system and of load perturbations in the master channel. The values of ω_0 are determined upon dynamic design of the control system together with other parameters that guarantee that given accuracy will be reached.
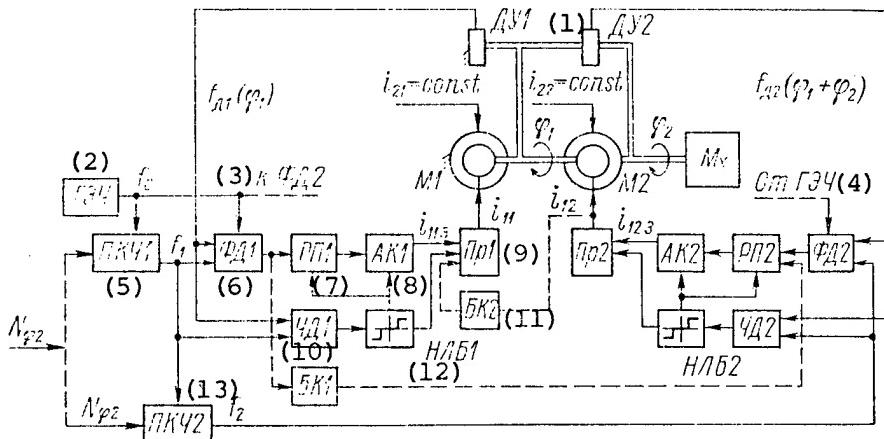
Figure 5.3. Functional Diagram of Two-Channel
Electric Drive for Angular Displacements

KEY:

1.	Angle-data transmitter	7.	Position regulator
2.	Reference frequency generator	8.	Analog keys
		9.	Current converter
3.	To phase discriminator	10.	Frequency discriminator
4.	From reference frequency generator	11.	Correction module
		12.	Nonlinear logic module
5.	Code-frequency converter	13.	Code-frequency converter
6.	Phase discriminator		

Two-channel control of precision angular and linear motions of actuating devices. A two-channel electric drive for angular precision motions is made by using DC or AC motors. This is of no principal significance for

200

development of an object motion control system. The difference is only in the structure of the electromagnetic circuits of the separate control systems. The structure of the mechanical part is made so that the rotor of one engine, the stator of which, making free motions in additional supports, is connected to the mechanism, is rigidly connected to the rotor of the other engine, the stator of which is connected to the base (Figure 5.3). The electric motors are controlled so that one of them operates in the motor mode while the other operates in the braking mode (in the recuperative braking mode). The mathematical description of the operating modes of electric motors is established directly from the equation of the balance of power. The system of equations of dynamics is written in the following form for this two-motor electric drive as a control object:

$$
\begin{bmatrix} \dot{\varphi}_1 \\ \dot{\omega}_1 \\ \dot{i}_{11} \\ \dot{i}_{12} \\ \dot{\omega}_2 \\ \dot{\varphi}_2 \end{bmatrix}
=
\begin{bmatrix}
0 & 1 & 0 & 0 & 0 & 0 \\
0 & 0 & \dfrac{c_{д1}}{J_{\Sigma1}} & \dfrac{c_{д2}}{J_{\Sigma2}} & 0 & 0 \\
0 & -\dfrac{c_{д1}}{L_{я1}} & -\dfrac{R_1}{L_{я1}} & 0 & 0 & 0 \\
0 & -\dfrac{c_{д2}}{L_{я2}} & 0 & -\dfrac{R_2}{L_{я2}} & -\dfrac{c_{д2}}{L_{я2}} & 0 \\
0 & 0 & 0 & \dfrac{c_{д2}}{J_{\Sigma2}} & 0 & 0 \\
0 & 0 & 0 & 0 & 1 & 0
\end{bmatrix}
\times
$$

$$
\times
\begin{bmatrix} \varphi_1 \\ \omega_1 \\ i_{11} \\ i_{12} \\ \omega_2 \\ \varphi_2 \end{bmatrix}
+
\begin{bmatrix}
0 & 0 \\
0 & 0 \\
\dfrac{1}{L_{я1}} & 0 \\
0 & \dfrac{1}{L_{я2}} \\
0 & 0 \\
0 & 0
\end{bmatrix}
\begin{bmatrix} e_1 \\ e_2 \end{bmatrix}
+
\begin{bmatrix}
0 & 0 \\
-\dfrac{1}{J_{\Sigma1}} & 0 \\
0 & 0 \\
0 & 0 \\
0 & -\dfrac{1}{J_{\Sigma2}} \\
0 & 0
\end{bmatrix}
\begin{bmatrix} M_{c1} \\ M_{c2} \end{bmatrix}.
$$

Here we have for electric motors M1 and M2, respectively: i_{11} and i_{12} are currents that determine the electromagnetic moments, M_{c1} and M_{c2} are moments of resistance, e_1 and e_2 are electromotive forces of control transducers, $L_{я1}$ and $L_{я2}$ are inductances, R_1 and R_2 are the active resistance, $c_{д1}$ and $c_{д2}$ are DC electric motors, $J_{я1}$, $J_{я2}$, $J_{ст}$, $J_{м}$ are moments of inertia of the armatures, free stator, and mechanism, and

$$J_{я1} + J_{я2} = J_{\Sigma1}, \quad \text{and} \quad J_{ст} + J_{м} = J_{\Sigma2}.$$

The positive feature of the considered system is that the mechanism can move smoothly even at superlow speeds w_2 due to the fact that the inner races of the bearing seats will rotate at given frequency w_0, at which the nonlinearities of dry friction inherent to low-speed mechanical systems will be manifested in the seats. The complexity in measuring the low speeds of precision motions of the mechanism is overcome by measuring the individual current values of angular displacements φ_1 and the sum of displacements $\varphi_1 + \varphi_2$. This is achieved by using a combination angle-data transmitter, which permits one to check the low rotational frequencies w_2 (up to zero values). (Footnote) (USSR inventor's certificate 635,587)

Development of a two-channel control system is based on the use of separate phase control systems with variable structure. Cross-couplings through the correction modules BK1 and BK2 of the control system, determined by the developed principle of its organization, appear in addition to the natural cross feedback of the electric drive system (Figure 5.3). A two-channel electric drive with mechanism Mx can be controlled on the principle of subordinate control. Using high-speed current regulation circuits i_{11} and i_{12} with pulse width converters at frequency of 10-15 kHz, one can consider that the closed current control circuits are inertialless and one can take them into account in the form of coefficients k_1 and k_2 of current transducers Pr_1 and Pr_2.

The phase systems contain angle-data transmitters DU1 and DU2, phase discriminators FD1 and FD2, position regulators RP1 and RP2, frequency discriminators ChD1 and ChD2, nonlinear logic modules NLB1 and NLB2, code-frequency converters PKCh1 and PKCh2, and analog keys AK1 and AK2, which switch the control channel structures from frequency discriminators to phase discriminators. The source of the reference frequency is a reference frequency generator GECh. The master signal for the control system is delivered in the form of a code N_{φ_2}.

Let us consider the possibility of controlling a two-motor electric drive without resorting to cross correcting couplings with PID position regulators in separate systems, which corresponds to control of the vector of state for an expanded object provided there is quasi-autonomy of separate systems.

Having written the equations of a closed system in the form:

$$\dot{x} = Ax + By + Df, \quad y = Cx$$

and going to the equation with transfer matrices, we find the equation with respect to the output, master and perturbing coordinates

202

$$
\begin{bmatrix} \varphi_1 \\ \varphi_2 \end{bmatrix} = [1 + W_3(p)]^{-1} \left\{ \begin{bmatrix} W_{\varphi_1}(p) & W_3(p) \\ -W_{\varphi_1}(p) W_{\varphi_2}(p) & W_{\varphi_2}(p) \end{bmatrix} \begin{bmatrix} \varphi_{13} \\ (\varphi_1 + \varphi_2)_3 \end{bmatrix} + \right.
$$

$$
\left. + \begin{bmatrix} -\dfrac{W_{\varphi_1}(p)}{W_1(p)} & \left(\dfrac{W_3(p)}{W_2(p)} - \dfrac{W_{\varphi_1}(p)}{W_1(p)} \right) \\ \dfrac{W_{\varphi_1}(p) W_{\varphi_2}(p)}{W_1(p)} & W_{\varphi_2}(p) \left(\dfrac{1}{W_2(p)} + \dfrac{W_{\varphi_1}(p)}{W_1(p)} \right) \end{bmatrix} \begin{bmatrix} M_{c1} \\ M_{c2} \end{bmatrix} \right\} ,
$$

<div align="right">(5.27)</div>

where $W_{\varphi_1}(p)$, $W_{\varphi_2}(p)$ are transfer functions of closed separate systems, considered as autonomous, $W_1(p)$ and $W_2(p)$ are transfer functions of parts of open separate systems from the input to the point of application of the perturbations, and $W_3(p) = W_{\varphi_1}(p) W_{\varphi_2}(p) W_1^{-1}(p) J_{\Sigma 2} p^2$.

Let us find the following relations for the first and second transfer matrices, respectively, of equation (5.27) to determine the conditions of diagonal dominance of the transfer matrices of the control system:

$$
\frac{|W_{11}(j\omega)|}{|W_{12}(j\omega)|} = \frac{J_{\Sigma 1}}{J_{\Sigma 2}} \frac{|W_{\varphi_1 \mathrm{p}3}(j\omega)|}{|W_{\varphi_2}(j\omega)|} ;
$$

$$
\frac{|W_{22}(j\omega)|}{|W_{21}(j\omega)|} = -\frac{1}{|W_{\varphi_1}(j\omega)|} ;
$$

$$
\frac{|W'_{11}(j\omega)|}{|W'_{12}(j\omega)|} = \left\{ - \left| \frac{W_3(j\omega) W_1(j\omega)}{W_{\varphi_1}(j\omega) W_2(j\omega)} \right| + 1 \right\}^{-1} ;
$$

$$
\frac{|W'_{22}(j\omega)|}{|W'_{21}(j\omega)|} = \left| \frac{W_1(j\omega)}{W_{\varphi_1}(j\omega) W_2(j\omega)} \right| + 1 .
$$

It follows from analysis of the first two relations that: 1) the independence of coordinate φ_1 on φ_2 is possible provided that $J_{\Sigma 1} \gg J_{\Sigma 2}$ or $\omega_{c1} \gg \omega_{c2}$, but the first inequality in precision systems is realized by an artificial increase of $J_{\Sigma 1}$, while the second results in the need to coarsen the second separate system, which contradicts the purposes of precision control of the mechanism; 2) the independence of coordinate φ_2 on φ_1 may not be realized by the parametric method due to the adopted method of developing the structure of the second separate system.

One can make similar conclusions on the basis of analyzing the second two relations. Thus, the condition of decomposition of separate systems may not be guaranteed purely parametrically in a closed system.

The presence of correlations results in an increase of the dynamic errors and of the vibration in the system, dependent on the ratio of the

total moments of inertia $J_{\Sigma1}$ and $J_{\Sigma2}$ and the speed of the control channels.
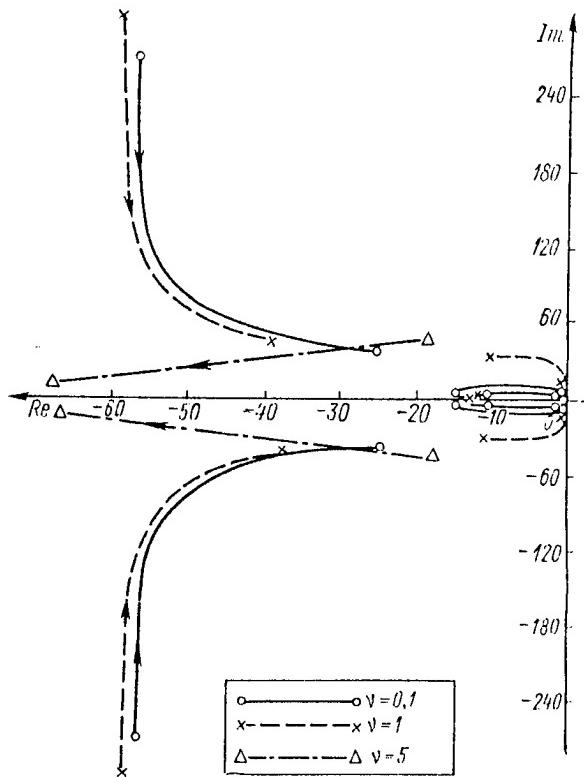
Figure 5.4.   Root Hodograph of Two-Channel Control System

The foregoing is illustrated by a root hodograph (Figure 5.4), plotted for the roots of the characteristic polynomial of a two-channel control system for different values of relative cutoff frequency $\nu_c = \omega_{c1}/\omega_{c2}$ (frequencies ω_{c1} and ω_{c2} correspond to separate systems, considered as autonomous) and of the relative coefficients of inertia $k_J = J_{\Sigma1}/J_{\Sigma2}$.

The hodograph is calculated according to the normalized signal graph of the control system (Figure 5.5). The notations of the transfer functions in Figure 5.5 correspond to the functional diagram presented in Figure 5.3. The hodograph reflects the motion of roots having minimal values and having the greatest influence on the dynamics of the system. The dependence of the mean square estimates of deviations of coordinates $\bar{\sigma}_{\varphi_1}^{(\varphi_1+\varphi_2)_3}$, $\bar{\sigma}_{\varphi_2}^{M_{c2}}$ on coefficient k_J at stepped changes of $(\psi_1 + \psi_2)_3$ and M_{c2}, calculated in the form of ratios to similar errors in the second separate system provided it is autonomous, corresponding to this hodograph, is shown in Figure 5.6, a and b.

204
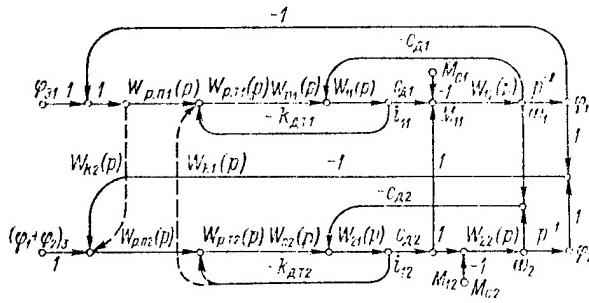
Figure 5.5. Normalized Signal Graph of Two-Channel
Control System

The given functions permit one to obtain estimates of the dynamic
characteristics of a two-channel control system for specific values of
the parameters of separate systems.
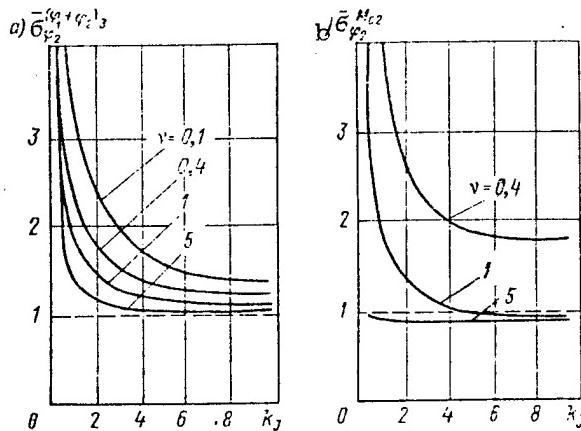
Figure 5.6. Dependence of Mean Square Estimates of
Deviations of Coordinates of Two-Channel System:
a--for master action; b--for perturbing action

Correcting cross couplings can be used to expand the bandwidth of the
second separate system according to the characteristic features of
developing the control system. Having written the transfer matrices of
a closed system with regard to transfer functions $W_{K1}(p)$ and $W_{K2}(p)$ of

these couplings and having assumed that the elements equal to zero are
nondiagonal, the form and values of $W_{K1}(p)$ and $W_{K2}(p)$ are determined.

The cross-couplings have single coefficients, i.e., $W_{K1}(p) = W_{K2}(p) = 1$,

if the transfer coefficients of the phase discriminators and current

sensors are equal. Technically, these correcting couplings are formed by high-frequency filters $W_{\phi}(p) = \tau p/(\tau p + 1)$, where $\tau \ll \omega_{c1}^{-1} \approx \omega_{c2}^{-1}$, from the output of the phase discriminator of the first channel to the input of the position regulator of the second channel and from the output of the current converter of the second channel to the input of the current converter of the first channel. Design of a such a two-channel system reduces to design of quasi-autonomous separate phase systems.

Enhanced sensitivity of the systems to variations of the parameters of cross couplings is observed when using cross correcting couplings in correlated control systems, it is important to determine the functions of relative sensitivities:

$$S^{W_{\varphi_2(\varphi_1+\varphi_2)_3}}_{W_{h1}}(p) = \frac{\partial \ln W_{\varphi_2(\varphi_1+\varphi_2)_3}(p,\,q)}{\partial \ln W_{h1}(p,\,q)};$$

$$S^{W_{\varphi_2(\varphi_1+\varphi_2)_3}}_{W_{h2}}(p) = \frac{\partial \ln W_{\varphi_2(\varphi_1+\varphi_2)_3}(p,\,q)}{\partial \ln W_{h2}(p,\,q)};$$

$$S^{W_{\varphi_2 M_{c2}}}_{W_{h1}}(p) = \frac{\partial \ln W_{\varphi_2 M_{c2}}(p,\,q)}{\partial \ln W_{h1}(p,\,q)};$$

$$S^{W_{\varphi_2 M_{c2}}}_{W_{h2}}(p) = \frac{\partial \ln W_{\varphi_2 M_{c2}}(p,\,q)}{\partial \ln W_{h2}(p,\,q)},$$

where   are transfer functions that link coordinate φ_2 to coordinates $(\varphi_1 + \varphi_2)_3$ and M_{c2}. $W_{\varphi_2(\varphi_1+\varphi_2)_3}(p,q)$, $W_{\varphi_2 M_{c2}}(p,\,q)$

These sensitivity functions for $\nu_c = 1$ and $k_J = 0.1$, calculated by the normalized graph of the system on a computer system, are shown in Figure 5.7. It follows from analysis of the functions that the system is more sensitive to variation of the cross-coupling parameters for transfer functions according to a given effect. Accordingly, measures must be adopted to reduce the sensitivity for precision systems, in which the intensity of measurement noise is significant compared to that of the perturbing actions. The use of adaptive control, at which the considered system is invariant to variation of the cross-coupling parameters, is effective.

A two-channel electric drive control system for linear displacements can be made similar to a two-channel electric drive system for angular displacements (Figure 5.8). The screw and nut of a screw gear (VP) of this system perform joint rotation. Linear perturbations of the mechanism are determined by the difference of the rotational frequencies of the electric motors and by coefficient $k_{\text{вп}} = v/(\omega_1 - \omega_2)$.

206
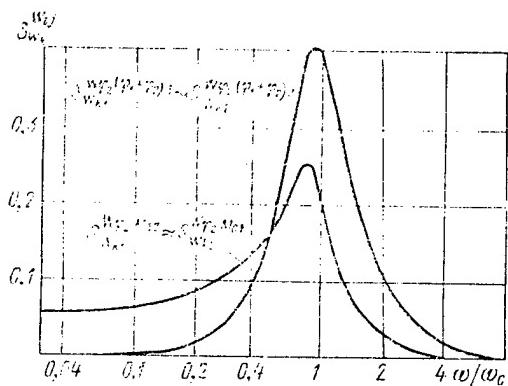
Figure 5.7. Function of Relative
Sensitivity of System
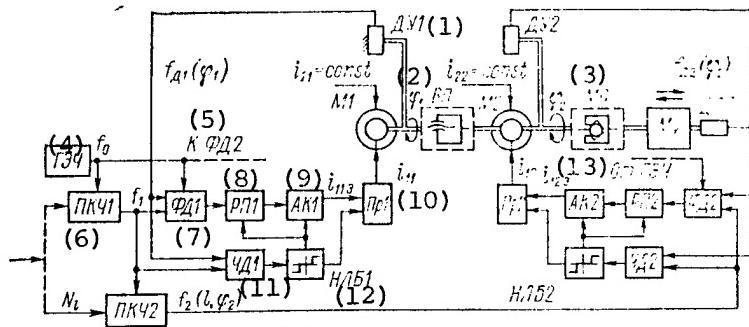
Figure 5.8. Functional Diagram of Two-Channel Electric
Drive for Linear Displacements

KEY:

1. Angle-data transmitter
2. Screw gear
3. Not further identified
4. Reference frequency
   generator
5. To phase discriminator
6. Code-frequency converter

7. Phase discriminator
8. Position regulator
9. Analog key
10. Current converter
11. Frequency discriminator
12. Nonlinear logic module
13. From reference frequency
    generator

An electric drive control system is made in the form of two separate
phase systems, containing internal current control circuits (current
converters). Without dwelling on analysis of the transfer matrices of
the equations of dynamics of a closed system, we note that the diagonal
dominance of the matrices is guaranteed provided that

207

$$\left| \frac{J_{_9}^2}{J_{_{\Sigma 1}} J_{_{\Sigma 2}}} [(1 + W_{_{\varphi_1 \text{раз}}}(j\omega))(1 + W_{_{\varphi_2 \text{раз}}}(j\omega))]^{-1} \right| \ll 1.$$

And this condition is guaranteed at ratios $J_{_9} \ll J_{_{я1}}$ and $J_{_9} \ll J_{_{я2}}$, which are almost always fulfilled in electric drives with screw gear due to the large values of their transfer coefficients $k_{_{вп}}$. Design of such a two-channel system reduces to design of quasi-autonomous separate phase systems. Known methods, for example, presented in [7] can be used for this.

6.1. Design Principles of Automatic Image Stabilization Systems for Information on Spatial Displacements of Moving Bases

General characteristic of displacement control devices of optical elements for image stabilization. Two variants of controlling the displacements of optical system components in inertial space are encountered in image stabilization problems: stabilization of these components or displacement with respect to fixed axes according to a given law.
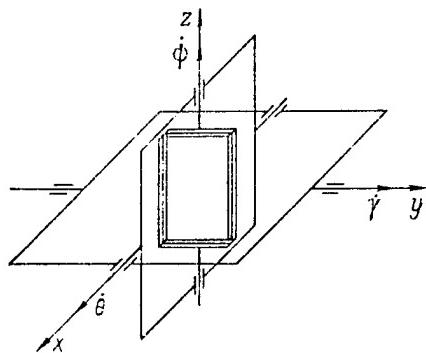
Figure 6.1. Layout of Three-Axis Gimbal Suspension of Stabilized Platform

The simplest method of solving the problem of stabilization is attachment of the entire optical instrument to a three-axis stabilized platform. A three-axis suspension of a platform is shown in Figure 6.1, while the order of rotation of the axes of the platform with respect to a fixed coordinate system is shown in Figure 6.2.

Projections of the angular velocities onto the axes of the platform can be found from the expressions:

$$\dot{\psi} = \frac{1}{\cos\Theta}\,(\Omega_x \sin\gamma - \Omega_z \cos\gamma);$$

$$\dot{\Theta} = -\Omega_x \cos\gamma - \Omega_z \sin\gamma;$$

$$\dot{\gamma} = -\Omega_x \sin\gamma\,\text{tg}\,\Theta - \Omega_y + \Omega_z \cos\gamma\,\text{tg}\,\Theta,$$

$$(6.1)$$

where Ω_x, Ω_y, and Ω_z are projections of the angular velocity of the base onto the axes of fixed coordinate system $O\xi\eta\zeta$, i.e., onto the axes of the platform, and ψ, Θ, and γ are the yaw, pitch, and bank angles of the base.

Expressions (6.1) degenerate at small angles of deflection of the base

$$\left.\begin{aligned} \dot{\psi} &= -\Omega_z; \\ \dot{\Theta} &= -\Omega_x; \\ \dot{\gamma} &= -\Omega_y. \end{aligned}\right\}$$

(6.2)

It is obvious that the design of the suspension is complicated considerably and the overall dimensions and mass of the device increase at significant dimensions of the optical instrument.
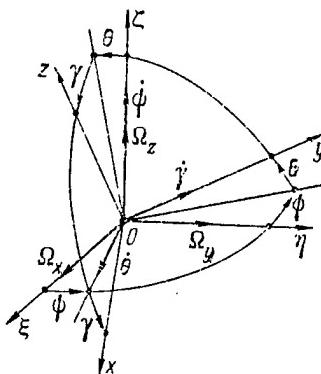
Figure 6.2.   Coordinate System of Platform

Image stabilization systems based on spatial orientation of entire instrument or of its individual components. The arrangement of an optical instrument on a platform, stabilized in inertial space (SP), is the most radical means of image stabilization. Stabilization systems are distinguished from each other in this case by the design version of the suspension, by the characteristics of arrangement of the sensors and by organization of the control channels. Let us consider the general design principles of these systems, using as an example a control system with three-axis gyroscopic sensors.

Drives M1, M2, and M3 are mounted on the suspension axes to displace or stabilize the outer (NK) and inner (VK) races in space (Figure 6.3). The control signals are fed to the drives from gyrosensors G1 and G2. The suspension axes of the gyrosensors are rationally oriented parallel to the axes of the stabilized platform (Figure 6.3). The signals from the angle-data transmitters of the gyroscope DUG1 and DUG3 of gyroscope

G1 can be used without preliminary conversion as the master signals to the inputs of control modules BU1 and BU2. Two position follow-up systems are formed in the space of the suspension races NK and VK of the stabilized platform with angle-data transmitters DU1 and DU3 in the feedback.

If gyroscope G2 is mounted on a base, the signal from the output of angle-data transmitter DUG2 should be converted in the coordinate converter PK according to expressions (6.1).
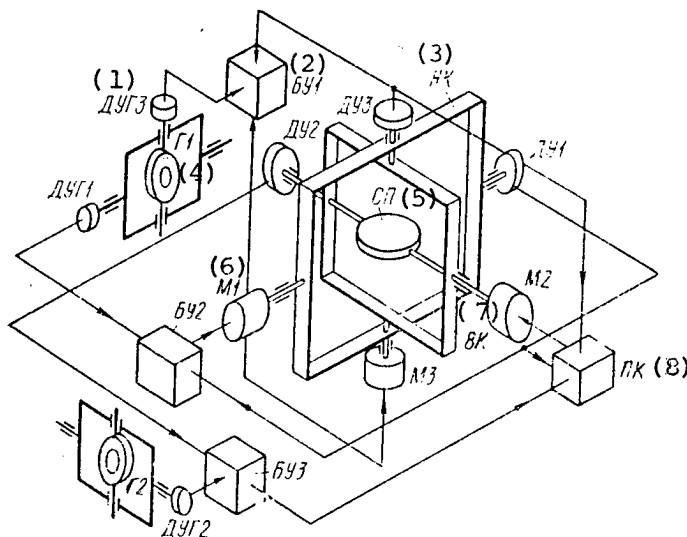
Figure 6.3. Layout of Three-Axis Gyro-Stabilized Platform

KEY:

1.	Angle-data sensor of gyroscope	5.	Inertial space-stabilized platform
2.	Control module	6.	Drive
3.	Outer race	7.	Inner race
4.	Gyroscope	8.	Coordinate converter

The signal from the output of the coordinate converter is used as a master to the control system of the third axis of the platform, formed by control module BU3, angle-data transmitter DU2, and by motor M2. The output signals of the gyrosystems mounted on the moving base for other purposes (for example, for control or orientation of the base), can be used instead of specially mounted gyro units. This circumstance simplifies considerably the device as a whole.

Obvious disadvantages of these stabilized platforms are the large overall dimensions and mass of the device. Moreover, it is difficult to provide sufficiently high stiffness of the structural elements of the suspension (especially with large dimensions of the optical instrument),

which reduces the accuracy capabilities of the drives. The dynamic range of the permissible input signals of the gyro units should exceed that of the possible variations of the displacement parameters of the base in the case under consideration. Under these conditions, the accuracy of the gyro units and of the device is comparatively low. Mounting the gyro units directly on the stabilized platform permits one to eliminate this deficiency. The range of the deflection angle of the sensitive element of the gyro units in this design may not exceed several degrees. Most classical gyro stabilizers (power and indicating) are designed in this manner. An extensive special literature, for example, [10, 63], is devoted to analysis and design of these instruments. Some characteristic features of using gyro stabilizers in image stabilization systems will be considered below.

The mass and size characteristics of an optical instrument with stabilized image field can be improved considerably, if one or several image shift compensators are used. These compensators can be designed on the basis of a one-axis gyro stabilizer. The sensitive element can be mounted on a moving element of the compensator, if this element is stabilized in space.
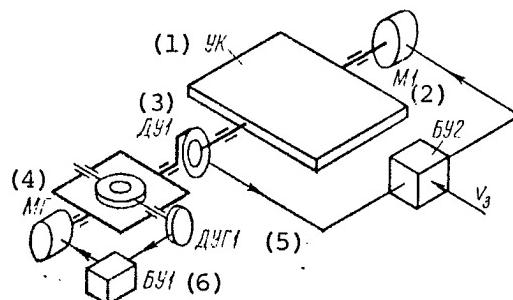
Figure 6.4. Layout of One-Axis Gyro-Stabilized Platform

KEY:

1. Compensator assembly
2. Motor
3. Angle-data transmitterilized
4. Relief motor
5. Angle-data transmitter of gyroscope
6. Control module

The moving element of the compensator should sometimes be displaced in space according to a specific law (for example, for reflecting compensators). This displacement can be easily realized in the design shown in Figure 6.4. The stabilized element is the stator of angle-data transmitter DU1 on the axis of the moving element of the compensator. The comparative smallness of the moment of inertia of the stabilized assembly permits one to achieve high stabilization accuracies in the circuit, formed by the gyroscopic angle-data transmitter DUG1, control module BU1 and relief motor MG. The motion of the moving assembly of

the compensator assembly UK in inertial space will be fully determined
by being given signal v_3 to the control circuit, which includes DU1,
control module BU2, and electric motor M1.

Let us consider versions of realizing this system. A functional diagram
of the stabilization system for one axis is presented in Figure 6.5.
Electric motors M1 and M2 set into rotation the rotors of pulsed angular
misalignment photosensors ID1 and ID2. The stators of ID1 are attached
to the base and to the gyro-stabilized platform (GSP). The stators of
ID2 are attached to the GSP and to the stabilized element (SE). The
gyro-stabilized platform has power drive along the stabilization axis
from electric motor M3, while the stabilized element has power drive
from electric motor M4. The power drive of the GSP is controlled from
gyroscope GP through control module BU3.
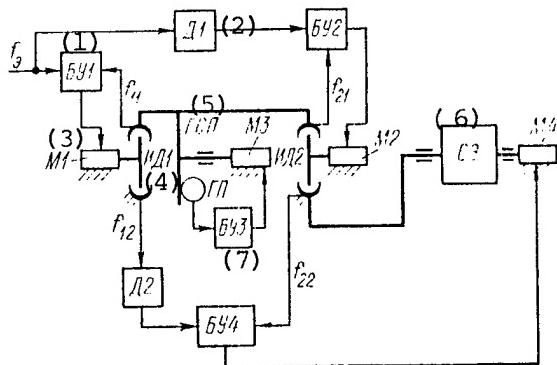
Figure 6.5. Functional Diagram of Position Control
System of Element to be Stabilized

KEY:
1. Control module
2. Frequency divider
3. Electric motor
4. Pulsed photosensor
5. Gyro-stabilized platform
6. Element to be stabilized
7. Gyroscope

The reference frequency f_3 in modules BU1 and BU2 is compared to signal
frequencies f_{11} and f_{21} from the stators of sensors ID1 and ID2 and
signals are generated to control electric motors M1 and M2. Electric
motor M4 is controlled from module BU4 from the results of comparing the
signal frequencies f_{12} and f_{22}. Frequency dividers D1 and D2 are also
included in the drive structure.

Let us denote the absolute angular velocities of the rotors of ID1 and
ID2 by Ω_1 and Ω_2, respectively. The signals of the sensors will then
have the frequencies:

213

$$f_{11} = k_1\Omega_1; \quad f_{12} = k_1 (\Omega_1 + \Omega_0);$$

$$f_{21} = k_2\Omega_2; \quad f_{22} = k_2 (\Omega_2 + \Omega_{c.9}),$$

where k_1 and k_2 are the transfer coefficients of the pulse sensors, Ω_0 is the absolute angular velocity of the base, and $\Omega_{c.9}$ is the absolute angular velocity of the element to be stabilized.

It follows from these relations:

$$\left.\begin{aligned}
\Omega_{c.9} &= \frac{f_{22}}{k_2} - \Omega_2 = \frac{1}{k_2}(f_{22} - f_{21}); \\
\Omega_0 &= \frac{f_{12}}{k_1} - \Omega_1 = \frac{1}{k_1}(f_{12} - f_{11}).
\end{aligned}\right\} \tag{6.3}$$

Let it be required to maintain a specific ratio between velocities

$$\Omega_{c.9} = a\Omega_0, \tag{6.4}$$

where a is a constant value.

One can write from expressions (6.3) and (6.4):

$$f_{22} - f_{21} = a\frac{k_2}{k_1}(f_{12} - f_{11}).$$

Let us denote $k_{\text{Д}} = ak_2/k_1$, and then

$$k_{\text{Д}}f_{12} - f_{22} = k_{\text{Д}}f_{11} - f_{21}.$$

According to the functional diagram (Figure 6.5) with operating frequency stabilization circuits f_{11} and f_{21}, one can write

$$f_{21} = k_{\text{Д}}f_{11} = k_{\text{Д}}f_9,$$

where f_9 is the reference frequency and $k_{\text{Д}}$ is the transfer coefficient of frequency divider D1.

214

The electric motor M4 should be controlled so as to maintain the ratio $f_{22} = k_{\text{Д}}f_{12}$. To do this, the transfer coefficient of frequency divider D2 should also be made equal to $k_{\text{Д}}$. The control system, designed according to Figure 6.5, permits one to establish any ratio between the speeds of the gyro-stabilized platform and the element to be stabilized, i.e., to formulate $a = \Omega_{c.э}/\Omega_0 = k_{\text{Д}}k_1/k_2$ by the appropriate selection of $k_{\text{Д}}$.

The condition $\Omega_{c.э} = 0$ should be provided to stabilize the SE in space. If the gyro-stabilized platform keeps its position in space unchanged, the closed circuit through BU1 becomes unnecessary. One should guarantee $f_{22} = f_{21}$ according to expression (6.3), which can be realized by feeding these signals to the inputs of BU4.

It is obvious that this device can also be used to realize displacements of the element to be stabilized in space according to a given program. If the rate of this displacement should be kept constant, it is sufficient to select the corresponding value of addition to a signal with frequency f_{22}. Maintaining a specific ratio of velocities Ω_0 and $\Omega_{c.э}$, one can achieve values k_1, k_2 and $k_{\text{Д}}$ by the appropriate selection. The input signal of the gyroscope (if there is a torque sensor along the precession axis) can also be used as a channel for controlling the position of the element to be stabilized. A disadvantage of the device, a functional diagram of which is shown in Figure 6.5, is the requirement of coaxial arrangement of all the drives, which increases the dimensions and complicates the design. The drive of the gyro-stabilized platform and the drive of the element to be stabilized are structurally divided into two identical assemblies, which can be placed independently of each other provided that the parallelism of the rotational axes is maintained, in a device whose functional diagram is shown in Figure 6.6. The notations in Figure 6.6 are the same as in Figure 6.5.

The following relations are valid for this system:

$$f_{12} = (\Omega_1 + \Omega_0)\,k_1; \quad f_{21} = (\Omega_2 + \Omega_0)\,k_2;$$
$$f_{11} = \Omega_1 k_1; \quad f_{22} = (\Omega_2 + \Omega_{c.э})\,k_2.$$

Hence, one can write:

$$\Omega_{c.э} = \frac{f_{22}}{k_2} - \Omega_2 = \frac{f_{22} - f_{21}}{k_2} + \Omega_0;$$
$$\Omega_0 = \frac{f_{12}}{k_1} - \Omega_1 = \frac{f_{12} + f_{11}}{k_1}.$$

215
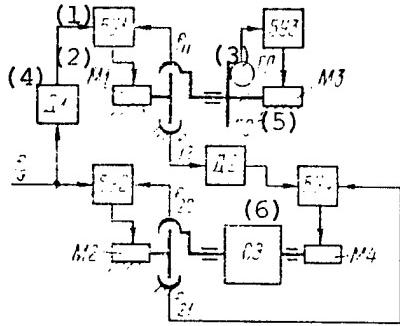
Figure 6.6. Functional Diagram of Variant of
Design Version of Position Control System of
Element To Be Stabilized

KEY:

1.	Control module	4.	Frequency divider
2.	Electric motor	5.	Gyro-stabilized platform
3.	Gyroscope	6.	Element to be stabilized

If the ratio $\Omega_{c.9} = a\Omega_0$ must be maintained, we find from the last expressions

$$(f_{12} - f_{11}) \frac{k_2}{k_1} (a - 1) = f_{22} - f_{21}.$$

Hence,

$$f_{12} \frac{k_2}{k_1} (a - 1) + f_{21} = f_{11} \frac{k_2}{k_1} (a - 1) + f_{22}.$$

Thus, the transfer coefficients of frequency dividers D1 and D2 (see Figure 6.5) should be

$$k_{\text{д}} = \frac{k_2}{k_1} (a - 1).$$

(6.5)

The drives should guarantee the ratio:

$$\begin{aligned} f_{21} &= -k_{\text{д}} f_{12}; \\ f_{22} &= -k_{\text{д}} f_{11}. \end{aligned}$$

(6.6)

216

The minus sign denotes that the rotors of sensors ID1 and ID2 should rotate in opposite directions.

One should find $\Omega_{c.9} = 0$ to stabilize the SE in space, which is possible at a = 0.

Having used expression (6.5), we find $k_\text{Д} = -k_2/k_1$ at a = 0.

The most frequently encountered problem of image stabilization using moving reflecting elements is that of guaranteeing the relation a = 0.5.
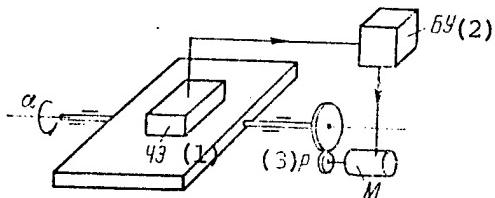
Figure 6.7. Layout of One-Axis Indicating
Gyro Stabilizer

KEY:
1. Sensitive element   3. Reduction gear
2. Control module   4. Electric motor

It is obvious that $k_\text{Д} = -0.5$ at $k_1 = k_2$. The drives should provide the following relations according to expressions (6.6):

$$f_{21} = 0{,}5f_{12}; \quad f_{22} = 0{,}5f_{11}.$$

This condition is easy to realize in practice.

Gyro stabilizers in image stabilization systems. One of the main components of an image stabilization system is the gyro stabilizer (GS), on which the optical circuit of the instrument or the entire optical instrument is mounted. The instrument should be mounted on a three-axis gyro stabilizer for total stabilization of the image, but a two-axis gyro stabilizer or a one-axis gyro stabilizer is used in most cases. Moreover, a multiaxial gyro stabilizer can be formally represented as a set of one-axis gyro stabilizers, mounted on different axes, at small stabilization errors. Most attention is devoted in [10] to a one-axis gyro stabilizer, and the derived expressions are then applicable to more complicated cases with regard to their characteristic features. Diagrams of a one-axis power-type indicating gyro stabilizer are presented in Figures 6.7 and 6.8.

217
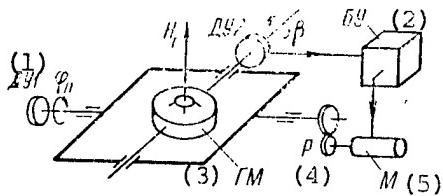
Figure 6.8. Diagram of One-Axis Power-Type
Gyro Stabilizer

KEY:

1. Angle-data transmitter   4. Reduction gear
2. Control module   5. Electric motor
3. Gyro motor

The difference between these two layouts of the gyro stabilizer is that
the gyroscope not only performs the role of sensitive element (ChE) of
misalignment of the platform to be stabilized, but also prevents this
misalignment due to a significant gyroscopic moment in the case of a
power gyro stabilizer. A drive containing an electric motor M and
reduction gear R, mounted on the stabilization axis, is used to reduce
the effects of the perturbing moments on the gyroscope and plays an
auxiliary role.

The gyroscopic moment in indicating gyro stabilizers is either
altogether absent or has a negligible value as a function of the type of
sensitive element to be used. Let us consider the equations of a
one-axis power gyro stabilizer with gyro motor (GM), presented in [10]:

$$
\begin{cases}
J_{\Sigma}\ddot{\varphi}_{\text{п}} + \dot{H}_{\text{г}}\beta + b_{1\text{э}}\dot{\varphi}_{\text{п}} = n M_{\text{дп}} + n\,|n + (-1)^{i}|\,J_{\text{я}}\ddot{\varphi}_{0} + b_{1\text{э}}\dot{\varphi}_{0}; \\[4pt]
J_{\text{г}}\ddot{\beta} - H_{\text{г}}\dot{\varphi}_{\text{п}} = M_{\text{к}},
\end{cases}
\tag{6.7}
$$

where $J_{\Sigma} = J_{\text{я}}n^{2} + J_{\text{п}}$ is the moment of inertia of the moving parts,

reduced to the stabilization axis, $J_{\text{я}}$ is the moment of inertia of the

armature of the relief electric motor, $J_{\text{п}}$ is the moment of inertia of

the platform to be stabilized, n is the gear ratio of the reducer, i is
the number of axes in the reducer, including the axes of the platform

and motor, $J_{\text{г}}$ is the moment of inertia of the gyroscope about the axis

of the inner gimbal, $\varphi_{\text{п}}$ is the angle of rotation of the platform about

the stabilization axis, φ_{0} is the angle of rotation of the base about

the stabilization axis, β is the angle of rotation of the gyroscope
about the precession axis, $H_{\text{г}}$ is the moment of momentum of the

gyroscope, $b_{\text{э}} = b_{\text{п}}n^{2} + b_{1}$ is the equivalent viscous friction

218

coefficient, b_1 is the coefficient of frictional forces along the stabilization axis, $b_я$ is the viscous friction coefficient on the axis of the electric motor armature, $M_{дв}$ is the moment of the electric motor, and $M_к$ is the correcting moment applied to the precession axis of the gyroscope.
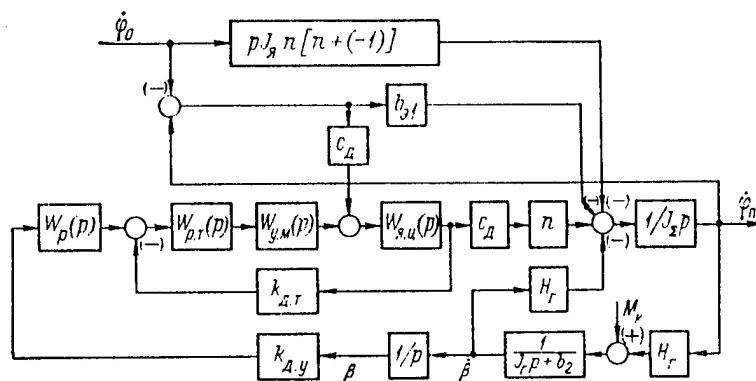
Figure 6.9.   Block Diagram of One-Axis Gyro Stabilizer

Let a DC electric motor, controlled in a system with subordinate feedback with respect to armature current, be used as the electric motor.   The current regulation circuit includes: a current regulator with transfer function $W_{p.т}(p)$, power amplifier with transfer function $W_{y.м}(p)$, current sensor of the armature with gear ratio $k_{д.т}$, and transfer function of armature circuit $W_{я.ц}(p)$.   A master signal is fed from the regulator with transfer function $W_p(p)$ to the input of the current circuit (Figure 6.9).   The block diagram of a one-axis stabilizer can thus be shown, according to expressions (6.7), in the form presented in Figure 6.9.   The following notations are introduced in this figure: $k_{д.y}$ is the gear ratio of the rotational angle-data transmitter β of the gyroscope, $c_д$ is the constant of the electric motor, and b_2 is the viscous friction coefficient on the precession axis.

If the speed of the current circuit is sufficiently high, there is no relationship with respect to the counter-emf of the electric motor and the block diagram can be converted to the form shown in Figure 6.10.

The following is denoted in Figure 6.10: $W_г(p) = k_г/(T_г p + 1)$ is the transfer function fo the gyroscope with respect to the measuring channel, where $k_г = H_г/b_2$ is the transfer coefficient of the gyroscope,

$T_\Gamma = J_\Gamma/b_2$ is the time constant of the gyroscope, $W_1(p) = k_{\text{д.у}} nc_{\text{д}} \times$

$\times \dfrac{1}{p} W_p(p) \; \Phi_{\text{к.т}}(p) \approx k_1 W_p(p)/p$, where $k_1 = k_{\text{д.у}} nc_{\text{д}}/k_{\text{д.т}}$; $\Phi_{\text{к.т}}(p) = W_\text{т}(p)/k_{\text{д.т}} [1 +$

$+ W_\text{т}(p)]$ is the transfer function of a closed current circuit, and

$W_\text{т}(p) = k_{\text{д.т}} W_{\text{р.т}}(p) \; W_{\text{у.м}}(p) \; W_{\text{д.н}}(p)$ is the transfer function of an open

current circuit, and $W_{06}(p) = pJ_{\text{д.н}} [n + (1)^{-i}]$ is the transfer function

of running-in.
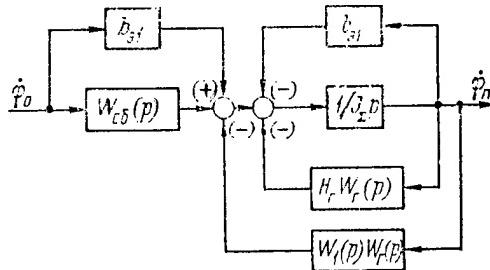
Figure 6.10. Transformed Block Diagram of
One-Axis Gyro Stabilizer

One can write for a circuit which includes transfer functions $H_\Gamma W_\Gamma(p) + b_{31}$

and $1/J_\Sigma p$:

$$\Phi_1(p) = \frac{1}{J_\Sigma p [1 + (H_\Gamma W_\Gamma(p) + b_{31})/J_\Sigma p]} =$$

$$= \frac{T_\Gamma p + 1}{\left(b_1 + \dfrac{H_\Gamma^2}{b_2} \right)(T^2 p^2 + 2\xi T p + 1)},$$

where $T^2 = \dfrac{J_\Sigma J_\Gamma}{\left(H_\Gamma^2 + b_1 b_2 \right)}$; $\xi = \dfrac{J_\Sigma b_2 + J_\Gamma b_1}{2\sqrt{J_\Sigma J_\Gamma - \left(H_\Gamma^2 + b_1 b_2 \right)}}$.

Accordingly, we have at $b_1 b_2 \ll H^2_\Gamma$:

$$\Phi_1(p) \approx \frac{T_\Gamma p + 1}{k_\Gamma H_\Gamma (T^2 p^2 + 2\xi T p + 1)},$$

where $T \approx \dfrac{\sqrt{J_\Sigma J_\Gamma}}{H_\Gamma^2}$; $\xi = \dfrac{1}{2 k_\Gamma} \sqrt{\dfrac{J_\Sigma}{J_\Gamma}}$.

The derived transfer function determines the operation of the gyroscope without a relief drive. It is obvious that if $H_r W_r(p) \ll J_\Sigma p$, then

$$\Phi_1(p) \approx \frac{1}{b_{01}(J_\Sigma p / b_{01} + 1)}.$$

Thus, if the reduced moment of inertia of the platform satisfies the expression $H^2_r \ll b_1 b_2$, one can disregard the stabilizing influence of the gyroscopic moment of the gyroscope in the low-frequency range. The gyroscope plays the role of only the sensitive element, which measures the angular deviations of the stabilized platform in space, which corresponds to indicating stabilization.

Let us now consider the operation of a circuit formed by the relief motor (Figure 6.10), i.e., the influence of transfer function $W_1(p)W_r(p)$. The transfer function of an open circuit can be written in the form

$$W^*(p) = \Phi_1(p)\, W_1(p)\, W_r(p) = \frac{k_r k_1 W_p(p)}{p\left(b_1 + H^2_r / b_2\right)\left(T^2 p^2 + 2\xi T_p + 1\right)}.$$

We find at $b_1 b_2 \ll H^2_r$

$$W^*(p) = \frac{K^* W_p(p)}{p\left(T^2 p^2 + 2\xi T_p + 1\right)},$$

where $k^* = k_r k_1 / H^2_r$.

The cut-off frequency ω_{cp} must be selected from the condition $\omega_{cp} \leq$

$\leq \frac{\xi}{T} \sqrt{1 - \xi^2}$, to eliminate the autooscillations of the gyro stabilizer.

This condition imposes constraints on the possible speed of the gyro stabilizer and, accordingly, on its accuracy capabilities. The transfer function of a closed relief circuit can be represented in the form $\Phi_2(p) = \Phi_1(p)\, \Phi^*_\Sigma(p)$, where $\Phi^*_\Sigma(p) = 1/(1 + W^*(p))$.

Hence, we have

$$W(p) = \dot\phi_\Pi(p)/\dot\phi_0(p) = [W_{06}(p) + b_{01}]\,\Phi_2(p).$$

One must guarantee the condition: $(1/T) > \omega_{cp} > (1/T_r)$ for a power gyro stabilizer and $(1/T) < (1/T_r) < \omega_{cp}$ for an indicating gyro stabilizer.

It follows from the transfer functions that a gyro stabilizer of any type effectively suppresses low frequencies. Moreover, the filtering properties of the gyro stabilizer do not vary for both a power and indicating gyro stabilizer at frequencies that exceed 1/T at proportional regulator. An increase of the astatism of the relief circuit of an indicating gyro stabilizer permits one to improve its filtering properties at low frequencies to frequency ω_{cp}. At high frequencies, $\omega \gg 1/T$ and $\omega \gg \omega_{cp}$ and one can write $\Phi_2(p) \approx \Phi_1(p)$ for the transfer function accroding to the angular motion speed of the base; therefore,

$$W(p) \approx W_{o6}(p)\,\Phi_1(p) \approx \frac{J_{\text{H}} n^2 p\,(J_{\text{I}} p + b_2)}{(H_r^2 + b_1 b_2)(T^2 p^2 + 2\xi T p + 1)} \approx \frac{J_{\text{H}} n^2}{J_\Sigma}.$$
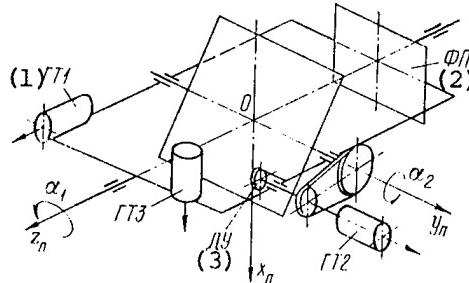
Figure 6.11. Kinematic Layout of AFA

KEY:
1. Gyro tachometer   3. Angle-data transmitter
2. Photodetector

If a reducerless drive is mounted along the stabilization axis, then

$W_{o6}(p) = b_{13}$; and $W(p) = b_1/J_\Sigma p$ at high frequencies.

Thus, the capability of the gyro stabilizer to filter high frequencies is independent of its type and is determined only by the design of the relief drive with respect to the stabilization axis. An important factor for image stabilization is the filtering capability of the gyro stabilizer at frequencies that exceed $\omega_3 = 2\pi/\tau_3$; therefore, one should provide $T \gg \tau_3$ for the power version of a gyro stabilizer and $\omega_{cp} \gg \omega_3$ for the indicating version of the gyro stabilizer. In this case, a reducerless relief drive is preferable, since it permits one to avoid the effect of vibrations.

Example of design of image stabilization system. Different versions of using mirror reflectors to design image stabilization systems were considered in Chapter 3. Let us consider the design of the image stabilization system of an AFA, based on the diagram presented in Figure 3.8.

The formulas that describe the displacements of the image in this AFA can be found from expressions (1.70). The photodetector is displaced in space at angular rate ω_ϕ. The projections of this rate onto the axes of the instrument are equal to: $\omega_{\phi x} = \omega_{xn};\ \omega_{\phi y} = \omega_{yn};\ \omega_{\phi z} = \omega_{zn} + \dot\alpha_1$.

Rotation of the mirror by angle α_1 (see Figure 3.8) results in corresponding variation of the angle of incidence of the ray on the mirror. If displacement of only the central ray is analyzed, one can assume that $\alpha_1 = 0$ in equations (1.70). Variation of the distance H_0 to the object of photography can be taken into account due to the corresponding correction of the parameters of vector ω_n.

We find for projections of the angular rate of displacement of the image:

$$\omega_{\delta x} = -\omega_{xn}\cos 2\alpha_2 + (\omega_{zn} + \dot\alpha_1)\sin 2\alpha_2;$$
$$\omega_{\delta y} = 2\dot\alpha_2 + \omega_{yn};$$
$$\omega_{\delta z} = \omega_{xn}\sin 2\alpha_2 + (\omega_{zn} + 2\dot\alpha_1)\cos^2\alpha_2.$$

One can find from these expressions the algorithm for compensation of image displacement from the condition $\omega_{\delta x} = \omega_{\delta y} = \omega_{\delta z} = 0$. Gyroscopes (usually gyro tachometers) can be used as the data sensor on displacements of elements of the optical system of the AFA for technical realization of this algorithm. One of them GT1 (Figure 6.11) should be mounted on the outer gimbal of a mirror and the axis of sensitivity of the gyroscope should be parallel to the rotational axis of this gimbal. The second gyroscope GT2 is mounted through a reducer with transfer coefficient 2 such that the axis of sensitivity of this gyroscope is parallel to the rotational axis of the mirror in the gimbal by angle α_2. The third gyroscope GT3 is attached to the gimbal so that the axis of sensitivity is perpendicular to those of gyroscopes GT1 and GT2.

There will be the following signals at the outputs of the gyroscopes:

$$\omega_{r1} = \omega_{zn} + \dot\alpha_1;$$
$$\omega_{r2} = 2\dot\alpha_2 + \omega_{yn};$$
$$\omega_{r3} = \omega_{xn}.$$

223

One can subsequently assume that the instrument axes $Ox_\pi y_\pi z_\pi$ are related to the outer gimbal of the mirror and are rotated by angle α_1 together with it. The motion of the mirror by angle α_2 is used for image stabilization during a comparatively short time interval, equal to the exposure time of the film. Thus, angle α_2 hardly differs from the nominal value. We assume that $\alpha_2 = 45° + \Delta\alpha_2$, where $\Delta\alpha_2 \ll 45°$.

One can write the approximate equalities

$$\sin 2\alpha_2 \approx 1 - 2\Delta\alpha_2^2; \quad \cos 2\alpha_2 \approx -2\Delta\alpha_2;$$
$$\sin^2 \alpha_2 \approx (1/2) - \Delta\alpha_2; \quad \cos^2 \alpha_2 \approx (1/2) + \Delta\alpha_2.$$

Using these equalities, one can find the following relations for the angular displacements of the output central ray with respect to the photodetector:

$$\omega_{\delta x} = (\omega_{z\pi} + \dot\alpha_1) + 2\Delta\alpha_2 [\omega_{x\pi} - \Delta\alpha_2 (\omega_{z\pi} + \dot\alpha_1)];$$
$$\omega_{\delta y} = \omega_{y\pi} + 2\dot\alpha_2;$$
$$\omega_{\delta z} = (\omega_{x\pi} + \dot\alpha_1) + 2\Delta\alpha_2 (\dot\alpha_1 - \Delta\alpha_2\omega_{x\pi} - \omega_{z\pi}).$$

Having substituted the expressions for the gyroscope signals into these equations, we find

$$\omega_{\delta x} = \omega_{r1} \left(1 - 2\Delta\alpha_2^2\right) + 2\Delta\alpha_2\omega_{r3};$$
$$\omega_{\delta y} = \omega_{r2};$$
$$\omega_{\delta z} = \omega_{r3} \left(1 - 2\Delta\alpha_2^2\right) - 2\Delta\alpha_2\omega_{r1}.$$

The image will thus be stabilized provided that:

$$\omega_{r1} \left(1 - 2\Delta\alpha_2^2\right) + 2\Delta\alpha_2\omega_{r3} = 0;$$
$$\omega_{r2} = 0;$$
$$\omega_{r3} \left(1 - 2\Delta\alpha_2^2\right) - 2\Delta\alpha_2\omega_{r1} = 0.$$

A simplified algorithm can be found at $\Delta\alpha_2 = 0$ in the following form:

$$\omega_{r1} = 0; \quad \omega_{r2} = 0; \quad \omega_{r3} = 0.$$

224
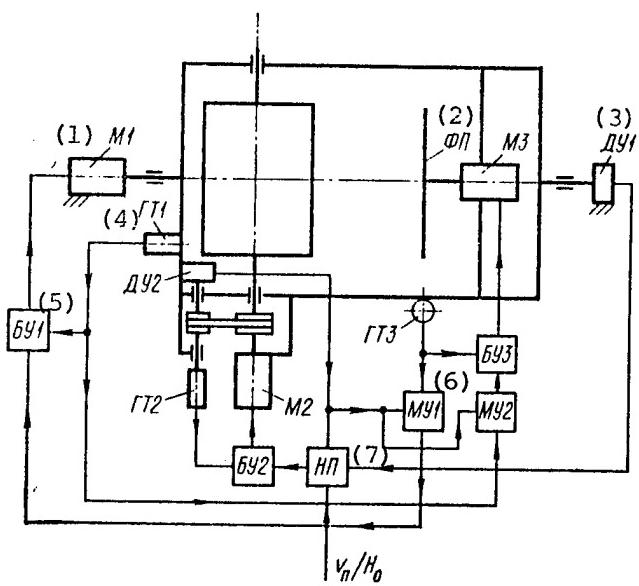
Figure 6.12. Functional Diagram of Image Stabilization
System of AFA (Version I)

KEY:
1. Electric motor
2. Photodetector
3. Angle-data transmitter
4. Gyroscope
5. Control module
6. Multiplier
7. Nonlinear converter

To compensate for displacement due to flight speed v_π, the vector of which can be directed along axis OZ_π, angular displacement should be accomplished along the mirror axis at angular rate

$$\dot{\alpha}_2 = - f' \, (v_u/H_0) \cos \alpha_1 \cos \Delta\alpha_2.$$

This condition can be realized if the drive control system according to the indicated rotational axis maintains the following ratio at the moment of exposure

$$\omega_{r2} = - 2f' \, (v_u/H_0) \cos \alpha_1 \cos \Delta\alpha_2.$$

A more accurate image stabilization algorithm can be realized if an angle-data transmitter DU is attached to the axis on which the gyroscope GT2 is mounted (Figure 6.11). We find a signal corresponding to angle $u_\text{Д} = 2\Delta\alpha_2$ at the output of this transmitter.

225

The stabilization algorithm thus assumes the form:

$$\omega_{r1} + \omega_{r3} u_{\pi} = 0;$$
$$\omega_{r2} = -2f' \, (v_{\pi}/H_o) \cos \alpha_1 \cos \Delta\alpha_2;$$
$$\omega_{r3} = \omega_{r1} u_{\pi}.$$

The functional diagram of the image stabilization system, which realizes this algorithm, is presented in Figure 6.12. Electric motors M1, M2, and M3 are controlled from the corresponding control modules BU1, BU2 and BU3. Signals are fed from gyroscopes GT1, GT2, and GT3 to the inputs of the control modules. Moreover, a signal is fed from the nonlinear converter (NP) to the input of module BT2. The nonlinear converter calculates the master signal to the control module BU2 $v_3 =$

$= 2f' \, (v_{\pi}/H_o) \cos \alpha_1 \times \cos \Delta\alpha_2$ according to information about the value of

v_{π}/H_0 and according to the value of α_1 and $\Delta\alpha_2$, measured by angle-data transmitters DU1 and DU2. Multipliers MU1 and MU2 are used to form the control signals of module BU1 and BU3.
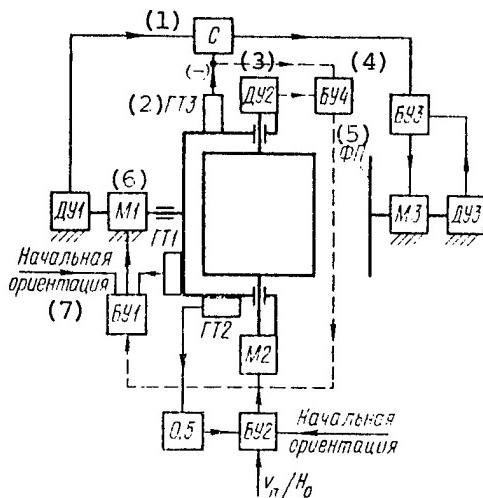
Figure 6.13. Functional Diagram of Image
Stabilization System of AFA (Version II)

KEY:

1. Adder   5. Photodetector
2. Gyro tachometer   6. Electric motor
3. Angle-data transmitter   7. Initial orientation
4. Control module

The photodetector may not be mechanically connected to the mirror from simplification and lightening of the design of the AFA. In this case

the photodetector should be a separate drive, the master to which is fed from angle-data transmitter α_1, mounted on the outer axis of the gimbal suspension. A diagram of this AFA is presented in Figure 6.13. The local drive of the photodetector is organized on electric motor M3, rotational angle-data transmitter DU3 and control module BU3. The control signal to the input of the BU3 is fed from rotational angle-data transmitter DU1 α_1 of the outer gimbal suspension of the mirror and from gyroscope GT3 through adder S. A layout for organization of an information channel, considered in Figure 6.12, can be used to eliminate the mechanical coupling of the gyroscope GT2 to the gimbal suspension of the mirror through a reducer. The dashed curve in Figure 6.13 denotes the additional coupling, which can be eliminated when using a simplified stabilization algorithm. The position of the mirror in space is determined before the beginning of photography and is corrected by using the initial orientation system.

When using a focal plane shutter, additional compensation of ground speed can be introduced with regard to the current position of the shutter. Let us denote the position coordinate of the focal plane on the frame by y_i. The condition of stabilization with respect to the inner axis of the gimbal suspension of the mirror is then written in the form:

$$\omega_{r2} \approx -2f'(v_n/H_o)\cos\alpha_1\cos\Delta\alpha_2[1 + (y_i/f')\operatorname{tg}\alpha_1].$$

This algorithm should be used only for short-focus objectives at large rotational angles α_1 of the AFA.

A functional diagram of the stabilization assembly of the outer gimbal axis is presented in Figure 6.14. In this figure, L1 is the dial of the pulse angle-data sensor, P1 is the platform for mounting the gyroscope, F1 is the first reading device from dial L1 (F1 is rigidly connected to the platform P1), F2 is the second readout device, rigidly connected to the outer gimbal axis, FD1 is the first phase discriminator, FD2 is the second phase discriminator, U1, U2, and U3 are correcting amplifier sections, SCh is the pulse counter, and GT1 is the gyroscope mounted on the platform P1.

The stabilization device operates in the following manner. The platform P1 is stabilized in space in the stabilization mode due to the feedback circuit U3-M5 of angle-data transmitter GT1. Since the signal from F1 is used to organize feedback with respect to the angular position of L1, the dial will rotate at constant angular velocity in space at constant master frequency f_3. The frequency fed from F2, $f_{\phi 2}$ will be equal to $(2\pi/N_1)(\Omega_n - \Omega_{zn})$, where N_1 is the the number of marks of L1, and Ω_n is the speed of the dial, i.e., it is proportional to the angular rotational speed of the base. The signal from F2 is used to organize feedback by the position of the external gimbal axis. To do this, it is

227

compared to frequency f_3 on FD2 and is fed through adders S1 and S2 and section U2 to the input of the actuating motor.
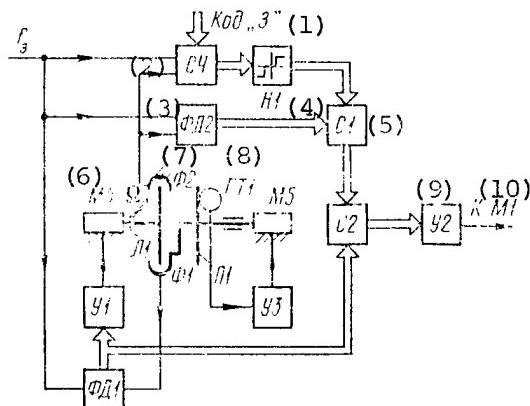

Figure 6.14. Functional Diagram of Outer Gimbal
Axis Stabilization System

KEY:

1.	Code "Z"	6.	Electric motor
2.	Reader	7.	Reader
3.	Phase discriminator	8.	Gyro tachometer
4.	Nonlinear element	9.	Correcting amplifier
5.	Adder	10.	To electric motor 1

A code is fed to the input of the adder of counter SCh, equal to the number of pulses of transmitter L1, by which the gimbal axis must be rotated, for reorientation of the outer axis. The signal from the adder is fed through the nonlinear element N1 to input U2, rotating the gimbal axis. When the code from counter SCh and the given code are compared, the system begins to stabilize its position. The presence of connection of output signals FD1 and FD2 permits one to obtain dynamic accuracy of the system, independent of rotational stability L1. Moreover, the total master frequency f_3 eliminates the error due to instability of f_3. The constant rotational speed of L1 and P1 in space minimizes the perturbing moments acting on the system, which permits one to use micromotors as M2 and M3, besides increasing the accuracy (see Figure 6.13). The functional diagram of the inner gimbal axis stabilization assembly is shown in Figure 6.15. In this figure, L1 and L2 are dials of pulse angle-data transmitters, FD1, FD2, and FD3 are phase discriminators, M1, M2, and M3 are the electric motors of the auxiliary drives, M4 is the electric motor of the mirror drive, P1 is the platform with gyroscope GT2 mounted on it, U1-U4 are correcting amplifiers, F1 and F3 are readers connected to the platform P1, F2 is a reader connected to the outer gimbal axis, and F4 is a reader connected to the outer gimbal axis.

228
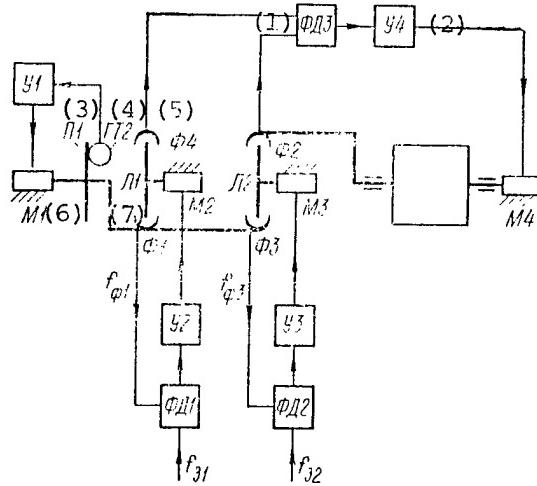
Figure 6.15. Functional Diagram of Inner
Gimbal Axis Stabilization System

KEY:

1. Phase discriminator   5. Reader
2. Correcting amplifier   6. Electric motor
3. Platform   7. Dial
4. Gyroscope

The mechanical part of the inner axis stabilization assembly differs
from the outer axis stabilization assembly by the presence of an
additional dial L2 and an electric motor M3 for driving it. The number
of pulses to rotate dial L1 is related to the number of pulses L2 in the
following manner: $N_1/N_2 = 0.5$, where N_1 is the number of marks of the
dial L1, and N_2 is the number of marks of dial L2.

Let us denote the velocity of separate assemblies in inertial space:
dial L1 by $\Omega_{\text{Л}1}$, dial L2 by $\Omega_{\text{Л}2}$, the platform P1 by $\Omega_{\text{П}1}$, the mirror axis
by Ω_3, and the base by Ω_0.

According to the functional diagram, the frequencies of readers F2 and
F4 are found in the ratio $f_{\phi 2} = f_{\phi 4}$. Multiplying out the equality, we
find $N_1 (\Omega_{\text{Л}1} - \Omega_0)/(2\pi) = N_2 (\Omega_{\text{Л}2} - \Omega_3)/(2\pi)$. and hence, $\Omega_3 = \Omega_{\text{Л}2} - 0.5\Omega_{\text{Л}1} + 0.5\Omega_0$.

The following equalities also follow from the functional diagram: $f_{31} =$
$= f_{\phi 1}; f_{32} = f_{\phi 3}$, where f_{31} and f_{32} are the corresponding master
frequencies, while $f_{\phi 1}$ and $f_{\phi 3}$ are frequencies F1 and F3.

Multiplying out the equalities, one can determine the angular velocities
of the dials:

229

$$\Omega_{\pi 1} = 2\pi f_{31}/N_1 + \Omega_{\text{п1}}; \quad \Omega_{\pi 2} = 2\pi f_{32}/N_2 + \Omega_{\text{п1}}.$$

We then find for the velocity of the mirror:

$$\Omega_3 = \pi \, (f_{32} - f)/N_1 + 0{,}5\Omega_{\text{п1}} + 0{,}5\Omega_{0y}.$$

Since the velocity of the platform is kept equal to zero, then

$$\Omega_3 = \pi \, (f_{32} - f_{31})/N_1 + 0{,}5\Omega_{0y}.$$

Thus, the image is stabilized with respect to axis Oy_k, and control of the velocity of the mirror in inertial space is also possible. To do this, one must fulfill the equality:

$$0{,}5 \, (v_{\text{п}}/H_0) \cos\alpha_1 [1 + (y_i/f') \, \text{tg}\,\alpha_1] = \pi \, (f_{32} - f_{31})/N_1.$$

If frequency f_{32} is kept constant, frequency f_{31} should vary by the law

$$f_{31} = f_{32} - (N_1 v_{\text{п}}/2\pi H_0) \cos\alpha_1 [1 + (y_i/f') \, \text{tg}\,\alpha_1].$$

Compensation links can be introduced to increase the dynamic accuracy of the system.

No rigid requirements are imposed on the photodetector stabilization assembly and the outer gimbal axis, since the velocity error causes the image to rotate about the optical axis, while the requirements on stabilization by this axis are not rigid. The position error may cause rotation of the field of blurring factors by some angle with respect to the shutter due to the linear velocity of the object.

6.2. Design Principles of Automatic Image Stabilization Systems by Information on Misalignment of Image

The different design principles of image stabilization systems were considered in Chapter 1. It was shown that introduction of an image misalignment sensor into the structure permits one to design a stabilization system on the closed principle, which considerably increases the accuracy of the entire system. It is obvious that image stabilization is possible upon organization of image shift or photodetector control systems in two-three coordinates. The sensors

considered in Chapter 4 yield information about the rate of image shift
along two mutually perpendicular axes. The field of the rates of image
shift has a complex configuration, dependent on the parameters of
displacement of the object. Thus, the characteristic features of the
transmitter determine the methodical errors in measurement of image
shift.
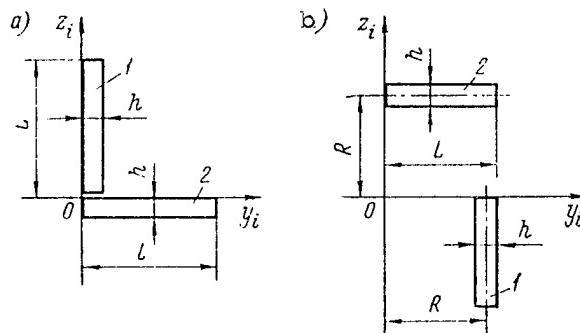
Figure 6.16. Variants of Arranging Mast Gates of
Image Misalignment Sensor:
a--arrangement of gates parallel to axes y, z;
b--arrangement of gates perpendicular to axes y, z

Let us consider the different variants of arrangement on the platform
frame, by which the integral estimate of the image shift rates is made.

A modulating array in the form of a spiral is considered in one of the
papers. (Footnote) (U.S. patent 3,511,510) If the mask gates are

arranged as shown in Figure 6.16, a, the estimate $\hat{z}$ of the projection of
the linear velocity $\dot{z}$ is made by the photodetector signal, mounted above
the notch 1 of the mask , which extends along axis Oz, while that of $\dot{y}_i$
is made by the photodetector signal, mounted above notch 2 of the mask
along axis Oy_i. Performing the integration within the given limits and
at $h \ll f$, $h \ll L$, $\varphi = 90°$, we find:

$$
\left.
\begin{aligned}
\widehat{\dot{y}}_i &\approx \omega_{xn}L/2 - f\omega_{zn} + v_{yn}f/H_o; \\
\widehat{\dot{z}}_i &\approx -\omega_{xn}L/2 + f\omega_{yn} + v_{zn}f/H_o.
\end{aligned}
\right\}
\tag{6.8}
$$

One can write in similar fashion for the arrangement of mask gates 1 and
2, shown in Figure 6.16, b:

231

$$\widehat{\dot{y}}_i = R\omega_{x\pi} - \frac{RL}{2f}\,\omega_{y\pi} + f\omega_{z\pi}\left(\frac{L^2}{3f^2} - 1\right) +$$

$$+ v_{x\pi}\frac{L}{2}\left(\sin\varphi + \frac{R}{L}\cos\varphi\right) + v_{y\pi}\frac{f}{H_0}\left(\sin\varphi + \frac{R}{f}\cos\varphi\right);$$

$$\widehat{\dot{z}}_i = -R\omega_{x\pi} - \frac{L^2}{3f}\,\omega_{y\pi} - \frac{RL}{2f}\,\omega_{z\pi} + v_{x\pi}\frac{L}{H_0}\left(\frac{1}{3f}\cos\varphi - \frac{1}{2}\sin\varphi\right) +$$

$$+ v_{z\pi}\frac{1}{H_0}\left(f\sin\varphi - \frac{L}{2}\cos\varphi\right).$$

We find at $L \gg h;\ f \gg h;\ f \gg L,\ R;\ \varphi = 90°$:

$$\widehat{\dot{y}}_i \approx R\omega_{x\pi} - f\omega_{z\pi} + v_{y\pi}\frac{f}{H_0};$$

$$\widehat{\dot{z}}_i \approx -R\omega_{x\pi} + \frac{f}{H_0}v_{z\pi}.$$

By analogy with the previous formulas for symmetrical arrangement of the mask notches with respect to axes Oz_i, Oy_i, one can write:

$$\widehat{\dot{y}}_i = R\omega_{x\pi} + \omega_{z\pi}\left(\frac{2}{3}\frac{L^2}{f} - f\right) + v_{y\pi}\frac{1}{H_0}(R\cos\varphi + f\sin\varphi);$$

$$\widehat{\dot{z}}_i = -R\omega_{x\pi} + \omega_{y\pi}f\left(1 - \frac{2}{3}\frac{L^2}{f^2}\right) +$$

$$+ v_{x\pi}\frac{2}{3}\frac{L^2}{fH_0}\cos\varphi + v_{z\pi}\frac{f}{H_0}\sin\varphi.$$

With differential photography of a signal from two notches of the mask, arranged diametrically opposite, we find for estimate $\widehat{\dot{y}}_i$ of the image speed along axis Oy_i

$$\widehat{\dot{y}}_i = \frac{1}{2}(\widehat{\dot{y}}_{i1} + \widehat{\dot{y}}_{i2}) = \omega_{z\pi}f\left(\frac{2}{3}\frac{L^2}{f^2} - 1\right) + \frac{v_{y\pi}}{H_0}f\sin\varphi.$$

We also find a similar expression for estimation of $\widehat{\dot{z}}_i$. Thus, differential photography of the signal permits one to obtain a signal, equivalent to the integral estimation of misalignment with respect to the field, limited by the dimensions of the notch. The given formulas permit one to calculate the methodical error of the image stabilization system, in which image misalignment sensors are used.
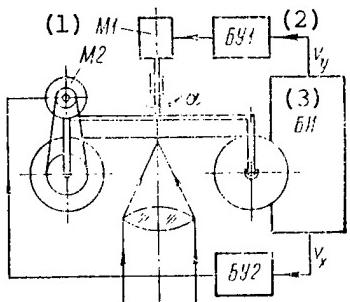
Figure 6.17. Layout of AFA With Two-Coordinate Image
Shift Rate Sensor

KEY:

1. Electric motor   3. Measuring module
2. Control module

Let us consider a device whose layout is shown in Figure 6.17 as an
example of designing an image stabilization system according to
information from the image misalignment sensor. The film holder can be
rotated by electric motor M1 by angle α about the vertical axis. The
signal to the motor M1 is formed in control module BU1 by the output
signal v_y of image misalignment perpendicular to the frame. The film
winding speed is dependent on the signal of the image motion speed v_x
along the frame. This signal is fed through control module BU2 to
electric motor M2. The rates of image misalignment are measured in a
measuring module BI.
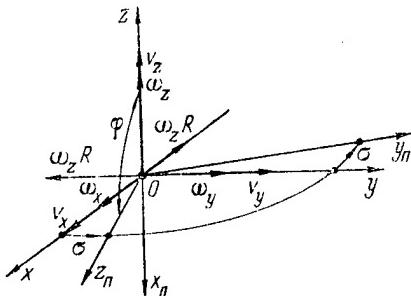
Figure 6.18. Coordinate System of AFA

The coordinate system Oxyz, bound to the base, and the coordinate system
$Ox_\Pi y_\Pi z_\Pi$, bound to the holder, are shown in Figure 6.18. The projections
of the linear and angular speeds of the image onto the axes of the base
are denoted by v_x, v_y, v_z and ω_x, ω_y, ω_z, respectively. Let the base of
the device not complete angular vibrations (i.e., $\omega_{x\Pi} = \omega_{y\Pi} = \omega_{z\Pi} = 0$),
while the principal optical axis of the device is perpendicular to the

233

plane of objects, i.e., $\bar{y} = 90°$. If the image shift is estimated by the entire image field, one can write for given conditions: $\dot{z}_{i\,cp} = v_{zn}f/H_0$; $\dot{y}_{i\,cp} = v_{yn}f/H_0$.

The device is rotated by angle σ about the principle optical axis until condition $\dot{y}_{icp} = 0$ is fulfilled. If the projections of the linear velocity of the base onto the axes of the base are equal to v_{x0}, v_{y0}, v_{z0}, we then find in projections onto the axes of the device:

$$v_{xn} = - v_{z0};$$
$$v_{yn} = v_{y0} \cos \sigma - v_{x0} \sin \sigma;$$
$$v_{zn} = v_{x0} \cos \sigma + v_{y0} \sin \sigma.$$

Hence, one can find the relation for the angle of rotation σ

$$\operatorname{tg} \sigma = v_{y0}/v_{x0}.$$

A signal proportional to the following value

$$\dot{z}_{i\,cp} = \frac{f}{H_0}\left(v_{x0} \cos \sigma + v_{y0} \sin \sigma\right) = \frac{f}{H_0}\frac{v_{x0}}{\cos \sigma} = \frac{f}{H_0}\sqrt{v_{x0}^2 + v_{y0}^2}.$$

will be formed at the second output of the image misalignment sensor.

Thus, the direction of motion of the film in the holder will coincide with the direction of the speed vector of the base in plane Ox_0y_0. If signal $\dot{z}_{icp}$ is used as the master at the input of the film motion speed control circuit, one can compensate the image shift caused by displacement of the base.

One can write from equations (1.21) with regard to Figure 6.18:

$$\dot{y}_i = z_i\omega_{xn} - \frac{\omega_{yn}y_iz_i}{f} + \omega_{zn}\left(\frac{y_i^2}{f} - f\right) + \frac{v_{xn}y_i}{H_0} + \frac{v_{yn}f}{H_0};$$

$$\dot{z}_i = - y_i\omega_{xn} + \omega_{yn}f\left(1 - \frac{z_i^2}{f^2}\right) + \frac{\omega_{zn}y_iz_i}{f} + \frac{v_{xn}z_i}{H_0} + \frac{v_{zn}f}{H_0}.$$

234

We find for projections of the angular speeds onto the axes of the device:

$$\omega_{x\pi} = \omega_{z0} + \dot{\sigma}; \quad \omega_{y\pi} = \omega_{y0} \cos \sigma - \omega_{x0} \sin \sigma;$$
$$\omega_{z\pi} = \omega_{x0} \cos \sigma + \omega_{y0} \sin \sigma.$$

Hence, we find for uncompensated displacements:

$$\Delta \dot{y}_i = z_i (\omega_{z0} + \dot{\sigma}) - \frac{\omega_{y\pi} y_i z_i}{f} - \frac{\omega_{z\pi} \left(z_i^2 - \frac{2}{3} z_m^2 \right)}{f} - \frac{v_{z0} y_i}{H_0};$$

$$\Delta \dot{z}_i = -y_i (\omega_{z0} + \dot{\sigma}) - \frac{\omega_{z\pi} y_i z_i}{f} - \frac{\omega_{y\pi} \left(\frac{2}{3} y_m^2 - y_i^2 \right)}{t} - \frac{v_{z0} z_i}{H_0}.$$

Specifically, the residual misalignment in the center of the frame is determined by the expressions:

$$\Delta \dot{y}_i = \frac{2}{3} \frac{w_{z\pi} z_m^2}{f};$$

$$\Delta \dot{z}_i = -\frac{2}{3} \frac{w_{y\pi} y_m^2}{f}.$$

The indicated components of misalignment do not affect the output signal of the image misalignment sensor and can therefore not be compensated.

The frequency band reproduced by a closed control system with respect to an image shift is determined by the spectral characteristics of the perturbations. The output signal of the sensor is in turn determined by the parameters of the angular and linear displacements of the base of the device. Let the maximum frequency of these displacements be ω^{max}_{BX}, while the image shift on this frequency should be suppressed by -40 dB by the stabilization system. It is then easy to find that frequency of photographing the signal from the sensor is determined from the

inequality $\omega_\pi \geqslant 25\omega_{Bx}^{max}$. with standard adjustment of the control circuit to the symmetrical optimum and provided that the excess of the modulation frequency of the pulse system above the cut-off frequency is not less than twofold. This condition is comparatively easy to realize in most designs of sensors. Thus, a frequency sensor with mechanical modulator in the form of a disk (with spiral bands in the center and with radial bands on the edge of the disk), having 30 spiral bands and 1,200 radial bands, is used in the above image stabilization system.

If the rotational speed of the disk is $\Omega_M = 120\pi$ s^{-1}, this corresponds to a modulation frequency through the first channel of $f_{M1} = 1.8$ kHz in the range of linearity of the charcteristic of ± 870 Hz, and that through the second channel of $f_{M2} = 72$ kHz at range of linearity of $\pm 2,000$ Hz.

The presence of two channels permits one to cover a wide range of frequencies of the input signals. If there are bright parts in the image, a correlation image misalignment sensor can be used. Thus, an image stabilization system for a lunar satellite is described in [88]. A cam, which moves the film holder with accuracy of not less than 10^{-6} m, was used as the actuating mechanism. An image with misalignment of not more than 2.5 μm at focal distance of the objective of 0.7 m was obtained with mass of the stabilization system of 4.53 kg and at consumed power of 8.5 W. These accuracies can be obtained only in a narrow range of variation of angular velocity, determined by the ratio v_Π / H_0.

6.3. Automatic Program Image Motion Control Systems

Reorientation systems of optical elements and devices. Program image motion control systems include optical element or device reorientation systems and also scanning systems. Any preset motions of optical elements or devices should be taken into account when designing image stabilization systems, since they can lead to considerable blurring of the image. The reorientation system is an optical element positioning system. The general principles of design calculation of position systems are outlined in [70]. The information channels of these systems are ordinarily constructed by using various types of code sensors. A disadvantage of systems with code sensors is level quantization, which results in limitation of the maximum achievable accuracy at the level of $\pm\delta$, where δ is the discreteness of the position information. Auto-oscillations of position systems may occur within this value. Taking into account that the problems of positioning of optical elements are continuously related to stabilization problems, the presence of auto-oscillations of position systems may have a significant influence on the errors of the stabilization systems. It becomes necessary in this regard to use different principles of arranging the control systems.

Specifically, systems with a reversing structure, when there is transition from a structure that realizes the positioning mode to one that realizes the stabilization mode, can be used. Different information channels are used. However, realization of these systems is related to considerable complication of them. Control systems whose information channels are based on pulsed photoelectric sensors, while the structure corresponds to that of a combination pulse-phase system using a one-axis gyro stabilizer, can also be organized.

236

Taking into account that optical devices are ordinarily reoriented in space, one must have both relative displacement sensors (for example, with respect to the base) and absolute displacement sensors in space.

Let us consider one-coordinate reorientation systems (Figure 6.19, a and b). The reorientation layout for the case of location of a gyro unit (GB) on a base is presented in Figure 6.19, a. The layout operated similar to that considered earlier in the "Stabilization" mode (see Figure 6.5). The difference is in the different design of the pulse sensor ID2 of the angle of rotation of the element to be stabilized SE. A four-channel photo impulse sensor is used in this device (Figure 6.20). The signals from outputs DU3 and DU4 are designed to measure the current position of the information systems with respect to the dial, while that of outputs DU1 and DU2 are designed to determine the mutual initial error of outputs DU2 and DU4 (channel I) and outputs DU1 and DU3 (channel II), and also to correct the current information about the angular error once every revolution of the dial. An angle of $180°$ with respect to the position of two information systems is taken as an error equal to zero.

The position error signal of the two sensor channels PD2 is taken from the output of the position error sensor IOP (see Figure 6.19, a). The error code is fed to the input of control module BU5, while the output signal of this module is used to control the electric motor M4 when the type of operation switch is set to the position "Correction." The master code of the IOP is fed from the output of adder S. Code "Z" (preset to rotation of the element to be stabilized) and the code of the current value of the angle of deflection of the base from the horizon with respect to the stabilization axis of the element to be stabilized are fed to the outputs of the adder. Information about the angle of deflection is fed from the onboard gyro unit VGB through the voltage-code converter (PNK).

The reorientation layout of the SE for the case of mounting the gyro unit directly on the element to be stabilized is presented in Figure 6.19, b. In this version of the circuit solution, a four-channel pulse angle-data transmitter is mounted in the gyro unit, while the reference frequency f_9 is received after conversion of reference code "E" in the code-frequency converter PKCh1.
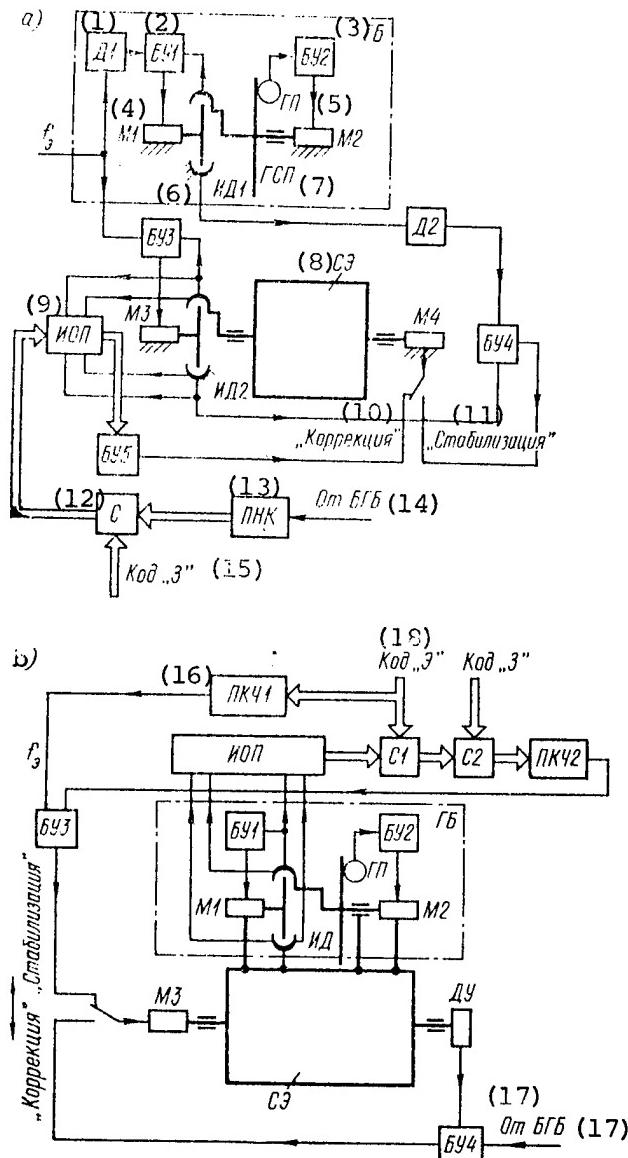
Figure 6.19.   functional Diagrams of One-Coordinate
Reorientation Systems:
a--with arrangement of the gyro unit on base;
b--with arrangement of gyro unit on element to
be stabilized

(Key on following page)

KEY:

1. Sensor
2. Control module
3. Gyro unit
4. Electric motor
5. Gyro platform
6. Pulse sensor
7. Gyro-stabilized platform
8. Element to be stabilized
9. Position error sensor
10. Correction
11. Stabilization
12. Adder
13. Voltage-code converter
14. From onboard gyro unit
15. Code "Z"
16. Code-frequency converter
17. From onboard gyro unit
18. Code "E"

Figure 6.20. Pulse Sensor of Angular
Position of Mirror

KEY:

1. Angle-data transmitter
2. Channel
3. Dial

The position error code from the output of the IOP is added to the
reference "E" and preset "Z" codes and is converted by the PKCh2 to the
frequency of the signal arriving at the second input of the BU3. Signal
f_9 is fed to the first input of the BU2. The spatial position of the SE
is stabilized in the "Stabilization" mode with the simultaneous
capability of rotating it with respect to the platform of the gyro
stabilizer in the gyro unit by the angle determined by the code "Z."
The "Correction" mode, in which the positioning system of the element to
be stabilized operates from control module BU4 by signals of the
relative angular position sensor of the element to be stabilized and the
onboard gyro unit VGB, is provided for periodic setting of the element
to be stabilized to the horizontal position and to compensate the effect
of the drift of the gyro unit. Let us consider one of the variants of
realizing the IOP.

The output information in the device is presented in binary code with
determination of the number sign. The device is designed to use a dial
with marks $N_\text{Л} = 1,800$, which permits one to measure the angular error in

239

the range of ±102° at the adopted digit capacity of the digital data processing assemblies. The maximum value of the measured error can be brought to 180° $(1 - N_\text{Л}/2)$ if the digit capacity is increased. The use of the device in automatic control systems permits one to achieve a positioning accuracy at the level of ±6'. An increase of accuracy is related to an increase of the number of marks on the dial.
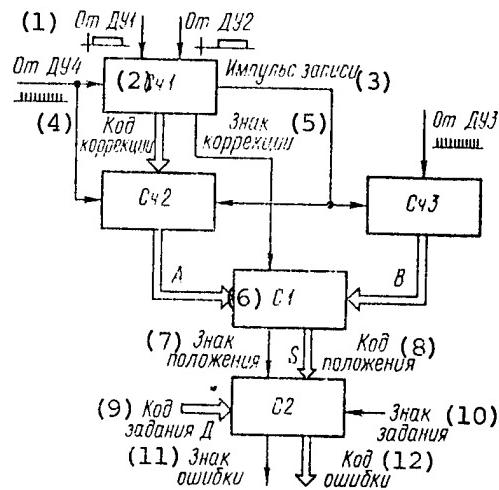

Figure 6.21. Information Processing Circuit in Mirror Position Control System

KEY:

1.	From data-angle transmitter	7.	Position sign
2.	Counter	8.	Position code
3.	Record pulse	9.	Preset code
4.	Correction code	10.	Preset sign
5.	Correction sign	11.	Error sign
6.	Adder	12.	Error code

The device (Figure 6.21) includes a circuit for initial setting and correction of the code and sign of the angular error Sch1. This circuit generates a record pulse, by which the initial conditions in counters Sch2 and Sch3 are established. Pulses are taken from angle-data transmitters DU1 and DU2. A signal of the sign of the correction code is generated as a function of the relative position of these pulses. The level of a logic 1 is taken here and further as the "plus" sign. The pulses following from the output of transmitter DU4 at frequency f = 900 $ω/π$ are calculated by counter Sch1. Counter Sch1 is set to zero at number of pulses of transmitter DU4 N = 511 and receives authorization to operate in the counting mode according to the pulse front from DU1 or due to a decrease of the pulse from DU2. If the number of pulses of transmitter DU4 is N < 511 and if the conditions for the pulses of transmitters DU1 and DU2 using delay lines are formed

240

under the same conditions, the pulses of code record, correction sign and setting the information to zero are formed in Sch1.

Counters Sch2 and Sch3 determine the current position of the information systems with respect to the dial. Variation of the codes recorded in counters Sch2 and Sch3 is presented on the working diagrams (Figure 6.22). It is assumed that the dial rotates at constant speed with respect to the first information system, which corresponds to a linear increase of the code in Sch2. The second information system performs arbitrary angular displacements. The information in Sch3 is set to zero and the correction code in Sch2 is recorded to eliminate the possibility of overflow of the counters by the recording pulse (see Figure 6.21).

The modulus code of relative angular position of the information systems is determined by adder S1. The direct output code of Sch2 and the inverse code of Sch3 are used. Adder S1 performs the arithmetic operation $|A| - |B|$ with regard to the ratio of codes A and B.

Determination of the position of the second information system not only with respect to the zero angle (see Figure 6.21), but also with respect to an arbitrary angle determined by code D and by the preset sign is determined to include an automatic control system in the device. An S2, which performs the arithmetic operation D - S, is introduced into this device. If signs D and S are identical, the calculation is made similar to the calculations in adder S1. If the signs of D and S are different, S2 operates like an ordinary adder with the exception of carry operations and inversion of codes.

Scanning systems. One of the methods of improving the image quality in optical systems is to use optical-mechanical scanning of the image by a scanner. Only part of the image near the principal optical axis of the device, where the aberrations introduced by the objective are minimal, is used. Moreover, this optical system permits one to encompass a large field of objects and does not introduce the distortions typical for wideband objectives.

However, introduction of scanners into the optical system results in the need to compensate for the resulting displacement of the image in the focal plane of the objective. This can be achieved by corresponding displacement of the photodetector provided there is accurate synchronization of the motion of the image and of the photodetector.

However, introducing a scanner into the optical system results in a need to compensate the resulting displacement of the image in the focal plane of the objective. This can be achieved by the corresponding displacement of the photodetector provided there is accurate synchronization of the motion of the image and photodetector.
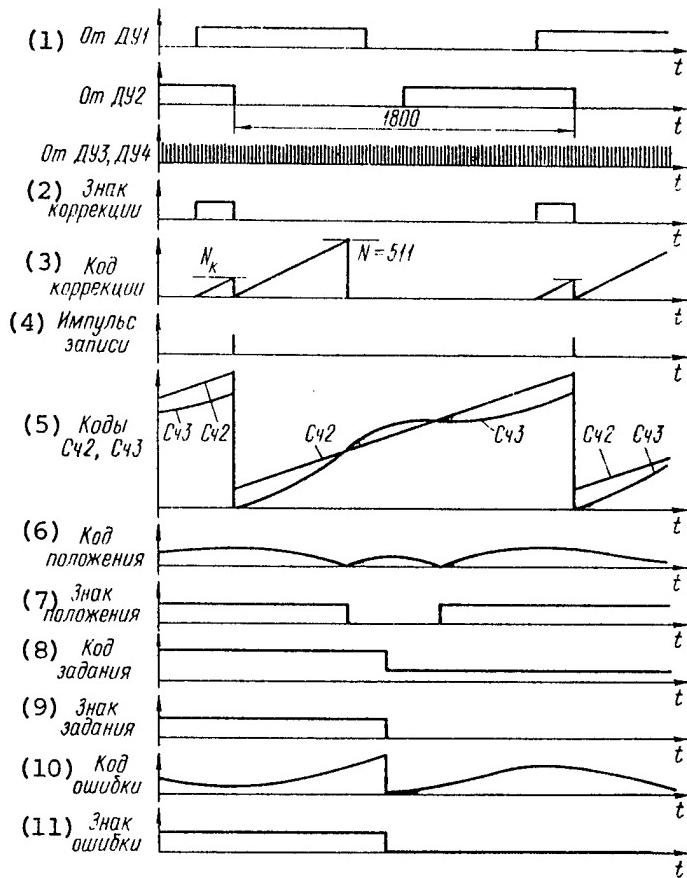
Figure 6.22.   Graphs of Time Processes in System

KEY:

1.	From data-angle transmitter	7.	Position sign
2.	Correction sign	8.	Preset code
3.	Correction code	9.	Preset sign
4.	Recording pulse	10.	Error code
5.	Codes of Sch2 and Sch3	11.	Error sign
6.	Position code		

Mirrors, prisms, optical wedges and so can be used as the scanning element, which permits one to change the direction of the incident ray in space. Let us consider the simplest scanner, shown in Figure 6.23, a. A flat mirror 1, rotating in front of an objective 2, scans the plane of objects, determined by the scanning angle $\pm \varphi_c$. An image of the field of objects, displaced at rate v_{H3}, will be formed in the focal plane 3 of the objective. The entire device is mounted on a moving base, moving at speed v_0 at altitude H_0. The band of coverage in the flight direction is determined by the width d of the film 4.
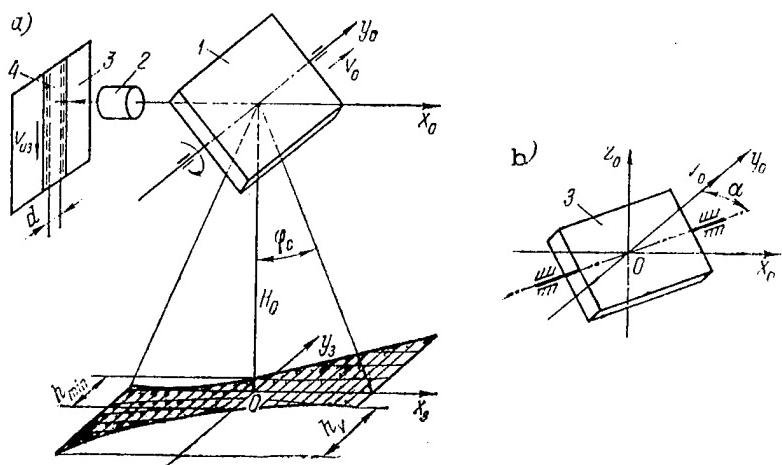
Figure 6.23. Layout of Scanner:
a--formation of image; b--rotation of mirror axes;
1--mirror; 2--objective; 3--focal plane;
4--photographic film

Let us have $h = dH_0/f \cos \varphi$, where φ is the actual scanning angle, for the coverage bandwidth on the plane of objects.

Part of the previous plane must ordinarily be repeated in the next frame, which is characterized by an overlap factor $k = b/d$, where b is the width of the unrepeated part of the image.

Let us have $h_{min} = k\, dH_0/f$ for the minimum width of the band on the plane of objects. The field of coverage in the flight direction, determined by the motion speed of the base $h_v = v_0 T_ц$, where $T_ц$ is the cycle time, $T_ц = k_н dH_0/(fH_0)$, is misalgined during the cycle.

We will have for the speed of the mirror (Z) on the working path

$$\omega_p = \frac{2\varphi_c}{k_2 T_ц} = \frac{2\varphi_c v_0 f}{k_1 k_2 dH_0} ,$$

where $k_2 = t_p/T_ц$ is the coefficient of symmetry of the cycle and t_p is the time of the working path.

To reduce the amplitude of the image shift perpendicular to the frame, the rotational axis of the mirror Z is rotated by angle α toward the direction of flight (Figure 6.23, b). The scanning angle φ'_c should be

243

determined by the formula $\varphi_c' = \text{arctg}\,(\text{tg}\,\varphi_c/\cos\alpha)$ to retain the field of coverage of the object plane. We find for the angular velocity of the mirror

$$\omega_p = \frac{2 f v_0\,\text{arctg}\,(\text{tg}\,\varphi_c/\cos\alpha)}{k_1 h_2\, d H_0}.$$

This expression determines the mean value of the angular velocity Z during the working pass. The law of variation of speed on the working segment can be selected arbitrarily. The motion speed of the image in the focal plane of the objective can be found from the expression

$v_{из} = 2\omega_p f \cos\alpha.$

The rate of shift of the image perpendicular to the frame, caused by motion of the mirror, will be

$$v_{из.\,поп} = 2\omega_p f \sin\alpha.$$

The simplest problem of synchronizing the motions of the image and of the photodetector can be solved for constant speed Z on the working pass. The exposure time will be independent of the angle of rotation of the mirror. The control system of the scanning element can be designed as a stabilization system, which permits one to achieve the highest accuracy with the most complete suppression of perturbations. The law of motion Z on the segment of the reverse pass can be selected arbitrarily with regard to the requirement of minimal energy expenditures at given cycle time.

The main task to be solved by the system is formulation of the required law of variation of the coordinates of motion of Z and to provide the necessary accuracy of maintaining the coordinates of motion during the working pass.

The mirror is equipped with a motor having sensors of the coordinates of motion to be checked and with a corresponding control system to formulate the required scanning law.

The graph of the scanning law of the mirror can be divided into two qualitatively different segments. The first is the segment of the working pass of the mirror and the second is the segment of the reverse and reverse pass of the mirror. The qualitative difference of these segments occurs due to different requirements on the accuracy of the motion of the mirror. The maximum accuracy of stabilizing the coordinates of motion of the mirror must be provided on the first segment. There are no requirements on the stabilization accuracy on the second segment, and if there are no constraints of any kind, the control

system should provide only the given time of motion of the mirror. The principal possibility of organizing the system on two actuating motors and with variable structure follows from this.

Another problem in development of scanners is compensation of the torques acting on the base and occurring mainly during reverses of the mirror. All the methods of compensating the reactive moment determine the presence of an inertial element (IE). The possible methods of compensation are based on development of a moment, equal in value, but opposite in direction, acting on the base, or of kinematic uncoupling of the scanner from the base by mounting the mirror together with the actuating motor on the inertial element. Compensation of the reactive moments acting on the base may result in difficulties of achieving the required accuracy of motion of the mirror during the working pass. Comparative analysis of different versions of designing scanning devices should be conducted to find the optimal solutions according to the criteria of accuracy and of the minimal moments acting on the base.

There is also the problem of improving the mass and size parameters of the scanner and of reducing the consumed power. This problem is very timely, for example, in the case of installing the device on an air/spacecraft. One of the methods of reducing the power losses in the scanner is to use various types of power recovery units (mechanical, electromechanical and so on). Selection of the recovery unit obviously determines the design of the entire device to a significant degree.

Let us consider realization of several scanners, distinguished by the method of preset motions and by the method of compensating the torque reaction acting on the base according to the above problems.

Scanner with mechanical recovery unit. A mechanical recovery unit is designed to reverse the mirror by exchanging the mechanical energy between the mirror and the inertial element through a flexible mechanical coupling introduced between them. A flywheel (M) can be used as the inertial element. This recovery unit permits one to reduce considerably the power consumed by the scanner (US), since the efficiency of the flexible coupling is usually much higher than that of the energy converters used to recover electric power with the electromechanical method of reversal.

The following mode is typical for the operation of this type of scanner. The flexible coupling between the mirror and flywheel, which are rotated in opposite directions, is switched on after the completion of the working pass of the mirror and power is exchanged between them. The sign and value of the speed of the mirror and flywheel are changed. The flexible coupling is switched off at the moment after reversal when the speed of the mirror and flywheel reach a maximum value. The mirror and flywheel then move separately. The flexible coupling is again switched on at a signal of the position data-angle transmitter, which provides information that the mirror has passed a given angle on the segment of the reverse pass, and the mirror and flywheel are again reversed. The

245

mirror is set at the initial point of the segment of the working pass at the end of the cycle.

The motion of the mirror and flywheel in the reverse segment are described in the first approximation by equations of dynamics of a two-mass flexible mechanical system:

$$
\begin{aligned}
J_\mathfrak{s}\ddot{\varphi}_\mathfrak{s} + c(\varphi_\mathfrak{s} - \varphi_\mathrm{M}) &= 0; \\
J_\mathrm{M}\ddot{\varphi}_\mathrm{M} - c(\varphi_\mathfrak{s} - \varphi_\mathrm{M}) &= 0,
\end{aligned}
\quad \Big|
\tag{6.9}
$$

where J_3 and J_M are the moments of inewrtia of the mirror and flywheel, respectively, c is the stiffness of the flexible coupling, and φ_3 and φ_M are the angular position of the mirror and flywheel, respectively.

Let us be given the initial conditions in the form: $\dot{\varphi}_\mathfrak{s} = \dot{\varphi}_{\mathfrak{s}0}$; $\dot{\varphi}_\mathrm{M} = \dot{\varphi}_{\mathrm{M}0}$; $\varphi_\mathfrak{s} = \varphi_\mathrm{c}$; $\varphi_\mathrm{M} = \varphi_{\mathrm{M}0}$ at t = 0, where $\dot{\varphi}_{30}$ is the speed of the mirror on the segment of the working pass, $\dot{\varphi}_{M0}$ is the speed of the flywheel when the mirror is moving on the segment of the working pass, φ is the scanning angle, and φ_{M0} is the angle of displacement of the flywheel during the working pass of the mirror.

The solution of equations of (6.9) will then have the form:

$$
\varphi_\mathfrak{s} = J_\mathrm{M} \frac{\dot{\varphi}_{30} - \dot{\varphi}_{\mathrm{M}0}}{\omega_y(J_\mathrm{M} + J_\mathfrak{s})} \sin \omega_y t + \frac{J_\mathfrak{s}\dot{\varphi}_{30} + J_\mathrm{M}\dot{\varphi}_{\mathrm{M}0}}{J_\mathfrak{s} + J_\mathrm{M}} t + \varphi_\mathrm{c};
$$

$$
\varphi_\mathrm{M} = J_\mathfrak{s} \frac{\dot{\varphi}_{\mathrm{M}0} - \dot{\varphi}_{30}}{\omega_y(J_\mathrm{M} + J_\mathfrak{s})} \sin \omega_y t + \frac{J_\mathfrak{s}\dot{\varphi}_{30} + J_\mathrm{M}\dot{\varphi}_{\mathrm{M}0}}{J_\mathfrak{s} + J_\mathrm{M}} t + \varphi_{\mathrm{M}0},
$$

where $\omega_y = \sqrt{c\dfrac{J_\mathfrak{s} + J_\mathrm{M}}{J_\mathfrak{s} J_\mathrm{M}}}$ is the frequency of elastic vibrations.

We find for the speeds of the mirror and flywheel, respectively,

$$
\dot{\varphi}_\mathfrak{s} = J_\mathrm{M} \frac{\dot{\varphi}_{30} - \dot{\varphi}_{\mathrm{M}0}}{J_\mathrm{M} + J_\mathfrak{s}} \cos \omega_y t + \frac{J_\mathfrak{s}\dot{\varphi}_{30} + J_\mathrm{M}\dot{\varphi}_{\mathrm{M}0}}{J_\mathfrak{s} + J_\mathrm{M}};
$$

$$
\dot{\varphi}_\mathrm{M} = J_\mathrm{M} \frac{\dot{\varphi}_{30} - \dot{\varphi}_{\mathrm{M}0}}{J_\mathrm{M} + J_\mathfrak{s}} \cos \omega_y t + \frac{J_\mathfrak{s}\dot{\varphi}_{30} + J_\mathrm{M}\dot{\varphi}_{\mathrm{M}0}}{J_\mathfrak{s} + J_\mathrm{M}}.
$$

The mirror and flywheel will reach the maximum speed $\dot{\varphi}_{31}$ and $\dot{\varphi}_{M1}$ after reversal at moment of time $t_1 = \pi/\omega_y$. The values of $\dot{\varphi}_{31}$ and $\dot{\varphi}_{M1}$ are determined by the formulas:

$$\dot{\varphi}_{31} = \frac{2J_M \dot{\varphi}_{M0} + \dot{\varphi}_{30}(J_3 - J_M)}{J_M + J_3};$$
$$\dot{\varphi}_{M1} = \frac{2J_3 \dot{\varphi}_{30} + \dot{\varphi}_{M0}(J_M - J_3)}{J_M + J_3}. \qquad (6.10)$$

The mirror and flywheel will move at these speeds after the flexible coupling on the segment of the reverse pass has been switched off. The operating time of the flexible coupling is $t_1 = \pi/\omega_4$. The angle traveled by the mirror and flywheel during the operating time t_1 of the flexible coupling, is determined by the equations:

$$\varphi_{31} = \frac{J_3 \dot{\varphi}_{30} + J_M \dot{\varphi}_{M0}}{J_3 + J_M} \frac{\pi}{\omega_y} + \varphi_c;$$

$$\varphi_{M1} = \frac{J_3 \dot{\varphi}_{30} + J_M \dot{\varphi}_{M0}}{J_3 + J_M} \frac{\pi}{\omega_y} + \varphi_{M0}.$$

The angular misalignment between the mirror and flywheel must be determined to calculate the parameters of the flexible coupling. This can be done if one assumes that the angular positions of the mirror and flywheel are equal to zero at the moment the flexible coupling is switched on, i.e., at $t = 0$. The equation of the angular misalignment between the mirror and flywheel will then have the form

$$\varphi_3 - \varphi_M = \frac{\dot{\varphi}_{30} - \dot{\varphi}_{M0}}{\omega_y} \sin \omega_y t.$$

The maximum angular misalignment at $\omega_y t = \pi/2$ will obviously be equal to $(\varphi_3 - \varphi_M)_{max} = (\dot{\varphi}_{30} - \dot{\varphi}_{M0})/\omega_y$.

The derived equations fully describe the motion of the mirror and flywheel when the flexible coupling is first switched on. The mirror and flywheel will move at speeds determined by expressions (6.10) after the flexible coupling has been switched off at moment of time $t_1 = \pi/\omega_y$ to moment of time t_2 of the second time the flexible coupling is switched on. The equations of motion on this segment will have the form:

$$\varphi_3 = \varphi_{31}(t - t_1); \quad \dot{\varphi}_M = \dot{\varphi}_{M1}(t - t_1);$$

$$\dot{\varphi}_3 = \dot{\varphi}_{31}; \quad \dot{\varphi}_M = \dot{\varphi}_{M1}; \quad \text{at} \quad t_1 < t < t_2.$$

The flexible coupling is switched on for the second time at moment t_2 and the initial system of equations (6.12) with variable initial conditions will be valid for the motion of the element to be stabilized and the inertial element:

$$\varphi_{32} = \varphi_{31} + \dot{\varphi}_{31}(t_2 - t_1); \quad \varphi_{M2} = \varphi_{M1} + \dot{\varphi}_{M1}(t_2 - t_1);$$

$$\dot{\varphi}_{32} = \dot{\varphi}_{31}; \quad \dot{\varphi}_{M2} = \dot{\varphi}_{M1} \quad \text{at} \quad t = t_2.$$

Since the operating time of the flexible coupling is independent of the initial conditions, it will be equal to the time the coupling is first switched on upon switching on the flexible coupling a second time, i.e., $t = \pi/\omega_y$.

The moment of time at which the flexible coupling is switched off after it is switched on a second time is determined by the expression $t_3 = t_2 + \pi/\omega_y$.

The total reversal time of the mirror Z is determined as the sum of the operating time of the flexible element and of the time of the return pass of the element to be stabilized $t_{pen} = 2\pi/\omega_y + (t_2 - t_1)$. The mirror and flywheel should cover angles equal to $\varphi_{33} = -\varphi_c; \quad \varphi_{M3} = -\varphi_{M0}$.

during the reversal time. This condition follows from the cyclic nature of operation of the scanner (US). The following equations can then be written for the law of motion of the mirror during one cycle:

$$\varphi_3 = J_M \frac{\dot{\varphi}_{30} - \dot{\varphi}_{M0}}{\omega_y(J_M + J_3)} \sin \omega_y t + \frac{J_3 \dot{\varphi}_{30} + J_M \dot{\varphi}_{M0}}{J_3 + J_M} t + \varphi_c,$$

$$\text{at} \quad 0 < t < t_1;$$

$$\varphi_3 = \dot{\varphi}_{31}(t - t_1) + \frac{J_3 \dot{\varphi}_{30} + J_M \dot{\varphi}_{M0}}{J_3 + J_M} \frac{\pi}{\omega_y} + \varphi_c,$$

$$\text{at} \quad t_1 < t < t_2;$$

$$\varphi_3 = J_M \frac{\dot{\varphi}_{31} - \dot{\varphi}_{M1}}{\omega_y(J_M + J_3)} \sin \omega_y \left(t - t_{pen} + \frac{\pi}{\omega_y}\right) +$$

$$+ \frac{J_3 \dot{\varphi}_{31} + J_M \dot{\varphi}_{M1}}{J_3 + J_M}\left(t - t_{pen} + \frac{\pi}{\omega_y}\right) -$$

$$- \frac{J_3 \dot{\varphi}_{31} + J_M \dot{\varphi}_{M1}}{J_3 + J_M} \frac{\pi}{\omega_y}, \quad t_2 < t < t_{pen};$$

$$\varphi_3 = \dot{\varphi}_{30}(t - t_{pen}), \quad \text{at} \quad t_{pen} < t < T_{II}.$$

248

Accordingly, we find the following for the motion speed of the mirror:

$$\dot{\varphi}_3 = J_M \frac{\dot{\varphi}_{30} + \dot{\varphi}_{M0}}{J_M + J_3} \cos \omega_y + \frac{J_3 \dot{\varphi}_{30} + J_M \dot{\varphi}_{M0}}{J_3 + J_M}, \quad \text{at} \quad 0 < t < t_1;$$

$$\dot{\varphi}_3 = \dot{\varphi}_{31}, \quad \text{at} \quad t_1 \leqslant t \leqslant t_2;$$

$$\dot{\varphi}_3 = J_M \frac{\dot{\varphi}_{31} - \dot{\varphi}_{M1}}{J_M + J_3} \cos \omega_y \left(t - t_p + \frac{\pi}{\omega_y} \right) +$$

$$+ \frac{J_3 \dot{\varphi}_{31} + J_M \dot{\varphi}_{M0}}{J_3 + J_M}, \quad \text{at} \quad t_2 < t \leqslant t_{pen};$$

$$\dot{\varphi}_3 = \dot{\varphi}_{30}, \quad \text{at} \quad t_{pen} < t \leqslant T_{II},$$

where $t_1 = \pi/\omega_{II}$; $t_2 = t_{pen} - 2\pi/\omega_y$; t_{pen} is the given reversal time of the mirror, and T_{II} is the cycling time.

The angular position of the mirror at moments of time t_1 and t_2 is determined by the expressions:

$$\varphi_{31} = \frac{J_3 \dot{\varphi}_{30} + J_M \dot{\varphi}_{M0}}{J_3 + J_M} \frac{\pi}{\omega_y} + \varphi_c;$$

$$\varphi_{32} = - \frac{J_3 \dot{\varphi}_{30} + J_M \dot{\varphi}_{M0}}{J_3 + J_M} \frac{\pi}{\omega_y}.$$

Based on the last expression, one can calculate the parameters of the scanner, which guarantees that the flexible coupling will be switched on at the end of the working pass and that it will be switched off after reversal of the mirror. This condition will be fulfilled when the angular position of the mirror at the time the flexible coupling is first switched off coincides with the angular positions of the mirror at the time the flexible coupling is switched on the second time, i.e., when the following equalities occur:

$$\varphi_{31} = \varphi_{32} \quad \text{or} \quad \varphi_c = - \frac{J_3 \dot{\varphi}_{30} + J_M \dot{\varphi}_{M0}}{J_3 + J_M} \frac{2\pi}{\omega_y}.$$

The parameters of the scanner can be fully calculated on the basis of the derived expressions.

The considered scanner is purely conservative. No control system on the reversal segment is required for it to operate. Realistically, any similar system has losses; therefore, the scanner should be considered with regard to the losses in the flexible coupling.

249

The equations of motion of the mirror and flywheel are written in the form:

$$J_3 \ddot{\varphi}_3 + b\,(\dot{\varphi}_3 - \dot{\varphi}_\text{M}) + c\,(\varphi_3 - \varphi_\text{M}) = 0; \\ J_\text{M} \ddot{\varphi}_\text{M} - b\,(\dot{\varphi}_3 - \dot{\varphi}_\text{M}) - c\,(\varphi_3 - \varphi_\text{M}) = 0,$$

(6.11)

where b is a coefficient that determines the losses in the flexible coupling.

The solution of the system has the following form for previously established initial conditions:

$$\varphi_3 = J_\text{M}\,\frac{\dot{\varphi}_{30} - \dot{\varphi}_{\text{M}0}}{(J_\text{M} + J_3)\,\omega'_y}\,e^{-at}\,\sin \omega'_y t + \frac{\dot{\varphi}_{30} J_3 + J_\text{M}\dot{\varphi}'_{\text{M}0}}{J_3 + J_\text{M}}\,t + \varphi_\text{c}; \\ \varphi_\text{M} = J_3\,\frac{\dot{\varphi}_{\text{M}0} - \dot{\varphi}_{30}}{(J_\text{M} + J_3)\,\omega'_y}\,e^{-at}\,\sin \omega'_y t + \frac{\dot{\varphi}_{30} J_3 + J_\text{M}\dot{\varphi}'_{\text{M}0}}{J_3 + J_\text{M}}\,t + \varphi'_{\text{M}0},$$

(6.12)

where ω'_y is the vibration frequency of the flexible system, equal to

$$\omega'_y = \omega_y \sqrt{1 - \frac{b^2}{4c}\,\frac{J_3 + J_\text{M}}{J_3 J_\text{M}}}; \quad a = -\frac{b\,(J_3 + J_\text{M})}{2J_3 J_\text{M}}.$$

One can find the equations for the motion speeds of the mirror and flywheel from expressions (6.12) after differentiation:

$$\dot{\varphi}_3 \approx J_\text{M}\,\frac{\dot{\varphi}_{30} - \dot{\varphi}_{\text{M}0}}{J_\text{M} + J_3}\,e^{-at}\,\cos \omega'_y t + \frac{\dot{\varphi}_{30} J_3 + \dot{\varphi}'_{\text{M}0} J_\text{M}}{J_3 + J_\text{M}}; \\ \dot{\varphi}_\text{M} \approx J_3\,\frac{\dot{\varphi}_{\text{M}0} - \dot{\varphi}_{30}}{J_\text{M} + J_3}\,e^{-at}\,\cos \omega'_y t + \frac{\dot{\varphi}_{30} J_3 + J_\text{M}\dot{\varphi}_{\text{M}0}}{J_3 + J_\text{M}}.$$

It is obvious from the derived expressions that the speeds of the mirror and flywheel will differ from those for a conservative system after the flexible coupling has been switched off. The speed of the mirror after the second reversal will be less by $\Delta\dot{\varphi} \approx \dot{\varphi}_{30}\,|1 - \exp\,(-a2\pi/\omega'_y)|$ on the working segment. An additional torque should be applied to bring the mirror to the given speed $\dot{\varphi}_{30}$ from the direction of the actuating motor of the motion control system of the mirror on the working segment. The accuracy of motion of the mirror on the initial segment of the working

pass thus deteriorates. To correct this negative phenomenon, the scanner is supplied with a control system of reversing of the mirror.

System for continuous control of mirror speed on reverse pass segment. This system permits one to monitor and control the motion of the mirror according to the required law of motion. The moments required to formulate this law of variation of speed are developed by the actuating motors of the mirror and flywheel and also by the flexible coupling of the mechanical recovery unit.

This system is described by the following equations, similar to equations (6.9):

$$\left.\begin{array}{l} J_{3}\ddot{\varphi}_{3} + b\,(\dot{\varphi}_{3} - \dot{\varphi}_{M}) + c\,(\varphi_{3} - \varphi_{M}) = M_{1}(t) + M_{B1}(t); \\ J_{M}\ddot{\varphi}_{M} - b\,(\dot{\varphi}_{3} - \dot{\varphi}_{M}) - c\,(\varphi_{3} - \varphi_{M}) = M_{2}(t) + M_{B2}(t), \end{array}\right\} \qquad (6.13)$$

where $M_1(t)$ and $M_2(t)$ are the moments of the actuating motors of the mirror and inertial element, respectively, and $M_{B1}(t)$ and $M_{B2}(t)$ are perturbing moments applied to the mirror and flywheel, respectively.

Introducing the Laplace transform, this system of equations is rewritten in the form:

$$J_{3}p^{2}\varphi_{3} + bp\,(\varphi_{3} - \varphi_{M}) + c\,(\varphi_{3} - \varphi_{M}) = M_{1}(p) + M_{B1}(p);$$
$$J_{M}p^{2}\varphi_{M} + bp\,(\varphi_{M} - \varphi_{3}) + c\,(\varphi_{M} - \varphi_{3}) = M_{2}(p) + M_{B2}(p).$$

After simple transformations, one can find the transfer functions of the coordinates of the system:

$$W_{11}(p) = \frac{\varphi_{3}(p)}{M_{1}(p)} = \frac{J_{M}p^{2} + bp + c}{J_{3}J_{M}p^{2}\left[p^{2} + bp\,(J_{3} + J_{M})/(J_{3}J_{M}) + c\,[(J_{3} + J_{M})/(J_{3}J_{M})]\right]};$$

$$W_{22}(p) = \frac{\varphi_{M}(p)}{M_{2}(p)} = \frac{J_{3}p^{2} + bp + c}{J_{3}J_{M}p^{2}\left[p^{2} + bp\,(J_{3} + J_{M})/(J_{3}J_{M}) + c\,[(J_{3} + J_{M})/(J_{3}J_{M})]\right]};$$

$$W_{12}(p) = \frac{\varphi_{M}(p)}{M_{1}(p)} = \frac{bp + c}{J_{3}J_{M}p^{2}\left[p^{2} + bp\,(J_{3} + J_{M})/(J_{3}J_{M}) + c\,[(J_{3} + J_{M})/(J_{3}J_{M})]\right]};$$

$$W_{21}(p) = \frac{\varphi_{3}(p)}{M_{2}(p)} =$$

$$= \frac{bp + c}{J_{3}J_{M}p^{2}\left(p^{2} + b\,(J_{3} + J_{M})p/(J_{3}J_{M}) + c\,[(J_{3} + J_{M})/(J_{3}J_{M})]\right)}.$$

It is obvious from the given expressions that the effect of the resonant link, taken into account in the transfer function according to the

251

control action $W_1(p)$, must be compensated to close the feedback with respect to speed or position of the mirror.

The frequency of this resonance at real scanning cycling time is in the low-frequency region with respect to the possible cut-off frequency of the closed system. It is easiest to compensate resonance by introducing coupling with respect to the torques of the actuating motors of the mirror and flywheel.

Let us determine the coupling coefficients with respect to torque. Let $M_2(p) = kM_1(p)$ and one can then write for the transfer function of the position of the mirror according to the control moment:

$$W_3(p) = W_{11}(p) + kW_{21}(p) =$$
$$= \frac{p^2 + bp(1 + k)/J_M + c(1 + k)/J_M}{J_3 p^2 [p^2 + bp(J_3 + J_M)/(J_3 J_M) + c[(J_3 + J_M)/(J_3 J_M)]]}.$$

One can establish from the derived expression that resonance is compensated if $k = J_M/J_3$. The transfer function on the control action at selected k will be equal to

$$W_3(p) = \frac{\varphi_3(p)}{M_1(p)} = \frac{1}{J_3 p^2}.$$

The torque coupling coefficient is independent of the parameters of the flexible coupling, but is related only to the moments of inertia of the mirror and flywheel, which do not change their values. Thus, one can recognize stable compensation of resonance in the control object and one can close the system at the cut-off frequency, lying in a large frequency range, which is unlimited by the resonance frequency of the flexible coupling. The control system reswitches the structure, according to the position of the mirror.

Scanners with reducer coupling between motor and scanning element. Realizing the law of scanning at short cycling time requires development of the drive of the mirror with large torque. This torque is developed by the drive mainly during reversal, i.e., the moment is pulsed in nature. On the other hand, the motion speeds of the mirror are comparatively low; therefore, either torque motors or stepdown reducer gears between the serial high-speed motor and mirror must be used to organize a drive with acceptable efficiency.

Some advantages both from the viewpoint of the mass and size characteristics of the entire device and from the viewpoint of compensating the torque reactions on the base can be found in the second case.

252

Let us consider the kinematic layout of a scanner using the reducer shown in Figure 6.24.
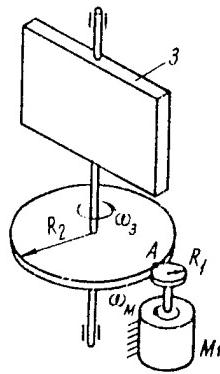
Figure 6.24. Scanner With Reducer Drive

The device consists of a scanning mirror Z, motor M1 and friction reducer that connects these elements.

Let the motor develop torque $M_{\text{ДВ}}$. Dut to the effect of this moment, the motor rotor picks up speed at acceleration ϵ_1, whereas the mirror Z will pick up speed at acceleration:

$$\epsilon_2 = i\epsilon_1, \tag{6.14}$$

where i is the gear ratio of the reducer.

One can write $M_{\text{ДВ}} = \epsilon_1 (J_1 + i^2 J_2)$, where J_1 and J_2 are the moments of inertia of the mass, related to the motor rotor and to the rotational axis of the mirror, respectively, can be written for the torque of the motor. One can write the following with respect to expression (6.14) for the torque of the motor

$$M_{\text{ДВ}} = \epsilon_2 (J_1 + i^2 J_2)/i. \tag{6.15}$$

One can determine from formula (6.15) the extreme values of the torque of the motor with respect to parameter i, which occur at gear ratio

$$i_{\text{ОПТ}} = \sqrt{J_1/J_2}$$

$$M_{\text{ДВ}}^{\min} = 2\epsilon_2 \sqrt{J_1 J_2}. \tag{6.16}$$

253

The necessary torque of the motor must be selected on the basis of expression (6.16) according to the known moment of inertia and required acceleration of the mirror.

If the reducerless version is compared to the considered version, the torques of the motors will be related to each other in the following manner:

$$\frac{M_{\text{дв}}}{M_{\text{дв б}}} = \frac{2\varepsilon_2 \sqrt{J_1 J_2}}{\varepsilon_2 (J_1 + J_2)} \approx 2 \sqrt{\frac{J_1}{J_2}},$$

where $M_{\text{дв б}} = \varepsilon_2 (J_1 + J_2)$ is the required torque of the motor in the reducerless version.

One can assume that $J_1 \ll J_2$ for the considered case, therefore, a considerable advantage in the torque of the drive motor of the mirror can be achieved when using the reducer version.

Compensation of reaction torques acting on base upon image stabilization. The presence of cyclicity or other forms of motion of the optical elements (OE) results in the need to develop angular accelerations, which are realized by using the corresponding drive moments of the optical elements. According to Newton's third law, a moment equal in value and opposite in sign to that applied to the optical element will be applied to the base from the direction of the drive. The moment applied to the base is called the reactive moment.

Let us determine the reactive moment acting on the base at known parameters of motion of the optical element.

Let the control system guarantee variation of the angular velocity of the optical element according to known law $\omega_{0.9}(t)$; the following moment should then be applied to the optical element from the direction of the actuating motor

$$M_{\text{дв}}(t) = J_{0.9} \frac{d\omega_{0.9}(t)}{dt} + M_c(t), \qquad (6.17)$$

where $J_{0.9}$ is the moment of inertia of the optical element about the rotational axis and $M_c(t)$ is the moment of resistance occurring between the optical element and the base (the effect of the other perturbing elements is disregarded).

The moments of the motor and the moment of resistance will then act on the base.

Hence, we have for the reactive moment on the base

$$M_{\text{p}} = - M_{\text{дв}}(t) + M_{\text{c}}(t).$$

With regard to expression (6.17), we find

$$M_{\text{p}} = - J_{\text{o. э}} \frac{d\omega_{\text{o. э}}(t)}{dt}. \qquad (6.18)$$

The base is displaced due to the action of this moment by the law determined by the equation

$$J_{\text{o}} \frac{d\omega_{\text{o}}}{dt} = M_{\text{p}}. \qquad (6.19)$$

Having substituted expression (6.19) into equation (6.18), we find

$$\frac{d\omega_{\text{o}}}{dt} = - \frac{J_{\text{o. э}}}{J_{\text{o}}} \frac{d\omega_{\text{o. э}}}{dt}. \qquad (6.20)$$

The angular rotational speed of the base can be found by integration of expression (6.20)

$$\omega_{\text{o}}(t) = - \frac{J_{\text{o. э}}}{J_{\text{o}}} \omega_{\text{o. э}}(t).$$

The derived expression can be used to formulate the criterion of the extent of compensation in the form

$$A < F \left[\omega_{\text{o}}(t), f_{\text{к}}(t) \right], \qquad (6.21)$$

where F is the estimate of the function, A is the permissible parameter of displacement of the object, and $f_{\text{K}}(t)$ is a function of the action of the compensating device.

It was established above that one of the requirements placed on scanners is the need to compensate the moments acting on the base. In the reducerless version, besides the moment applied to the base and caused by operation of the mirror drive, there is an additional moment due to the characteristics of the kinematic layout of the device.

Let us consider Figure 6.24 to determine this moment. A force
determined by the expression $F = J_2\epsilon_2/R_2$, where R_2 is the radius of the
reducer gear connected to the mirror, should be applied to the mirror so
that it speeds up at angular acceleration ϵ_2, in $(\cdot)A$. By considering
the moments about the rotational axes of the motor and mirror, it is
easy to ascertain that forces equal to force F will be applied to these
axes. The directions of the effect of these forces are such that they
result in the occurrence of a moment acting on the base in a direction
opposite to the effect of the moment of the motor. The value of this
moment is determ,ined in the form $M_K = F(R_1 + R_2)$, where R_1 is the radius
of the reducer gear, connected to the motor.

Multiplying out F, we find $M_K = J_2\epsilon_2(i + 1)$. The total moment acting on
the base can be found from the expression

$$M_p = M_{\text{дв}} - M_{\text{к}} = \epsilon_2\left(\frac{J_1}{i} + kJ_2\right) - J_2\epsilon_2(1 + i) = \epsilon_2\left(\frac{J_1}{i} - J_2\right).$$

$$(6.22)$$

It follows from expression (6.22) that the reactive moments acting on
the base can be compensated for the reducerless version of a drive
without any additional measures whatever. The gear ratio of the
reducer, to guarantee condition $M_p = 0$, should be equal to

$$i = J_1/J_2.$$

$$(6.23)$$

The moment which the motor should develop is determined after
substituting the value of the gear ratio with respect to formula (6.23)
into expression (6.15) $M_{\text{дв}} = \epsilon_2 J_2(1 + i) \approx \epsilon_2 J_2$ at $i \ll 1$.
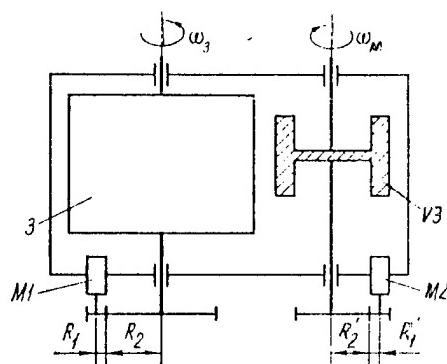
Figure 6.25. Scanner With Compensation of
Reactive Moment on Base

The use of a reducer coupling with the scanning element is one of the directions in development of various types of layouts for compensating the moments acting on the base. For example, the layout of a scanner, in which the mirror is connected to the motor directly, while the mirror is mechanically connected to the flywheel through a reducer to compensate for the moments acting on the base, is presented in a patent. (Footnote) (British patent 1,520,845) It is obvious that all the above formulas are valid for this case, but the motor should be selected with respect to torque according to acceleration ϵ_1 and its moment of inertia J_1. The necessary moment of the motor in this device is determined from the formula

$$M'_{\text{дв}} = \epsilon_1 \left(J_1 + \frac{J_1^2}{J_2} \right) = \epsilon_1 \frac{J_1}{J_2} (J_1 + J_2).$$

If one takes into account that the moment of inertia of the flywheel is selected from the relation $J_2 \ll J_1$ to reduce the overall dimensions and mass of the device, then the motor should develop a significant torque. It is one of the deficiencies of the considered device. Another disadvantage is the circumstance that the moments of resistance acting on the flywheel shaft result in motion with considerable amplification due to the large gear ratio of the reducer. This inevitably causes a reduction of the motion accuracy of the scanning element.

The electric drive motor of the mirror is designed in some practical cases for minimum developed moment with respect to formula (6.16), while the moment acting on the base is compensated by developing the design shown in Figure 6.25. The reaction moment is compensated by introducing an additional inertial element IE, having a drive from an electric motor M2 and rotating in a direction opposite to the direction of rotation of the mirror. The required moment acting on the base is required for the compensating device at minimum overall dimensions and minimum moment of the motor. This requirement is equivalent to the problem of determining the maximum reaction moment at given parameters of the device. To solve this problem, let us write the expression for the acceleration of the flywheel, which follows from formula (6.15)

$$\epsilon_2 = iM_{\text{дв}}/(J_1 + J_2 i^2). \tag{6.24}$$

After substituting expression (6.24) into equation (6.22), we find:

$$M_{\text{p}} = \frac{M_{\text{дв}} i (J_1/i - J_2)}{J_1 + J_2 i^2} = \frac{M_{\text{дв}} (J_1 - iJ_2)}{J_1 + J_2 i^2}. \tag{6.25}$$

Let us find the maximum moment acting on the base with respect to the gear ratio of the reducer. To do this, let us calculate the partial derivative

$$\frac{\partial M_{\text{p}}}{\partial i} = \frac{M_{\text{дв}} \left(J_2^2 i^2 - 2J_1 J_2 i - J_1 J_2 \right)}{(J_1 + J_2 i^2)^2}.$$ (6.26)

From the condition of the extreme value of function (6.26) follows

$$J_2^2 i^2 - 2J_1 J_2 i - J_1 J_2 = 0.$$ (6.27)

The roots of equation (6.27) are equal to

$$i_{1,2} = \frac{1}{-1 \pm \sqrt{1 + J_2/J_1}}.$$ (6.28)

Study of the second derivative shows that the values of the gear ratio of the reducer, determined by expression (6.28), yield the maximum values of the reactive moment on the base.

It makes sense to consider only one value of the root

$$i = i_1 = \frac{1}{-1 + \sqrt{1 + J_2/J_1}},$$

since $i_1 > 0$.

Ordinarily, $J_2/J_1 \gg 1$; therefore, we find for the gear ratio of the reducer

$$i \approx \sqrt{J_1/J_2}.$$ (6.29)

The maximum moment applied to the base is determined at the calculated gear ratio of the reducer from expressions (6.25) and (6.29)

$$M_{\text{p}} = 0{,}5 M_{\text{дв}} \left(1 - \sqrt{J_2/J_1} \right).$$

One can determine from this expression the required moment of the inertia of the flywheel for the selected motor

$$J_2 \geqslant J_1 (2M_p/M_{\text{дп}} + 1)^2.$$

Realization of this scanner is the result of solving the following contradictory requirements: provision of minimal mass, overall dimensions and power consumption. One or another version is achieved as a function of the combination of these requirements in quantitative expression.
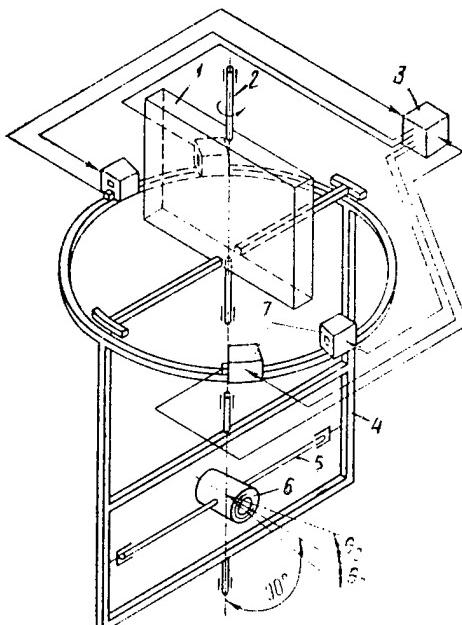
Figure 6.26. Scanner With Gyro Compensator of
Reactive Moment on Base:
1--mirror; 2--rotational axis; 3--control module;
4--outer gimbal; 5--inner gimbal; 6--gyroscope;
7--position sensors

The mirror Z can be uncoupled kinematically from the base by introducing a free gyroscope in the scanner.

A block diagram of the scanner with gyro compensator is shown in Figure 6.26. The actuating motor of the motion control system of the mirror 1 is connected to it in one or another manner and is mounted on the inner gimbal 4 of the gyroscope 6. The actuating moment develops a torque upon reversal of the mirror that decelerates the mirror and then accelerates it in the opposite direction. The same moment, but opposite

259

in sign, will be applied to the outer gimbal of the gyroscope and will cause precession of it about the axis of the inner gimbal 5. The action of the reactive moment will be compensated by the resulting gyroscopic moment, while no moment will be applied to the base. The rotor of the actuating motor is rigidly connected to the scanner, while the stator is located on the inner gimbal of the free gyroscope. The mirror moves during the working pass by inertia, while the actuating motor is switched on through the control module 3 and reverses the mirror at the end of the working segment by signals of the position sensors 7.

The corresponding control circuit and position sensor (or speed sensor) of the mirror can be used to create active control during the working pass.

The method of control on the working segment of the cycle is selected by the above principle.

The use of a free gyroscope instead of various types of flywheel as the inertial element permits one to improve considerably the mass and size characteristics of the scanner.

Let us consider the method of designing a scanner with gyro compensator. Let us assume that the kinematic connection between the outer gimbal of the gyroscope and the mirror Z is formed only for the brief reversal time, while the actuating motor (or the device that replaces it) provides reversal according to the law of elastic collision. The following moment will be applied to both the mirror and gyroscope

$$M_{\text{Д}} = k_{\text{п}} \varphi_c, \tag{6.30}$$

where $k_{\text{п}}$ is the coefficient of the equivalent stiffness of the drive, which reversal provides, and φ_c is the angle of rotation of the mirror from the point of beginning of application of the moment $M_{\text{Д}}$.

It should be noted that a spring mechanism, attached to the gimbal of the gyroscope, or two magnets with oppositely mounted poles, one of which is attached to the gimbal of the gyroscope and the other of which is attached to the mirror Z, can be used as the reverse drive of the mirror.

On the other hand, the moment $M_{\text{Д}}$ applied to the mirror causes accelerated motion of the mirror, determined by the expression

$$M_{\text{д}} = J_{\text{э}}\ddot{\varphi}_{\text{с}}, \tag{6.31}$$

where J_3 is the moment of inertia of the mirror.

Solving the system of combined equations (6.30) and (6.31), let us determine the law of variation of $M_{\text{Д}}$ as a function of time t

$$M_{\text{Д}}(t) = M_{\text{од}} \sin q_{\text{с}} t, \tag{6.32}$$

where $M_{\text{од}} = k_{\text{н}}\dot{\varphi}_{\text{с0}} \sqrt{J_{\text{с}}/k_{\text{н}}}$ is the amplitude of the moment to be applied and $q_{\text{с}} = \sqrt{k_{\text{н}}/J_{\text{с}}}$ is the frequency of free vibrations of the system.

Since moment $M_{\text{Д}}$ is applied through the motor stator to the outer gimbal of the gyroscope, this causes precession of the gyroscope rotor about the axis of the inner gimbal, determined by a system of equations with slight deviations of Θ from Θ_0

$$\left. \begin{aligned} J_{\text{н}}\ddot{\Theta} + J_{\text{р}}\Omega\dot{\psi}\cos\Theta_0 &= 0; \\ J_{\text{н}}\ddot{\psi} - J_{\text{р}}\Omega\dot{\Theta}\cos\Theta_0 &= M_{\text{Д}}(t), \end{aligned} \right\} \tag{6.33}$$

where $J_{\text{в}}$ and $J_{\text{н}}$ are the moments of inertia of the inner and outer gimbals of the gyroscope about their rotational axes, $J_{\text{р}}$ is the moment of inertia of the gyroscope rotor, Ω is the angular velocity of the gyroscope rotor, Θ is the angle of rotation of the gyroscope about the axis of the inner gimbal, ψ is the angle of rotation of the gyroscope about the axis of the outer gimbal, and Θ_0 is the initial angle of rotation of the gyroscope about the axis of the inner gimbal.

Solution of the system of these equations has the form:

$$\Theta(t) = \Theta_0 - \frac{M_{\text{од}}J_{\text{р}}\Omega\cos\Theta_0}{q_{\text{с}}\left(J_{\text{р}}^2\Omega^2\cos^2\Theta_0 - J_{\text{в}}J_{\text{н}}q_{\text{с}}^2\right)}(1 - \cos q_{\text{с}} t);$$

$$\psi(t) = \frac{M_{\text{од}}J_{\text{в}}}{\left(J_{\text{р}}^2\Omega^2\cos^2\Theta_0 - J_{\text{в}}J_{\text{н}}q_{\text{с}}^2\right)q_{\text{с}}}\sin q_{\text{с}} t.$$

The inequality $(J_{\text{р}}\Omega\cos\Theta_0)^2 \gg J_{\text{в}}J_{\text{н}}q_{\text{с}}^2,$ is fulfilled at $\Theta_0 \ll \pi/2$; therefore, simpler expressions can be written for angles $\Theta(t)$ and $\psi(t)$:

$$\Theta\left(t\right) \approx \Theta_0 - \frac{M_{0\text{д}}}{q_c J_{\text{p}} \Omega \cos \Theta_0}\left(1 - \cos q_c t\right);$$

$$\psi\left(t\right) \approx \frac{M_{0.\text{д}} J_{\text{в}}}{q_c J_{\text{p}}^2 \Omega^2 \cos^2 \Theta_0} \sin q_c t.$$

It follows from these equations that the amplitude of the rotational angle of the gyroscope is much less with respect to angle ψ than with respect to angle Θ.

Since moment $M_{\text{Д}}(t)$ acts only in the interval $0 \leq t \leq \pi/q_c$, we find after reversal of the mirror (at $t \geq \pi/q_c$):

$$\Theta^* = \Theta_0 - 2\frac{M_{0\text{д}}}{q_c J_{\text{p}} \Omega \cos \Theta_0}; \qquad \psi^* = 0.$$

Let $\Theta^* = -\Theta_0$, and then $\cos \Theta_0 \approx 1$ and the required moment of momentum of the gyroscope can then be found in the form

$$J_{\text{p}} \Omega = \frac{M_{0\text{д}}}{q_c \Theta_0} = \frac{\dot\varphi_{c0} J_{\text{э}}}{\Theta_0}.$$

We find for the ratio of the moments of inertia of the gyroscope rotor and mirror:

$$\frac{J_{\text{p}}}{J_{\text{э}}} = \frac{\dot\varphi_{c0}}{\Omega\Theta_0}.$$

Thus, the required moment of inertia of the gyroscope rotor is found to be several orders less than the moment of inertia of the mirror Z, which leads to a reduction of the mass and size of the entire device and is one of the main advantages of this type of device.

6.4. Shock Absorbers in Image Stabilization Systems

Both force and kinematic perturbations act on the optical device (OP) during its operation. (Footnote) (The section was written jointly with V. F. Putkov) The force perturbations include the moments and forces occurring upon relative displacements of the assemblies of the optical device. The kinematic perturbations appear upon angular or linear accelerations of the base with respect to the optical device. The simultaneous action of these factors is a significant feature of the optical device as an object to be cushioned. It is known on the basis

of [10, 38] that angular misalignments of the optical device affect observation quality to the greatest degree. The mean square deviation of the angular position of the optical device at given spectral densities of the force and kinematic perturbing actions can be used as the criterion of optimality when working out the design of the suspension of the optical device on shock absorbers.
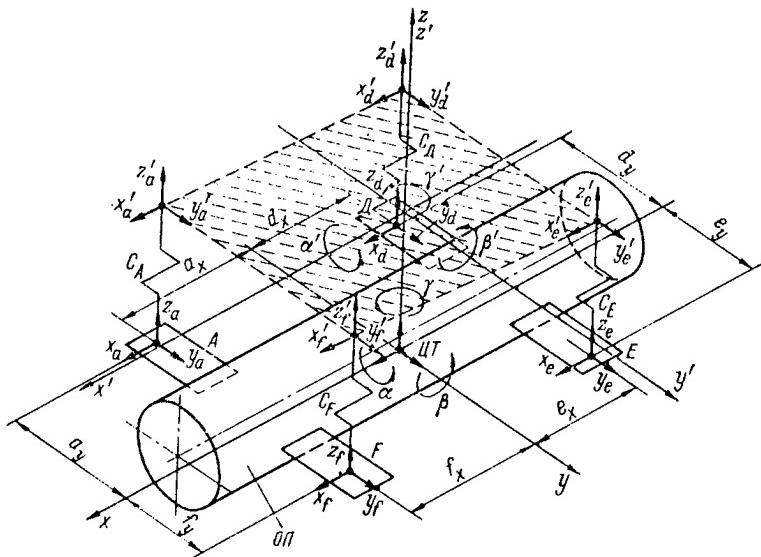
Figure 6.27. Layout of Cushioning System of
Optical Device

A layout of the suspension of an optical device to a base on four shock absorbers, which have finite stiffness coefficients c_A, c_D, c_E, and c_F with respect to axes x, y, z, is presented in Figure 6.27.

The perturbing force actions are simulated by the forces and force moments, applied to the center of gravity of the optical device and directed along axes x, y, z, with respect to these axes. All the different perturbing force actions can be transformed to this case by known relations. The perturbing kinematic actions are simulated by the vectors of displacements of the points of attachment of the shock absorbers to the carrier, directed along the unit vectors of coordinate system x', y', z'.

The vector of the generalized coordinates is formed from the rotational angles α, β, γ with respect to coordinate system x, y, z, passing through the center of gravity of the optical device, and linear misalignments of the center of gravity with respect to the axes of this coordinate system. The linear misalignment of the points of attachment of the optical device to the shock absorbers are then related to the

vector of the generalized coordinates by the coupling equations of the coordinates:

$$
\begin{aligned}
x_a &= x - a_y\gamma; & y_a &= y + a_x\gamma; & z_a &= z - a_y\alpha - a_x\beta; \\
x_d &= x + d_y\gamma; & y_d &= y - d_x\gamma; & z_d &= z - d_y\alpha + d_x\beta; \\
x_e &= x - e_y\gamma; & y_e &= y - e_x\gamma; & z_e &= z + e_y\alpha + e_x\beta; \\
x_f &= x + f_y\gamma; & y_f &= y + f_x\gamma; & z_f &= z + f_y\alpha - f_x\beta,
\end{aligned}
\quad (6.34)
$$

where a_x, a_y, d_x, d_y, e_x, e_y, f_x, f_y are the coordinates of the points of attachment of the optical device to the shock absorbers.

The mathematical description of the optical device on a flexible suspension is easier to compile in the multidimensional case by using a Lagrange equation of second kind with regard to losses in the shock absorbers

$$
\frac{d}{dt}\left(\frac{\partial T}{\partial \dot{q}_i}\right) - \frac{\partial T}{\partial q_i} + \frac{\partial \Pi}{\partial q_i} + \frac{\partial \Phi}{\partial \dot{q}_i} = N_i, \quad (6.35)
$$

where T and Π are the kinetic and potential energy of the system, Φ is a dissipative Rayleigh function, $N(i)$ are external forces, and q is a generalized coordinate.

One can generally write:

$$
T = \frac{1}{2}\sum_{i=1}^{k}\mu_i \dot{q}_i^2; \quad \Pi = \frac{1}{2}\sum_{j=1}^{g}c_j\left(q_i - q_i'\right)^2; \quad \Phi = \frac{1}{2}\sum_{j=1}^{g}b_j\left(\dot{q}_i - \dot{q}_i'\right)^2,
$$

where μ_i is the generalized coefficient of inertia, c_j is the stiffness coefficient of the j-th flexible link that connects the generalized coordinates q_i and q'_i, and b_j is a coefficient of the dissipative forces of the j-th flexible link.

The expressions for the kinetic and potential energy of the system and for the dissipative function have the form in the case under consideration:

264

$$T = \frac{1}{2} m\dot{x}^2 + \frac{1}{2} m\dot{y}^2 + \frac{1}{2} m\dot{z}^2 + \frac{1}{2} J_x \dot{\alpha}^2 + \frac{1}{2} J_y \dot{\beta}^2 + \frac{1}{2} J_z \dot{\gamma}^2;$$

$$\Pi = \frac{1}{2} c_x [(x_a - x_a')^2 + (x_d - x_d')^2 + (x_e - x_e')^2 + (x_f - x_f')^2] +$$

$$+ \frac{1}{2} c_y [(y_a - y_a')^2 + (y_d - y_d')^2 + (y_e - y_e')^2 + (y_f - y_f')^2] +$$

$$+ \frac{1}{2} c_z [(z_a - z_a')^2 + (z_d - z_d')^2 + (z_e - z_e')^2 + (z_f - z_f')^2];$$

$$\Phi = \frac{1}{2} \{ b_x [(\dot{x}_a - \dot{x}_a')^2 + (\dot{x}_d - \dot{x}_d')^2 + (\dot{x}_e - \dot{x}_e')^2 +$$

$$+ (\dot{x}_f - \dot{x}_f')^2] + \frac{1}{2} b_y [(\dot{y}_a - \dot{y}_a')^2 + (\dot{y}_d - \dot{y}_d')^2 +$$

$$+ (\dot{y}_e - \dot{y}_e')^2 + (\dot{y}_f - \dot{y}_f')^2] + \frac{1}{2} b_z [(\dot{z}_a - \dot{z}_a')^2 + (\dot{z}_d - \dot{z}_d')^2 +$$

$$+ (\dot{z}_e - \dot{z}_e')^2 + (\dot{z}_f - \dot{z}_f')^2] \},$$

(6.36)

where m is the mass of the optical device, J_x, J_y, and J_z are the polar moments of inertia of the optical device with respect to the corresponding axes, c_x, c_y, and c_z are the stiffness coefficients of the shock absorbers with respect to axes x, y, and z, b_x, b_y, and b_z are the viscosity coefficients of the shock absorbers along axes x, y, z, x'_i, y'_i, z'_i, i = a, d, e, f are linear displacements of the points of attachment of the shock absorbers to the base, which are kinematic perturbing actions for the optical device.

Solution of equation (6.35) with respect to expressions (6.36) for T, Π and Φ with regard to (6.34) results in a system of equations of dynamics of the optical device on a flexible suspension, which in operator matrix form has the form:

$$A(p) \mathbf{x}(p) = B(p) \mathbf{f}(p),$$

(6.37)

where

$$A(p) = \begin{bmatrix} A_{11}(p) & 0 & A_{13}(p) & 0 & 0 & 0 \\ 0 & A_{22}(p) & A_{23}(p) & 0 & 0 & 0 \\ A_{31}(p) & A_{32}(p) & A_{33}(p) & 0 & 0 & 0 \\ 0 & 0 & 0 & A_{44}(p) & A_{45}(p) & A_{46}(p) \\ 0 & 0 & 0 & A_{54}(p) & A_{55}(p) & A_{56}(p) \\ 0 & 0 & 0 & A_{64}(p) & A_{65}(p) & A_{66}(p) \end{bmatrix},$$

moreover:

$$A_{11}(p) = mp^2 + 4b_x p + 4c_x,$$

$$A_{13}(p) = A_{31}(p) = -(e_y + f_y - a_y - d_y)(b_x p + c_x),$$

$$A_{22}(p) = mp^2 + 4b_y p + 4c_y,$$

$$A_{23}(p) = A_{32}(p) = -(d_x + e_x - a_x - f_x)(b_y p + c_y),$$

$$A_{33}(p) = J_z p^2 + [b_x(a_y^2 + d_y^2 + e_y^2 + f_y^2) + b_y(a_x^2 + d_x^2 + e_x^2 + f_x^2)] p +$$
$$+ c_x(a_y^2 + d_y^2 + e_y^2 + f_y^2) + c_y(a_x^2 + d_x^2 + e_x^2 + f_x^2),$$

$$A_{44}(b) = mp^2 + 4b_z p + 4c_z,$$

$$A_{45}(p) = A_{54}(p) = -(a_y + d_y - e_y - f_y)(b_z p + c_z),$$

$$A_{46}(p) = A_{64}(p) = -(a_x + f_x - d_x - e_x)(b_z p + c_z),$$

$$A_{55}(p) = J_x p^2 + b_z(a_y^2 + d_y^2 + e_y^2 + f_y^2) p + c_z(a_y^2 + d_y^2 + e_y^2 + f_y^2),$$

$$A_{56}(p) = A_{65}(p) = -(d_x d_y + f_x f_y - a_x a_y - e_x e_y)(b_z p + c_z),$$

$$A_{66}(p) = J_y p^2 + b^2 + b_z(a_x^2 + d_x^2 + e_x^2 + f_x^2) p + c_z(a_x^2 +$$
$$+ d_x^2 + e_x^2 + f_x^2);$$

$\mathbf{x}(p) = |xy\gamma z\alpha\beta|^{\mathbf{T}}$ is the vector of the generalized coordinates;

$$\mathbf{B}(p) = \begin{vmatrix} 1 & 0 & 0 & 0 & 0 & 0 \cdot B_{11}(p) & 0 \\ 0 & 1 & 0 & 0 & 0 & 0 \cdot 0 & B_{22}(p) \\ 0 & 0 & 1 & 0 & 0 & 0 \cdot B_{31}(p) & B_{32}(p) \\ 0 & 0 & 0 & 1 & 0 & 0 \cdot 0 & 0 \\ 0 & 0 & 0 & 0 & 1 & 0 \cdot 0 & 0 \\ 0 & 0 & 0 & 0 & 0 & 1 \cdot 0 & 0 \end{vmatrix}$$

$$\begin{vmatrix} B_{13}(p) & 0 & 0 & 0 \\ B_{23}(p) & 0 & 0 & 0 \\ B_{33}(p) & 0 & 0 & 0 \\ 0 & B_{44}(p) & B_{45}(p) & B_{46}(p) \\ 0 & B_{54}(p) & B_{55}(p) & B_{56}(p) \\ 0 & B_{64}(p) & B_{65}(p) & B_{66}(p) \end{vmatrix},$$

and:

$$B_{11}(p) = 4b_x p + 4c_x, \quad B_{13}(p) = B_{31}(p) =$$
$$= (a_y + d_y - e_y - f_y)(b_x p + c_x),$$
$$B_{22}(p) = 4b_y p + 4c_y, \quad B_{23}(p) = B_{32}(p) = (a_x + f_x - d_x - e_x) \times$$
$$\times (b_y p + c_y),$$
$$B_{33}(p) = [b_x (a_y^2 + d_y^2 + e_y^2 + f_y^2) + b_y (a_x^2 + d_x^2 + e_x^2 + f_x^2)] p +$$
$$+ c_x (a_y^2 + d_y^2 + e_y^2 + f_y^2) + c_y (a_x^2 + d_x^2 + e_x^2 + f_x^2),$$
$$B_{44}(p) = 4b_z p + 4c_z;$$
$$B_{45}(p) = B_{54}(p) = (e_y + f_y - a_y - d_y)(b_z p + c_z),$$
$$B_{46}(p) = B_{64}(p) = (d_x + e_x - a_x - f_x)(b_z p + c_z),$$
$$B_{55}(p) = (a_y^2 + d_y^2 + e_y^2 + f_y^2)(b_z p + c_z),$$
$$B_{56}(p) = B_{65}(p) = (a_x a_y + e_x e_y - d_x d_y - f_x f_y)(b_z p + c_z),$$
$$B_{66}(p) = (a_x^2 + d_x^2 + e_x^2 + f_x^2)(b_z p + c_z);$$

$\mathbf{f}(p) = |F_x F_y M_\gamma F_z M_\alpha M_\beta x' y' \gamma' z' \alpha' \beta'|^{\mathsf{T}}$ is the vector of the perturbing

effects.

Matrices A(p) and B(p) have latticed shape and the mathematical model of the suspension of the optical device can be broken down. In this case, equation (6.37) is written in the form:

$$\boldsymbol{A_1}(p)\,\mathbf{x_1}(p) = \mathbf{B}_1(p)\,\mathbf{f}_1(p);$$
$$\boldsymbol{A_2}(p)\,\mathbf{x_2}(p) = \mathbf{B}_2(p)\,\mathbf{f}_2(p),$$

where

$$\boldsymbol{A_1}(p) = \begin{bmatrix} A_{11}(p) & 0 & A_{13}(p) \\ 0 & A_{22}(p) & A_{23}(p) \\ A_{31}(p) & A_{32}(p) & A_{33}(p) \end{bmatrix};$$

$$\boldsymbol{A_2}(p) = \begin{bmatrix} A_{44}(p) & A_{45}(p) & A_{46}(p) \\ A_{51}(p) & A_{55}(p) & A_{56}(p) \\ A_{64}(p) & A_{65}(p) & A_{66}(p) \end{bmatrix};$$

$$\mathbf{B}_1(p) = \begin{bmatrix} 1 & 0 & 0 \cdot B_{11}(p) & 0 & B_{13}(p) \\ 0 & 1 & 0 \cdot 0 & B_{22}(p) & B_{23}(p) \\ 0 & 0 & 1 \cdot B_{31}(p) & B_{32}(p) & B_{33}(p) \end{bmatrix};$$

$$\mathbf{B}_2(p) = \begin{bmatrix} 1 & 0 & 0 \cdot B_{44}(p) & B_{45}(p) & B_{46}(p) \\ 0 & 1 & 0 \cdot B_{54}(p) & B_{55}(p) & B_{56}(p) \\ 0 & 0 & 1 \cdot B_{64}(p) & B_{65}(p) & B_{66}(p) \end{bmatrix};$$

$$\mathbf{x}_1(p) = [x y \gamma]^T; \quad \mathbf{x}_2(p) = [z \alpha \beta]^T;$$
$$\mathbf{f}_1(p) = [F_x F_y M_y x' y' \gamma]^T;$$
$$\mathbf{f}_\alpha(p) = [F_z M_\alpha M_\beta z' \alpha' \beta']^T.$$

Analysis of the non-diagonal elements of matrices $A_1(p)$ and $A_2(p)$ shows that the independence of the free motions of the generalized coordinates of the system can be guaranteed if the specific relations between the point coordinates of the suspension of the optical device on shock absorbers is fulfilled. The total invariance of the free motions is reached if the following conditions are fulfilled:

$$\left.\begin{array}{r}
a_x + f_y - d_x - e_x = 0; \\
a_y + d_y - e_y - f_y = 0; \\
a_x a_y + e_x e_y - d_x d_y - f_x f_y = 0,
\end{array}\right\} \tag{6.38}$$

fulfillment of which is similar to the requirement that the center of gravity coincide with the center of the suspension of the optical device [38].

The independence of the forced motions of the optical device along different generalized coordinates provided that equalities (6.38) are fulfilled is guaranteed only if there is no mutual correlation between the elements of the vector of the perturbing effects. The absence of cross-correlation is possible, if all the force perturbations are concentrated in the center of gravity of the optical device, which is ordinarily not fulfilled in practice.

If the mathematical model of the suspension may not be broken down, its dynamic properties are completely described by n × m transfer matrix $W(p) = A^{-1}(p)B(p)$ of dimension n × m, where n is the number of generalized coordinates and m is the number of perturbing effects. The analytical solution does not yield a clear result, since it is related to finding the reciprocal matrix $A^{-1}(p)$.

Let us assume for analysis of the dynamic characteristics of the flexible suspension of the optical device that the conditions of decomposition of the mathematical model are fulfilled, matrix A(p) has diagonal shape, and the equations of dynamics then acquire the form:

268

$$(mp^2 + 4b_x p + 4c_x)\, x(p) = F_x(p) + (4b_x p + 4c_x)\, x'(p);$$

$$(mp^2 + 4b_y p + 4c_y)\, y(p) = F_y(p) + (4b_y p + 4c_y)\, y'(p);$$

$$\{J_z p^2 + [b_x(a_y^2 + d_y^2 + e_y^2 + f_y^2) + b_y(a_x^2 + d_x^2 + e_x^2 + f_x^2)]\, p +$$
$$+ c_x(a_y^2 + d_y^2 + e_y^2 + f_y^2) + c_y(a_x^2 + d_x^2 + e_x^2 + f_x^2)\}\, \gamma(p) =$$
$$= M_\gamma(p) + \{[b_x(a_y^2 + d_y^2 + e_y^2 + f_y^2) +$$
$$+ b_y(a_x^2 + d_x^2 + e_x^2 + f_x^2)]\, p + c_x(a_y^2 + d_y^2 + e_y^2 + f_y^2)\}\, \gamma'(p);$$

$$(mp^2 + 4b_z p + 4c_z)\, z(p) = F_z(p) + (4b_z p + 4c_z)\, z'(p);$$

$$[J_x p^2 + b_z(a_y^2 + d_y^2 + e_y^2 + f_y^2)\, p +$$
$$+ c_z(a_y^2 + d_y^2 + e_y^2 + f_y^2)]\, \alpha(p) =$$
$$= M_\alpha(p) + [b_z(a_y^2 + d_y^2 + e_y^2 + f_y^2)\, p + c_z(a_y^2 + d_y^2 + e_y^2 + f_y^2)]\, \alpha'(p);$$

$$[J_y p^2 + b_z(a_x^2 + d_x^2 + e_x^2 + f_x^2)\, p + c_z(a_x^2 + d_x^2 + e_x^2 + f_x^2)]\, \beta(p) =$$
$$= M_\beta(p) + [b_z(a_x^2 + d_x^2 + e_x^2 + f_x^2)\, p +$$
$$+ c_z(a_x^2 + d_x^2 + e_x^2 + f_x^2)]\, \beta'(p).$$

These equations have identical form $(\mu_i p^2 + b_i p + c_i)\, q_i(p) = f_i(p) + (b_i p + c_i)\, q_i'(p)$.
where μ_i, b_i, and c_i are the generalized coefficients of inertia, viscosity and stiffness, respectively, $q_i(p)$ is the i-th generalized coordinate, and $f_i(p)$ and $q'_i(p)$ are the generalized force and kinematic perturbing effects, respectively, on the i-th generalized coordinate.

The transfer functions for the force and kinematic effect can then be written in the form:

$$\left.
\begin{aligned}
W_i^f(p) &= \frac{q_i(p)}{f_i(p)} = \frac{1}{c_i}\, \frac{1}{T_y^2 p^2 + 2\xi T_y p + 1}; \\
W_i^q(p) &= \frac{q_i(p)}{q_i'(p)} = \frac{2\xi T_y p + 1}{T_y^2 p^2 + 2\xi T_y p + 1},
\end{aligned}
\right\}
\tag{6.39}$$

where $T_y^2 = \mu_i/c_i$; $\xi = b_i/(2c_i T_y)$ is the damping coefficient.

The spectral density of the i-th generalized coordinate is determined by the following formula if there is no correlation between the force and kinematic perturbing effects

$$S_i(\omega) = \left| W_i^f(j\omega) \right|^2 S_f(\omega) + \left| W_i^q(j\omega) \right|^2 S_\sigma'(\omega),$$

where $S_f(\omega)$ and $S'_q(\omega)$ are the spectral density of the force and kinetimatic perturbing effects, respectively, on the i-th generalized coordinate and $\left| W_i^f(j\omega) \right|$, $\left| W_i^q(j\omega) \right|$ are the moduli of the amplitude frequency characteristics for the force and kinematic perturbing effects.

The optimal value of the damping coefficient ζ can be determined for known $S_f(\omega)$ and $S'_q(\omega)$ by the values of the mean square of the generalized coordinate $\bar{q}_i^2 = \dfrac{1}{2\pi} \displaystyle\int_{-\infty}^{\infty} S_i(\omega)\, d\omega$.

The optimal value of the damping coefficient can be determined analytically in the case of a kinematic perturbing effect, presented in the form of white noise. The mean square of the generalized coordinate is determined from the equation

$$q_i^2 = \frac{1}{2\pi} \int_{-\infty}^{\infty} \frac{1 - 4\xi^2 T_y^2 (j\omega)^2}{[T_y^2 (j\omega)^2 + 2\xi T_y j\omega + 1]^2}\, N\, d\omega = \frac{4\xi^2 + 1}{4\xi T_y}\, N.$$

To find the minimum value of the last expression, let us set the first derivative equal to zero with respect to the damping coefficient

$$\frac{1}{T_y} - \frac{1}{4T_y \xi^2} = 0.$$

Hence, we find $\zeta_{\text{опт}} = 0.5$. In this case, $q^2{}_i = NT_y$.

A value of $\zeta = 0.2$ is recommended in [38] for the case of a determinant kinematic perturbing effect at frequency $\omega = T^{-1}{}_y$. Thus, one can conclude that the spectra of perturbing effects actually existing in the systems must be taken into account when developing flexible suspensions of optical devices.

Filtration of the force and kinematic perturbations, as follows from equation (6.39), is improved if the time constant of the elastic vibrations T_y, the value of which is bounded above by the requirement of guaranteeing the required static stiffness of the shock absorbers, is increased [9]. The filtering properties of the flexible suspension can be improved in the low-frequency region to $\omega = T^{-1}{}_y$ if active vibration-protection systems are used. It is assumed that the bandwidth of these systems exceed at least the lowest range of flexible vibrations of the suspension of the optical device on shock absorbers. The active vibration-protection system filters the perturbing effects in its own

bandwidth, while the high-frequency components of perturbations are filtered mainly by the flexible suspension of the optical device.

Several perturbing force effects R_i, $i = \overline{1, n}$, which have arbitrary directions and different points of application, are ordinarily active during operation on the optical device. The forced motions of the optical device are correlated even if the mathematical model breaks down, i.e., if conditions (6.38) are fulfilled. This can also be said about the forced motions of the suspension exposed to kinematic perturbations. Misalignment of the image, which is a criterion of the quality of the flexible suspension of an optical device, is determined by the formula

$$\delta(p) = L W^l(p) K r + L W^q(p) q, \qquad (6.40)$$

where $L = [l_\alpha(\alpha, \beta, \gamma) \; l_\beta(\alpha, \beta, \gamma) \; l_\gamma(\alpha, \beta, \gamma)]$ is the transformation matrix of the angular misalignments of the optical device with respect to its center of gravity (TsT) to misalignment of the image, the elements of which are dependent on a specific version of the optical device, $W^l(p)$ is the matrix of transfer functions by the perturbing force effects in the case of no breakdown of the mathematical model, equal to

$$W^l(p) =$$

$$= \begin{bmatrix} W^l_{\alpha\alpha}(p) & W^l_{\alpha\beta}(p) & 0 & 0 & 0 & W^l_{\alpha z}(p) \\ W^l_{\beta\alpha}(p) & W^l_{\beta\beta}(p) & 0 & 0 & 0 & W^l_{\beta z}(p) \\ 0 & 0 & W^l_{\gamma\gamma}(p) & W^l_{\gamma x}(p) & W^l_{\gamma y}(p) & 0 \end{bmatrix};$$

K is the reduction matrix of the perturbing force actions toward the center of gravity of the optical device, determined in the form

$$K = \begin{bmatrix} k_{\alpha 1} & k_{\beta 1} & k_{\gamma 1} & k_{x 1} & k_{y 1} & k_{z 1} \\ \cdot & \cdot & \cdot & \cdot & \cdot & \cdot \\ \cdot & \cdot & \cdot & \cdot & \cdot & \cdot \\ k_{\alpha i} & k_{\beta i} & k_{\gamma i} & k_{x i} & k_{y i} & k_{z i} \\ \cdot & \cdot & \cdot & \cdot & \cdot & \cdot \\ \cdot & \cdot & \cdot & \cdot & \cdot & \cdot \\ k_{\alpha n} & k_{\beta n} & k_{\gamma n} & k_{x n} & k_{y n} & k_{z n} \end{bmatrix}^T,$$

and $k_{\alpha i} = y_{0i} \cos \vartheta_i - z_{0i} \cos \psi_i$; $k_{\beta i} = z_{0i} \cos \varphi_i - x_{0i} \cos \vartheta_i$; $k_{\gamma i} = x_{0i} \cos \psi_i - y_{0i} \cos \varphi_i$; $k_{xi} = \cos \varphi_i$; $k_{yi} = \cos \psi_i$, $k_{zi} = \cos \vartheta_i$, x_{0i}, y_{0i}, z_{0i} are the coordinates of application of the R_i, $\cos \varphi_i$, $\cos \psi_i$, and $\cos \vartheta_i$ are the direction cosines of R_i, $r = |R_1 R_2 \ldots R_n|^T$ is the vector of the perturbing force effects, $W^q(p)$ is a amtrix of the transfer functions for the perturbing kinematic effects in the absence of decomposition of the mathematical model, equal to

$$\overline{W}^q(p) =$$
$$= \begin{bmatrix} W_q^{\alpha\alpha}(p) & W_{\alpha\beta}^q(p) & 0 & 0 & 0 & W_{\alpha z}^q(p) \\ W_{\beta\alpha}^q(p) & W_{\beta\beta}^q(p) & 0 & 0 & 0 & W_{\beta z}^q(p) \\ 0 & 0 & W_{\gamma\gamma}^q(p) & W_{\gamma x}^q(p) & W_{\gamma y}^q(p) & 0 \end{bmatrix};$$

and $q = |\alpha'(p)\ \beta'(p)\ \gamma'(p)\ x'(p)\ y'(p)\ z'(p)|^T$ is the vector of the perturbing kinematic effects.

The spectral density of image misalignment is determined from the expressions

$$S_\delta(\omega) = |L W^f(j\omega) K|^2 S_f(\omega) + [L W^q(j\omega)]^2 S_q(\omega),$$

where $S_f(\omega) S_q(\omega)$ are the vectors of the spectral densities of the force and perturbing kinematic effects and $W^f(j\omega)$, $W^q(j\omega)$ are the matrices of the frequency transfer functions.

Hence, the mean square of image misalignment is determined by the relation

$$\bar{\delta}^2 = \frac{1}{2\pi} \int\limits_{-\infty}^{\infty} S_\delta(\omega)\, d\omega.$$

The problem of optimal synthesis of the parameters of a flexible suspension is formulated in the following manner:

$$\min \{\bar{\delta}^2(h), \quad h \in H\},$$

272

where h is the vector of the variable parameters whose elements are the coordinates of the reduction points and the coefficients of stiffness and viscosity of the shock absorbers.

Constraints in the form of inequalities $h_{i\,min} \leqslant h_i \leqslant h_{i\,max}$, where $h_{i\,min}$, $h_{i\,max}$ are the lower and upper bounds of variation of the i-th parameter.

The given method of parametric design is oriented toward the use of the computer and is based on the iterative search procedure $h_{опт}$, corresponding to the minimum $\bar{\delta}^2$. The main difficulties in performing this design are the large expenditures of machine time in calculation of $\bar{\delta}^2$ at each step of the iteration.

The design procedure is simplified considerably if the conditions of decomposition of the mathematical model of the flexible suspension of the optical device are fulfilled. The values contained in matrix equation (6.40) assume the form:

$$\mathbf{W}_1^f(p) = \begin{bmatrix} W_{\alpha\alpha}^f(p) & 0 & 0 \\ 0 & W_{\beta\beta}^f(p) & 0 \\ 0 & 0 & W_{\gamma\gamma}^f(p) \end{bmatrix};$$

$$\mathbf{K} = \begin{bmatrix} k_{\alpha 1} & \cdots & k_{\alpha i} & \cdots & k_{\alpha n} \\ k_{\beta 1} & \cdots & k_{\beta i} & \cdots & k_{\beta n} \\ k_{\gamma 1} & \cdots & k_{\gamma i} & \cdots & k_{\gamma n} \end{bmatrix};$$

$$\mathbf{W}_1^q(p) = \begin{bmatrix} W_{\alpha\alpha}^q(p) & 0 & 0 \\ 0 & W_{\beta\beta}^q(p) & 0 \\ 0 & 0 & W_{\gamma\gamma}^q(p) \end{bmatrix};$$

$$q_1 = [\alpha'\beta'\gamma']^T.$$

The constraints in the form of equalities (6.38) must be taken into account during parametric design. Since the numerators of the elements of transfer matrices $W^f_1(p)$ and $W^q_1(p)$ are second order, one can avoid the need for numerical integration of the spectral densities during determination of δ^2 at each step of the iteration and one can use the tabulated integrals [10] of form

$$I_n = \frac{1}{2\pi} \int_{-\infty}^{\infty} \frac{G(j\omega)\,d\omega}{A(j\omega)\,A(-j\omega)},$$

273

where $A(j\omega)$ and $G(j\omega)$ are polynomials of $j\omega$ of n-th and (2n - 2)-th power. It should be noted that this approach requires additional time expenditures when preparing the problem of parametric design for solution of the computer.

BIBLIOGRAPHY

1. Zeldovich, S. M., M. I. Maltinskiy, O. M. Okon et al., "Avtokompensatsiya instrumentalnykh pogreshnostey girosistem" [Autocompensation of the Instrument Errors of Gyro Systems], Leningrad, Izdatelstvo "Sudostroyeniye", 1976.

2. Apeko, M. I. and A. S. Dubovik, "Prikladnaya optika" [Applied Optics], Moscow, Izdatelstvo "Nauka", 1982.

3. Chemodanov, B. K., V. L. Danilov, V. D. Nefedov et al., "Astrosledyashchiye sistemy" [Astronomical Tracking Systems], Moscow, Izdatelstvo "Mashinostroyeniye", 1977.

4. Babayev, A. A., "Amortizatsiya, dempfirovaniye i stabilizatsiya bortovykh opticheskikh priborov" [Shock Absorption, Damping and Stabilization of Airborne Optical Instruments], Leningrad, Izdatelstvo "Mashinostroyeniye", 1984.

5. Babayev, A. A., "Stabilizatsiya opticheskikh priborov" [Stabilization of Optical Instruments], Leningrad, Izdatelstvo "Mashinostroyeniye", 1975.

6. Barb, D. F. and S. Campana, "Charge-Coupled Imaging Devices," "Dostizheniya v tekhnike peredachi i vosproizvedeniya izobracheniy" [Advances in Transmission and Reproduction of Images], translated from English by V. A. Hertel and V. V. Rakitina, Vol 3, Moscow, Izdatelstvo "Mir", 1980.

7. Basharin, A. V., V. A. Novikov, and G. G. Sokolovskiy, "Upravleniye elektroprivodami" [Control of Electric Drives], Leningrad, Energoizdat, 1982.

8. Beloglazov, I. N. and V. P. Tarasenko, "Korrelyatsionno-ekstremalnyye sistemy" [Correlation Extreme Systems], Moscow, Izdatelstvo "Sovetskoye radio", 1974.

9. Bessekerskiy, V. A. and Ye. P. Popov, "Teoriya sistem avtomaticheskogo regulirovaniya" [The Theory of Automatic Control Systems], Moscow, Izdatelstvo "Nauka", 1975.

10. Bessekerskiy, V. A. and Ye. A. Fabrikant, "Dinamicheskiy sintez sistem giroskopicheskoy stabilizatsii" [Dynamic Design of Gyroscopic Stabilization Systems], Leningrad, Izdatelstvo "Sudostroyeniye", 1968.

11. Bespalov, Yu. I., "Using Thin Layers of Liquid in Geodetic Surveying Instruments," IZVESTIYA VUZOV. GORNY ZHURNAL, No 8, 1978.

12. Bespalov, Yu. I., "Optical Plumb With Liquid Compensator," IZVESTIYA VUZOV. SERIYA GEODEZIYA I AEROFOTOSYEMKA, No 2, 1976.

13. Bespalov, Yu. I., "Optical Centering Device With Liquid Compensator," IZVESTIYA VUZOV. SERIYA GEODEZIYA I AEROFOTOSYEMKA, No 6, 1981.

14. Biberman, L. N., "Rastry v elektroopticheskikh ustroystvakh" [Patterns in Electrooptical Devices], translated from English by V. I. Proskuryakov, Moscow, Izdatelstvo "Energiya", 1969.

15. Bron, M. and E. Wolf, "Osnovy optiki" [Fundamentals of Optics], translated from English, edited by G. P. Motulevich, Moscow, Izdatelstvo "Nauka", 1973.

16. Braslavskiy, D. A. and V. V. Petrov, "Tochnost izmeritelnykh ustroyst" [The Accuracy of Measuring Devices], Moscow, Izdatelstvo "Mashinostroyeniye", 1976.

17. Brykov, V. G. and A. V. Mochalov, "Errors of Three-Axis Laser Gyroscope Module With General Initial Misalignment," IZVESTIYA VUZOV. SERIYA PRIBOROSTROYENIYE, Vol 26, No 6, 1983.

18. Bychkov, S. I., D. P. Lukyanov and A. I. Bakalyar, "Lazerny giroskop" [The Laser Gyroscope], Moscow, Izdatelstvo "Sovetskoye radio", 1975.

19. Zeyger, S. G., Yu. L. Klimontovich, P. S. Landa et al., "Volnovyye i fluktuatsionnyye protsessy v lazerakh" [Wave and Fluctuation Processes in Lasers], Moscow, Izdatelstvo "Nauka", 1974.

20. Volosov, D. S., "Fotograficheskaya optika" [Photographic Optics], Moscow, Izdatelstvo "Iskusstvo", 1978.

21. Vyskub, V. G., B. S. Rozov, and V. I. Savelyev, "Pretsizionnyye tsifrovyye sistemy avtomaticheskogo upravleniya" [Precision Digital Automatic Control Systems], Moscow, Izdatelstvo "Mashinostroyeniye", 1984.

22. Gabor, D., "Displacement Sensors and Drives for Control of Segmented Main Mirror," "Opticheskiye i infrakrasnyye teleskopy 90-kh godov" [Optical and Infrared Telescopes of the 1990's], Moscow, Izdatelstvo "Mir", 1983.

23. Graym, N. N., "Opticehskiye dalnomery i vysotomery geometricheskogo tipa" [Optical Rangefinders and Geometric-Type Altimeters], Moscow, Izdatelstvo "Nedra", 1983.

24. Gusev, N. A., "An Autoreduction Optical Plumb Line With Liquid Lens," ZAPISKI LENGRADSKOGO GORNOGO INSTITUTE IMENI PLEKHANOV, Vol 67, No 1, 1975.

25. Gusev, N. A., "Two-Liquid Compensator for Mining Leveling," NAUCHNYYE DOKLADY VYSSHIKH SHKOL. SERIYA GORNOYE DELO, No 2, 1959.

26. Gusev, N. A., "A Liquid Compensator," GEODEZIYA I KARTOGRAFIYA, No 9, 1958.

27. Denisov, A. A. and D. N. Kolesnikov, "Teoriya bolshikh sistem upravleniya" [The Theory of Large Control Systems], Leningrad, Znergoizdat, 1982.

28. Gerald, A and J. N. Berg, "Vvedeniye v matrichnuyu optiku" [Introduction to Array Optics], Moscow, Izdatelstvo "Mir", 1978.

29. Petrov, V. I., V. A. Polkovnikov, L. V. Rabinovich et al., "Dinamika sledyashchikh privodov" [The Dynamics of Follow-Up Drives], Moscow, Izdatelstvo "Mashinostroyeniye", 1982.

30. Zhovinskiy, V. N. and V. F. Arkhovskiy, "Korrelyatsionnyye ustroystva" [Correlation Devices], Moscow, Izdatelstvo "Energiya", 1974.

31. Gorenshteyn, I. A., I. A. Shulman, A. S. Safaryan et al., "Inertsialnaya navigatsiya" [Inertial Navigation], Moscow, Izdatelstvo "Sovetskoye radio", 1962.

32. Katys, G. P., "Optiko-elektronnaya obrabotka informatsii" [Optical Electronic Data Processing], Moscow, Izdatelstvo "Mashinostroyeniye", 1973.

33. Katys, G. P., "Opticheskiye informatsionnyye sistemy robotov i manipulyatorov" [Optical Information Systems of Robots and Manipulators], Moscow, Izdatelstvo "Mashinostroyeniye", 1977.

34. Kozlov, Yu. A., "Linear and Angular Image Misalignment Stabilization and Measuring Devices," IZVESIYA LETI. AVTOMATIZATSIYA PROIZVODSTVENNYKH PROTSESSOV I USTRANOVOK, No 239, 1978.

35. Kozlov, Yu. A. and V. A. Solntsev, "Effect of Parameters of Photoelectric Sensor Elements on Operation in Optical Image Shift Compensation System," "Sbornik nauchnykh trudov Khabarovskogo politekhnicheskogo instituta. Voprosy teorii i rascheta elementov i sistem avtomatizirovannogo elektroprivoda" [Collection of Scientific Papers of Khabarovsk Polytechnical Institute. Problems of the Theory and Design of Elements and Systems of an Automated Electric Drive], 1982.

36. Kozlov, Yu. A. and V. A. Solntsev, "Optical Image Shift Compensation System," "Sbornik nauchnykh trudov Khabarovskogo politekhnicheskogo instituta. Voprosy teorii i rascheta elektromekhanicheskikh sistem" [Collection of Scientific Papers of Khabarovsk Polytechnical Institute. Problems of the Theory and Design of Electromechanical Systems], 1980.

37. Kozubovskiy, S. F., "Korrelyatsionnyye ekstremalnyye sistemy: Spravochnik" [Extreme Correlation Systems: A Handbook], Kiev, Izdatelstvo "Naukova dumka", 1973.

38. Kolovskiy, M. Z., "Avtomaticheskoye upravleniye vibrozashchitnymi sistemi" [Automatic Control of Vibration-Protection Systems], Moscow, Izvatelstvo "Nauka", 1967.

39. Komarov, V. M. and G. B. Yatskevich, "Laser Systems in Location and Navigation," ZARUBEZHNAYA RADIOELEKTRONIKA, No 2, 1978.

40. Kondourov, I. N., A. V. Mirolyubov, and V. A. Solomatin, "Calculation of Parameters of Analyzer in Phase Optoelectronic Velocity Sensors," OPTIKO-MEKHANICHESKAYA PROMYSHLENNOST, No 5, 1983.

41. Solntsev, V. A., P. N. Kopanygin, Yu. A. Kozlov et al., "Checking the Parameters of Motion of an Optical Image," IZVESTIYA LETI. AVTOMATIZATSIYA PROIZVODSTVENNYKH PROTSESSOV I USTANOVOK, No 292, 1981.

42. Konyukhov, N. Ye., A. A. Plyut, and V. M. Shapovalov, "Optoelektronnyye izmeritelnyye preobrazovateli" [Optoelectronic Measuring Converters], Leningrad, Izdatelstvo "Energiya", 1977.

43. Korn, G. and T. Korn, "Spravochnik po matematike (dlya nauchnykh rabotnikov i inzhenerov)" [Handbook on Mathematics (for Scientific Workers and Engineers], translated from English, edited by I. G. Aramanovich, Moscow, Izdatelstvo, Nauka, 1973.

44. Korshak, F. A., "Tsentralnoye proyektirovaniye dvizhushchimsya puchkom luchey v fotogrammetrii" [Central Design of Moving Bundle of Rays in Photogrammetry], Makhachkala, Dagestanskiy Gosudarstvennyy universitet, 1962.

45. Kochetov, F. G., "Niveliry s kompensatorami" [Levels With Compensators], Moscow, Izdatelstvo "Nedra", 1985.

46. Kravtsov, N. V. and Yu. V. Strelnikov, "Pozitsionno-chuvstvitelnyye datchiki opticheskikh sledyashchikh sistem" [Position-Sensitive Sensors of Optical Tracking Systems], Moscow, Izdatelstvo "Nauka", 1969.

47. Kravtsov, N. V., L. Ye. Chirkov, and V. L. Polyachenko, "Elementy optoelektronnykh informatsionnykh sistem" [Elements of Optoelectronic Information Systems], Moscow, Izdatelstvo "Nauka", 1970.

48. Kruksunov, L. Z., "Spravochnik po osnovam infrakrasnoy tekhniki" [Handbook on Fundamentals on Infrared Technology], Moscow, Izdatelstvo "Sovetskoye radio", 1978.

49. Batrakov, A. S., M. M. Butusov, G. P. Grechka et al., "Lazernyye izmeritelnyye sistemy" [Laser Measuring Systems], Moscow, Izdatelstvo "Radio i svyaz", 1981.

50. Miroshnikov, M. M., "Teoreticheskiye osnovy optiko-elektronnykh priborov" [Theoretical Fundamentals of Optoelectronic Instruments], Leningrad, Izdatelstvo "Mashinostroyeniye", 1983.

51. Mikhelson, N. N., "Opticheskiye teleskopy. Teoriya i konstruktsiya" [Optical Telescopes. Theory and Design], Moscow, Izdatelstvo "Nauka", 1976.

52. Nikolayev, P. V. and Yu. A. Sabinin, "Fotoelektricheskiye sledyashchiye sistemy" [Photoelectric Tracking Systems], Leningrad, Izdatelstvo "Energiya", 1969.

53. Novoselov, B. V., "Proyektirovaniye kvazioptimalnykh sledyashchikh sistem kombinirovannogo regulirovaniya" [Design of Quasi-Optimal Combination Control Tracking Systems], Moscow, Izdatelstvo "Energiya", 1972.

54. Nosov, Yu. R., "Optoelektronika" [Optoelectronics], Moscow, Izdatelstvo "Sovetskoye radio", 1977.

55. Artobolevskiy, I. I., V. A. Genkin, V. K. Grinkevich et al., "Optimization in LP-Search Computer Theory," DOKLADY AKADEMII NAUK SSSR, No 6, 1971.

56. Osmolovskiy, P. F., "Iteratsionnyye mnogokanalnyye sistemy avtomaticheskogo upravleniya" [Multichannel Iterative Automatic Control Systems], Moscow, Izdatelstvo "Sovetskoye radio", 1969.

57. Pavlov, A. V., "Optiko-elektronnyye pribory. Osnovy teorii i rascheta" [Optoelectronic Instruments. Fundamentals of Theory and Design], Moscow, Izdatelstvo "Energiya", 1974.

58. Pelpor, D. S., "Giroskopicheskiye sistemy orientatsii i stabilizatsii: Spravnochnoye posobiye" [Gyroscopic Orientation and Stabilization Systems: A Reference Manual], Moscow, Izdatelstvo "Mashinostroyeniye", 1982.

59. Pogarev, G. V., "Opticheskiye yustirovochnyye zadachi: Spravochnoye posobiye" [Optical Adjusting Problems: A Reference Manual], Leningrad, Izdatelstvo "Mashinostroyeniye", 1974.

60. Pogarev, G. V., "Yustirovka opticheskikh priborov" [Adjustment of Optical Instruments], Leningrad, Izdatelstvo "Mashinostroyeniye", 1968.

61. Popov, G. M., "Asfericheskiye poverkhnosti v astronomicheskoy optike" [Aspherical Surfaces in Astronomical Optics], Moscow, Izdatelstvo "Nauka", 1980.

62. Rivkin, S. S., "Stabilizatsiya izmeritelnykh ustroystv na kachayushchemsya osnovanii" [Stabilization of Measuring Devices on a Rocking Base], Moscow, Izdatelstvo "Nauka", 1978.

63. Rivkin, S. S., "Teoriya giroskopicheskikh ustroystv" [The Theory of Gyroscopic Devices], Book 2, Leningrad, Izdatelstvo "Sudostroyeniye", 1964.

64. Rigley, W., W. Hollister, and W. Denhard, "Teoriya, proyektirovaniye i ispytaniye giroskopov" [The Theory, Design and Testing of Gyroscopes], Moscow, Izdatelstvo "Mir", 1972.

65. Rouse, A., "Zreniye cheloveka i elektronnoye zreniye" [Human Vision and Electronic Sight], Moscow, Izdatelstvo "Mir", 1977.

66. Savchuk, A. A., "Space-Dependent Image Distortions Caused by Motion and Restoration of Image," "Obrabotka izobrazheniya pri pomoshchi TsVM" [Image Processing Using a Digital Computer], Moscow, Izdatelstvo "Mir", 1973.

67. Sergeyev, V. I., "Instrumentalnaya tochnost kinematicheskikh i dinamicheskikh sistem" [Instrumental Accuracy of Kinematic and Dynamic Systems], Moscow, Izdatelstvo "Nauka", 1971.

68. Sergeyev, V. I. and I. N. Statnikov, "On the Randomized Discrete Search for Optimal Solutions in Problems of Projection of Mechanisms and Machines," "Resheniye zadach prikaldnoy mekhaniki na EVM" [Computer Solution of Problems of Applied Mechanics], Moscow, Izdatelstvo "Nauka", 1978.

69. Sergeyev, G. A. and D. A. Yanutsh, "Staticheskiye metody issledovaniya prirodnykh obyektov" [Statistical Methods of Studying Natural Objects], Leningrad, Gidrometoizdat, 1973.

70. Vavilov, A. A., A. D. Valchikhin, I. A. Karasin et al., "Sintez pozitsionnykh sistem programmnogo upravleniya" [Design of Program Control Position Systems], Leningrad, Izdatelstvo "Mashinostroyeniye", 1977.

71. Bleyz, Ye. S., Yu. A. Danilov, V. F. Kazmirenko et al., "Sledyashchiye privody" [Follow-Up Drives], Books 1 and 2, Moscow, Izdatelstvo "Energiya", 1976.

72. Slyusarev, G. G., "Metody rascheta opticheskikh sistem" [Methods of Calculating Optical Systems], Leningrad, Izdatelstvo "Mashinostroyeniye", 1969.

73. Smirnov, A. Ya., "Matematicheskiye modeli teorii peredachi izobrazheniy" [Mathematical Models of the Theory of Image Transmission], Moscow, Izdatelstvo "Svyaz", 1979.

74. Strelkov, S. P., "Vvedeniye v teoriyu kolebaniy" [Introduction to Vibration Theory], Moscow, Izdatelstvo "Nauka", 1964.

75. Tomovich, R. and M. Vukobratovich, "Obshchaya teoriya chuvstvitelnosti" [The General Theory of Sensitivity], Moscow, Izdatelsvto "Sovetskoye radio", 1972.

76. Tudorovskiy, A. I., "Teoriya opticheskikh priborov" [The Theory of Optical Instruments], Vol 1, Moscow, Akademii Nauk SSSR, 1948.

77. Kozlov, Yu. A., V. A. Solntsev, P. N. Kopanygin et al., "A Photoelectric System for Checking the Parameters of Motion of an Optical Image," IZVESTIYA LETI. SERIYA AVTOMATIZATSIYA PROIZVODSTVENNYKH PROTSESSOV I USTANOVOK, No 268, 1980.

78. Himmelblau, D., "Prikladnoye nelineynoye programmirovaniye" [Applied Nonlinear Programming], Moscow, Izdatelstvo "Mir", 1975.

79. Chung Ki-Kim, "The Physics of Charge-Coupled Devices," "Pribory s zaryadovoy svyazyu" [Charge-Coupled Devices], Moscow, Energoizdat, 1981.

80. Sheynis, N. V., "Wedges With Variable Refracting Angle," OPTIKO-MEKHANICHESKAYA PROMYSHLENNOST, No 3, 1971.

81. Shcherbakov, Ya. Ye., "Raschet i konstruirovaniye aerofotoapparatov" [Calculation and Design of Aerial Cameras], Moscow, Izdatelstvo "Mashinostroyeniye", 1979.

82. Yakushenkov, Yu. G., "Opticheskiye sistemy fotoelektricheskikh ustroystv" [Optical Systems of Photoelectric Devices], Moscow, Izdatelstvo "Mashinostroyeniye", 1966.

83. Yakushenkov, Yu. G., "Osnovy optiko-elektronnogo priborostroyeniya" [Fundamentals of Optoelectronic Instrument Building], Moscow, Izdatelstvo "Sovetskoye radio, 1977.

84. Aroyan, G. F., "The Technique of Spatial Filtering," PROCEEDINGS OF IRE, Vol 47, No 9, 1959.

85. Altor, J. T., "Image Velocity Sensing With Parallel-Split Reticles," JOURNAL OF THE OPTICAL SOCIETY OF AMERICA, Vol 54, No 12, 1963.

86. De Ponteves, D. and R. Rafat, "Stabilisation de la visee par systeme gyroscopique" NOUVELLE REVUE D'OPTIQUE APPLIQUE, No 1, 1972.

87. Erfle, H, "Über die durch ein Drehkeilpaar erzeugte Ablenkung und über eine als Kennzeich für die Beibehaltung des Hauptschnittes dienende Sinusbedigung," ZEITSCHRIFT FÜR PHYSIK, No 1, 1920.

88. Fourner-Siere, A. and C. Sicourt, "Le FOC in instrument europeen pour le telescope spatial," L'AERONAUTIQUE ET L'ASTRONAUTIQUE, No 4, 1980.

89. Hair, T., J. Bluthe, and W. Ager, "An Optical Method of Measuring Transverse Surface Velocity," ACTA IMECO, Vol 2, 1968.

90. Hayashi, A. and Y. Kitogawa, "Image Velocity Sensing Using an Optical Fiber Array," APPLIED OPTICS, Vol 21, No 8, April 1982.

91. Itakura, Y, S. Tsutsumi, and T. Takagi, "Statistical Properties of the Background Noise for the Atmospheric Windows in the Intermediate Infrared Region," INFRARED PHYSICS, Vol 14, No 1, 1974.

92. Levi, L., "Motion Blurring With Decaying Deflector Response," APPLIED OPTICS, Vol 10, 1971.

93. Truscott, N. R., "Image Transforms With Fused Fiber Optics," PROCEDDINGS OF SOCIETY OF PHOTO-OPTICAL INSTRUMENT ENGINEERING, Vol 306, 1981.

94. Vander, Ingt A., "Optical Processing," PROCEEDINGS OF DEVELOPMENT IN HOLOGRAPHY, SPIE. SEMINAR PROCEEDINGS, Vol 25, 1971.

95. Wood, G. D., "An Airborne Video (Motion Picture Surveillance System)," JOURNAL OF THE SMPTE, No 9, 1974.

- END -

SUBSCRIPTION/PROCUREMENT INFORMATION